PhD thesis

Institute of Physical Chemistry
Polish Academy of Sciences
Kasprzaka 44/52
01-224 Warszawa, Poland

Electrodes modified

with carbon nanoparticles and enzymes

Katarzyna Szot

PhD thesis

This dissertation was prepared within the International Ph.D. in Chemistry Studies
at Institute of Physical Chemistry of the Polish Academy of Sciences

Supervisor: Prof. dr hab. Marcin Opallo
Department of Electrode Processes

Warszawa, January 2012

Acknowledgements

First of all, I would like to express my sincere gratitude to my supervisor Prof. Marcin Opallo for his scientific assistance, understanding, patience, and guidance.

I would like to thank Prof. Gunther Wittstock for instructive visits in his laboratory.

I gratefully acknowledge Dr. Joanna Niedziolka-Jönsson, Dr. Ewa Rozniecka, Dr. Martin Jönsson-Niedziolka, Dr. Wojciech Nogala, Wojciech Adamiak and Dr. Adam Lesniewski for scientific discussions, help and support.

Also I would like to thank for all help from Dr. Carolina Nunes Kirchner, Dr. Barbara Pałys; Dr. Cecile Rizzi; Dr. Laurent Gaillon; Prof. Frank Marken and his formers PhD students (Dr. Stuart MacDonald and Dr. John D. Watkins); Adam Presz; and Prof. Jerzy Rogalski.

Many thanks to all colleagues from the Department of Electrode Processes, for making a great atmosphere in the laboratory and for the help they provided me.

I would like to thank my family for their love and understanding.

Also I would like to thank my friends for their faith and support.

Finally I would like to thank My Marcin for his love, faith and invaluable help.

This dissertation is dedicated to Marcin Karpiński who always gives me a boost.

Abstract

The aim of this thesis was the development of preparation procedures and study of the electrochemical properties of electrodes modified with hydrophilic carbon nanoparticles and enzymes. The carbon nanoparticles were immobilized onto electrode surfaces via the application of various methods like chemically and electrochemically generated sol-gel processes and/or layer-by-layer assembly method. In the latter method the electrostatic interactions between negatively and positively charged carbon nanoparticles or between negatively charged carbon nanoparticles and imidazolium functionalized silicate were utilized for film formation. The obtained films were characterized by atomic force microscopy, scanning electron microscopy and reflection absorption infrared spectroscopy.

On the surface of modified electrodes redox active enzymes such as laccase, bilirubin oxidase, myoglobin and glucose oxidase were immobilized. Most of electrodes modified with laccase or bilirubin oxiadase exhibit mediated and mediatorless bioelectrocatalysis of oxygen reduction. This reaction was studied by scanning electrochemical microscopy. The application of redox competition mode enabled the study of the catalytic activity of laccase co-encapsulated with carbon nanoparticles within silicate matrix. The electrodes modified with laccase or bilirubin oxidase were applied as biocathodes in Zn-dioxygen hybrid cells. In turn the direct signal from the enzyme's active center was recorded for the electrodes modified with myoglobine and glucose oxidase. The effect of the presence of hydrogen peroxide or glucose on the electrochemical properties of these electrodes was also observed.

Streszczenie

Celem niniejszej rozprawy było opracowanie sposobów modyfikacji, oraz poznanie elektrochemicznych właściwości, elektrod modyfikowanych nanocząstkami węgla i enzymami. Do unieruchomienia nanocząstek węgla na powierzchni elektrody wykorzystano chemicznie lub elektrochemicznie generowany proces zol-żel, i/lub metodę „warstwa po warstwie" (ang. *layer-by-layer*). W przypadku tej ostatniej do otrzymania filmu, wykorzystano elektrostatyczne oddziaływanie pomiędzy ujemnie i dodatnio naładowanymi nanocząstkami węgla lub pomiędzy ujemnie naładowanymi nanocząstkami węgla i polikrzemianem z imidazoliowymi grupami funkcyjnymi. Otrzymane warstwy zostały scharakteryzowane następującymi metodami: mikroskopii sił atomowych, skaningowej mikroskopii elektronowej oraz odbiciowo-absorpcyjnej spektroskopii podczerwieni.

Na powierzchni modyfikowanych elektrod zostały unieruchomione takie redoks-aktywne enzymy jak lakaza, oksydaza bilirubiny, mioglobina i oksydaza glukozy. Większość elektrod modyfikowanych lakazą lub oksydazą bilirubiny wykazywała zarówno mediatorową, jak i bezmediatorową bioelektrokatalityczną redukcję ditlenu. Proces bioelektrokatalitycznej redukcji ditlenu został zbadany dodatkowo za pomocą skaningowej mikroskopii elektrochemicznej przy wykorzystaniu trybu, w którym próbka i próbnik konkurują o ten sam substrat. To umożliwiło zbadanie rozkładu aktywności lakazy unieruchomionej wraz z nanocząstkami węgla w matrycy polikrzemianowej. Elektrody modyfikowane lakazą i oksydazą bilirubiny zostały wykorzystane, jako biokatody w ogniwach cynkowo-ditlenowych. Natomiast bezpośredni sygnał od centrum aktywnego enzymu uzyskano tylko w przypadku elektrod modyfikowanych mioglobiną lub oksydazą glukozy. Właściwości elektrochemiczne tych elektrod zależą także od obecności glukozy lub nadtlenku wodoru w roztworze elektrolitu.

Major abbreviations

AA	ascorbic acid
ABTS^{2-}	2, 2'-azinobis (3-ethylbenzothiazoline-6-sulfonate)
AChE	acetocholinesterase
AFM	atomic force microscopy/ microscope
BFC	biofuel cell
BOx	bilirubin oxidase
CA	chronoamperometry
Cat	catalase
CCE	carbon ceramic electrode
CNPs	carbon nanoparticles
CE	counter electrode (auxiliary electrode)
CNTs	carbon nanotubes
CV	cyclic voltammetry or cyclic voltammogram
CVD	chemical vapour deposition
Cyt c	cytochrome c
DA	dopamine
DET	direct electron transfer
DNA	deoxyribonucleic acid
EIS	electrochemical impedance spectroscopy
FAD	flavin adenine dinucleotide
Fc(CH$_2$OH)$_2$	ferrocenedimethanol
FMCA	ferrocene monocarboxylic acid
GCE	glassy carbon electrode
GN	graphene
GOx	glucose oxidase
Hb	haemoglobin
HET	heterogeneous electron transfer
HRP	horseradish peroxidase
IL	ionic liquid
IR	infrared spectroscopy
ITO	tin-doped indium oxide coated glass

Major abbreviations

IUPAC	International Union of Pure and Applied Chemistry
LbL	layer-by-layer
Lc	laccase
Mb	myoglobin
MCOx	multicopper oxidases
MET	mediated electron transfer
MTMOS	methyltrimethoxysilane
MWCNTs	mutli-walled carbon nanotubes
NADH	nicotinamide adenine dinucleotide
NB	nitrobenzene
NHE	normal hydrogen electrode
OCP	open circuit potential
ORR	oxygen reduction reaction
OTEOS	*n*-octyltriethoxysilane
PG	pyrolytic graphite electrode
RE	reference electrode
SCE	saturated calomel electrode
SEM	scanning electron microscopy / microscope
SECM	scanning electrochemical microscopy/ microscope
SWCNTs	single-walled carbon nanotubes
Syr	3, 5-dimethoxy-4-hydroxybenzaldehydazine (syringaldazine)
*t*BuFc	*tert*-butylferrocene
TMOS	tetramethoxysilane
WE	working electrode
UA	uric acid
UME	ultramicroelectrode

Table of content

1. Introduction

There is scientific interest in environmentally friendly power sources as fuel cells. To be applicable for powering portable electronics or *in vivo* devices such fuel cells have to fulfil several nontrivial conditions; they have to efficiently operate in room temperature without substantial heating, contain and produce disposable products and use only selective catalysts instead of expensive noble metals. The cell also has to be small enough to be placed in the device or biological organisms and produce energy from available fuels (glucose or ascorbic acid). In terms of efficiency (current and power density) and stability, the cell should deliver power of the order of miliwatts while maintaining long-term stability. Conventional batteries lack many of the above features. They contain and produce harmful compounds and in some cases nonselective catalysts which make them nonbiodegradable, and makes it obligatory to use hard to miniaturize sealings. Some of them produce excessive heat which could cause damage to (in case of *in vivo* applications) neighbouring tissues or vulnerable device elements. They also have a narrow choice of fuels. On the contrary, fuel cells utilizing redox enzymes i.e. enzymatic biofuel cells might fulfil all of these criteria. Biofuel cells which generate a high power density [1] as well as biofuel cells which operate in physiological conditions [2] have already been created. However, their stability is still an issue and there have yet been no reports on systems simultaneously fulfilling both of these requirements. Apart from their application as energy sources, bioelectrodes similar to those used in biofuel cells can also be employed as detectors in sensors capable of measuring concentrations of various analytes.

This thesis is an attempt to approach this goal in this dynamically developing branch of electrochemistry. In particular it is focused on redox proteins and similarly sized carbon nanoparticles modified electrodes. These materials due to their ability to create well developed surfaces could have a significant role in the development of biofuel cells and biosensors. The various procedures for preparation of enzymes and carbon nanoparticles modified electrodes are created in attempt to improve stability and efficiency of the bioelectrocatalytic process.

1

2

Literature review

2. Modified electrodes

When considering an electrode designed for power generation, conversion or detection of analyte one is interested in the following desired attributes: (i) surface development (ii) improved electrocatalysis and sensitivity (iii) freedom from surface fouling and (iv) exclusion of side reactions that might compete with the studied electrode process.

All of above mentioned are together hard to come by when only bare electrodes are taken into account. To overcome these limitations researchers started to experiment with new, often complex materials and dedicated catalysts. Using them they started to create so called chemically modified electrodes. The pioneering work in that field was presented by Lane and Hubbard in 1973 [3]. Since that time the branch of electrochemistry studying these newly developed electrodes has seen remarkable growth, and numerous important results were achieved. According to IUPAC there are four main avenues for modifying electrode surfaces through chemisorption, covalent bonding, polymer film coating and composite [4]. Some of these approaches can also be utilized for enzyme-modified electrodes.

The studies of enzyme-modified electrodes started even earlier than chemically modified ones. Such an interest arose due to their feasible biomedical applications. In 1962 Leland C. Clark Jr. − the father of biosensors − for the first time demonstrated a glucose biosensor [5]. The authors modified an oxygen electrode with two glucose permeable membranes with the glucose oxidase entrapped in between. The constructed device was utilized for detection of glucose during cardiovascular surgeries through monitoring of the changes of the oxygen[*] partial pressure consumed in the bioelectrocatalytic reaction [5]. Later, Updike and Hicks followed Clark's tracks and modified the oxygen electrode with acrylamide gel with immobilized glucose oxidase [6]. Ten years later Yeah and Kuwana [7], and Eddowes and Hill [8] made a real breakthrough in the bioelectrochemistry. They independently adsorbed cytochrome *c* on tin doped indium oxide [7] and 4,4'-bipyridyl modified gold electrodes [8] and for the first time observed direct electron transfer.

---

[*] In this thesis the term "oxygen" instead of "dioxygen" is used.

With the advent of nanotechnology various new materials such as carbon-based nanomaterials, metal and metal oxide nanoparticles, have emerged. The uniqueness of nanomaterials when applied for electrodes modification is based on their remarkable surface properties. Their surface to volume ratio increases with their size decrease.

Such outcome leads to a well developed surface area and significant amelioration of sensitivity, electrical conductivity, and selectivity of the electrode modified with such materials. Additionally, used nanomaterials and biomolecules are of similar dimensions enabling nanomaterials to operate as an electrical wire, between the electrode surface and protein's active center. Therefore, the combination of "nano" with "bio" has opened a wide window for development of innovative electrodes with possible application in electrochemical biosensors and biofuel cells.

The present dissertation focuses on electrodes modified with carbon nanoparticles (CNPs) and various enzymes. It presents diverse approaches for depositing carbon nanoparticles at the electrode surface and studies of their electrochemical behaviour in the absence and presence of adsorbed biomolecules.

3.   Carbon-based nanomaterials in electroanalysis

As other natural sciences, electrochemistry has been vastly enriched by the recent developments in the field of nanotechnology. Nanotechnology's kingpin is the development of novel nanomaterials. These, no larger than 100 nm, one or more dimensional, materials of unique physical and chemical properties, find various applications in fields from chemistry, physics, engineering and computer science to medicine. Among such materials one can find those comprised of e.g. metal and metal oxides nanoparticles, quantum dots or various carbon-based structures. The later group draw special attention from electrochemists, owing to their remarkable electrochemical properties (e.g. superb electrical conductivity and high surface area), and their ability for being utilized as an element for modification of electrodes. This in turn has already led to the generation of new sensors, and devices for energy storage and conversion.

The carbon nanoparticles are the main material that was utilized for the modification of the electrodes in this thesis. Owing to that, special attention has been paid to other related carbon-based nanomaterials (carbon nanotubes, graphene, and carbon nanoparticles) in this chapter. They have been described in terms of their

4

properties and impact on the electrochemical behaviour of the electrodes modified with them and the potential electroanalytical applications.

3.1. Carbon nanotubes

The first report on the material called later carbon nanotubes (CNTs) came from Radushkevich and Lukyauovich in 1952 [9]. However in 1991 it was carefully studied by Sumio Iijima [10]. Since that time these materials have held the attention of a wide scientific audience.

CNTs are one dimensional well-ordered, hollow graphitic nanostructures made of sp^2-hybridized carbon atoms. Structurally, they are divided into two classes: multi-walled carbon nanotubes (MWCNTs) and single-walled carbon nanotubes (SWCNTs). MWCNT is composed of several concentric tubes of graphite sharing a common longitudinal axis whereas SWCNTs are a single layer of graphene rolled into a tube. Typically, the length of CNTs can range from several hundred nanometers to several millimeters while diameters are 0.4 - 2 nm and 2 - 100 nm for SWCNTs and MWCNTs, respectively [11]. The CNTs behave either like a metal (SWCNTs, MWCNTs) or a semiconductor (SWCNTs). The electrical conductivity of SWCNTs depends on their chirality and diameter while for MWCNTs such dependence is not observed. The unique properties of CNTs such as superb strength, stiffness, chemical and thermal stability, electrical conductivity, high surface area of 1600 m^2 g^{-1} (SWCNTs), and the presence of a hollow core suitable for storing guest molecules, have revolutionized various fields such as electronics and medicine [12]. CNTs are also applicable in various energy storage devices (supercapacitors, fuel cells, and accumulators), transistors, photovoltaic devices, sensors and biosensors [12-15].

There are numerous ways of preparation of CNTs modified electrodes for example through chemical vapour deposition (CVD) [16], laser evaporation [17] or arc discharge [18]. The CNTs owing to following advantages: small size with large surface area, high sensitivity to target analyte, fast response time in analyte detection, and diminishing surface fouling effects have found wide application in the electrochemical sensing [19].

The CNTs thin film modified electrodes can be prepared through depositing the CNTs at the electrode's surface via CVD [16], electrodeposition [20], electrophoretic deposition [21], drop coating of CNTs solution suspension on the electrode surface

5

followed by evaporating of the solvent [22, 23], abrasion [24] or the layer-by-layer (LbL) assembly method [25]. The CNTs modified electrode can be also obtained through e.g.: mixing CNTs with carbon paste [26] or embedding with a polymer [27] or sol-gel silicate matrix [28]. These immobilizing techniques were found to form a random tangle of CNTs at the electrode surface. However such an arrangement might hinder the electron transfer. In order to improve the electrical contact between the sensing element and the physical transducer and avoid any impurities originating from solvents or binders vertically aligned CNTs forests are also applied as an electrode. However, so far the most attractive presented design of CNTs electrode is the utilization of the unique properties of a single CNT as a nanoelectrode [13, 29].

CNTs gain considerable attention in modified electrodes area, because of enhancement of their electrochemical sensing performance through their functionalisation by covalent bonding or non-covalent attachment of various objects (e.g conducting polymer, metal nanoparticles, ionic liquids (IL) or graphene Fig. 3.1) to the CNTs sidewalls [25, 30]. Even the impurities that may remain after synthesis, such as metallic compounds or nanoparticles, have an great impact on their electrocatalytic activity [31].
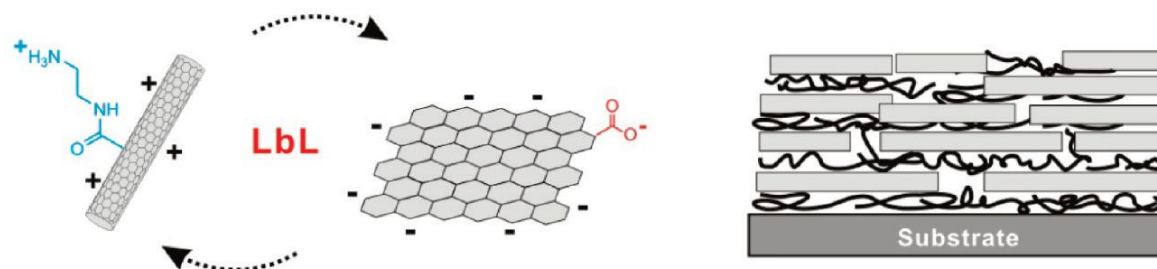
Fig. 3.1 A schematic representation of hybrid LbL multilayer of functionalized MWCNTs and graphene oxide [25].

The first CNTs-modified electrode was constructed 15 years ago. Britto *et al.* used MWCNTs mixed with bromoform as a binder and packed them into a glass capillary to study the electrochemical oxidation of dopamine (DA) [32]. The MWCNTs-modified electrode exhibited significant improvement in the oxidation of DA that occurred at a low potential with a higher rate of heterogeneous electron transfer rate constant, compared with other carbon electrodes [32]. Since that time CNTs-based electrochemical sensors became a 'hot' topic in electroanalysis.

6

One can find an enormous amount of analytes which have been studied using CNTs modified electrodes such as NADH [22], hydrogen peroxide [33], hormones [34], uric and ascorbic acid, neurotransmitters [35], amino acids [36], epinephrine [24], anesthetics [37], heavy metals ions [38], explosive substances [39]. For example Salimi *et al.* reported the development of an epinephrine electrochemical sensor based on MWCNTs attached to basal plane pyrolytic graphite electrodes via abrasion [24]. Electrochemical measurements showed that the MWCNTs modified electrode provides excellent matrices for the amperometric detection of epinephrine in the presence of the common interferences such as ascorbic acid (AA), and that the optimized electrochemical sensor exhibited long linearity, high stability and very good reproducibility for the detection of epinephrine [24]. The application of CNTs modified electrodes enhances the sensitivity for NADH [22] and hydrogen peroxide [33], due to their high electrical conductivity that promotes the electron-transfer reaction, which is attributed to the presence of edge plane defects at their end caps. Wang *et al.* demonstrated that electrodes modified with SWCNTs and MWCNTs significantly decreased the overpotential for NADH oxidation and diminished NADH surface fouling effects during amperometric sensing [22]. As one can see in the Fig. 3.2 the oxidation peak of NADH at the bare glassy carbon electrode at +0.82 V (Fig. 3.2A) is shifted to more negative values for MWCNTs and SWCNTs modified electrodes (Fig. 3.2B,C). The peak currents are 1.6 and 2.3-fold higher than the one obtained at the bare electrode [22]. Good catalytic ability towards the oxidation of NADH at the CNTs was also demonstrated by Dong's group [40]. The authors observed remarkable catalytic oxidation current at the multilayer CNTs/thionine film modified ITO electrode occurring at ca. 0.0 V. That is more negative than that of the bare ITO electrode (ca. 0.6 V) [40] and graphene [22, 41] CNPs [42] or CCE [43] based biosensors. The obtained results are promising for the development of numerous oxidase and dehydrogenase based amperomatric biosensors.

7
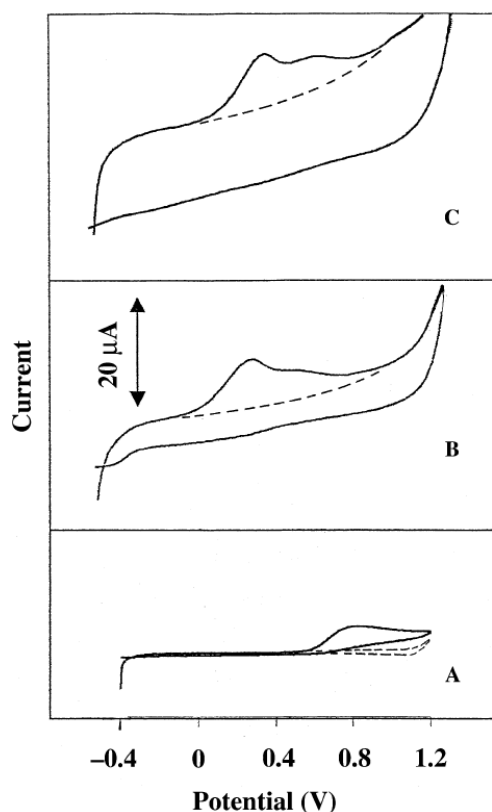
Fig. 3.2 Cyclic voltammograms for NADH oxidation obtained at unmodified (A), MWCNTs-modified (B), SWCNTs-modified (C) glassy carbon electrodes (solid lines), and background respone (dotted lines) [22].

The usage of the CNTs/metal composites for the construction of efficient ultratrace heavy metals ions electrochemical sensors has become a popular. Xu *et al.* proposed such a sensor based on MWCNTs and bismuth film electrode [38]. The MWCNTs were dispersed in Nafion solution and drop-coated onto GCE, after drying on the premodified electrode the bismuth film was electrodeposited (MWCNTs-Nafion/Bi). The obtained composite combines properties of its individual components such as higher electrical conductivity, well developed electroactive area, strong absorptive ability of CNTs, and heavy metal ions detection sensitivity, with a synergistic effect [38]. Differential pulse anodic stripping voltammetry shows, that MWCNTs-Nafion/Bi is a sensing platform to detect lead and cadmium ions with good sensitivity (25 ng L^{-1} for Pb^{2+} and 40 ng L^{-1} for Cd^{2+}), stability and reproducibility [38], and are comaparable with Nafion/graphene coated bismuth film electrodes [44].

8

With the advent of nanotechnology and microfabrication, the requirements given to nanomaterials are higher. In that context the main drawback of CNTs is the difficulty to assemble them in a controllable manner and obtain complex sensors or other devices, due to undesired effects of their high aspect-ratio. In contrast, graphene, a relatively new material, is highly amenable to microfabrication, which makes it more applicable for the development of such devices [13].

3.2. Graphene

In 2004 the Geim group separeted a new form of carbon named graphene (GN) sheets [45]. It is built of a set of two-dimensional sheets of sp^2 hybridized carbon atoms [45]. Due to its unique properties such as a very large surface area of 2630 m^2 g^{-1}, excellent thermal and electrical conductivity [46], high mobility of the charge carriers (200 000 cm^2 V^{-1} s^{-1}), high mechanical strength and elasticity, it attracted wide scientific interest [47-49]. Its potential applications might be in bioscience, developing electronics, sensors, energy storage and conversion devices. Some scientists declared that it might be even viewed as a substitute for silicon in electronics [13, 50].

Geim *et al.* obtained GN by the so called scotch-type method but it is not a technique for well-controlled synthesis, and processing [45]. Therefore other procedures for obtaining graphene have been developed [48]. Currently its synthesis might occur via CVD [51], substrate-free gas-phase synthesis [52], arc discharge [53], chemical reduction of graphite oxide [54], direct synthesis of graphene from graphite or its derivatives [55], electrochemical synthesis [56], epitaxial growth of graphene on silicon carbide [57] or unzipping carbon nanotube into graphene nanoribbon [58].

Owing to its unusual properties, GN serves as an excellent electrode material by allowing to develop electrodes with high electronic conductivity, wide electrochemical potential window, fast kinetics for a number of mediators, and opens new avenues for various modifications of the surface of the electrode. Thus it has found wide application in electroanalysis, mainly as base component of thin films used for electrode modification [49, 50, 59].

Graphene modified electrodes can be obtained through depositing the graphene sheets at the electrode's surface via CVD [51], spray-coating [60], vacuum filtration [61] or electrophoretic deposition [62]. Also such techniques like LbL [63], Langmuir–

9

Schaefer [64] and Langmuir–Blodgett [65], electrostatic attraction [66] and noble-metal-promoted macroassembly [67] are utilized for preparation of graphene based electrodes. Furthermore, in order to enhance GN properties and applicability there were attempts to synthesize high-quality GN-inorganic nanomaterials hybrids via incorporation of such materials as metal nanoparticles [68], metal oxides [69], ionic liquids [70-72], quantum dots [73] and carbon nanotubes [25].

Graphene in contrast to currently, commercially available carbon nanotubes, does not contain any impurities hence it offers more reproducible sensing response [13, 49]. GN-based electrochemical sensors also exhibit extremely low detection limits compared with SWCNTs-based ones due to its noise levels being one to two orders of magnitude smaller [13].

Recent studies have focused on developing amperometric GN based electrochemical sensors for detecting a wide range of chemical compounds such as DA in the presence of ascorbic acid and uric acid (UA) [41, 74], acetaminophen [41], free bases of DNA [41], hydrogen peroxide [41], NADH [41], heavy metal ions [44, 75], chlorpromazine [76], and explosive substances [72].

An interesting GN based electrochemical sensor for detecting hydrogen peroxide has been proposed by Zhou *et al.* [41]. As one can see on Fig. 3.3, the obtained GN-modified GCE, compared with a graphite modified one and a bare electrode, shows an increased electron transfer rate. Such a sensor compared with SWCNTs-based one exhibits a wider detection range, better selectivity and sensitivity (Fig. 3.3) [41].
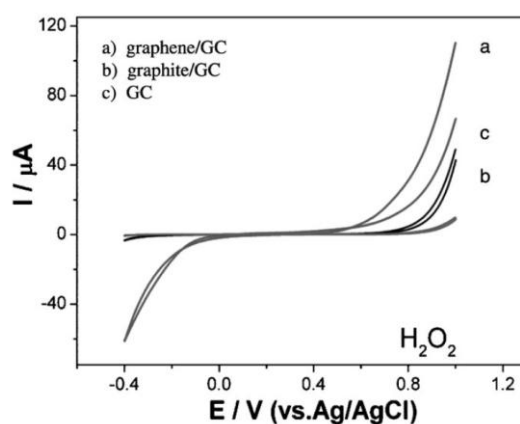
Fig. 3.3 CVs obtained in the presence of H_2O_2 obtained at graphene (a) graphite (b) and bare glassy carbon electrode (c) [41].

10

Shang *et al.* showed that GN-based electrodes also can be applied as electrochemical sensors for simultaneous determination of DA, ascorbic and uric acid. The voltammetric peaks were well-resolved and shifted to a lower potential in comparison with a bare electrode (Fig. 3.4A,B). That indicates fast heterogeneous electron transfer (HET) in graphene based materials [74].

(A) **(B)**
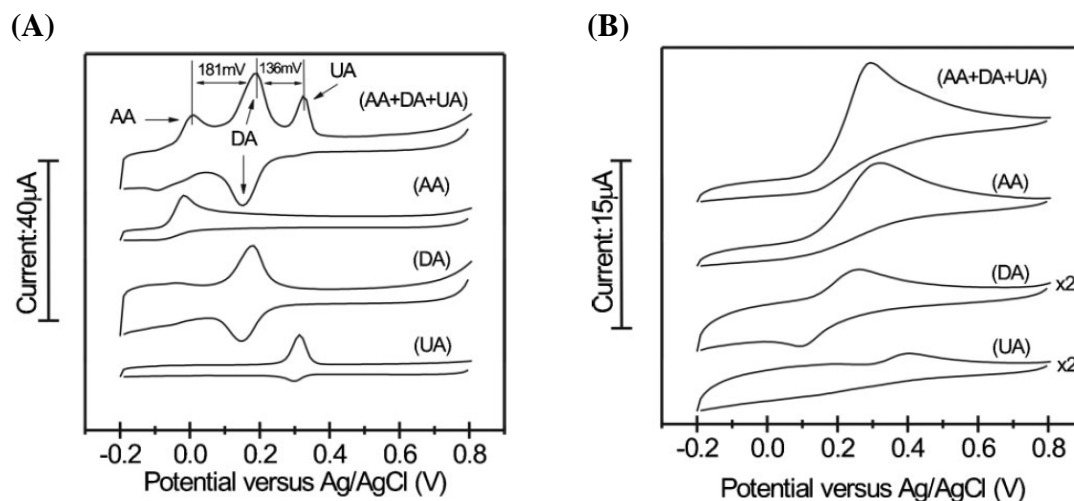
Fig. 3.4 CVs obtained at multilayer graphene nanoflakes films on Si substrate(A) and bare GCE electrodes (B), in the presence of ascorbic acid, dopamine,and uric acid [74].

The range of potential electroanalytical applications of GN based electrodes is still increasing. For example a new electrochemical sensor for detecting ultratraces of trinitrotoluene was constructed. The authors obtained an IL–graphene paste electrode, by combining an IL and a three-dimensional (3D) graphene material with large surface area and well defined mesopores [72]. Such an electrode provides a larger electroactive surface area and lower charge transfer resistance compared to IL–CNTs and IL–graphite paste electrodes. It exhibits high sensitivity for detecting trinitrotoluene, low detection limit and reproducibility that is superior to that demonstrated by the IL–CNTs and IL–graphite paste electrodes [72]. Recently, GN materials and noble metals nanoparticles are being utilized for the formation of heterojunction. Its interface might be a promising platform for Surface Enhanced Raman Scattering-sensors and catalysis [77].

The number of applications of GN is skyrocketing, therefore the technique of its synthesis - capable of producing high-quality GNs on a large scale and in a low-cost manner - should be drawn up. For example the Institute of Electronic Materials

11

Technology in Warsaw is one of the world leading institutions that specialize in synthesis of GN.

Even though the GN materials exhibit outstanding properties it should be taken into account that not all reports are so optimistic [78, 79]. Pumera *et al.* showed that contrary to the widely accepted opinion, it is not always beneficial to exfoliate graphitic structures to single-layer graphene to achieve maximum electrochemical performance [78]. This can be seen as a special case of more general phenomenon that the actually exhibited properties of GNs materials depend highly on the procedure of synthesis of such material, e.g. whether it is obtained in the form of several tens of stacked graphene sheets or only a few layers. They demonstrated that multilayered structures provide higher capacitance than the single-layer sheets due to better availability of the graphene sheets' edges [78]. Also the use of graphene oxide, as electrochemical detector in microfluidics devices for neurotransmitters or nitroaromatic explosives separation, is of no advantage in terms of sensitivity or selectivity over that of graphite microparticles based detectors [79].

Summarising at the moment there is no clear advantage of graphene as compared to CNTs in electrochemical sensing [13].

3.3.   Carbon nanoparticles

In addition to the newly applied materials as CNTs or GNs many nanoparticulate forms of carbon are well-established electrode materials. Quite recently hydrophilic carbon nanoparticles with phenyl sulfonic acid functionalities were introduced as one of them. This material is commercially available from Cabot Corporation (Emeror 2000) and its production is based on diazonium chemistry [80] or controlled vapour-phase pyrolysis of hydrocarbons [81]. Unlike the carbon nanotubes or graphene, it has been known for many years and hence it is widely used in industry, for example as a filler or a pigment. It offers most of the advantages of nanocarbons like extremely high surface area, high level of interfacial edge sites, reactive surface sites and good electrical conductivity. Furthermore, in contrast to other nanocarbon materials, their phenylsulfonate functionalities (negative charge) have a great impact on its hydrophilicity. Therefore, they are used for electrode surface modification.

Phenylsulfonated carbon nanoparticles deposition at the electrode has been achieved for example by encapsulation in polymer [82], using electrostatic interactions

12

with polyelectrolytes [83-85] or with positively charged objects (gold nanoparticles [86] and functionalized silicate submicrometer particles [87, 88]), sol-gel processed silicate film [89], or just by drop-coating the CNPs suspension on the electrode surface [90, 91]. These electrodes were mainly developed by Marken's group. For example these authors assembled thin chitosan-carbon nanoparticle films onto ITO electrodes in a layer-by-layer deposition process. In such a system chitosan, as a cationic polyelectrolyte, provides binding sites for immobilization of redox systems via physisorption of dianionic indigo carmine or chemisorption of 2-methyleneanthraquinone. The authors investigated the binding effect of these redox systems and the stability of voltammetric responses as a function of pH [84]. As is presented at Fig. 3.5A the voltammetric response of, for instance, indigo carmine adsorbed on the modified electrode is increasing with the amount of the chitosan-carbon nanoparticles layers deposited on the electrode surface and the chitosan's concentration during the deposition Fig. 3.5B. The authors also suggest that such modification may help in developing new, fast and sensitive sensor electrodes [84].
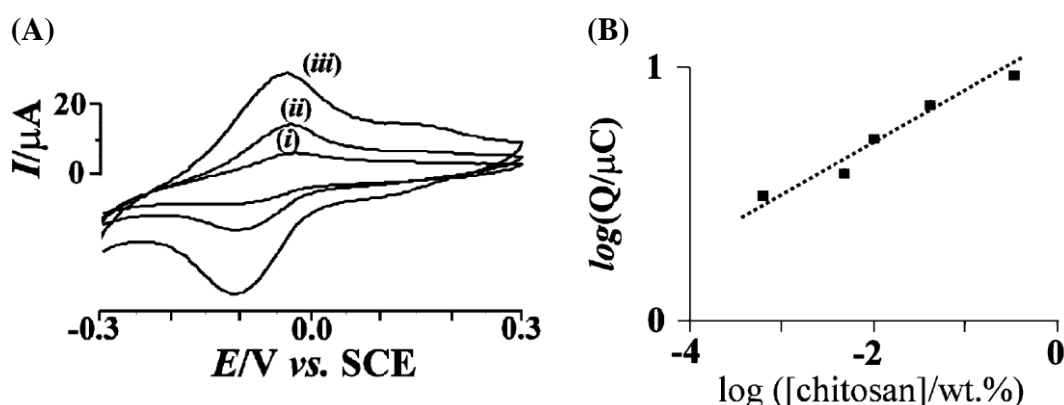
Fig. 3.5 (A) CVs for the reduction and re-oxidation of indigo carmine adsorbed into a (i) 2-layer, (ii) 5-layer and (iii) 10-layer chitosan-CNP film electrode (B) Dependence of the charge under the peak current on the deposition concentration of chitosan during the LbL coating, obtained at the 10-layer chitosan-CNP with adsorbed indigo carmine [84] .

Recently, a similar avenue for electrode modification with CNPs by applying the LbL technique was presented by the Opallo group [86-88]. Two types of three dimensional CNPs film electrodes were prepared from oppositely charged particles. As

13

a positively charged material and linker, gold conductive particles [86] and functionalized silicate submicroparticles [87, 88] were applied. The voltammetric responses from measurements of the capacitive current show that surface of the modified electrodes, is well developed and electrochemically active. Even for nonconductive silicate submicroparticles the good electrical contact is assured due to the formation of percolation paths across the films (Fig. 3.6A) [88]. The effect of surface development was also confirmed for the AuNP-CNPs electrode. The results from voltammetric experiments show that the catalytic current of oxygen reduction in acidic solution is increasing with the amount of AuNPs deposited on the electrode surface [86]. Similar electrodes were also prepared for the research described in this thesis.

The first electroanalytical application of CNPs' was reported by Zimer *et al.* [82]. The authors modified ITO electrodes with a polyaniline-template carbon nanoparticle mixture via drop coating. The new electrode exhibited excellent chemical and physical stability. The anodic stripping voltammetry measurements revealed that such nanocomposite based electrodes can be applied as an electrochemical sensor for detecting heavy metals ions such as lead and copper at very low concentrations [82].

One can find applications of CNPs based electrodes for sensing of biologically important substances: simultaneously acetaminophen and tramadol [90], naltrexone [91], azathioprine [92], piroxicam [93], dopamine in the presence of ascorbate [83, 88], and benzophenone or triclosan [94]. Some of these electrodes were employed for the immobilization of redox probes [83-85, 95] or catalysts [96].

The carbon nanoparticles were also utilizied as surface-active nanomaterials for designing liquid | liquid interfaces or modification of sensor electrode surfaces in particular for electroanalytical applications [97]. For example Marken *et al.* used that material for stabilizing the liquid | liquid interfaces allowing emulsion microdroplets of organic liquids to be deposited onto ITO electrode surfaces. The applied CNPs formed conducting pathways for electrons at the nanoparticle surface which resulted in effective catalysis of simultaneously electron transfer and ion transfer at triple phase boundary [97].

Also the CNPs have successfully been used for the construction of electrochemical sensors for neurotransmitters [83, 88]. Celebanska *et al.* applied CNPs-

14

silicate submicroparticles modified electrode as a selective, sensitive and stable amperometric sensor for dopamine detection in the presence of interferences (AA, UA) [88]. From differential pulse voltammetry experiments (Fig. 3.6B) it is clearly visible that the DA peak current is proportional to the dopamine concentration [88]. Also Marken *et al.* presented the application of CNPs based electrodes for detecting DA. The obtained detection limit at their electrode is slightly lower than that of the above described electrode [83].

(A)   **(B)**
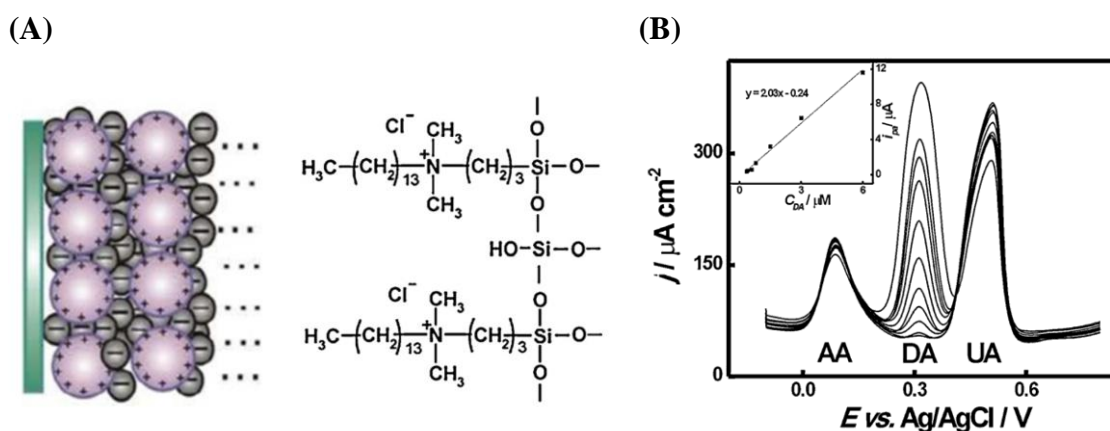
Fig. 3.6 (A) Idealized scheme of the film prepared form silicate submicroparticles and carbon nanoparticles with positively and negatively charged functionalities and a scheme of the structure of silicate with tetradecyldimethylammonium functionalities. (B) Differential pulse voltammograms obtained with TDA these electrodes in the presance of ascorbic acid, uric acid, and various concentrations of dopamine [88].

For further application of those CNPs in electroanalysis two attempts have already been made to replace the phenyl sulfonic acid functionalities with other groups [98, 99]. The authors employed negatively charged material as a precursor to obtain positively charged one but identical in size [98] and then used the resulting one to covalently attach the anthraquinone functional groups [99]. As one can see at Fig. 3.7 the conversion was carried out via sulfonylchloride formation followed by reaction with amines to give sulphonamides with single or multiple positive charges [98].

15
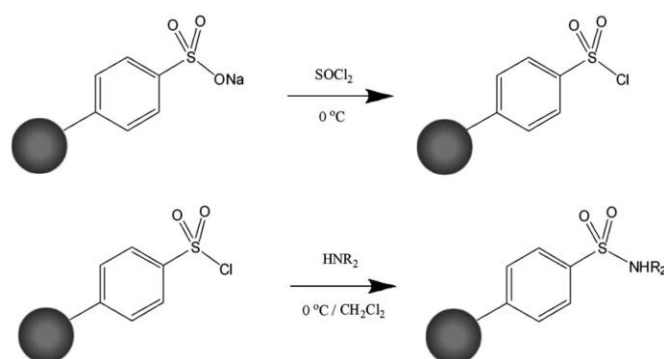
Fig. 3.7 Schematic illustration of preparation of positively charged carbon nanoparticles from sulfonated ones [98].

The obtained nanoparticles were characterized by Raman spectroscopy AFM, XPS, and voltammetric methods. They form a stable thin film on glassy carbon electrodes. Such electrodes after dipping into solutions of the anionic redox probe indigo carmine then rinsed with distilled water and placed into fresh electrolyte, shows a well defined reversible peaks corresponding to the electrochemical redox reaction. That confirms irreversible redox probe adsorption on the surface of the modified electrode and additionally allows characterization of the surface properties as a function of pH [98].

The phenylsulfonated and ammonium functionalized carbon nanoparticles will be also employed in the present study as a material for electrode modification.

3.4. Carbon ceramic electrode

Carbon ceramic electrodes (CCE) are specific combinations of carbon particles and a silicate matrix. These electrodes were introduced by Lev and co-workers in 1994 [100]. They are prepared by mixing carbon black or graphite powder with the sol-gel precursor and solvent. A porous and rigid carbon composite material is formed after the sol-gel process, aging and drying (usually lasting ca. 24 hours).

The utilized sol-gel process for the CCE preparation involves few steps: hydrolysis under acidic or basic conditions, followed by condensation and polycondesation of organometallic compounds (usually, silicon alkoxide). After the hydrolysis of the silicon alkoxide, silanol groups are formed, which in further steps are transformed into silanol and siloxanes groups, as shown in Eqs. 3.1-3.2, and then

16

undergo gelation, aging and drying processes, resulting in the porous silicate matrix formation [101].

$$(RO)_3SiR' + 3\ H_2O\ \rightarrow\ (HO)_3SiR' + 3ROH \tag{3.1}$$

$$2(HO)_3SiR' \rightarrow\ (HO)_2SiR'\text{-}O\text{-}SiR'(OR)_2 + 2H_2O \tag{3.2}$$
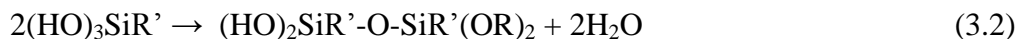
The sol-gel process is a powerful technique that enables the formation of silicate matrices with controlled structure, morphology, composition or porosity. Also the wettability of that material can be tailored by selecting proper alkoxide precursors. For example hydrophilic matrices can be obtained with tetramethoxysilane (TMOS) or tetraethoxysilane, whereas the utilization of methyltrimethoxysilane (MTMOS) ensures its hydrophobicity.

The carbon particles immobilized within the silicate matrix are interconnected forming efficient electron percolation pathways [100]. The size and the fraction of the utilized carbon grains have a significant impact on the electrical properties of such CCE. As one can see from Fig. 3.8 the conductivity percolation threshold varies from a few weight percent for carbon black to ca. 30% for large carbon particles [102].
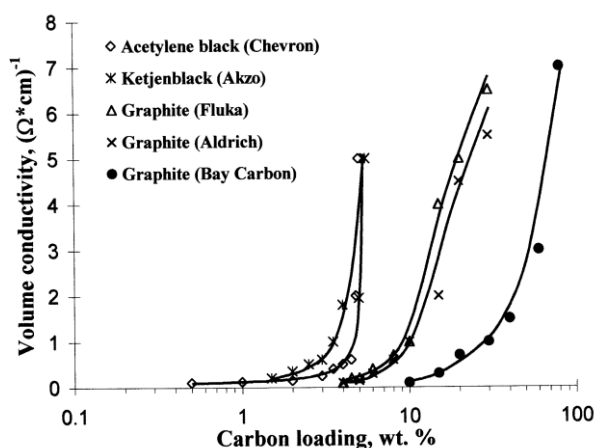
Fig. 3.8 Dependence of the specific conductivity of CCEs on carbon loading for different carbon materials [102].

The physicochemical properties of the CCE can also be easily manipulated by e.g. covalent modification of the carbon (micro)particles, or by changing the silicate matrix properties via application of suitable precursors or sol-gel dopants [102].

17

The CCE due to their outstanding properties such as renewable surface, high porosity, conductivity and stability, fast kinetics for mediators, wide operational potential window, and high signal to background current ratio, are applied as substrates for electrochemical sensors construction or energy conversion and storage devices [102]. The CCE have already been applied as an electrochemical sensors for detecting such analytes like e.g.: acetaminophenol [103], adrenaline [104], ascorbic acid [103], bromate [105], cysteine, dopamine, glucose [106], glutathione [107], hydrazine [108], hydrogen peroxide [109], NADH [43], pH [110], phenolic compounds [111], silver [112] and uric acid [103, 104].

An interesting avenue for the fabrication of an enzymeless CCE biosensor for detecting glucose in the presence of interferences was proposed by Salimi *et al.* [106]. In order to obtain a highly sensitive electrode exhibiting long-term stability, the authors used a sol-gel technique to prepare a uniform film consisting of nickel and Nafion in a graphite composite lattice. The graphite particles provide efficient percolation conductivity through the interconnected carbon grains whereas the introduction of a selective catalyst such as nickel the effect of avoids interferences. The Nafion membrane eliminates the interferences but also prevents electrode fouling. The electrochemical measurements show that the modified electrode displayes excellent reproducibly, high stability, fast response and activity for the determination of glucose in buffer as well as in human serum samples [106].

Another electrochemical CCE sensor presented by Salimi's group was employed for hydrazine determination [108]. In order to obtain a sensitive sensor the authors proposed an easy and fast method for adsorbing chlorogenic acid, the mediator that catalyzes the electrooxidation of hydrazine on the CCE surface. The adsorbed chlorogenic acid is electroactive, very stable and its properties depend on pH, as anticipated for quinone/hydroquinone functionalities. It was presented that the modified electrode shows high catalytic activity towards hydrazine electrooxidation at wide a pH range. The optimized amperometric sensor with the aid of mediator exhibited good performance for hydrazine sensing with a rapid response (1 s), wide linear range (0.1 μM - 1.0 mM), low detection limits (0.02 μM with a signal-to noise ratio of 3), high stability and reproducibility [108]. The obtained results are comparable to hydrazine sensors based on CNT [23] composite electrodes.

18

Nogala *et al.* were successful in attaching laccase mediators, 2,2'-azinobis(3-ethylbenzothiazoline-6-sulphonate) ($ABTS^{2-}$) and syringaldazine (Syr), to CCE surfaces (Fig. 3.9) [113, 114]. The authors applied a simple procedure for stable and non covalent immobilization of mediators by confining them within the hydrophobic porous silicate-carbon heterogenous structure of CCE. The electrochemical measurements revealed that the obtained mediator modified carbon ceramic electrodes exhibit stable voltammetry corresponding to a surface confined oxidation-reduction process and after enzyme immobilization the electrodes show electrocatalytic activity towards the oxygen reduction reaction (ORR) [113, 114].

(A) **(B)**
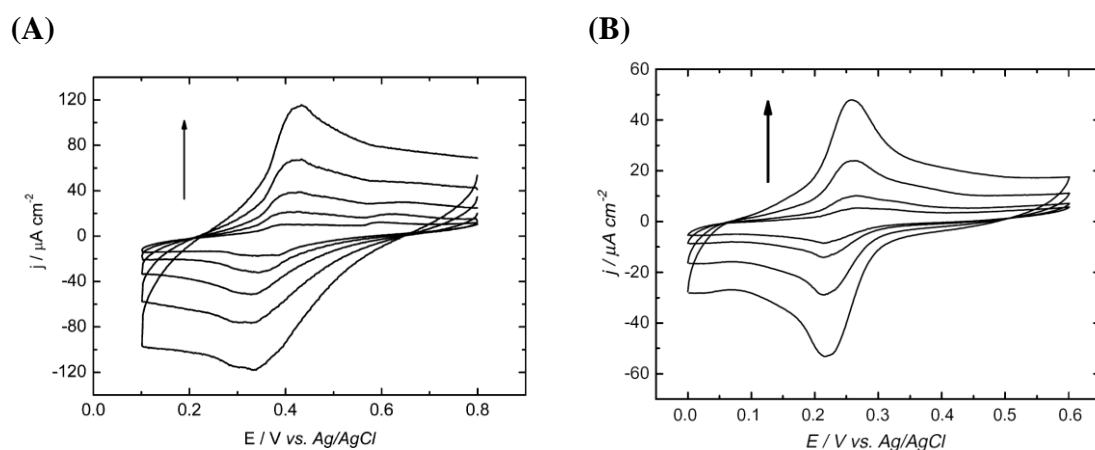
Fig. 3.9 CVs of $TMOS_{gel}$ coated (A) ABTS and (B) syringaldazine modified CCE immersed in O_2-saturated phosphate buffer at various scan rates. Arrow indicates increasing scan rate [113, 114].

19

4. Bioelectrocatalysis with redox enzymes

Redox enzymes owing to their unique ability to efficiently catalyze electrode reactions are being widely applied as key elements of modified electrodes. At the beginning studies in this area were difficult, and did not bring any successful results due to enzymes' sensitivity to various factors such as temperature or pH, changes of which can diminish enzymes' biological activity or even denature them [115]. Thus the biggest obstacle to successful utilization of the enzymes was ensuring electrical contact of the enzymes with the electrode, and concurrently their protection from the denaturization. Both of these are nowadays achieved mostly by immobilization of the enzyme on the electrode surface.

The first successful immobilization, reported in the 1950s, was achieved for α-amylase on activated carbon and other carbon based materials via the adsorption methode. However, real progress in bio-immobilization happened in the second half of the sixties [116]. From that time the enzyme immobilization has become the core aspect of the studies of enzyme modified electrodes, and thus is also in the center of this thesis.

Since electrodes based on redox proteins (bilirubin oxidase (BOx), glucose oxidase (GOx), myoglobin (Mb) or laccase (Lc)) were constructed as part of this PhD thesis the chapter is focused on those biomolecules.

4.1. Enzyme immobilization

The development of efficient procedures of enzyme immobilization at the electrode has made a breakthrough in bioelectrochemistry allowing the construction of new classes of biosensing devices [117-122]. In order to prolong the enzyme's activity and stability other attempts have also been made such as modification of the enzyme's functional groups or protein engineering by changing of the amino acid sequence [123]. These immobilization procedures can be utilized effectively only if they assure: high surface concentration, activity and stability of the enzyme, good access to the enzyme's active center for the substrate and fast response time [116]. Achieving all of the above has proved to be a challenging task; therefore one can find in the literature various approaches that attempt to fulfill them. Generally, the immobilization methods can be

20

classified into three sub-groups, based on the utilized entrapment process: physical adsorption, covalent bonding and encapsulation [124].

- **Physical adsorption** – methods based on this tends to be the easiest and so far most often used. They exploit attractive forces between the proteins and a conductive substrate. In these techniques biocatalysts can be immobilized to the surface of a bare electrode or one modified for example with carbon nanomaterials, through hydrophobic or ionic interactions, van der Waals forces or the formation of hydrogen bonds. Such a modification preserves the native structure of the enzyme. Nevertheless, the main drawback of that technique is the continuous leaching out of the adsorbed protein from the support. This harmful desorption process can be triggered through changes in temperature, pH, and ionic strength. If these parameters are controlled one could avoid leaching problems and effectively stabilize the proteins.

- **Covalent bonding** – in this approach a covalent bond is formed between the functional groups present on the protein's surface and a carrier such as a membrane, polymer, or directly between the enzyme molecules. The diversity of the bonds between proteins and different functional groups on the support is myriad. Some of them have been depicted in Fig. 4.1. Even though the covalent bonding might unfavorably alter the biomolecule's conformational structure, the enzyme immobilized in that way often exhibit better stability, sensitivity and activity comparing to physical adsorption.

21
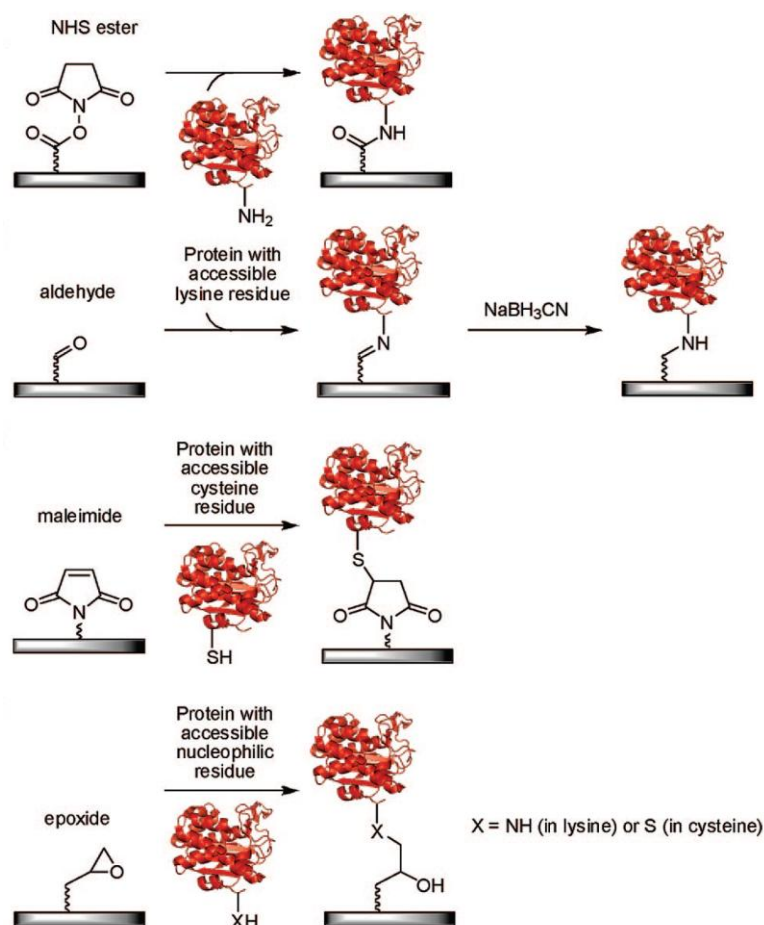
Fig. 4.1 Some surface modification methods for covalent immobilization of proteins [125]

Covalent bonding can be brought about by cross-linking, which enables enzyme entrapment, via the creation of bonds between enzymes' active groups causing the ezymes to form 3D aggregates. The most often applied cross-linkers are a bi- or multifunctional reagents, such as carbodiimide or glutaraldehyde. Covalent bonding and cross-linking are generally applied to attach enzymes on self-assembled monolayers.

For example Pellissier *et al.* covalently immobilized a GOx layer on glassy carbon electrodes, functionalized through electrochemical reduction of *in situ* generated aryldiazonium salts bearing carboxylic acid groups [126]. The authors demonstrated that such modification has a considerable effect on the electrodes' stability. Even after 6 weeks the immobilized enzyme maintained much of its intial catalytic activity [126].

22

- **Encapsulation** – the variety of new materials have given researchers the opportunity for the development of new, advanced matrices for enzyme encapsulation where proteins are stable and their selectivity might be improved. The enzymes can be encapsulated in materials like: liposome, polymer or polyelectrolytes matrices, sol- or hydro-gels, and cubic phases. This method improve the protein's stability with minimal unfolding of the enzyme. Additionally, the mismatch between protein and pore size prevents the protein from leaking out of the electrode surface.

The application of the sol-gel process for enzyme immobilization has been known from over half a century [127]. However, the real breakthrough came in the 1990s when Avnir reported that enzymes like alkaline aspartase and alkaline phosphatase after entrapping within a silica matrix retained their catalytic activity longer [128]. The sol-gel materials are biocompatible and have numerous pores and channels within their framework. Owing to such structure the mass transfer through silicate materials is more efficient than in other materials not exhibiting these features. The size of the majority of the pores is sufficiently small to entrap enzymes effectively. One can 'tailor' silicate matrices' physicochemical properties by careful selection of e.g. the metal alkoxide precursor, catalyst and its concentration, solvent or ambient conditions (temperature and humidity). An interesting example of such phenomenon was presented by Avnir and Frenkel-Mullerad [129]. The authors demonstrated that one can actually "deceive" the immobilized enzyme to operate in a pH in which it is not active by coentrapping it with the proper surfactant within the silicate matrix (Fig. 4.2) [129].

23
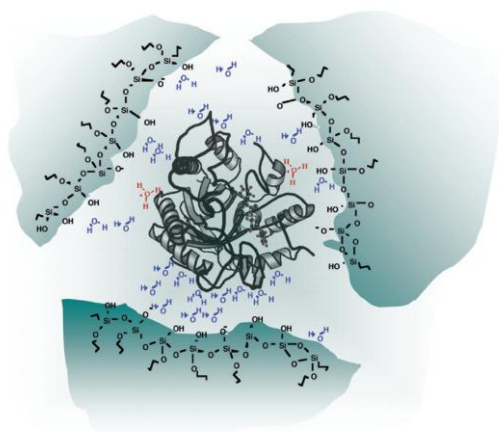
Fig. 4.2 A schematic presentation of enzyme coentrapped with cationic surfactant within silicate matrix [129].

The sol-gel method enables the formation of thin films on electrode surface by catalyst electrogeneration [130]. They can be deposited at the electrode surface via electrodeposition and dip-, spray or spin-coating methods. For example Xia's group presented a one-step and alcohol-free method to entrap horseradish peroxidase (HRP) in a silicate matrix [131]. The authors used, as a precursory solution, a mixture of a buffer solution of HRP and solution of ammonium hexafluorosilicate $((NH_4)_2SiF_6)$. After applying a negative potential to a working electrode the reduction of water occurs. The evolved hydrogen bubbles serve as a dynamic template that takes part in the formation of a porous silica matrix, catalyzed by the generated hydroxyl ions (Fig. 4.3). The obtained silica matrix is porous, uniform and enables free mass transport, in that way providing a biocompatiable environment [131].
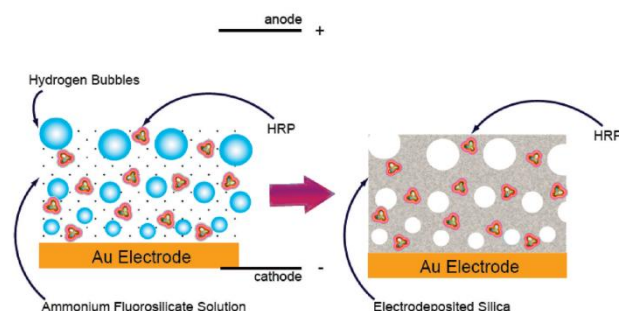
Fig. 4.3 A schematic illustration of HRP immobiliztion within electrodeposited porous silica matrix [131].

24

As mentioned above, the main drawback in the attachment of enzyme via physical adsorption is its poor stability caused by leakage of the enzyme from the electrode surface. To overcome that problem the LbL assembling method was developed to stabilize biomolecule within the polyelectrolyte. This method was pioneered by Ilner [132] and rediscovered by Decher and Hong [133]. It is a powerful technique for fabricating protein multilayer thin films of controlled architecture and composition [134]. The most conventional LbL approach is based on alternative adsorption of oppositely charged species from their solutions through electrostatic interactions [133, 135]. The proteins immobilized in these films retain their native structure and electraocatalytic activity.

As was demonstrated by Tachikawa's group glucose oxidase can be immobilized between negatively charged SWCNTs only if it is deposited from the solution whose pH value is lower than the enzyme's iso-electric point [136]. Under conditions the GOx is positively charged, and stabilized through electrostatic interaction with the SWCNTs within the multilayer film. Electrochemical measurements show that entrapped GOx exhibits direct electron transfer of the FAD/FADH$_2$ redox cofactor and electrocatalytic response towards glucose oxidation (Fig. 4.4). The redox peak currents of GOx increased linearly with the number of deposited enzymatic layers indicating that the LbL assamble technique enables effective GOx immobilization maintaining 85% of its initial biological activity after a month [136].
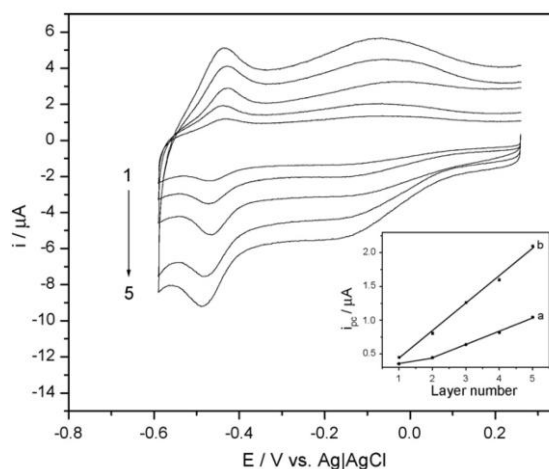
Fig. 4.4 CVs of the GOx immobilized within SWCNTs (1-5 layers) via LbL method on the electrode. The insert presents the relationship between cathodic currents and the number of layers (a) cathodic peak near -0.14 V; (b) cathodic peak near -0.485 V [136].

25

Recently, a novel multiprotein layer architecture that comprised two biomolecules such as cytochrome *c*, and bilirubin oxidase together with the polyelectrolyte sulfonated polyaniline, was presented by Lisdat *et al.* (Fig. 3.5) [137]. The authors demonstrated that such modification promotes the transport of electrons from the electrode's surface through the multiple proteins layers to the O_2 in the solution producing a catalytic reduction current whereas the electrode modified with only one protein, does not exhibit electrocatalytic behaviour. The catalytic currents increase as the number of layers increase indicating effective electrical chain between multiple proteins layers and the electrode surface [137].
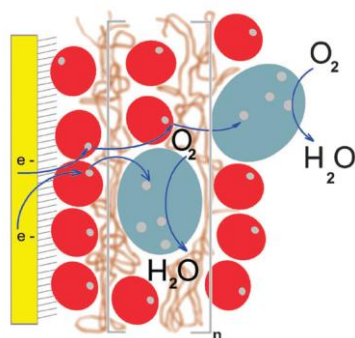
Fig. 4.5 Scheme of the redox chain between Cyt c (red circles)/BOx (blue shapes) multilayer electrode of the bioelectrocatalytic ORR [137].

4.2. Characterization of redox proteins

For over a half of the century, the interest in the application of redox proteins and enzymes in electrochemistry has been increasing. Such popularity can be traced to their ability to catalyze electrochemical reactions. They operate as biocatalysts in the cells of living organisms, mediating in the catabolic and anabolic pathways, thereby decreasing the activation energy of biochemical reactions. That in turn leads to the formation of new reaction pathways whose intermediate product's free energy is lower than the one obtained without the enzymes. Enzymes are also known for their high specificity towards their substrates compare to most inorganic catalysts. Therefore, they have found wide application in industry (e.g. in pharmacy, biorecycling or in construction of biosensors and biofuel cells). The rate of the chemical reaction catalyzed by proper enzymes might be accelerated even 10^6-10^{11} times.

26

As one can notice in the literature there is a slight disambiguity regarding whether all the redox proteins, as they by definition can catalyze redox reactions, can also be considered redox enzymes. From electrochemical and molecular points of view it's hard to present any important differences. But in accordance with [115], in this thesis, as redox enzymes will be regarded only those proteins which natural primary function is the catalysis of the redox reactions, whereas proteins with other primary functions, only exhibiting reductase, and peroxidase-like activity will be refered to as simply redox proteins. Nevertheless both the redox proteins such as myoglobin, hemoglobin and cytochrome *c* as well as the redox enzymes are widely used in electroctroanalysis for studying their electrochemistry and constructing biodevices.

Enzyme-based electrodes were constructed as the main part of this PhD thesis, therefore the next subsections are devoted to several redox enzymes (laccase, bilirubin oxidase and glucose oxidase) and one protein (myoglobin) which were used in this research. The choice was determined by the type of reaction they catalyze and their potential application. Lc and BOx were selected as enzymes that catalyze the oxygen reduction reaction, and owing to that they are utilized for producing biocathodes in biofuel cells. GOx and Mb, which catalyze glucose oxidation and hydrogen peroxide reduction, respectively were applied as model enzyme and protein to study their bioelectrocatalytic activity on modified electrodes.

4.2.1. Multicopper oxidases

Multicopper oxidases (MCOx) such as Lc, BOx or copper efflux oxidase are produced by numerous fungi, plants, bacteria and insects [138, 139]. They catalyze the oxidation of organic substrates (particularly products of lignin degradation or bilirubin, in the case of BOx), and the reduction of molecular oxygen directly to water without any intermediates being formed [140]. Owing to the latter, these enzymes have found wide application as biocatalysts in biofuel cells [119, 138, 141, 142].

All MCOx have similar structure. Their active centres are comprised of four copper ions which are classified into three types: T1 (blue copper), T2 (normal copper) and T3 (two coupled coppers) [138]. The T1 is ca. 0.13 nm away from other sites (0.04 nm) forming a trinuclear cluster (TNC) through bonding the copper ions from T3 with T2 via two histidines. All the ions are surrounded by amino acids, mainly

27

histidines and cysteines, that take part in the transport of electrons from T1, where the substrates are oxidized, through a tripeptide His-Cys-His chain to the outlying T2/T3 cluster where O_2 is reduced directly to water, (Fig. 4.6) [138, 143].
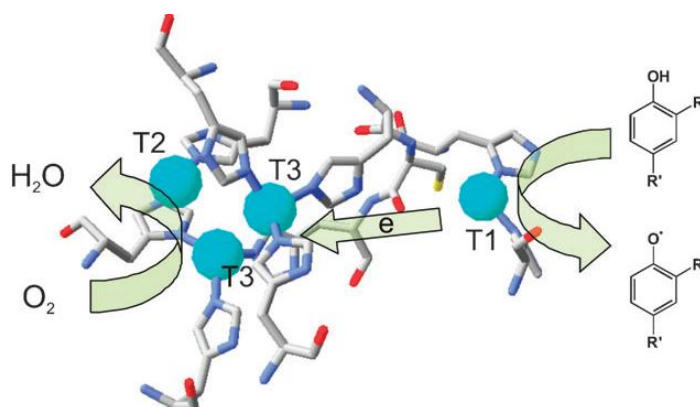
Fig. 4.6 Structure of copper site of Trametes hirsuta laccase and representation of its catalytic reactions [143].

Recently, the crystallographic structure of BOx, which in contrast to laccase was unknown for a long time, has been solved for the version extracted from *Myrothecium verrucaria* (*Mv*) [144, 145]. The structure reveals that the T1 site has an unusual environment consisting of two non-coordinating hyrodrophilic amino acids, asapargine and threonine, not previously observed in the structures of other MCOx (Fig. 4.7) [145].

(A)   **(B)**
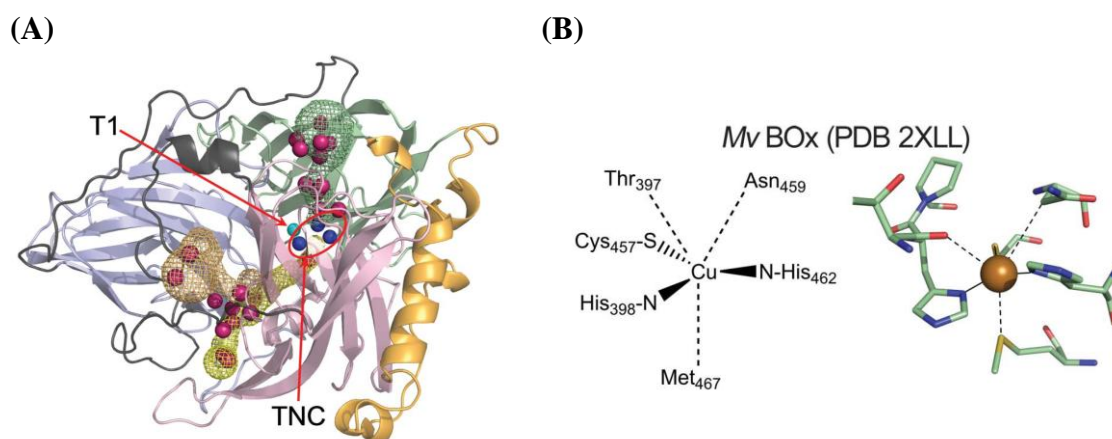
Fig. 4.7 (A) A scheme of the X-ray determined crystal structure of Mv BOx. (B) The T1 geometry in Mv BOx [145].

28

The presence of the hydrophilic pocket near the T1 site was employed by Blanford's group as a binding site of *Mv* BOx with its substrate, bilirubin, to stabilize the enzyme on a pyrolytic graphite electrode (PG) [145]. Such electrode exhibited an enhanced electrocatalytic response towards ORR compared to unmodified PG with bilirubin (Fig. 4.8) [145].

If one compares the studies on enzyme modified electrodes, it is worth noting that the enzymes utilized, can be procured from various sources. For that reason the activity of identically denoted enzymes can differ markedly between studies.
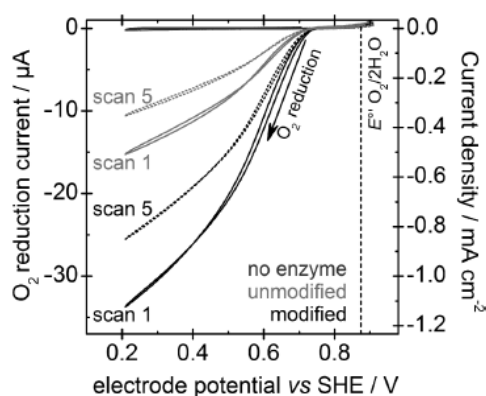
Fig. 4.8 Electrocatalysis of ORR by BOx on a pyrolytic graphite 'edge'electrode modified with bilirubin and an unmodified electrode at 25°C in pH 6 with rotation rate 4000 rpm [145].

The redox potential of the enzyme is crucial for its application as cathode catalyst in biofuel cells. In the case of laccases the T1 site is an electroactive center so it determines the redox potential of the enzyme which can vary from 0.43 V to 0.78 V vs. NHE [146, 147]. Due to such diversity the laccases can be divided into three groups: low, medium and high potential. Low potentials are laccases that originate from trees e.g *Rhus vernicifera* (for which the redox potential of T1 is 0.43 V vs. NHE [148]). Medium ones are isolated from fungi e.g. *Rhizoctonia solany* with redox potential in the range of 0.47 – 0.71 V vs. NHE [149, 150]. The high potential ones, also from fungi with redox potentials of ca. 0.78 V and 0.75 V vs. NHE for laccases from *Trametes* [147] and *Cerrena* [151-153] species respectively e.g *T. hirsuta*, *T. versicolor* and *C. unicolor.*

The optimum pH at which fungi-laccases operate is in the range of 3-5, making those biocatalysts unsuitable for *in vivo* applications where the pH is 7.4. Moreover, all

29

the laccases are inhibited by halide ions such as chloride or fluoride which are ubiquitous in the human fluids [154]. Therefore, to circumvent these problems, bilirubin oxidase, an enzyme that retains a relatively high activity at neutral pH and in the presence of chloride ions, might substitute laccase in these applications. The redox potential of BOx is akin to high-potential laccase at 0.69 V [155].

The oxygen reduction reaction is a slow chemical reaction. In the literature one can find a few proposed mechanisms for the laccase catalysed reaction. From the spectroscopic studies Solomon *et al.* were able to observe MCOx's O_2 intermediates proving that O_2 reduction to H_2O consists of two 2 electron transfer steps (Fig. 4.9) [156]. The first one is slow and rate-determining, while the second is fast. As depicted in Fig. 4.9, the process begins from the native intermediate (NI), the oxidized state of copper ions. Then the substrate reduces the copper centers, starting from T1 which accepts and transfers electron to the TNC where O_2 is reduced. Subsequently, two mechanisms for the reduction are possible. The first leads to a form with fully reduced copper ions that bind the molecular oxygen to T2/T3, resulting in a peroxy intermediate formation (PI) (the rate-determining step). Afterwards, the cleavage of the O-O occurs, which is proton-assisted from the Glu near T3, and terminates the catalytic cycle, releasing the water molecule (the fast step). In the case of the second mechanism of reduction, the NI is first interconverted to a fully oxidized so called "resting" form, and finally to the fully reduced one. In the latter mechanism the T1 can be continuously reduced by the substrate but the transport of the electron is too slow to impact the catalytic cycle [156].
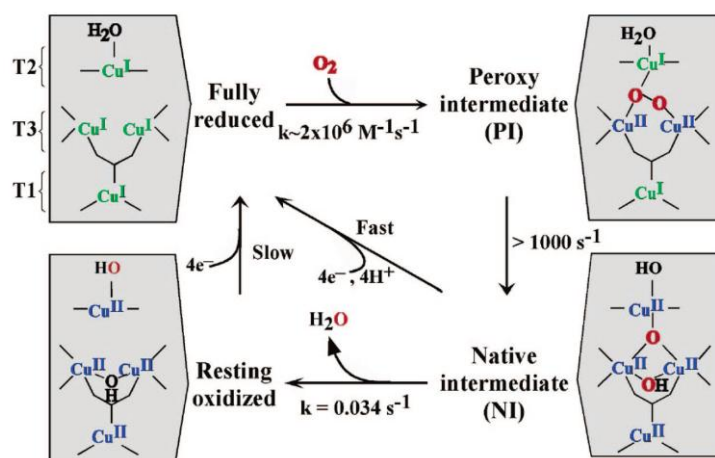
Fig. 4.9 Schematic illustration of mechanism of oxygen reduction catalyzed by MCOx [156].

4.2.2. Glucose oxidase

Glucose oxidase from the fungus *Aspergillus niger* is a flavin, and one of the most resistant enzymes with molecular mass of 150–180 kDa that consists of two identical polypeptide chains, each containing a flavin adenine dinucleotide (FAD) as redox prosthetic groups which are tightly bond together (Fig. 4.10A) [157]. The $FAD/FADH_2$ is deeply buried ca. 0.13 nm within the globular structure of the GOx which hinders the electron transfer between the enzyme and the electrode. The biological function of GOx is to catalyze the oxidation of glucose into gluconolactone, which then hydrolyses into gluconic acid (Fig. 4.10B) [82]. That process is accompanied by O_2 reduction to hydrogen peroxide (more details in Chapter 6). Owing to the first reaction the GOx is widely applied as biocatalyst for glucose biosensor construction [157, 158] or on the anode of the glucose/O_2 biofuel cell [2, 159, 160].

(A)   **(B)**
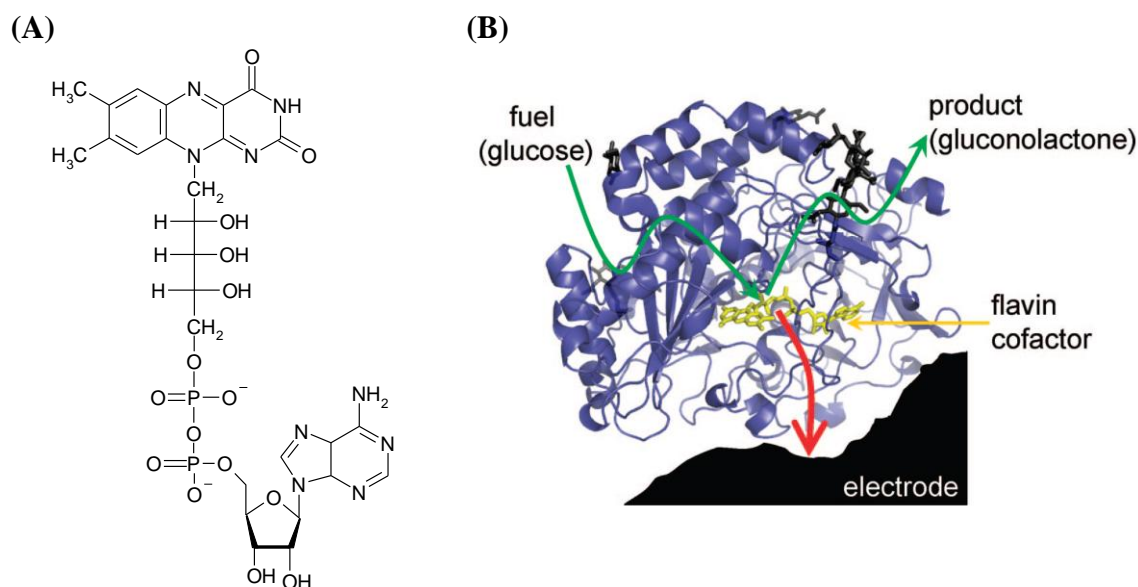
Fig. 4.10. (A) A glucose oxidase cofactor – flavine adenine dinucleotide (FAD). (B) A scheme of electron transfer from FAD domaine of glucose oxidase to the electrode surface [161].

4.2.3. Myoglobin

Myoglobin (Mb) is an iron heme, globular protein found in cardiac and red skeletal muscle tissues, responsible for oxygen storage and transport. It comprises a single polypeptide chain of 160 amino acid residues and a porphyrin known as protoporphyrin IX which is an iron complex (Fig. 4.11), as a prosthetic group [162]. The iron heme

31

group is electroactive so if the Mb is properly immobilized at the electrode surface the Fe(III)/Fe(II) couple undergoes a single electron, single proton reversible electrochemical reaction, described by the following equation [162]:

$$MbFe(III) + H^+ + e- \rightarrow Mb(II) \tag{4.1}$$

These relatively small molecules of ca. 17 kDa molecular weight, are usually isolated from whale sperm, and do not reveal any important *in vivo* enzymatic functions [115, 162]. However, they exhibit catalytic properties towards hydrogen peroxide, O_2, nitric oxide and trichloroacetic acid or nitrite reduction reaction, so it might serve as a relatively cheap "enzyme-mimic" for studying the biological functions of heme proteins or enzymes, and their applications in biosensors and the biocatalytic area [115, 163-165].

(A)   **(B)**
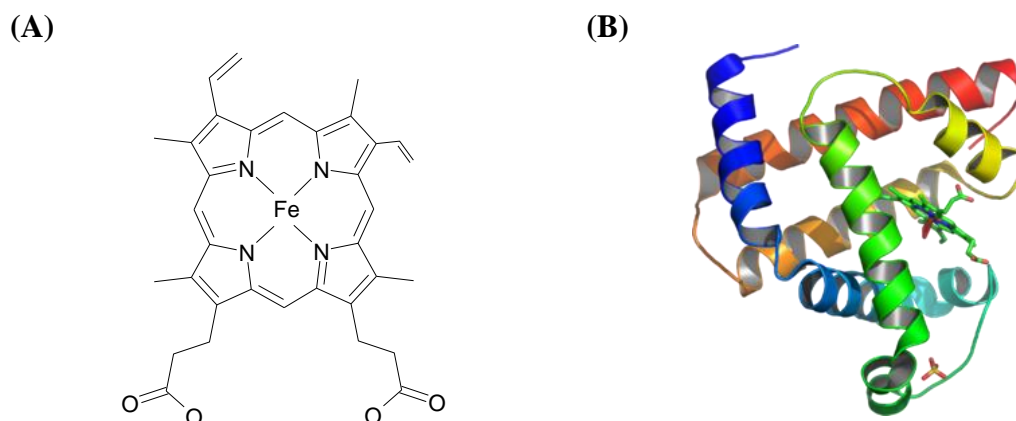
Fig. 4.11 (A) Protoporphyrin IX, heme b as found in myoglobin (B) A scheme of the structure of Mb [166].

5. Carbon-based nanomaterials for redox protein modified electrodes

5.1. Carbon nanotubes

Carbon nanotubes, due to their large chemically active surface area, excellent electrical conductivity, and easy protein immobilization with maintenance of its activity can promote the electron-transfer reaction and enhance the electrochemical reactivity of biomolecules. For instance vertically alligned CNT behave like a molecular wire which can penetrate the protein shell to get to deeply buried redox centers in that way improving the electrical contact between the biomolecule and the electrode surface [167, 168]. Therefore the employment of CNTs in developing biosensors or biofuel cells has significant impact on the progress in manufacturing a new generation of biosensing devices [12, 29, 169-172].

Diverse CNT based modified electrodes were applied to achieve direct electron transfer and to study the electrochemical behaviour both of proteins whose redox centres are close to the electrode's surface such as peroxidases [173, 174], cytochrome *c* (Cyt *c*) [175], myoglobin [176], catalase (Cat) [177] or azurin [175], and of glucose oxiase [178], multicopper oxidases [178-181], hydrogenases [182] and dehydrogenases [183] whose redox centres are deeply buried within the protein structure and would not normally be electrochemically active. These biomolecules can be immobilized on the CNTs surface through covalent binding and affinity interactions, entrapment during polymerization or by adsorption onto the polymer or the walls of the SWCNTs utilizing electrostatic or hydrophobic interaction, as is depicted in Fig. 5.1 [169].
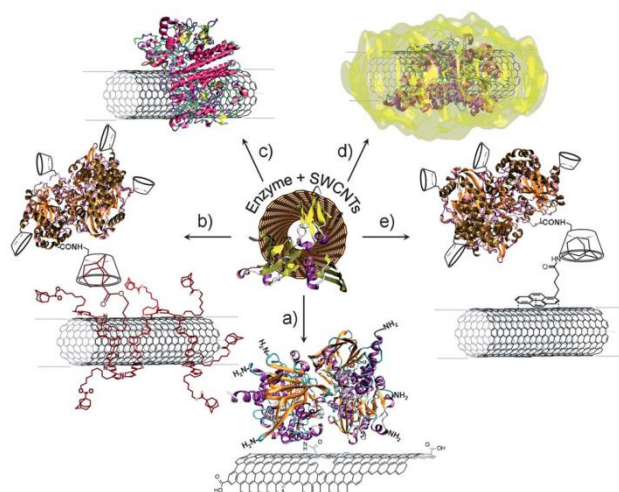
Fig. 5.1 A schematic illustration of various strategies of enzymes immobilization on SWCNTs: (a) covalent binding; (b) electrodeposition; (c) adsorption; (d) entrapment; and (e) immobilization via affinity interactions onto functionalized nanotubes [169].

Lojou *et al.* described an interesting example of a biosensing device that also potentially might find application as a bioanode in fuel cells. They utilized amine-modified and carboxyl-functionalized SWCNTs as a platform for hydrogenase immobilization at gold and graphite electrodes [182]. Hydrogenase is a microbial enzyme that catalyses with high rate the oxidation of hydrogen into protons or the evolution of hydrogen from the reduction of protons. Therefore, with the potential advent of the hydrogen economy it might be important to fabricate highly developed surface area electrodes for entrapment of that enzyme and utilization of the electrodes as bioanodes in fuel cells. The authors demonstrated that hydrogenase adsorbed on the carboxylic acid functionalized CNTs-coated pyrolytic graphite (PG) electrodes exhibits direct electron transfer towards hydrogen oxidation, reaching a catalytic current at least one order of magnitude higher than at a bare PG electrode [182].

Currently, CNTs are also leading materials for the construction of biocathodes [2, 120, 184]. Generally, as biocatalysts for cathode construction, enzymes from the oxidoreductase group are used e.g. laccases, whose application is limited by their susceptibility towards chloride ions, and the more costly bilirubin oxidases. However, recently the relatively cheap peroxidases, that are resistant to chloride ions and active in neutral pH have found application as a biocatalyst in the cathodic compartment of a biofuel cell [185]. An example of such a biocathode modified with CNTs, has been recently presented [173]. Schuhmann's group adsorbed horseradish peroxidase at

34

hierarchical carbon microfiber (CMF)/carbon nanotube composite materials, directly grown on a graphite rod electrode that was postmodified with pyrene-1-hexanoic acid using π–π interactions. The HRP immobilized on this modified electrode exhibits direct bioelectrocatalytic activity towards H_2O_2 reduction reaction on potentials as high as that obtained for high potential laccases, about +0.600 V vs. Ag|AgCl [173]. Such high value of potential is obtained only in few cases like an astonishing bioelectrocatalytic effect on specially treated electrified interfaces. Generally the onset potential of H_2O_2 reduction is obtained at potentials of about +50 to 100 mV vs. Ag|AgCl. The obtained results suggest that the crucial factor is that the carbon nanostructures formed on top of the CMFs during CNT growth are leading to an improved orientation of the HRP thus enhance the specific interaction between the heme-cofactor of HRP and the carbon nanostructured-based electrode [173].

Another employment of CNTs as a material for biosensing devices [12, 29, 172] and biofuel cells [2, 186] construction was presented by Mao's group. A laccase/MWCNT-based electrode was proposed as a novel electrochemical biosensor for selective determination of dopamine, in the presence of the most potential electrochemical interferents such as ascorbic acid (AA) and dopamine's metabolite – 3,4-dihydroxyphenylacetic acid (DOPAC) [179]. The laccase catalyzes the oxidation of DA into dopamine-o-quinone which can cyclize and be oxidized by laccase again to form 5,6-dihydroxyindoline quinone that is readily reduced electrochemically at the MWNTs. Its reduction occurs at a negative potential of -0.15 V vs. Ag|AgCl that is far from those of the redox processes of AA and DOPAC. Xiang *et al.* show that the utilization of the multifunctional catalytic properties of laccase and the excellent electrochemical properties of carbon nanotubes enable to obtain selective, simple and stable DA biosensors [179]. However, its sensitivity for bioanalytical applications should be improved.

Recently, the application of the layer-by-layer assembly method for the preparation of CNTs modified electrodes have gained considerable attention because that technique provides thinner and more dispersed CNTs-based films, which improves and enhances the interaction between the CNTs and entrapped biomolecules. The Simonian group constructed a hybrid nanocomposite electrode based on the interaction of anionic/cationic biomolecular layers structured with MWCNTs [187]. The obtained

35

results suggest that integration of the CNTs with biopolymers enhance the direct electron transfer, increase the electrochemically active surface area and improve the mechanical stability of such a nanocomposite. Fig. 5.2 depicts such a surface modification. As one can see, firstly on the negatively charged surface of the GCE a supporting bilayer of oppositely charged MWCNT-polyethyleneimine (PEI) and MWCNT-DNA was deposited. Then on that cushioning support a positively charged complex of MWCNT and organophosphorus hydrolase (OPH), that catalyses the hydrolysis of a variety of organophosphate neurotoxins, was adsorbed [187]. The authors proposed that sandwich-like LbL structure for sensitive detection of p-nitrophenol (PNP), the catalytic product of the hydrolysis of paraoxon. The electrochemical results show that the peak current of the PNP electro-oxidation increases linearly with increasing number of active layers. The demonstrated nanocomposite biosensor is relatively simple, does not require complex synthesis, shows high sensitivity and a low detection limit [187].
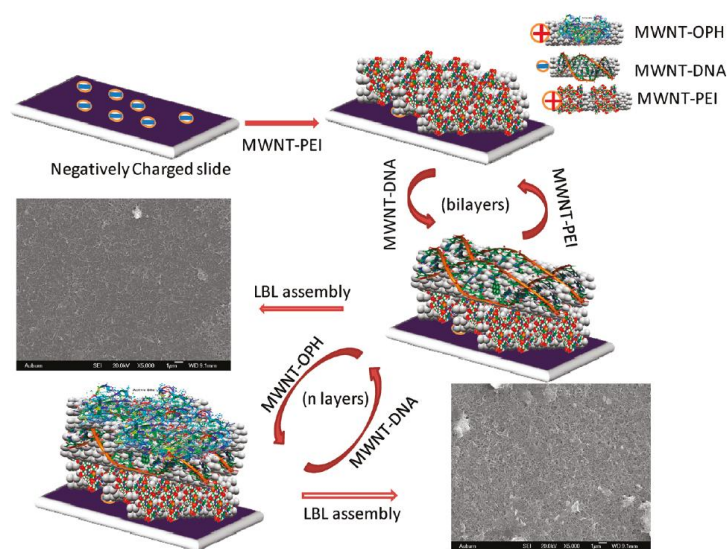
Fig. 5.2 A scheme of the multilayers film formation via LbL method. The initial layers of MWCNT-PEI and MWCNT-DNA provide support for subsequent layers of MWCNT-OPH and MWCNT-DNA [187].

Carbon nanotubes have recently emerged as a new option for an unconventional barcode construction [188]. Such device might serve as medical diagnostic models or multiplexed bioanalytical assays for detection of multiple proteins or single molecules of DNA and could have a wide variety of tagging applications. Strack *et al.* chose

36

a macroscopic aggregate of carbon nanotubes, as highly electrically conductive, and enzymes (Lc) adsorbing material, to generate a directly readable barcode [188]. It was generated from monitoring the amperometric laccase's response, in the bioelectrocatalytic reaction of oxygen reduction, in the electrolyte of controlled oxygen content. The system demonstrated long-lived biocatalytic activity and retention of DET under continuous flow [188].

5.2. Graphene

As mentioned in the Chapter 3 graphene is sometimes called a "wonder material" for its remarkable properties [48, 189]. Those same features enable it to find applications in fields such as biosensors [13, 49, 189, 190] and biofuel cell [191, 192] development. Various graphene based modified electrodes were applied to study the electrochemical behaviour of redox proteins. The direct electrochemistry and electrocatalysis of heme-containing metalloproteins (myoglobin [71, 164], cytochrome *c* [164, 193], horseradish peroxidase [164], haemoglobin (Hb) (Fig. 5.3A) [194]) were studied, but also other redox enzymes like glucose oxidase [70], alcohol dehydrogenase [195], bilirubin oxidase [192], laccase [196], polyphenol oxidase [197], acetocholinesterase (AChE) [198], and catalaze [199] were examined.

(A)

(B)
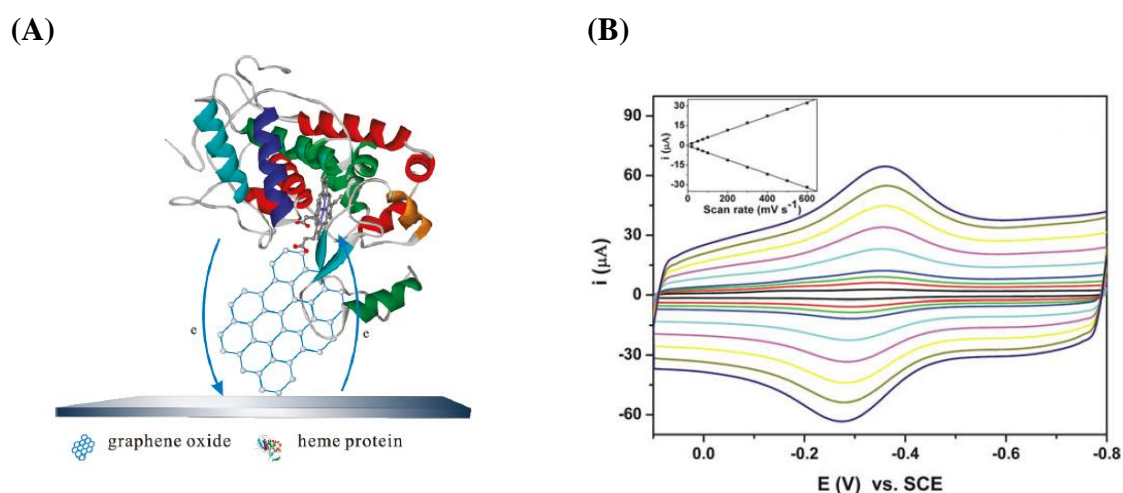
Fig. 5.3 (A) A scheme of electron transfer between the graphene oxide and a heme protein at a glassy carbon electrode [164]. (B) Scan rate depandance of Hb adsorbed on the PDDA/RTIL graphene nanosheets modified GCE. Inset: plots of peak currents vs. scan rates [194].

However, the development of GN modified electrodes for biological applications might be limited by its hydrophobicity. This is an inherent problem of carbon based nanomaterials like carbon nanotubes that they form agglomerates or even re-graphitize to graphite (in the case of graphene) due to the van der Waals interactions and strong π –π stacking [48].

Therefore the improvement of GN hydrophilicity through its covalent or noncovalent functionalization facilitates biomolecule immobilization [48]. For example Hb adsorbed on graphene nanosheets functionalized with poly(diallyldimethylammonium chloride) (GN-PDDA) combined with room temperature ionic liquid modified electrode, exhibits fast direct electron transfer [194]. Cyclic voltammetry experiments of the described system show well-defined and quasi-reversible redox peaks from the heme group (Fig. 5.3B) that vary linearly with the scan rates, as shown in the inset of Fig. 5.3B, indicating that the process is surface controlled [194].

Shan *et al.* presented the first graphene based glucose biosensor using a polyvinylpyrrolidone-protected graphene/polyethylenimine-functionalized ionic liquid electrode [70]. Physically adsorbed GOx on such a surface maintained its biological activity and was successfully applied for developing glucose biosensors. The prepared biosensor exhibits a wide linear glucose response (2 to 14 mM, *R*= 0.994), good reproducibility (*RSD*=3.2 % for current response to 6 mM at -0.5 V and *N*=10), and high stability [70].

One can find in the literature a plethora of glucose biosensors based on various carbon materials [29, 70, 168, 200]. However, as was reported lately by Zhou *et al.* graphene based biosensors are getting to be the leading ones, owing to their low limit of detection (2 μM), wide linear range (0.01 – 10 mM), high sensitivity (20.21 μA mM cm^{-2}), reproducibility, and high stability [41].

Another example of a GN based biosensor was presented by Wang *et al.* [201]. The authors developed a rapid, simple and highly sensitive AChE biosensor for organophosphorous pesticides (Ops) based on immobilization of AChE onto CdS–decorated graphene (CdS–G) nanocomposite. The immobilized enzyme on such modified electrode possesses higher enzymatic activity and affinity to acetylthiocholine chloride due to the excellent electron-transfer channels of the nanocomposite [201].

38

GN based electrodes, due to their fast electron transfer kinetics and excellent electrocatalytic characteristics, compared to other carbon based electrodes, are also a novel platform for laccase (*Rhus vernicifera*) immobilization and for studying the mediated bioelectrocatalytic reaction of oxygen reduction. Such system was demonstrated by Wu *et al.* [196]. They obtained the nanocomposite material via dispersion of graphene sheets in ABTS solution. Then laccase was assembled on such prepared surface utilizing the π-π and the electrostatic interactions between graphene and ABTS, respectively. As one can see from Fig. 5.4 a well defined sigmoidal curve (curve b) is obtained [196]. The catalytic current density obtained at pH 7.4 was higher than 120 μA cm^{-2} at 0.33 V. Under these conditions oxygen electroreduction commences at 0.580 V vs SCE, a value close to the formal potential of T1 redox center of the laccase and similar to other results obtained for carbon-laccase based electrodes. Despite the presence of the mediator at the electrode surface, such system was applied for detection of extracellular oxygen released from human erythrocytes [196]. The results show that the detection limit of this system is comparable with CNTs-chitosan-laccase modified electrodes [202] while its sensitivity is higher than at CNTs-laccase boron-doped diamond electrode [153]. The presented electrode might also find another application for example as a biocathode in a biofuel cell.
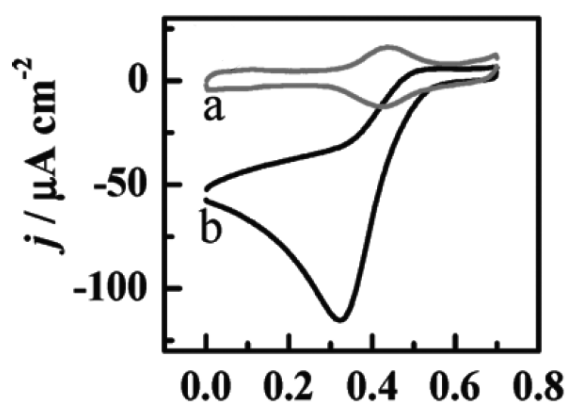
Fig. 5.4 Electrocatalysis of ORR by laccase immobilized at ABTS-graphene GCE in oxygen free (curve a) and O₂-saturated (curve b) PBS [196].

Recently Liu *et al.* constructed the first enzymatic membraneless biofuel cell based on silica sol–gel immobilized graphene sheets/enzyme composite gold electrodes

[192]. Bilirubin oxidase and glucose oxidase were employed as the cathodic and anodic enzymes, respectively. Additionally, the required mediators were incorporated within the sol (Fig. 5.5). The maximum power density of such biofuel cell is two times greater than that of a comparable SWCNT-based biofuel cell [192]. Nevertheless, more attractive for commercialization is a construction of a mediatorsless biofuel cell. Such a biofuel cell based on nanographene plateles was presented recently by Zheng *et al.* [191]. Its maximum power density is two times higher compared to the one presented by Liu *et al.* [192].
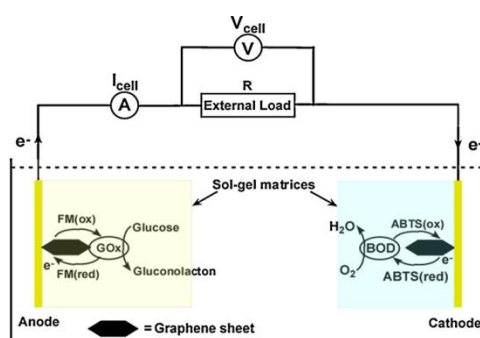
Fig. 5.5 A schematic illustration of graphene based membraneless glucose-O₂ biofuel cell with GOx/FM and BOx/ABTS functionalized electrodes as anode and cathode, respectively [192].

5.3. Carbon nanoparticles

The history of the application of CNPs as a support for enzymes's immobilization is relatively short. The important property of hydrophilic carbon nanoparticles is the presence of sulfonate groups that increases their solubility. It is also essential for electrode preparation and biomolecule immobilization. All these features make CNPs one of the most promising materials for development of amperometric enzyme modified electrodes. Parallel to my reaserch, other reports have appeared about successful applications of sulfonated CNPs as biocathode material [86, 87, 203].

An example of such a biocathode was presented by Lesniewski *et al.* [86, 87]. The authors constructed a three dimensional film electrode using the LbL technique by alternative immersion of ITO into a suspension of positivly (gold nanoparticles [86] or imidazolium functionalised silicate submicroparticles [87]) and negativly charged particles. The obtained electrodes, after the laccase [87] or bilirubin oxidase [86] adsorption, exhibited mediatorless electrocatalysis towards oxygen reduction (Fig. 5.6).

40

(A)   **(B)**
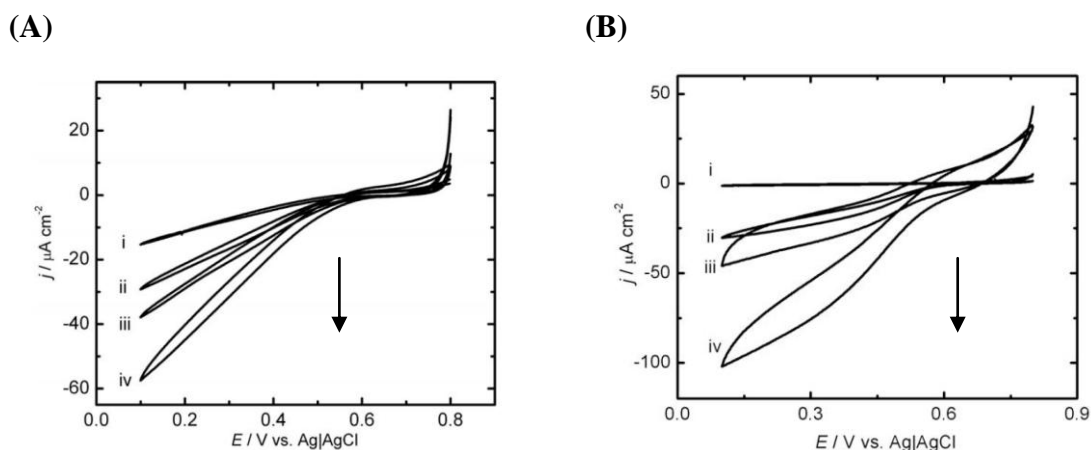
Fig. 5.6 Electrocatalysis of ORR by (A) BOx on AuNPs-CNP [86] (B) and Lc on imidazolium functionalised silicate submicroparticles – CNP [87] ITO electrode modified by increasing number of immersion and withdrawal steps as shown by arrows.

It was shown, that the current density of the bioeletrocatalytic process increases with the amount of the carbon material deposited at their surfaces (Fig. 5.6) [86, 87]. These results confirm that carbon nanoparticles form effective percolation paths that allow for appropriate electron transport and a high amount enzyme loading. Nevertheless, the maximal efficiency of these electrodes is still not as high as some other carbon-based biocathodes [204-206]. For example Nogala *et al.* through incorporation of hydrophilic carbon nanoparticles in a carbon ceramic electrode, increased its catalytic efficiency ca. two times [205].

Apart from the electrodes modified with enzymes there has been research on electrodes employing bacterial organisms as biocatalyst. Yuan *et al.* fabricated a microbial fuel cell (MFC) with an anode made from a mixture of a bacteria (*Proteus vulgaris*) suspension with unmodified carbon nanoparticles and Teflon emulsion [207]. Such carbon paste with entrapped bacteria was spread on carbon cloth. The introduction of carbon nanoparticles with immobilized bacteria facilitates the electron transfer. Thereby, the performance of the assembled MFC is enhanced ca. 2.5 times compared with the MFC at which carbon nanoparticles were not applied and bacteria was unimmobilized [207].

41

An interesting example of electrochemically generated carbon nanoparticles on a glassy carbon electrode and the application of such a surface (called as surface-nanocrystalline GC electrode) as a platform for glucose oxidase immobilization was presented by Xu *et al.* [208]. The modified electrode compared with the bare one showed higher electrocatalytic activity in direct electrochemistry of GOx, due to a higher proportion of edge sites (Fig. 5.7) [208].
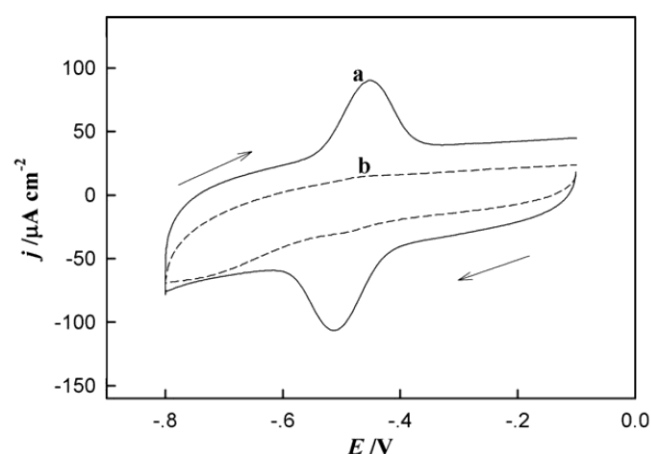
Fig. 5.7 CVs obtained for GOx adsorbed on carbon nanoparticles modified (a) and unmodified glasy carbon electrode (b) [208].

Also hemoglobin immobilized within a 3D-nanoporous hybrid material composed of CNPs without sulfonate gropus and polyvinyl alcohol (Hb-CNP-PVA), exhibits direct electrochemistry and bioelectrocatalytic activity towards oxygen, hydrogen peroxidase (Fig. 5.8) and nitrite reduction [209]. However, their analytical performance is not as good as hemoglobin-graphene based biosensors in the determination of nitrite [194].
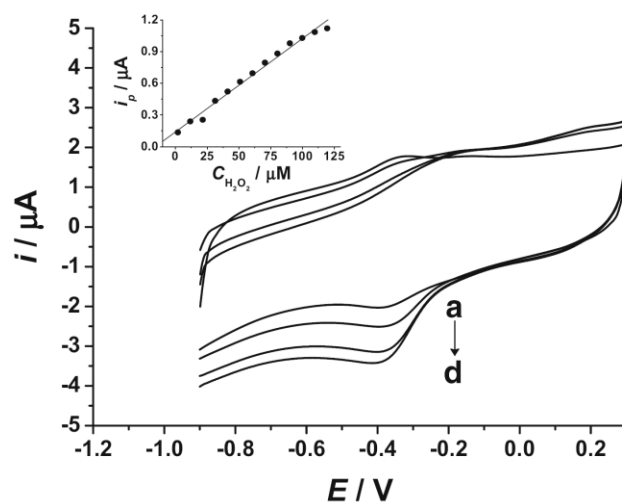
Fig. 5.8 CVs of Hb-CNP-PVA modified GCE electrode at differenet concentration of hydrogen peroxide in buffer solution [209].

One can also find CNP based electrochemical immunosennsors for detetection of α-fetoprotein (as a model protein) in clinical immunoassays [210].

5.4. Carbon ceramic electrode

As it was mentioned in Chapter 3, the CCEs due to their unique properties are found to be a suitable support for the construction of electrochemical sensing devices. Moreover, the sol-gel process which is utilized for electrode preparation provides favorable conditions for stable protein immobilization. Therefore, one can observe an extensive progress in the application of CCEs in the biosensing area. Hitherto, the CCEs were employed as a platform for the immobilization of enzymes like glucose oxidase [100, 200], lactate oxidase [211], horseradish peroxidase [212], xantine oxidase [213], laccase [87, 111, 113, 114], bilirubin oxidase [203] and tyrosinase [214].

One of the first reports on the application of a CCE in the biosensing area, was presented by Gun and Lev [200]. The authors modified the CCE electrode with the redox mediator ferroceneacetic acid and GOx covalently bonded to its surface. It enables effective wiring of the enzyme to the silicate matrix and maintaining of its bioelectrocatalytic activity towards glucose oxidation. The presence of the graphite dispersion improved the long range electron transfer through formation of percolation paths. The immobilized mediator facilities short range electron shuttling from the active center of the glucose oxidase to the carbon dispersion by an electron hopping

43

mechanism [200]. The main advantage of this biosensor is its renewable surface regenerated by polishing. Nevertheless the biosensors with immobilized mediator are not so enticing.

The application of CCE as platform for laccase immobilization was proposed by Gorton's group [111]. The authors demonstrated that the presence of the silanol groups on the sol-gel lattice in the CCE additionally stabilize the enzyme, resulting in its stronger adsorption than onto spectrographic graphite or highly ordered pyrolytic graphite electrodes. Physically adsorbed laccase on the surface of CCE exhibit electrocatalytic activity towards oxygen reduction and phenolic compound oxidation [111]. Electrochemical measurements show that not the T1 center of Lc, but more probably the T2/T3 cluster, is responsible for the direct electron transfer, as it is usually observed for carbon-based electrodes. The optimized electrochemical biosensor, in comparison with the graphite based biosensor, offers a lower detection limit and a wider linear dynamic range for the detection of phenolic compounds. Its performance is comparable with recently prepared CNTs based biosensors [215, 216].

Also a sol–gel-derived ceramic–carbon nanotube nanocomposite film prepared by doping MWNTs into a silicate gel matrix was successfully used to immobilize HRP [212]. The combination of silicate gel matrix and MWCNTs enables the fabrication of a uniform, stable, and biocompatible film that promotes electron transfer. The HRP immobilized on such an electrode exhibits direct electrochemistry of the heme couple and electrocatalytic activity. The presented biosensor exhibits good sensitivity, stability and fast response in determination of H_2O_2 [212].

Recently, CNPs-enriched CCEs with adsorbed bilirubin oxidase was proposed by Nogala *et al.* as an air-breathing biocathode for studying the biocatalytic reaction of oxygen reduction (Fig. 5.9) [203]. In such a system, substrate (oxygen) is supplied from the outer gas phase (porous material), which in turn makes it more accessible to the biocatalyst than from the electrolyte, where its transport towards the electrode is the rate-limiting step of the bioelectrocatalysis. As a result the oxygen mass transport rate through the air-breathing biocathode is two times higher than from aqueous solution [203].

44
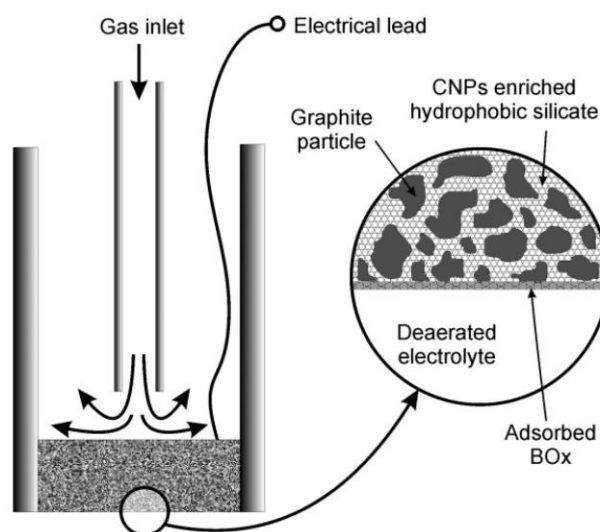
Fig. 5.9 A schematic illustration of air-breathing CNPs-enriched CCE biocathode [203].

6. Biodevices

With the progressof nanotechnology a number of various nanomaterials have been fabricated. This accelerated research on enzyme and nanomaterials-modified electrodes for biofuel cell or biosensing. In the next subsections the development of the biofuel cell and the zinc-oxygen hybrid cell is discussed. Since biocathodes based on DET and MET were constructed as part of this PhD thesis a review of these electrodes, and the Zn-oxygen hybrid cell based on them, is presented.

6.1. Biofuel cells

Biofuel cells (BFCs) convert chemical directly electrical energy using the capabilities of biocatalysts, mostly enzymes, on at least one electrode. Biofuel cells where the biocatalyst is employed at only one electrode are called hybrid biofuel cells. As biocatalysts most often enzymes are used (i.e. enzymatic fuel cells), but recently there has been a rise in the application of complete living cells for that purpose again (i.e. microbial fuel cell) [118]. In enzymatic BFCs electrons generated at the anode by fuel oxidation (e.g. of sugars or alcohols) in enzymatic reaction (utilizing respectively: glucose oxidase, or fructose, cellobiose, aldehyde or alcohol dehydrogenases) are transferred to cathode via external electric circuit (Fig. 6.1). At the cathode the enzymatic (e.g. of laccase, bilirubin oxidase or horseradish peroxidase) reduction of

45

oxidant (oxygen or hydrogen peroxide) occurs consuming electrons produced on the anode [118-120]. The enzymes can replace conventional inorganic catalysts, owing to their ability to operate under mild conditions with a minimal overpotential of diffusion-controlled oxidant reduction reaction, broader choice of fuels, higher selectivity, and catalyst renewability and disposability. Nevertheless, the low stability of enzymes, and their low turnover number are still the limiting factors for constructing applicable BFCs. Therefore there is still room for improvement in their stability and electrical connection with the electrode (which is crucial for the cell's efficiency) for example via redesigning of biocatalyst by random mutagenesis approach or reducing the glycolisation's level [123].

It is believed that the power output of BFCs still could be increased by 1-2 orders of magnitude to few milliwatts per square centimeter [2]. However considering the lower power deinsity of currently available biofuel cells (compared to conventional fuel cells) and their intrinsic biocompatibility, initially they might find mostly biomedical, clinical and health applications such as pacemakers, glucose sensors for diabetics, small valves for bladder control or biosensors.
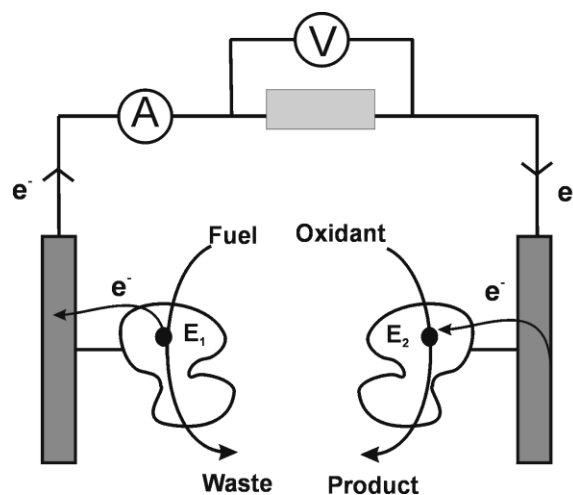
Fig. 6.1 Schematic illustatration of an enzymatic biofuel cell with a cathode and an anode modified with enzymes E_1 and E_2, respectively.

The first microbial fuel cell was constructed by Potter in 1910, who utilized yeast and E.coli in the anodic compartment using Pt electrodes to generate electrical power, while the first enzymatic glucose-oxygen (O_2) fuel cell was demonstrated by Davis and

Yarborough in 1962 [217] and later by Yahiro in 1964 [218]. However, a real extensive interest in the development of enzymatic biofuel cells was observed more than decade ago. At the beginning two compartment BFCs were constructed with a membrane [141, 219]. Later on, the work on one compartment BFCs (membraneless) for potential *in vivo* applications began. The first examples were presented by Katz (Fig. 6.2) [220] and Heller [159]. In such devices the transport of the electrons between electrode and enzyme can be conducted in two ways: with mediator immobilized at the electrode surface (MET) or by direct electron transfer (DET). The immobilization of mediator and enzyme prevents side reactions (e.g. between the cathodic and anodic mediator) from taking place and in case of *in vivo* applications naturally prevents mediator molecules from leaving the fuel cell and potentially harming host's cells. Recently, devices that employ DET, despite their low current density, have been favored. Their distinctive advantages are simplicity, greater potential miniaturization (and hence better chances of successful *in vivo* application), lack of thermodynamic losses taking place due to mismatch between enzyme and mediator redox potentials, and lower cost than that of cells employing mediators.
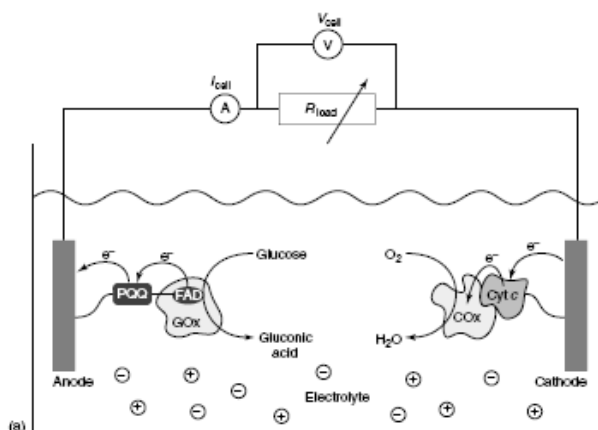
Fig. 6.2 Schematic illustration of membraneless and glucose-O_2 biofuel cell in which the cathode and anode are modified with enzymes – cytochrome c and glucose oxidase, respectively [220].

6.1.1. Biocathode based on mediated electron transfer

In order to construct and miniaturize a membraneless biofuel cell for *in vivo* application various avenues are undertaken to immobilize the mediator at the electrode surface. Most biocathodes consist of copper oxidoreductases like laccase or bilirubin oxidase

47

from various sources. Although, these enzymes fulfill crucial requirements for application in biofuel cell [147, 184] their active centers are deeply buried within the protein structure, which causes that the transfer of electrons directly between the enzyme and the electrode surface is not always possible. Therefore one strategy to obtain efficient electron transfer is based on immobilization of the mediator.

Mediators are low molecular weight redox species, with fast and reversible electrochemistry that transfer electrons to/from the electrode surface. Both their oxidized and reduced forms should be stable and it redox potential has to be close to that of the enzyme [141]. Research carried out by Palmore *et al.* showed that for high potential laccase ABTS^{2-} (2,2'-azinobis-(3-ethylbenothiazoline-6-sulfonate)) (Fig. 6.3) is the best electron shuttling molecule among those studied [141].
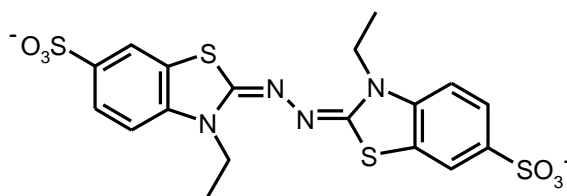
Fig. 6.3 2,2'-azinobis (3-ethylbenzothiazoline-6-sulfonate) ABTS^{2-} [221].

Other compounds that were sucessfully used as mediators for that enzyme include osmium polymer [159, 222-224] and syringaldazine (Syr) [114, 225, 226]. Their main advantages over ABTS^{2-} are flexibility [224], and lower toxicity of the oxidized form (electroneutral) [114], respectively. However, the low redox potential of Syr and its pH dependence exlude that mediator for being applied in biofuel cells [114]. The major drawback of the utilization of ABTS^{2-} is that the oxidized form is an anion radical (ABTS$^{\bullet-}$) which not only significantly deteriorate enzyme activity [227-229], but also can harm life tissue, effectively eliminating it from *in vivo* applications. Nevertheless, it is still the most studied mediator for laccase and bilirubin oxidase modified biocathodes for oxygen reduction.

It is worth emphaisizing that the enzymes utilized in the research covered in the subsections devoted to MET and DET based biocathodes were procured from various sources (e.g. companies delivering commercially available species), and in some cases were prepared through dedicated procedures in order to e.g. produce specially mutated

48

species. For that reason the activity of the identically denoted enzymes can differ markedly between studies. That in turn makes it hard to directly compare effieciency of the biocathodes obtained.

As ABTS^{2-} based biocathodes were constructed as part of this PhD thesis therefore the literature part devoted to MET focuses on various approaches for ABTS^{2-} immobilization at the electrode surface.

6.1.1.1.   Laccase-biocathode

One can find in the literature several different methods for ABTS^{2-} and Lc immobilization at the electrode surface. Amore *et al.* encapsulated laccase and ABTS^{2-} in silica coated and high surface area carbon electrode [230]. The authors suggest that within such a matrix, fluid microdomains are formed, which are permeable to oxygen and water from the electrolyte solution, therefore efficient bioelectrocatalysis of oxygen reduction is recorded [230]. A similar avenue was repeated by Nogala *et al.* [113]. The authors presented a simple procedure for the noncovalent and relatively stable immobilization of ABTS^{2-} and laccase (*Cerrena unicolor*). First mediator was adsorbed within a porous hydrophobic silicate-carbon heterogeneous structure of a carbon ceramic electrode and then on its surface a thin hydrophilic silicate film with encapsulated enzyme was deposited (Fig. 6.4). Such electrodes with adjacent hydrophilic and hydrophobic silicate matrices exhibit high bioelectrocatalytic activity, which indicates good electronic contact between mediator and laccase [113].
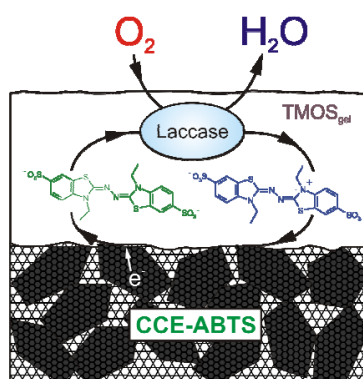
Fig. 6.4 Schematic diagram of the structure of ABTS-CCE covered by a thin film of sol-gel processed hydrophilic TMOS-gel based silicate with encapsulated laccase and the mechanism of mediated ORR [231].

49

Nazaruk *et al.* demonstrated that lyotropic liquid-crystalline cubic phase is a biocompatible material for ABTS^{2-} and Lc embedding [160]. In order to increase the surface area and improve the electrical conductivity and stability of the biocathode, SWCNTs were introduced [232, 233]. CNTs and graphene are excellent materials for ABTS^{2-} immobilization due to π–π interactions [192, 196, 234-236]. In an attempt to exploit this feature the authors modified the surface of the CNTs with ABTS^{2-} via adsorption. Glassy carbon was modified with such SWCNTs separately, and then covered with a cubic phase with entrapped Lc (*Cerrena unicolor*) [232]. Opallo's group utilized encapsulated MWCNT in sol-gel matrix [236] and VACNT [234] for ABTS^{2-} adsorption. After Lc immobilization these electrodes exhibit bioelectrocatalytic activity towards ORR [234, 236]. Similar strategy was proposed by Karnicka *et al.* with Nafion used for encapsulation [235]. The ABTS^{2-} can be also attached to the SWCNTs via covalent binding (Fig. 6.5) [232, 233]. Such modified CNTs were also employed as mediator in biocathodes [232, 233, 237].
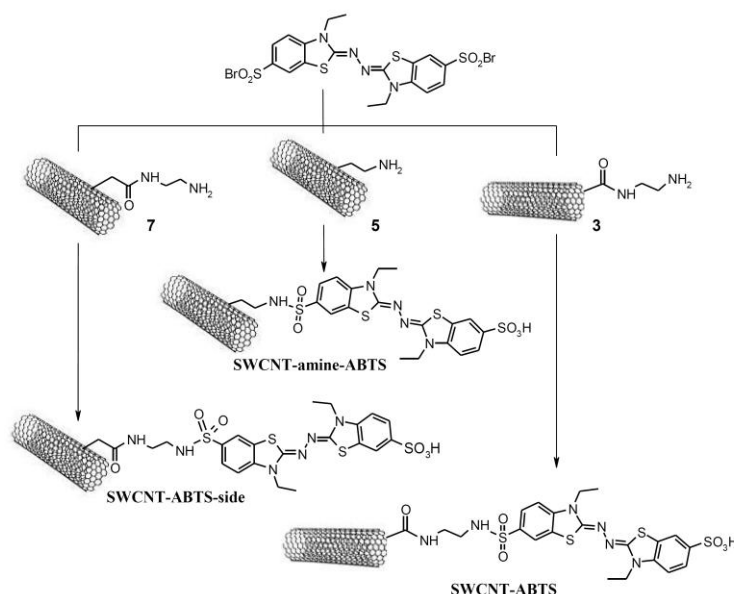
Fig. 6.5 Schematic illustration of three routes for SWCNTs covalent modification with ABTS residues [233].

Conducting, biocompatible polymers, such as polypyrrole, are also widely used for Lc and ABTS^{2-} entrapment at the electrode surface [238, 239]. Such polymer films of controlled thickness reveal good electrical conductivity, polycationic nature, water

50

solubility of its monomer. They were applied for simultaneous entrapment of the enzyme and mediator by electrodeposition on the glassy carbon electrode [238, 239].

Recently Cosnier *et al.* proposed a cheap, fast and simple method for immobilization of Lc and $ABTS^{2-}$ by mechanical compression with graphite particles [240]. Such electrode was additionally covered by Nafion to avoid leakage of the hydrophilic mediator. The assembled enzymatic BFC based on that electrode revealed good stability: after operating for a week it lost only 18-20% of its activity [240]. That result shows that such strategy is effective and can be an important step towards the development of more stabile biofuel cells. The same group also presented another stable mediator-based biocathode. $ABTS^{2-}$ was intercalated within layered double hydroxides particles [241]. Finally these particles were positively charged which allowed utilizing the electrostatic interactions with negatively charged SWCNTs to immobilize Lc. The use of SWCNTs and electroactive nanohybrid materials improved the current density of the electrode for ORR (ca. 100 $\mu A\ cm^{-2}$) [241], but not enough for applying successfully that electrode as biocathode in biofuel cell.

6.1.1.2.   Bilirubin oxidase-biocathode

Bilirubin oxidase exhibits better biological activity and affinity towards the substrate than laccase [154]. However, one can find in the literature fewer reports about biocathodes modified with BOx and $ABTS^{2-}$ than for Lc.

Tingry *et al.* entrapped $ABTS^{2-}$ and BOx onto porous carbon covered with electropolymerized polypyrrole films (Fig. 6.6) [242]. The obtained material is uniform and conducting [242]. However, this method did not allow varying the amount of immobilized enzyme.

51
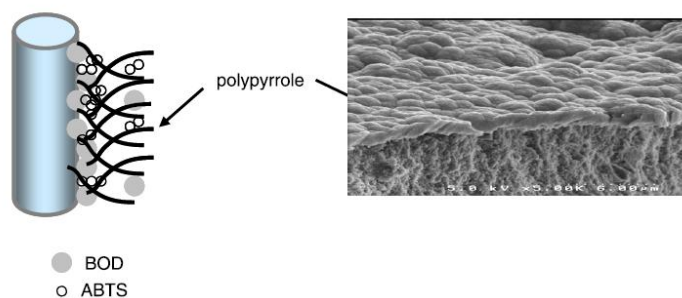
Fig. 6.6 Schematic view of the polypyrrole-ABTS^{2-}-BOx based biocathode and SEM image of the polypyrrole deposited at the electrode surface [242].

In other study the same authors utilized a matrix of the microporous carbon material Vulcan and Nafion for mediator and enzyme immobilization at the porous carbon electrode [243]. Such modification has great positive impact on proton transfer in the vicinity of the electrode. Moreover, the presence of the carbon material increases the active surface area and enhances the electrical conductivity. Hence, that biocathode exhibits better performance, such as higher current density and lower overpotential, as compared to a polypyrrole film based biocathode [242], and was propitiously applied in a hybrid biofuel cell [243]. Recently, another avenue for achieving highly efficient ABTS^{2-}-BOx-based biocathodes was presented by Hussein *et al.* It involves the application of BOx-decorated buckypaper-based nanostructured electrodes [244] and the current density exceeds that of recently reported on carbon-based BOx biocathode [243, 245].

Lately, graphene has been employed for fabrication of a mediator-based biocathode [192]. The BOx and ABTS^{2-} were co-immobilized with graphene, using a silica sol-gel matrix at a gold electrode. The resulting electrode has successfully been applied in the membraneless biofuel cell [192].

6.1.2. Biocathode based on mediatorless electron transfer

A good electrical contact between the redox center of the enzyme and the electrode is a crucial factor for obtaining highly efficient and stable electrodes for biofuel cells. This may be achieved by enforcing proper orientation of the enzyme towards the conductive substrate and thereby shortening the distance between the active site (T1 of multicopper oxidases) and the electrode's surface [122, 142]. Other key issues are the enzyme's

52

stability and well developed electrode surface area, both of which can be achieved by immobilizing enzymes on a proper material utilizing various nanomaterials.

As has been mentioned in Chapter 4 Lc and BOx catalyse the four electron electroreduction of oxygen to water [138, 142] and therefore have found wide application as biocatalysts in various researches aiming to obtain a biocathode for biofuel cells [118-120, 122, 222, 230].

The pioneering work in mediatorless bioelectrocatalysis of oxygen to water was done by Tarasevich *et al.* in the late seventies of the 20th century [246, 247]. They proposed to use nanostructured carbon electrodes as laccase-adsorbent and electro-conducting material at which he was able to achieve a substantial current density of 1 mA cm^{-2} [248]. Since that time an abundance of similar papers can be found with the majority of them describing biocathodes constructed to employ BOx, Lc or copper eflux oxidase (see for example [249, 250]) as biocatalysts for ORR. The next two subsection concerns biocathodes modified with Lc or BOx exhibiting mediatorless catalysis.

6.1.2.1.   Laccase-biocathode

Laccase adsorbed on smooth electrodes like bare and thiol modified gold [142, 251, 252], and carbon-based ones exhibits direct electron transfer towards oxygen reduction [142]. Efficient mediatorless bioelectrocatalysis with laccase was also noticed on electrodes composed of carbon materials like carbon black [253], mesoporous carbon [254], mesoporous carbon aerogel [255], colloidal carbon [256], or multilayered carbon nanoparticle-silicate particle film [87].

The mechanism of electron transport within the laccase depends on the electrode material applied [142]. The T1 center of Lc is responsible for accepting electrons at carbon-based electrodes, while at gold ones though it is the T2 center that plays that role (Fig. 6.7) [142].

(A)   **(B)**
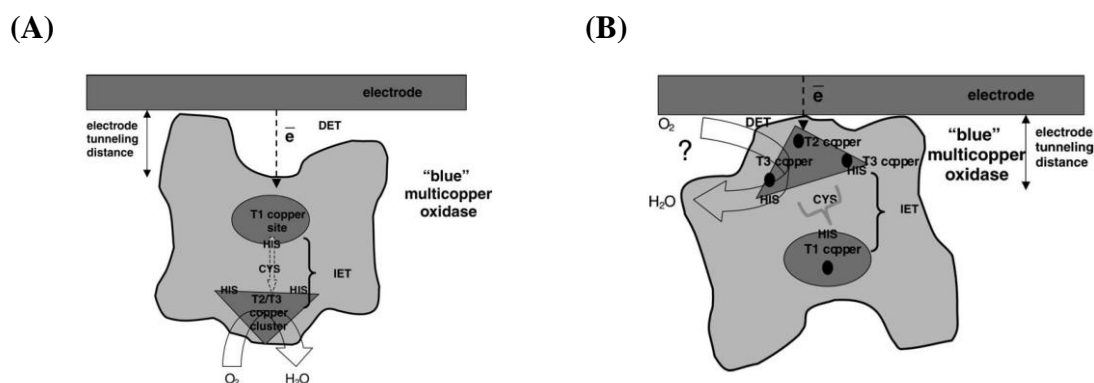
Fig. 6.7 Schematic illusitration of direct electron transfer from (A) T_1 to the surface of carbon electrode (B) T_2 to the gold surface electrode [142].

Multi-walled [2, 257] and single-walled carbon nanotubes [186, 258-260] or graphene sheets [191] films were also found to be suitable promoters of the mediatorless oxygen electroreduction. For example non-covalently (pyrene sulfonated [259]) and covalently (arylated [260]) functionalized SWCNTs-modifed electrode enhance the bioelectrocatalysis. Moreover, electrodes modified with multilayer films of Lc (*Trametes versicolor*), poly-L-lysine (PLL) and MWCNTs [204] or with Lc (*Cerrena unicolor*), and vertically aligned pyrene-functionalized carbon nanotubes facilitates DET of ORR (Fig. 6.8) [234]. Recently, an interesting study has shown that laccase immobilized on directly grown SWCNTs via liquid induced shrinkage provides an outstanding catalytic current density of up to 4 mA cm^{-2} [1].

Laccase adsorbed on gold nanoparticulate electrode also exhibits mediatorless ORR electrocatalysis [261, 262]. For example Dong *et al.* constructed an electrode modified with a gold nanoparticles (GNP) and Lc multilayered film whose highest achieved value of current density was 0.8 mA cm^{-2} but the onset potential of ORR was about 0.2 V lower [261] compared with other gold materials [262]. However, the addition of GNP to a carbon felt electrode modified with a composite film which consisted of partially sulfonated (3-mercaptopropyl)-trimethoxysilane sol–gel, Lc and chitosan enabled to obtain large current density (4.5 mA cm^{-2}) and decrease the overpotential by 0.24 V [263].

54

(A)

(B)
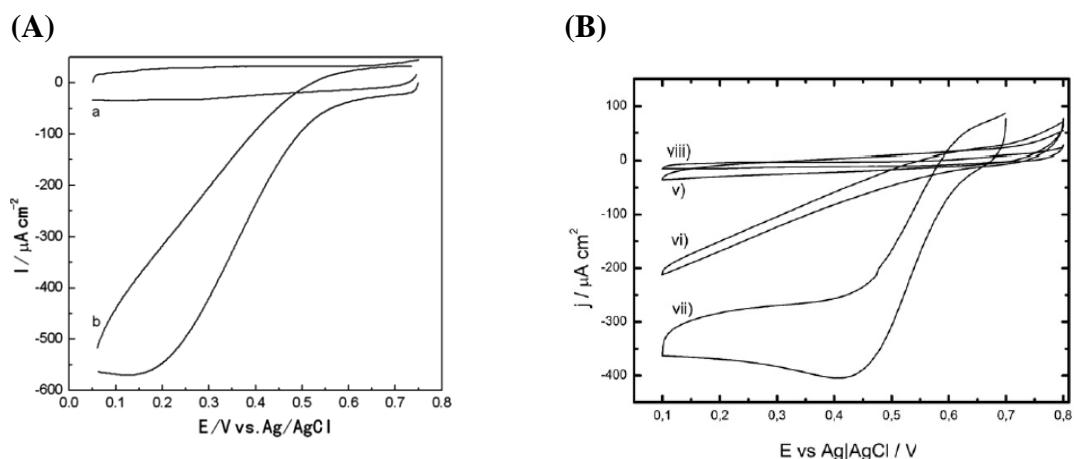
Fig. 6.8 Voltammetry at (A) the multilayered film of MWCNTs, PLL and Lc on ITO electrode in (a) deareated and (b) air saturated PBS (pH 6) [204] and (B) the VACNTs modified with (v) Lc, (vi) MTMOS/Lc, (vii) PSA/MTMOS/Lc in O_2-saturated McIlvaine buffer (pH 4.8) and (viii) MTMOS/Lc in deaerated buffer [234].

Another challenge is to improve the performance of biocathodes by enforcing the proper enzyme orientation towards the electrode surface. Hitherto a few surface modification techniques of carbon [264-266] and gold [143, 267, 268] have been proposed. Some of these electrodes exhibit the superior properties such as high magnitude and long-term stability of the current response [264, 265], low overpotential of ORR [267] and resistance to chloride anions [268].

Lately, another approach for creating efficient biocathodes has emerged based on gas-diffusion electrodes [269-271]. Although, oxygen is abundant in the environment, it exhibits poor aqueous solubility and a small diffusion coefficient in aqueous solutions. As a result its transport to the electrode surface is often a rate-limiting step in the bioelectrocatalysis of ORR [272]. Therefore it is essential, to design materials that are both oxygen permeable and hydrophobic, allowing them to serve as membranes making oxygen from the gas phase access the biocatalyst [269-271]. Atanassov *et al.* made a two-layered biocathode (known also as *an air-breathing biocathode*) that comprised of a mixture of teflonized carbon and untreated carbon black with adsorbed laccase as a hydrophic gas diffusion layer and hydrophilic biocatalytic layer, respectively (Fig. 6.9) [270]. This electrode exhibits high current

55

density up to 1 mA cm^{-2}, low overpotential for the ORR and increased stability up to one month [270].
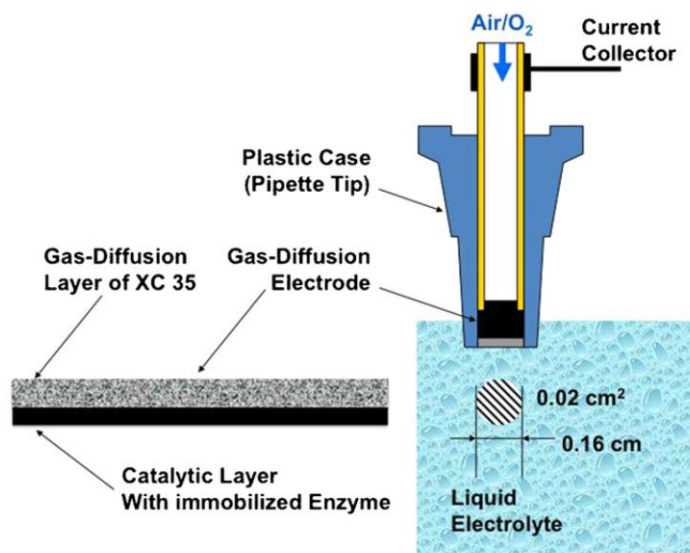
Fig. 6.9 A schematic illustration of Lc-based air-breathing biocathode [270].

6.1.2.2. Bilirubin oxidase-biocathode

It is known that electrodes modified with BOx quite often promote direct electron transfer between the electrode surface and enzyme's active center. A sophisticated approach for preparation efficient biocathodes was presented by Willner *et al.* [273]. The procedure is based on the electropolymerization of BOx and platinum nanoparticle composite crosslinked by means of oligoaniline bridges onto a roughened gold electrode (Fig. 6.10). The obtained high current density (ca. 1 mA cm^{-2}), and an onset potential of 0.72 V vs. NHE of ORR clearly indicate that such electrode modification significantly enhances the bioelectrocatalytic process [273]. The application of gold nanoparticle modified electrodes for adsorption bilirubin oxidase was also successfully conducted by Ohno *et al.* (the current density reaches ca. 0.5 mA cm^{-2}) [274].

56
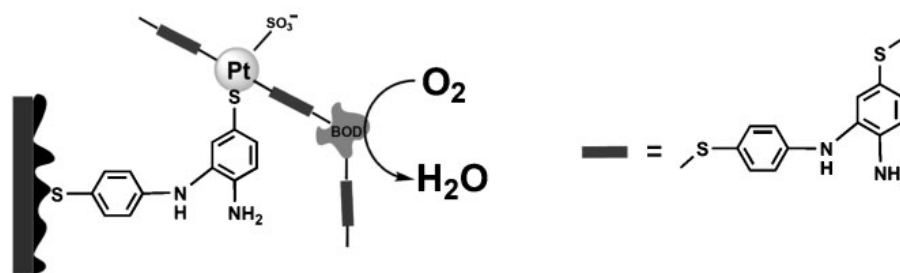
Fig. 6.10 Schematic presentation of ORR catalyzed by electropolymerized BOx and platinum nanoparticles composite crosslinked by means of oligoaniline bridges onto a roughened gold electrode [273].

Carbon-based electrode materials has proven to provide favourable conditions for direct electron exchange with BOx [142, 275, 276], and for mediatorless oxygen reduction bioelectrocatalysis [247, 276-280]. The electrode materials from that group tested so far includes different forms of graphite [142, 275-278], porous carbon [281], carbon ceramic electrode enriched with carbon nanoparticles [203], carbon nanotubes [257, 275, 278-280], nanostructured sol–gel/carbon nanotube composite electrodes (Fig. 6.11) [181, 282], pyrene-functionalized CNTs [181, 257] or multilayered gold-carbon nanoparticulate films [86].
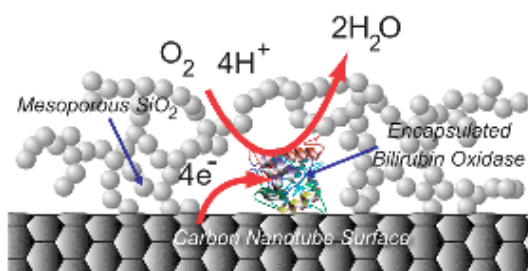
Fig. 6.11 Schematic presentation of ORR catalyzed by BOx encapsulated in nanostructured sol–gel/carbon nanotube composite electrode [282].

This application of new carbon-based nanomaterials, driven by their good electrical conductivity and biocompatibility, has a great impact on the design of new platforms for enzyme immobilization [184]. Recent Mano's and Tsujimura's studies have shown that three dimensional and highly porous materials increase electroactive surface area and enzyme loading. The authors propose to use carbonaceous

57

micro/macrocellular foams [206] as the biocathode and carbon aerogel [255] as bilirubin oxidase adsorbent and electroconductive material to utilize observed properties of these nanomaterials. The obtained current densities for these electrodes are high (2.1 mA cm^{-2} [206] and 3.5 mA cm^{-2} [255] at 1000 rpm) but better mechanical stability was reported for the first one. Recently the efficient bioelectrocatalysis (ca. 1.2 mA cm^{-2} current density and 0.74 V vs. NHE the onset potential of ORR) was also reported for single-walled carbon nanohorn-modified carbon fiber microelectrodes with adsorbed BOx [283].

Additionally, improvement of BOx based biocathodes' performance was achieved with air breathing electrode [203, 284]. However the highest current density was reported for copper efflux oxidase (20 mA cm^{-2}) [250]. Unfortunatly, the onset potential of ORR is too negative to apply this electrode in BFC.

It can be concluded that the diversity of the nanomaterials that might be potentially utilized for mediatorless biocathodes is large, through metal nanoparticles to various types of carbon-based nanomaterials. Most of this research was done in paralell to the research presented in this thesis.

6.1.3. Enzymatic fuel cell based on mediatorless electron transfer

Some of the biocathodes have been successfully applied in various types of BFC [1, 261, 263, 273, 283]. However, keeping in mind that BFCs might be applicable as *in vivo* power sources, BOx is a more preferable biocatalyst than laccase. Even though the overpotential decrease of oxygen reduction is smaller than that of high potential laccase, its superiority to Lc manifests in activity under simulated physiological conditions (at neutral pH and in the presence of chloride anions) [154, 247, 277, 285]. However, still the main drawback of BOx is its high cost, leading to continued research in aimed at improving laccases' properties. Only a few ways for improving its stability in the presence of inhibitors (mainly Cl^{-}) have yet been presented [268, 286]. The authors demonstrated that Lc (*Trametes hirsute*) covalently bound to an electrochemically modified graphite electrode [268] or incorporated into an optimized Os-complex modified hydrogel [286], was not inhibited in presence of Cl^{-}.

Apart from Cl^{-} other blood components like ascorbic acid (AA) and urate [287] could also disturb biofuel cell operation *in vivo*. In order to avoid it, additional enzyme – ascorbate oxidase (AaOx) [278] or ion selective membrane made of cubic phase [287]

58

were sucessfully applied, respectively. In the first case, the AaOx is immobilized on both SWCNT modified carbon fibers microelectrodes along with GOx and BOx, suppressing its electrochemical oxidation. In the artificial serum the maximum power density for such glucose/O_2 biofuel at 0.35 V equaled 35 μW cm^{-2} [278]. Although this performance is poor it can operate in artificial serum. Also the BFC based on spectrographic graphite electrodes with adsorbed BOx and cellebiose dehydrogenase was tested in human serum [288]. However, the electrical contact between the active centre of the enzyme and the electrode should be definitely improved. An example of biofuel cells in which such a problem was circumvented, were presented by Nishizawa's [1] and Cosnier's [2] groups. The first group employed directly grown SWCNTs with immobilized Lc and fructose dehydrogenase, separately, through liquid-induced shrinkage [1]. The second group used pellets as biocathode and bioanode fabricated by mechanical compression of MWCNTs and appropriate enzymes (Lc and GOx together with catalase that decompose harmful hydrogen peroxide) (Fig. 6.12) [2]. The first biofuel cell reached by far the highest power density (1.8 mW cm^{-2} at 0.45 V in pH 5) [1]. The second one that was tested under physiological conditions delivered power density of up to 1.3 mW cm^{-2} at 0.6 V [2].
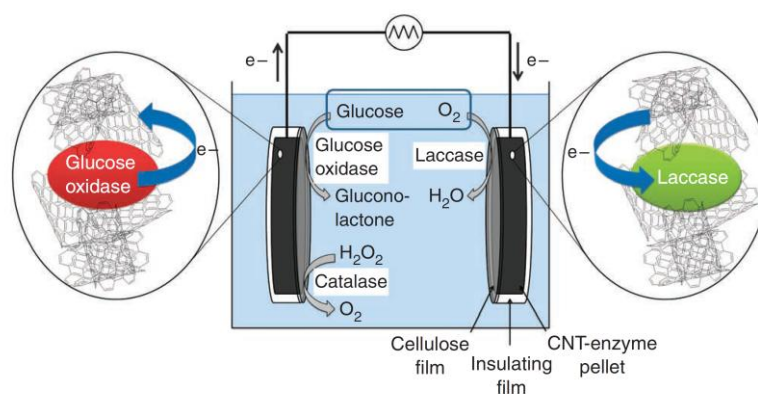
Fig. 6.12 Schematic illustration of the oxygen-glucose enzymatic biofuel cell based on MWCNTs biocathode and bioanode with immobilized laccase and glucose oxidase with catalyse, respectively [2].

Another interesting example of carbon-materials based enzymatic BFC was reported by Zhang *et al.* They utilized graphene, as a conductive material and a platform for enzymes (GOx and Lc) immobilization [191]. Even though the efficiency of such

glucose/O_2 biofuel cell is meager (57.8 μW cm^{-2}, 0.22 V) such approach could be perspective for future development of novel carbon-based nanomaterials BFC device.

6.1.4. Zinc-O_2 hybrid cell

The concept of zinc-oxygen hybrid cell as alternative of oxygen-glucose biofuel cell was proposed by Heller [289]. It consists of a miniature of a Nafion-coated Zn anode [290] and a biocathode for oxygen reduction (Fig. 6.13) [289, 290].
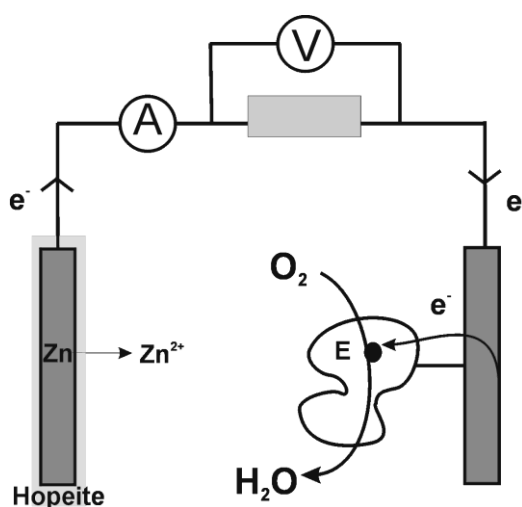
Fig. 6.13 A schematic illustration of Zn-O_2 hybrid cell that consists on Zn wire covered with hopeite as an anode and a biocathode with attached enzyme (E) that catalyses the reduction of oxygen to water.

During discharging in physiological saline buffer solution, the Nafion-coated Zn anode is overgrown by lamellar polymer called hopeite [$Zn_3(PO_4)_2 \cdot 4H_2O$] [290]. Its structure protects Zn wire against the corrosion by blocking the transport of oxygen, while preventing Zn^{2+} dissolution. A hybrid cell based on Zn anode provides one of the utmost negative potential (E^0 = -0.76 V vs. NHE [291]) so its operating voltage is larger than typical biofuel cell. Recent studies have already demonstrated possible Zn-anode's combinations with biocathodes modified with multicopper oxidases [181, 203, 234, 260, 264, 289, 292-295] and horseradish peroxidase [185]. Diverse materials such as a conductive ink [292], functionalized CNTs [181, 234, 260, 295], graphitized carbon cloth [294], carbon particles [203] and ITO nanoparticles [293], were utilized for biocathodes preparation. The highest power density so far (above 1 [264] and 2 mW cm^{-2} [260]) were obtained with laccese modified cathodes. The graphite

60

covalently modified with 4-[2-aminoethyl] benzoic acid [264], and glassy carbon electrode coated with arylated (covalently modified with anthracene or anthraquinone) SWCNTs and coated with a layer of neutralized Nafion [260], were used there as a support for laccase. In terms of operating voltage (1.5 V) the Zn-oxygen hybrid cell proposed by Zloczewska *et al.* [234] is superior at the moment. These authors applied vertically aligned pyrene-functionalized carbon nanotubes embedded in hydrophobic matrix for enzyme's immobilization [234].

Recently Feraponotova group proposed a stable Zn-oxygen hybrid cell with a biocathode made of a graphitized carbon cloath with immobilzed Lc that was able to power a 1.5 V domestic device for 38 days [294].

However the performances of all these hybrid cells have yet not been tested in artificial serum.

The Zn-oxygen hybrid cells construction is also described in this PhD thesis.

6.2. Electrochemical biosensing

According to IUPAC's definition, an electrochemical biosensor is a self-contained integrated device that provides specific quantitative or semiquantitative analytical information based on the recognition system utilizing a biochemical reaction [296]. Here this mechanism is a conversion of substrate in enzymatic reaction involving electron transfer reaction of immobilized redox protein. These reactions allow for transformation, via electrochemical transduction element, of concentrations of substrates into an electrical potential (potentiometric) or current signal (amperometric). Then signal is amplified, processed and then is ready for further use (like displaying in a user-friendly fashion or transmision to some other system as one of the input signals) (Fig. 6.14) [121, 296, 297].
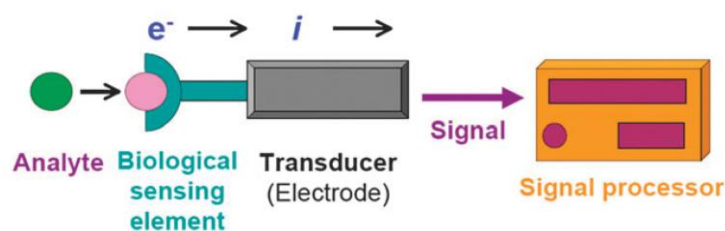

Fig. 6.14 A schematic presentation of electrochemical biosensor [297].

61

The glucose biosensors are the most widely studied class of biosensors since there is constant demand for diabetes control [117]. The amperometric glucose sensors based on the most resistant enzyme glucose oxidase (GOx) have played a leading role in the entire biosensors market. Distinctive advantages of such devices are: low cost of production, disposability of electrodes, reproducibility, simplicity and compactness of the measuring instruments [117, 157, 158, 298]. The biomolecules' intrinsic, high selectivity and sensitivity outweigh their low stability as compared to inorganic catalysts [157]. Additionally, biomolecules' stability is increased by employing various techniques for their immobilization [2, 136, 160, 167, 168, 200, 299, 300].

The first biosensor based on glucose oxidase was reported by Clark and Lyons in 1962 [5] and since that time there is extensive development of biosensors based on redox proteins. Desired features of such devices are stability, efficiency and exhibition of direct electron transfer (leading to lower cost as no mediator is needed). Therefore the application of nanomaterials − such as carbon nanotubes [12, 13, 29], graphene sheets [13, 49, 189] or nanoparticles [301] which are known for their good electrical conductivity, well developed surface and are capable of immobilizing various redox proteins − could have a significant impact in developing such devices. It has to be emphasized that good applicable biosensor should not only be tested with aqueous buffer but first of all with biological samples. Furthermore the components from which it is made should be biocompatible [302]. Some already published biosensors-based articles are trying to fulfill all these criteria with various successes [298, 303, 304].

Since electrodes based on GOx and Mb, which catalyze glucose oxidation and hydrogen peroxide reduction, were constructed as part of this PhD thesis a review of these electrodes is presented.

6.2.1. Glucose biosensing

Diabetes mellitus is a serious health problem around the world that might trigger off heart disease, blindness and kidney failure. So far its management often relies on periodically controlling concentration of the glucose in the bloodstream. Therefore, the development of new biosensing device for continuous monitoring and assay glucose's is extremely important [157, 158, 298].

The amperometric glucose biosensors are categorized into three generations depending on the mechanism of electron transport in which the natural secondary

62

substrate (first), artificial redox mediator (second) and direct electron transfer (third) are used (Fig. 6.15) [158]:

- First generation sensors are based on the use of natural oxygen as a cosubstrate and detection of generated hydrogen peroxide that is presented via following reactions and at the Fig. 6.15A [305]:

$$\text{Glucose} + \text{GOx-FAD} \rightarrow \text{gluconolactone} + \text{GOx-FADH}_2 \qquad (6.1)$$

$$\text{GOx-FADH}_2 + O_2 \rightarrow \text{GOx- FAD} + H_2O_2 \qquad (6.2)$$

$$H_2O_2 \rightarrow 2e^- + O_2 + 2H^+ \qquad (6.3)$$
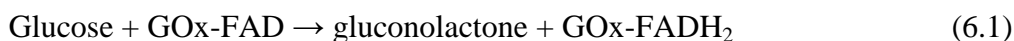
The concentration of oxygen in physiological fluid is substantially lower then the glucose that results in a fluctuation in the oxygen concentration causing so called "oxygen deficit". Although this type of biosensors is simple, still its main drawbacks are the oxygen problem mentioned above, and the denaturation of enzyme by hydrogen peroxide.

- Second generation sensors replaces oxygen as (natural) cofactor with artificial mediators (M) (Fig. 6.15B) [306]:

$$\text{Glucose} + \text{GOx-FAD} \rightarrow \text{gluconolactone} + \text{GOx-FADH}_2 \qquad (6.4)$$

$$\text{GOx-FADH}_2 + M_{(ox)} \rightarrow \text{GOx- FAD} + M_{(red)} \qquad (6.5)$$

$$M_{(red)} \rightarrow M_{(ox)} + ne \qquad (6.6)$$

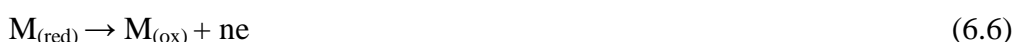The most often applied diffussional mediators for GOx are: ferrocene derivatives [307], ferricyanide [308], conducting organic salts (tetrathiafulvalene-tetracyanoquinodimethane) [309], quinone compounds [308] and dyes [310], tetrathiafulvalene [311], transition-metal complexes [157], and phenothiazine and phenoxazine compounds [157]. A significant disadvantage of these biosensors is the possibility of mediator leaking from the electrode's surface. Several approaches to avoid this problem have been proposed as: applying a nondiffusional mediator-tethered complexes of $Os^{2+/3+}$ redox center stabilized by ligands attached to polymer backbone [223], covalent attachment of mediators groups e.g ferrocene to the redox center of GOx [312] or

63

employing nanomaterials such as vertically alligned CNTs [167, 168] or gold nanoparticles [299] as an electrical connector between the enzyme's redox center and electrode's surface.

- Third generation sensors are based on direct electron transfer between the enzyme (GOx) and the electrode surface (Fig. 6.15C):

$$Glucose + GOx\text{-}FAD \rightarrow gluconolactone + GOx\text{-}FADH_2 \qquad (6.7)$$

$$GOx\text{-}FADH_2 \rightarrow GOx\text{-}FAD + 2e^- + 2H+ \qquad (6.8)$$

The transport of electrons might occur via conducting polymer such as a polypyrrole [313] and various nanomaterials such as carbon nanotubes [167] or metal nanoparticles [301]. This type of biosensor is currently the leading one and is the most prospective of all three generations.
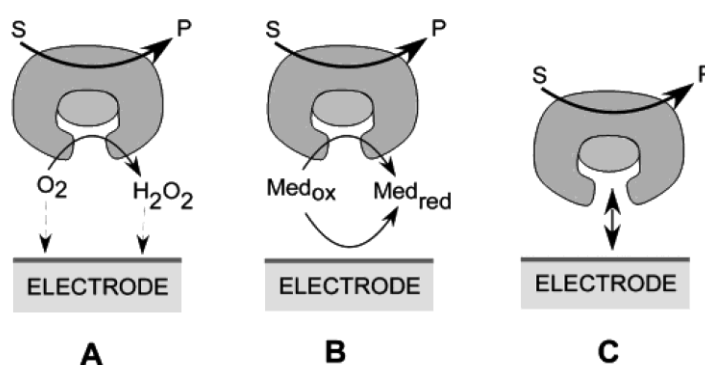
Fig. 6.15 A schematic illustration of the (A) first (B) second and (C) third generations biosensors depending on the mechanism of electron transport [158].

Most of these biosensors are based on electrochemical assays with glucose oxidase, glucose dehydrogenase or cellobiose dehydrogenase, as a biological recognition element [117]. The GOx is mainly applied due to its biochemical stability and the exhibition of direct electron transfer. Moreover, the glucose dehydrogenase does not require an oxygen cofactor and is therefore more desirable for construction of the third generation biosensors [117, 158]. Also a proper enzyme's immobilization might improve such biosensors performance in terms of its stability. Many immobilization techniques of GOx immobilization onto various carbon nanomaterials have been developed in the past years such as layer-by-layer assembly [136], mixing in a carbon

64

paste [200], and adsorption from the enzyme solution onto boron-doped carbon nanotubes [314], SWCNTs [315], MWCNTs [316], graphene sheets [70].

It is also worth mentioning another approach to glucose assaying – the bienzymatic glucose biosensor [317-319]. All biosensors from this family consist of two enzymes (HRP and GOx) which are covalently immobilized onto e.g. carboxylic-derived MWCNTs [319]. This example functions in the following way: GOx catalyses the oxidation of glucose in the presence of oxygen as a natural cosubstrate. Hydrogen peroxide generated in that enzymatic reaction engages in a reaction with HRP and aniline and as a result polyaniline (PANI) is formed (Fig. 6.16) [319]. Subsequently square wave voltametry is used to measure PANI peak current which corresponds to initial glucose concentration. The main advantage of such systems of that class is the possibility to detect glucose at very low applied potentials where the noise level and amount of the interfering compounds is negligible [318].
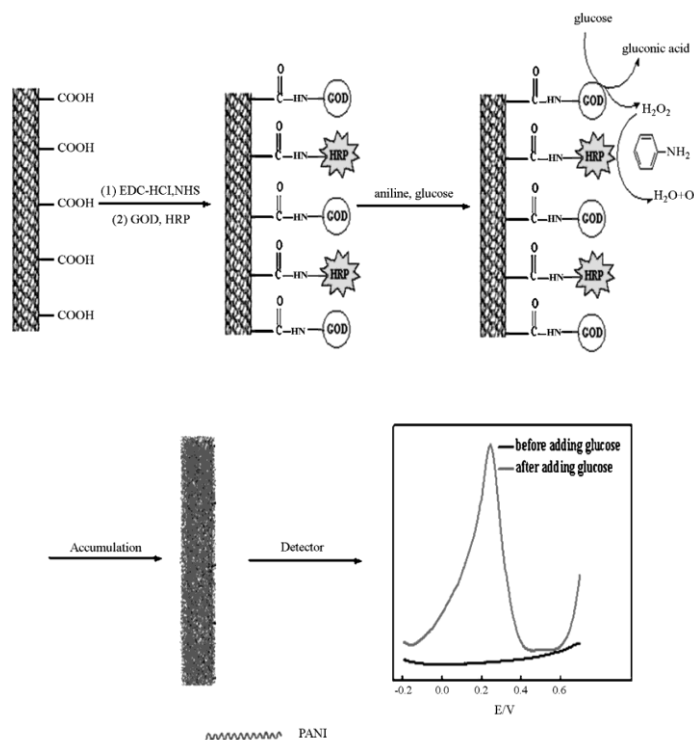

Fig. 6.16 Schematic illustration of glucose biosensor based on bienzyme-catalyzed deposition of PANI on MWCNTs in which the detection of glucose occurs via measurment of the PANI peak current [319].

65

6.2.2. Hydrogen peroxide biosensing

The hydrogen peroxide biosensors have found wide application in electroanalysis or biomedical diagnostics e.g in DNA hybridization assays [320], immunoassays [210], construction of bienzymatic biosensors [317-319] and biofuel cells [2, 173, 185, 321, 322]. The enzymes from peroxidase group catalyze the reduction of H_2O_2 to water and are often used, as a tags or additional biocatalysts in the glucose biosensors [317]. They are also used for bioanode modification in the biofuel cell to decompose H_2O_2 [2, 322], where H_2O_2 is the product of the reactions catalyzed by a large number of oxidases. They may be applied as biocatalysts at the biocathodes to reduce oxidant (H_2O_2) [173, 185]. The most popular redox proteins employed as hydrogen peroxide reduction reaction biocatalysts are heme proteins e.g: Cyt *c* [175], Cat [199], horseradish [174] or soybean [323] peroxidases, Mb [174] and Hb [324]. Recently extensive development of carbon-based nanomaterials has been observed, that has sparked new ideas like enzymes immobilization and their application in constructing third generation biosensors' for hydrogen peroxide [71, 164, 173, 174, 209, 325-327].

He *et al.* developed an electrochemical biosensing platform for hydrogen peroxide based on carbon-based nanomaterials [324]. The authors applied a room temperature ionic liquid functionalized graphene for hemoglobin immobilization at carbon ceramic electrode (Nafion/Hb-IL-GR/CCE). Such graphene based nanocomposite electrode promote the direct electron transfer of hemoglobine's heme Fe(III)/Fe(II) couple and retains enzyme's bioelectrocatalytic activity for the reduction of H_2O_2 to water [324]. The demonstrated biosensor showed good response towards the detection of H_2O_2 with a fast response time, wide linear range, high sensitivity and good reproducibility and is a promising one to develop the graphene-based third generation biosensors [324]. Its performance is batter than that of other carbon materials-based electrodes, such as carbon nanotubes [328], carbon nanoparticles [209] or carbon black [329].

Rusling group applied highly oriented SWCNT forests and iron heme enzyme for detection of H_2O_2 [174]. The authors covalently linked Mb and HRP separately, to the untethered ends of stable SWNT forests assembled on pyrolytic graphite electrode [174]. Voltammetric studies of Mb and HRP immobilized on the premodified PG electrode show quasi-reversible redox behaviour for Fe(III)/Fe(II) and demonstrate

66

their bioelectrocatalytic activity in the presence of H_2O_2. The biosensor is easy to fabricate, exhibited high stability, long linearity and the limit of detection lower then on the other carbon nanomaterial like: vertically aligned CNT forests [330] or graphene based nanocomposite electrode [71] with attached Mb, for the detection of H_2O_2. Moreover it offers new promising approaches for the development of biosensors on the nanometer scale such as multielement nanobiosensor arrays [174].

Also the Mb adsorbed onto bicontinuous gyroidal mesoporous carbon modified CCE exhibits direct electron transfer and electrocatalytic activity towards H_2O_2 reduction reaction. The authors demonstrate that good sensitivity of the obtained electrode is due to mesoporous character of carbon material which makes it a suitable enviroment for Mb immobiliaztion [331].

The catalase adsorbed on a nanocomposite film consisting of amine functionalized graphene and gold nanoparticles modified glassy carbon electrode, also exhibits direct electron transfer of heme couple and sensitivity towards the bioelectrocatalytic reduction of H_2O_2 [199]. The Cat based electrode combined with glucose oxidase enables a development of efficient bioanode. Recently, an interesting example, of such a setup for fabrication of functional and implanatable, glucose biofuel cell was presented by Cosnier's group [322]. The obtained bioanode contained a mixture of graphite, ubiquinone (mediator), GOx and Cat. The role of catalase in that system is to decompose the produced H_2O_2 in the side reaction of GOx with O_2 [322].

67

GOAL

The main aim of this thesis is the preparation and characterization of electrochemical properties of carbon nanoparticulate film electrodes. These are applied for bioelectrocatalytic reactions such as oxygen reduction, hydrogen peroxide reduction and glucose oxidation. The thesis focuses on immobilization of carbon nanoparticles onto electrode surfaces via the application of various methods like sol-gel processing, layer-by-layer assembly, and electrodeposition assisted by a three-phase junction. The intention of these studies is to utilize the generated platforms for immobilization of redox proteins such as laccase, bilirubin oxidase, myoglobin and glucose oxidase, through adsorption or encapsulation. The final objectives are to examine the efficiency of the carbon nanoparticulate enzyme-modified electrodes, their stability, and potential applicability in power generation or biosensing.

Experimental

7. Methods

In this thesis mainly the electrochemical techniques (cyclic voltammetry, chronoamperometry and chronopotentiometry) were applied for studying electrochemical properties of carbon nanoparticulate film ITO with or without adsorbed enzymes. Additionally, the optical profilometry, spectroscopy (electrochemical impedance spectroscopy, infrared spectroscopy) and microscopy (scanning electrochemical microscopy, scanning electron microscopy and atomic force microscopy) methods were employed for characterizing these electrodes.

A summary of these methods is presented in this chapter.

7.1. Cyclic voltammetry

Cyclic voltammetry (CV) provides essential information about the thermodynamics of electrode process such as the redox potential, kinetics of heterogeneous and catalytic reactions, coupled chemical reaction and adsorption processes [291]. One can also obtain information regarding qualitative and quantitative composition of the studied system. For these reasons it has been utilized in this research.

A potentiostat is required for performing cyclic voltammetry in three-electrode cell. It maintains a constant, predefined potential between the working (WE) and reference (RE) electrodes by enforcing a flow of electric current between the counter and working electrodes.

In a cyclic voltammtery experiment the potential of the working electrode varies linearly in time with rate, called scan rate (Fig. 7.1A). The polarization of the working electrode starts with the initial potential (E_i) at which the electrode reaction does not run and the measured current is the capacitive current only. Then, the potential is gradually changed to the values at which the reduction and oxidation processes occur until it reaches the end potential (E_e).
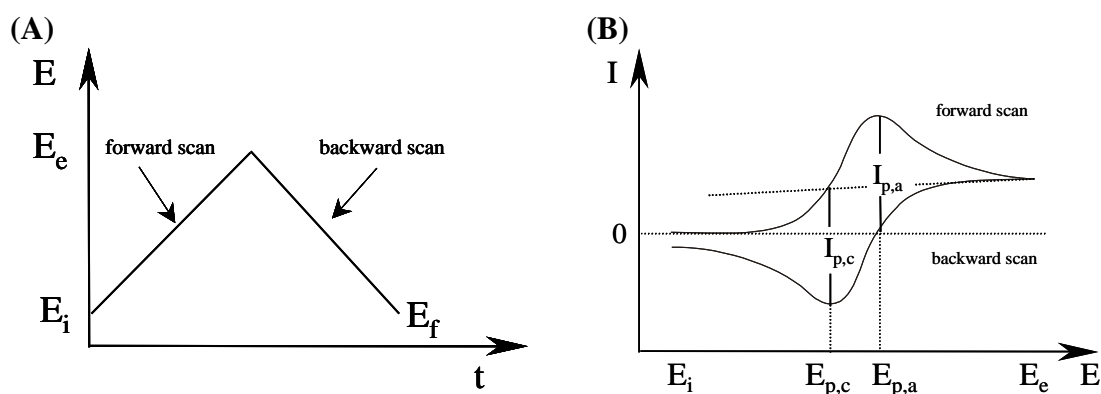
Fig. 7.1 (A) Plot of the potential program applied in CV, (B) resulting cyclic voltammorgam [291].

The relation between current and polarization potential depends, on the rate of the charge transfer process, and the rate of the diffusion of electroactive species towards the electrode surface. In case of a reversible process, in which the rate of the electrode reaction is controlled by the rate of the diffusion, on the cyclic voltammogram the oxidation and reduction peaks are developing with the difference of peak potential equaling 57/n mV at 25 °C (Fig. 7.1B). The value of the cathodic or anodic peak currents depends on the concentration of electroactive species in the solution C^* (mol cm^{-3}), its diffusion coefficient D (cm^2 s^{-1}), the projected area of the electrode A (cm^2), the number of transferred electrons n and the scan rates v (V s^{-1}). In the case of linear diffusion at 25 °C that dependence is described by the Randles-Sevcik equation [291]:

$$i_p = (2.69 \cdot 10^5)n^{2/3}AC^*D^{1/2}v^{1/2} \tag{7.1}$$

In the case where redox species such as redox active protein, is adsorbed on the electrodes surface the i_p varies linearly with the scan rate and is described by the following equation [291]:

$$i_p = \frac{n^2 F A \Gamma_T v}{4RT} \tag{7.2}$$

where F is Faraday's constant (96 487 C mol^{-1} of electrons), Γ_T is the total surface concentration of electroactive species (mol cm^{-2}), R is the gas constant and T is temperature in Kelvins.

72

If the studied reaction is a surface controlled process, it is predicted that on cyclic voltammogram the oxidation and reduction peaks are developing with the difference of peak potential and the width at half height equal zero and 90.6/n mV at 25 ºC, respectively. The total concentration of adsorbed molecules can be estimated from the charge integration (Q in Coulombs) of each peak in cyclic voltammogram, given by Faraday's law [291]:

$$Q = nFA\Gamma_T \tag{7.3}$$

Often, in the literature one can find a term *protein-film voltammetry*, introduced by Armstrong, which is used to describe the electrochemistry of adsorbed redox protein [332].

Enzymes may catalyze electrochemical reactions (Chapter 4). If enzyme is dissolved or adsorbed at the electrode surface, it decreases the overpotential and increases faradaic current at given potential. Such a phenomenon is called bioelectrocatalysis. This type of reaction was described by Nicholson and Shain [333], and its mechanism is presented in Eqs. 7.4 – 7.5, where O and R refer to the respective redox forms of mediator, Z is the oxidized enzyme and $k_f = k[Z]$ is the pseudo-first-order rate constant for the reoxidation of the mediator with the reaction with enzyme.

$$O + ne \overset{k}{\leftrightarrow} R \tag{7.4}$$

$$R + Z \overset{k_f}{\rightarrow} O \tag{7.5}$$

The overall catalytic system is controlled either by diffusion (7.4) or kinetic of the reaction (7.5). The value of the ratio k_f/a determines which of them dominates (Fig. 7.2), where a is defined as $a = nFv/RT$. If the ratio is small the reaction is diffusion controlled and the current can be described by Eq. (7.6). In the case if it is high the second reaction is fast and the catalytic current (i_{cat}) is given by the equation [333]:

$$i_{cat} = nFAC^*D^{1/2}k_f^{1/2} \tag{7.6}$$

73

where i_{cat} is directly proportional to $(k_f)^{1/2}$ and independent of the scan rate. Under these conditions a catalytic curve is recorded, which is similar to polarographic waves, instead of peak-shaped cyclic voltammogram.
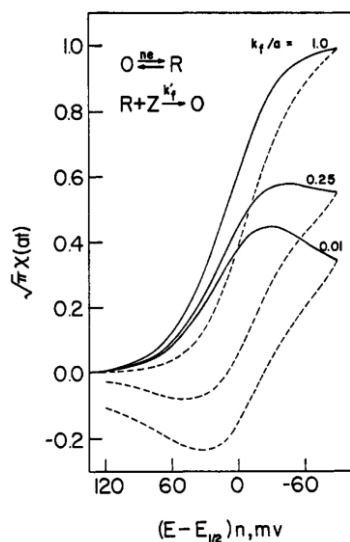

Fig. 7.2 Plot of the current functions ($\sqrt{\pi\chi}$ (at)) for a catalytic reaction with reversible charge transfer vs potential for different values of the ratio k_f/a [333].

7.2.   Chronoamperometry

Chronoamperometry (CA) is perhaps the simplest electrochemical method in which the current is measured as a function of time. As is depicted in Fig. 7.2A a double step potential is applied to the working electrode. In the first step when the initial potential (E_1) is applied to the working electrode, redox species that is present in the electrolyte does not undergo any electrochemical reaction, and the measured current is equal zero. Then, the potential is shifted to the E_2 at which the diffusion controlled redox reaction occurs. That in turn leads to decrease of the faradaic current. During the electrochemical reaction (τ) the concentration of the redox species, in the vicinity of the electrode is diminishing, resulting in a diffusion layer formation.
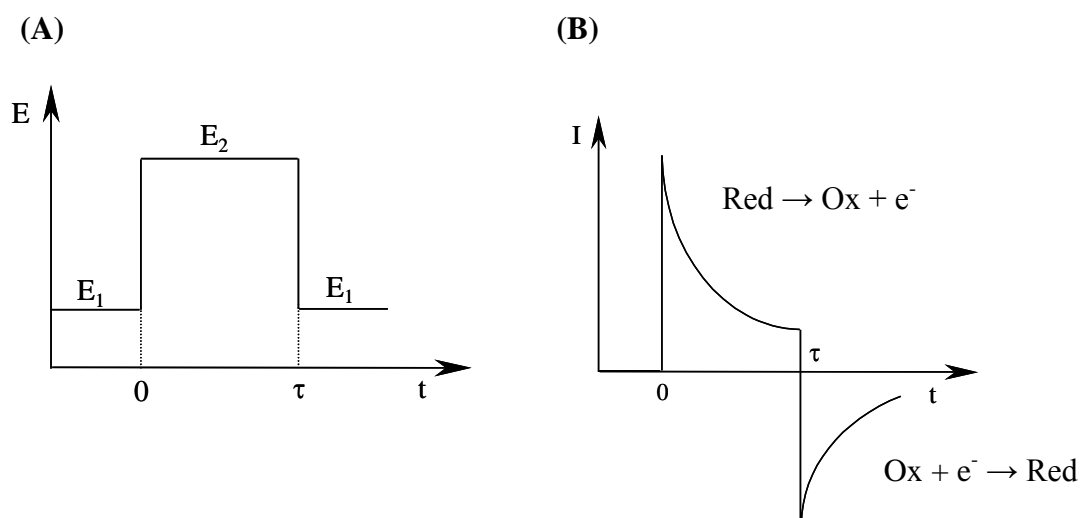
(A)

(B)

Fig. 7.2. (A) Plots of the double step potential program in CA, (B) and current response [291].

The changes of the current in time are described by the Cottrell equation [291]:

$$i = z_i A F \frac{D_{Ox}^{1/2} C_{Ox}^*}{\pi^{1/2} t^{1/2}} \tag{7.7}$$

where C_{Ox}^* is the bulk concentration of species *Ox*, z_i is the charge number of electrochemical reaction. In the case where the mass transport is diffusion-controlled the *i* varies linearly with the reciprocal of the square root of time (*t*) [291].

CA method is usually applied for the determination of the diffusion coefficient of the redox probe or electroactive surface area of the working electrode. Also like it is presented in that thesis CA might be employed for testing electrodes stability in time.

7.3. Chronopotentiometry

Chronopotentiometry (CP) is a method where the potential of the working electrode is measured in time at constant current. Usually, the experiment is performed in the three-electrode electrochemical cell. The applied potential to the working and counter electrodes (CE) impose the flow of the current, whereas the potential of the working electrode is measured [291].

In our studies that method was applied for measuring the voltage of the two-electrode set up – the Zn-O_2 hybrid cell for 100 s at different current loads to give the

75

voltage time to stabilise, resulting in the voltage-current characteristic. That in turn provides information about the efficiency about the studied cell.

7.4. Electrochemical impedance spectroscopy

Electrochemical impedance spectroscopy (EIS) is an effective technique applicable for studying of surface modified electrodes. It is based on the measurement of the impedance of the working electrode conducted when low amplitude sinusoidal voltage is applied – E(t).

$$E(t) = E_0\cos(\omega t) \tag{7.8}$$

or it might be presented as imaginary part:

$$E(t) = E_0\exp(j\omega t) \tag{7.9}$$

where E_0 is voltage signal amplitude, t is a time, and $\omega = 2\pi f$ is a frequency and f excitation frequency .

In response to sinusoidal voltage signal system generates also sinusoidal signal current – $I(t)$ with equal frequency but with phase shifted by angle ϕ.

$$I(t) = I_0\cos(\omega t - \phi) \tag{7.10}$$

or it might be presented as imaginary part:

$$I(t) = I_0\cos(j\omega t - j\phi) \tag{7.11}$$

where I_0 is current signal amplitude.

Probing the system with sinusoidal voltage signals with various frequencies, and recording resulting currents and their phase angles allow to determine system's impedance (Z) as function of frequency:

$$Z = \frac{E(t)}{I(t)} = \frac{E_0\cos(\omega t)}{E_0\cos(\omega t - \phi)} = |Z|\frac{\cos(\omega t)}{\cos(\omega t - \phi)} \tag{7.12}$$

or it might be presented as imaginary part

$$Z = \frac{E_0(t)}{I_0(t)} = \frac{E_0\exp(j\omega t)}{I_0\exp(j\omega t - j\phi)} = |Z|\exp(j\phi) = |Z|(\cos\phi + j\sin\phi) \tag{7.13}$$

$$Z = |Z|\cos\phi + j|Z|\sin\phi \tag{7.14}$$

$$Z = Z_{Re} + Z_{Im} \tag{7.15}$$

The impedance of the working electrode is measured at its equilibrium potential or when it is polarized at established potential or current. The results are usually presented as impedance spectrum. It can be presented as Nyquist plot (imaginary parts

76

of impedance Z_{im} (or -Z") vs. real Z_{re} (or Z')) [291]. If the redox probe is presence in the solution it usually consists of semicircle part at high frequencies corresponding to the electron transfer limited process, and a linear part at low frequencies which provides information about the diffusion controlled process. The electron transfer resistance is equal of the semicircle diameter (Fig. 6.3A) [291].

The Randles equivalent circuit is used for fitting the impedance spectrum in the presance of redox probe in the solution (Fig. 6.3B) [291]. It consisting of the ohmic resistance of the electrolyte solution (R_s), the double layer capacitance (C_{dl}), the Warburg impedance related to the diffusion of the redox probe in the solution (*W*), and the heterogeneous electron transfer resistance (R_{ct}). Therefore, this method was utilized for characterizing the electrical properties of: bare and hydrophilic silicate matrix with embedded CNP and Lc modified with ITO electrodes.
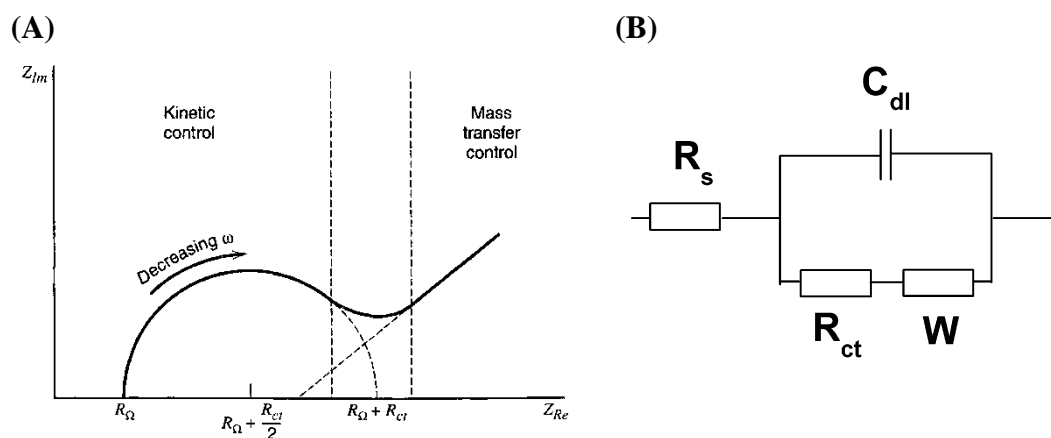
(A)

(B)

Fig. 6.3 (A) Impedance plot for an electrochemical system and (B) Randles equivalent circuit diagrams [291].

7.5. Scanning electrochemical microscopy

Scanning electrochemical microscopy (SECM) is a probe scanning technique developed by Bard and co-workers in late eighties of the 20th century. It is in its heyday over the last few decades, owing to its broad applications in the studies of the corrosion processes, biological systems, catalytic electrodes, fuel cells and surface analysis and is not limited to conductive samples [334]. For electrode studies the SECM system consists of four electrodes: two working, reference and counter electrode. The potential

of the working electrodes versus the reference and counter ones is controlled by bipotentiostat. One of the working electrodes is the studied sample whereas the second one is a movable microelectrode – so called ultramicroelectrode (UME) or SECM tip. The SECM tip is attached to a 3D piezo positioner controlled by an electronic system capable of recording acquired data. The positioner, capable of moving horizontally (in x, y directions) and vertically (in z direction), enables performing scans of a sample with UME at constant distance above it (d). The UME owing to its size (diameter smaller than 30 μm) exhibits hemispherical diffusion which in turn leads to more efficient mass transport to the electrode surface comparing to planer electrode. In these conditions the resulting, steady-state current, $i_{T,\infty}$ is given by the following formula (7.16) [335]:

$$i_{T,\infty} = g(RG)nFDr_T C^* \hspace{4cm} (7.16)$$

where F is the Faraday constant, n is the number of electrons transferred per molecule, D and C^* are the diffusion coefficient and the bulk concentration of the reagent, respectively, and r_T is the tip radius. RG is the shape factor described as the ratio of the insulating sheath (r_{glass}) to the r_T ($RG = r_{glass}/r_T$), and g is the geometry-dependent factor that depends on the thickness of the insulting sheath (Fig. 7.4). For the infinitely large insulator it assumes the value of 4.
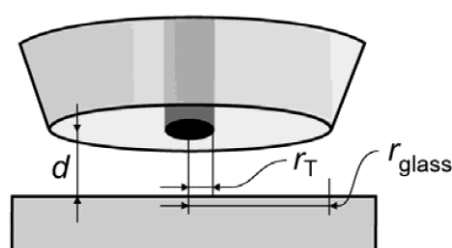
Fig. 6.4 A schematic illustartation of SECM tip's dimensions with characteristics parameters: tip-substrate separation d, radius of the SECM tip r_T, radius of the insulating sheath r_{glass} [335].

The SECM experiments can be performed in various modes: feedback (FB), generation-collection mode (GC), direct mode and redox competition mode [334, 335].

- Feedback mode – in that mode the UME is immersed in the electrolyte that contains one form of the redox probe (R↔O + ne⁻). Depending on the potential

that is applied to the UME the redox species might be oxidized or reduced, and the diffusion limited current is detected at the UME. When the tip is far from the substrate the steady-state current is recorded at the UME, and is given by the equation 16.3. Its value serves as a reference for further experiments. When the UME approaches a non-conductive surface the regeneration of the redox probe is hindered, and that in turn leads to a decrease of faradaic current r_T at the SECM tip. This phenomenon is known as "negative feedback". Opposite phenomenon (i.e. "positive feedback") occurs when the UME is moved towards the conductive surface that enables regeneration of the redox species, and results in an increment of faradaic current that is recorded at the UME. Generally these modes are applied for extracting information about the kinetics of the process at the substrate.

- Generation-collection mode – in that mode during initial conditions a solution does not contain any electroactive species. These species can only be generated on a tip or sample via applying a suitable potential, and their further detection occurs at the sample or tip, respectively. The first mode is described as tip-genaration/sample collection (TG/SC) whereas the latter one is a sample-generation/tip collection (SG/TC). These measurements are generally applied for studying the immobilized enzymes and cells. A decisive advantage of that mode over the FB is a high sensitivity.

- Direct mode – in that mode the function of the counter electrode for UME is taken over by the sample. The UME's current is neutralized by the sample one, which is of the same size but oppositely directed. That mode has been utilized mainly for analyzing defining area or local surface modification.

- Redox competition mode – a mode that was recently presented by Schumann's group [336, 337]. In this mode the SECM tip is situated closely to the sample, and the same potential is applied to both working electrodes. That leads to a competition for the same substrate (e.g. oxygen), between these electrodes. In order to avoid O_2 depletion in the space between the UME and the substrate, a two-step potential program is applied to the UME (Fig. 7.5). In the first step, the UME potential E_T is set to water oxidation potential. Next UME tip is shifted

79

to the potential at which the oxygen reduction reaction occurs. While the UME is located over the electrocatalalytic spots e.g. enzyme's molecules, its ORR current is smaller because of oxygen consumption by the enzyme at the substrate.

This mode is generally applied for studies of catalytic and biocatalytic oxygen electroreduction at modified surfaces with various sizes. Therefore it has been used in my research for studying the bioelectrocatalytic reaction of ORR catalyzed by Lc immobilized with CNPs within hydrophilic silicate matrix.
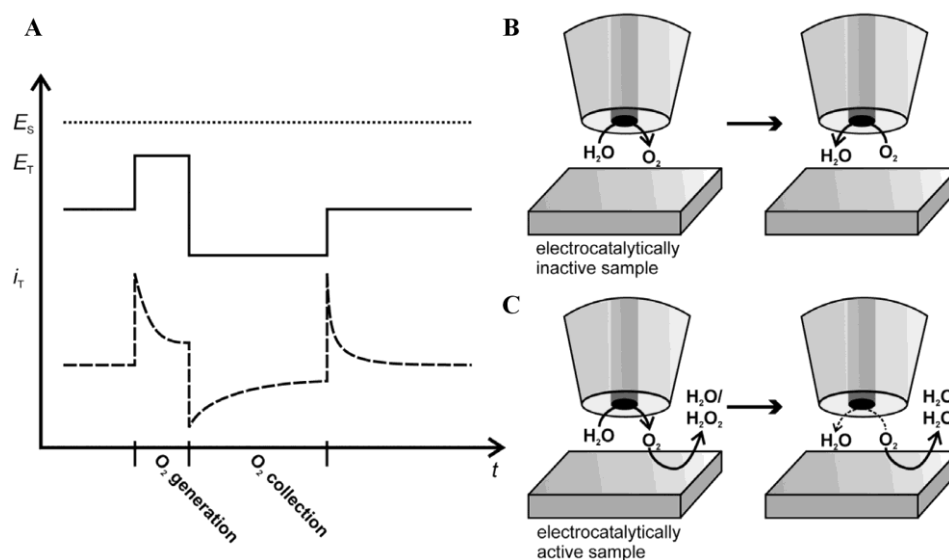

Fig. 7.5 General principles of the RC mode. (A) Pulse program at the SECM tip: $E_S(t)$ (dotted line), $E_T(t)$ (solid line), and $i_T(t)$ (dashed line). (B) O_2 is generated and re-collected at the SECM tip an electrocatalytically inactive substrate. (C) O_2 is generated at the UME and partly consumed at an electrocatalytically active substrate [335].

7.6. Scanning electron microscopy

In scanning electron microscopy (SEM) image is generated through analysis of the results of scattering of electronic beam on the surface of the studied sample. SEM comprise of cathode so called gun, which emits electrons, which in turn are being focused into a beam, and accelerated in the direction of the anode. With high enough voltage applied the velocity of electrons reaching anode can get to values close to the speed of light. Microscope is also equipped with a system capable to deflect the beam in a controllable manner, making it possible to scan the surface of the studied material in

80

preprogrammed fashion, and thus allowing to create the resulting image line-by-line. When formed and deflected beam hits the surface of the sample the results of these interactions is being recorded by the dedicated detector. After the interaction of the beam with the surface, several types of radiation can be generated: backscuttered electrons, secondary electrons, X-rays and visible light. Backscuttered electrons emition takes place when energy of the reflected electrons is almost identical to the energy of the beam electrons. Secondary electrons generation occurs when low energy electron is being emitted from the surface layer of the sample.
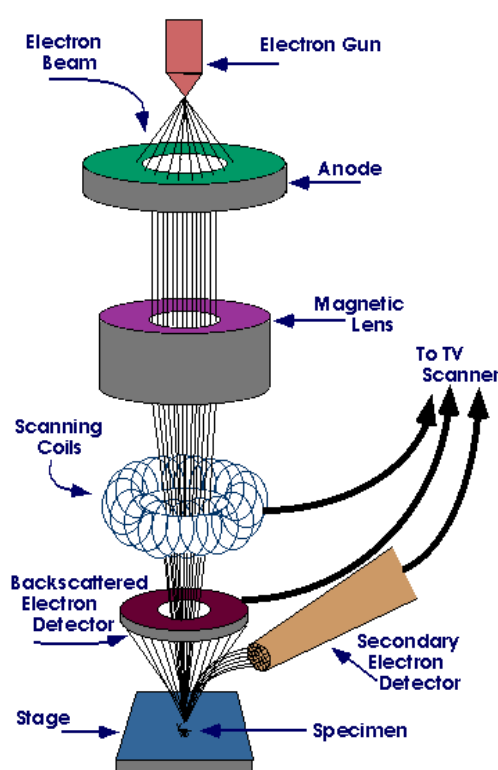
Fig. 7.6 A schematic illustration of the SEM [338].

Since the electrons are unable to flow through the sample the image produced from the data stored by the detector represents topography and composition of the surface only. In order to obtain higher quality images, the process is being carried out in the vacuum to prevent electrons from the beam from interacting with air.

SEM provides valuable information about the topography of the studied samples. Owing to that it was applied in this research for analyzing various carbon nanoparticles based materials.

81

7.7. Atomic force microscopy

Atomic force microscopy (AFM) is a type of microscope with a scanning probe. With such microscope it is possible to obtain images with atomic resolution. It operates by scanning the surface of the sample material with sharp needle like probe (so called tip) placed on an elastic cantilever. A laser beam is cast on the back side of the cantilever and is reflected towards array of photodiodes. Since the cantilever's orientation changes monotonically as a function of the depth of the surface in the point currently under the probe, measuring the location of the reflected beam on the detector enables calculating that depth. The signal from the detector may also be used as an input signal for feedback loop allowing probe to automatically maintain distance from the surface at which the signal is constant. There are two operating modes of AFM – the contact and tapping mode. The contact mode works with constant exerted force, and owing to that usually is applied for imaging hard sample (Fig. 7.7). In the case of the tapping mode the presence of piezoelectric actuator allows for retaining an appropriate distance between the sample and the tip. This in turn enables imaging fragile and rough samples e.g. carbon nanoparticulate films.
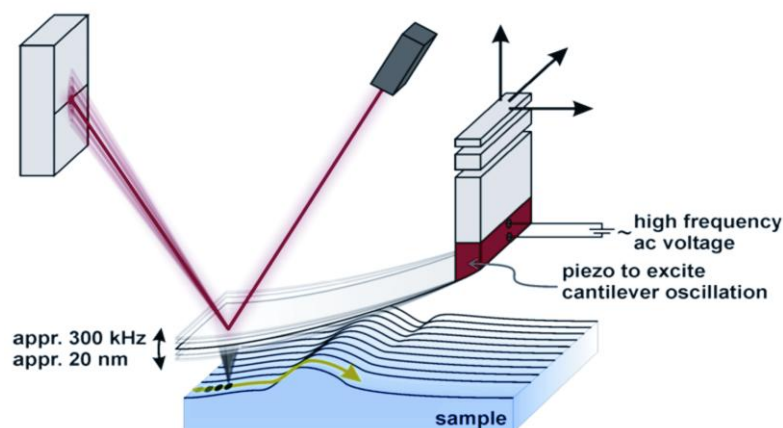

Fig. 7.7 A schematic illustration of the AFM tapping mode [339].

The AFM was used in that thesis for analysis of carbon nanoparticulate film electrodes topography. Also it enables determination of the thickness of the studied samples from the measurement of AFM profiles.

7.8. Infrared spectroscopy

Infrared spectroscopy (IR) is a widely applied research technique that provides qualitative information about the studied sample mainly by allowing to identify specific functional groups present in the molecules. Atoms in each molecule are continuously oscillating, bonds between its atoms are stretched or bended with frequencies specific to the given molecule. This in turn leads to specific molecule's vibrations. If the molecule is irradiated with electromagnetic radiation from the infrared region (1000 – 20000 nm, near, middle and far IR) with frequency that matches the energy of one vibrational modes, then the photon is absorbed (with some probability), and the molecule transits to a higher vibrational energy state [340]. By irradiating the sample with IR radiation with various wavelengths one can gather molecule's IR spectrum, called "molecular fingerprint". Since this spectrum is highly specific, the IR measurements are very valuable for identification of bonds functional groups or whole molecules in studied samples. However, the infrared radiation is absorbed only by molecules in which the change in dipole moment can occur, for diatoms and symmetrical molecules such behaviour is not observed so they are inactive at the IR spectrum [340].

The IR spectrum is usually presented as a graph of absorbance (A) or % transmittance (T) – the percentage of the energy of the radiation of a particular wavelength that is not adsorbed by the sample – versus radiation's wavenumber. The absorbance and transmittance fulfil Beer-Lambert law [340]:

$$T = \frac{I}{I_0}100\% = e^{-\varepsilon l c}100\% \qquad\qquad (7.17)$$

$$A = \ln\frac{I_0}{I} = -\ln T \qquad\qquad (7.18)$$

where I_0 and I are the intensities of the incident and transmitted light, respectively. C is the molar concentration of absorbing species, ε is a molar absorptivity (extinction coefficient), and l is the path length.

Herein IR spectroscopy was used to confirm the gel network formation in one of the alkoxide precursors – n-octyltriethoxysilane, which is known for its difficulty in gelating, owing to the increased steric hindrance. Also the homogenity of the obtained

83

silicate materials prepared from that precursor was studied via performing the infrared map. The experiments were carried out using the reflectance mode (that is one in which the ration of the reflected IR radiation to the incident one is measured), non-destructive method which enables studies of surfaces coated with thin films.

7.9. Optical profilometry

Optical profilometry is a nondestructive, fast and high resolution (vertical and lateral resolutions are in the nanometre and micrometre level, respectively) technique that provides information about the topography and roughness of the studied sample. In the profilometer the light generated by the lamp is split into two beams. One of them (so called "internal beam") is directed into a reference mirror whereas the other one onto the studied surface. The reflected beam from the sample interferes with the internal beam. As a result interference fringes are formed, creating various patterns. Those interference patterns in turn are digitalized, and using dedicated software transformed into a reconstructed model of the surface's 3D profile [341].
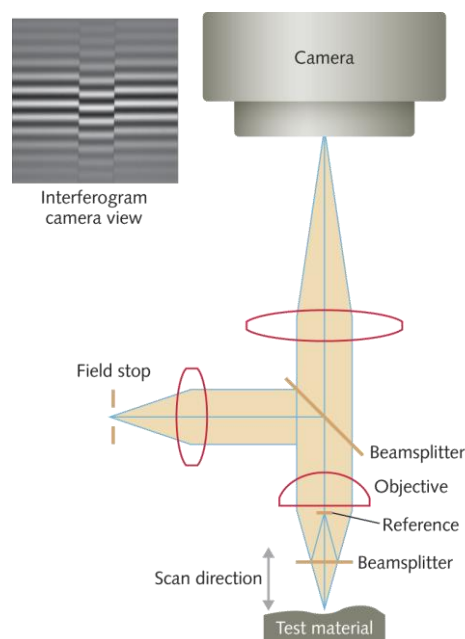

Fig. 7.8 A schematic illustration of the optical profilometer [341].

The optical profilometer was used in that thesis for determination of the thickness CNPs-imidazolium functionalized silicate multilayers film electrodes.

8. Chemicals and materials

- 2,2'-azino-bis(3-ethylbenzothiazoline-6-sulfonate) ($ABTS^{2-}$, 98%, Sigma-Aldrich)

- Argon (N5. 0, Multax)

- Bilirubin oxidase from *Myrothecium sp.* fungus (EC 1.3.3.5, Amano Enzyme Inc.)

- Carbon nanoparticles with phenylsulfonic acid surface functionalities (ca. 7.8 nm mean diameter, Emperor 2000, Cabot Corporation)

- Carbon nanoparticles with sulfonamide group (obtained from Prof. Frank Marken, synthesized according to procedure described in literature [98])

- Citric acid monohydrate ($C_6H_8O_7 \cdot H_2O$, Merck)

- Disodium hydrogen phosphate (Na_2HPO_4, POCH)

- Ethanol (C_2H_5OH, 96 %, Chempur)

- 1,1'-Ferrocenedimethanol ($Fc(CH_2OH)_2$, 99 %, Aldrich)

- Formic acid (HCOOH, 98 %, POCH)

- Ferrocenemonocarboxylic acid (FMCA, $\geq$ 97%, Fluka)

- Glucose ($C_6H_{12}O_6$, 99.5 %, Sigma-Aldrich)

- Glucose oxidase from *Aspergillus niger* fungus (EC 1.1.3.4, Amano Enzyme Inc.)

- Hexaammineruthenium (III) chloride ($[Ru(NH_3)_6]Cl_3$, Sigma-Aldrich)

- Hydrochloric acid (HCl, 35 %, POCH)

- Hydrogen peroxide (H_2O_2, 30 %, Chempur)

- Laccase from *Cerrena unicolor* fungus (EC 1.10.3.2, isolated and purified by Prof. Rogalski group according to procedure described in literature [342])

- Methanol (CH_3OH, 99.8%, Chempur)

- Methyltrimethoxysilane (MTMOS, 98%, Sigma-Aldrich)

- 1-Methyl-3-(3-trimethoxysilylpropyl)imidazolium bis(trifluoromethylsulfonyl) imide (P(TMOS)MIMNTF2, synthesized by dr Cecile Rizzi from University of Pierre and Marie Curie-Paris, France)

- Monosodium phosphate hydrate ($NaH_2PO_4 \cdot H_2O$, POCH)

- Myoglobin from horse heart (90 %, Sigma-Aldrich)

- Nafion ® (5 % solution in 2-propanol, Sigma-Aldrich)

- Nitrobenzene ($C_6H_5NO_2$, 99 %, POCH)

- *n*-Octyltriethoxysilane (OTEOS, 97%, ABCR)

- Oxygen (N5. 0, Multax)

- Phosphoric acid (H_3PO_4, 85 %, Chempur)

- Platinum wire (10 μm diameter, Goodfellow)

- Potassium chloride (KCl, Sigma-Aldrich)

- Potassium hexacyanoferrate (II) trihydrate ($K_4[Fe(CN)_6] \cdot 3H_2O$, POCH)

- Potassium hexacyanoferrate (III) ($K_3[Fe(CN)_6]$, Sigma-Aldrich)

- 2-Propanol ($CH_3CH(OH)CH_3$, ≥99.8 %, Merck)

- Sodium chloride (NaCl, Chempur)

- Sodium fluoride (NaF, POCh)

- Sodium hydroxide (NaOH, POCH)

- Sodium perchlorate ($NaClO_4$, Fluka)

- Sodium sulfite (Na_2SO_3, POCH)

- Sulfiric acid (H_2SO_4, 95 %, Chempur)

- Tin-doped indium oxide coated glass (ITO, resistivity 15 and 8-12 Ω per square, Image Optics Components Ltd., and Delta Technologies, respectively)

- *tert*-butylferrocene (*t*BuFc, 98%, ABCR)

- Tetramethoxysilane (TMOS, 99%, Sigma-Aldrich)

- Water (H_2O, resistivity >15 Ω·cm, demineralized with ELIX system, Milipore)

- Zinc wire (250 μm diameter, 99.95%, Goodfellow)

All reagents were used as received.

9.   Instrumentation

Potentiostats, bipotentiostats

- Autolab PGSTAT 30 (Eco Chemie)

- µBIP (Schramm, Heinrich Heine University, Düsseldorf, Germany)

Optical microscope

- Nikon Eclipse LV150 metallurgical microscope (Nikon)

Infrared spectroscopy

- Nicolet iN10-MX-FTIR microscope (Thermo Scientific)

The experiments were carried out using the reflectance mode and the 2-D MCT detector. The sampled area for a single spectrum was equal to 25 µm2. The spectral resolution was equal to 4 cm^{-1} and typically 12 scans were averaged for a single spectrum. So as to allow for superposition of visible and infrared maps, both sets of optics of the microscope were aligned to exactly the same spot on the sample. The correlation maps were obtained using the standard correlation algorithm implemented in the OMNIC PICTA software provided with the microscope.

Atomic force microscopy

- Veeco Dimension 3100 microscope and Nanoscope IIIA controller (Veeco Instruments Inc.)

- Veeco Nanoscope SPM

Scanning electrochemical microscopes

- Home-built (for study of ABTS-CCE/Lac, Syr-CCE/Lac and CCE-CNP/BOx) [343]
    - Stepper motor positioning system (Märzhäuser Wetzlar GmbH & Co KG)
    - PCI-DAS 1602/16 analog-digital converter board (Plug-in Electronic GmbH)
    - Analog µBiP3 bipotentiostat (M. Schramm, Heinrich Heine University of Düsseldorf)

The motor positioning and data acquisition were controlled by the homemade SECMx software. The in-house developed package MIRA [344] was used for data analysis and extraction of the averaged currents from redox competition measurements.

Profilometry

- WYKO163 NT100 optical profiler

Scanning electron microscope

- JEOL JSM6310 or with a Leo 1530 field emission gun scanning electron microscope system

- SEM SUPRA (Carl Zeiss SMT Inc.)

Dip-coater

- KSV dip-coating unit (KSV Instruments Ltd.)

pH-meter

- CG 837 pH-meter (SCHOTT)

- pH-meter 605 (Methrom GmbH)

Balance

- AB204-S analytical balance (Mettler Toledo)

- CP124S analytical balance (Satorius AG)

Ultrasonic bath

- Sonorex RK 31 (Bandelin electronic GmbH & Co.)

Furnance

- Tube furnace (Barnstead Inc.)

10.   Electrode modification procedures

10.1.   Electrode modification with silicate and carbon nanoparticles

The essential part of that thesis was the preparation of the carbon nanoparticles-based electrodes, which in turn had a significant impact on the bioelectrocatalysis. Five procedures have been utilized for immobilization CNPs. One of them leads to generation of the material in the form of stripe whereas the others enable films formation. The applied techniques for electrodes' modification such as sol-gel process, electrodeposition and LbL assembly, can be divided into a single and multi-step procedures. The latter one was used for preparing multilayer film through LbL assembly while the single step procedure was applied for the development of the thin silicate film and stripe, respectively. One of the procedures generates the pure carbon film whereas others carbon-silicate films.

In all modification procedures ITO was used as a substrate. Before preparation it was cleaned with ethanol, then with deionized water and finally heated for 30 minute in a tube furnace (Barnstead International) at 500 °C in air. The area of modified electrode was defined by masking off 0.2 cm^2 with scotch tape, except electrodes modified by electrochemical method (see in subsection 10.1.1.3). The electric contact was assured by a piece of copper tape.

The details of electrodes modification procedures are described in the following sections.

10.1.1. Single step procedures

Single step procedures were utilized for the preparation of thin silicate film and stripes in the sol-gel drop coating method and electrodeposition processes, respectively (Fig. 10.1). The CNPs were embedded in silicate matrices prepared from sol-gel precursors: hydrophilic (TMOS) and hydrophobic ones (MTMOS and OTEOS).
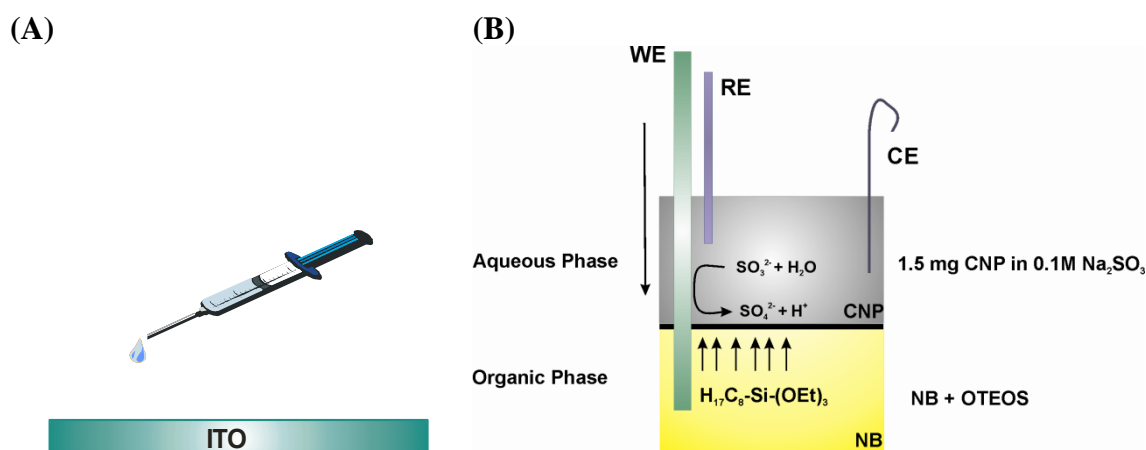
89

Fig. 10.1 Schemes of single-step preparation of carbon nanoparticulate-silicate based electrodes via (A) drop coating and (B) electrodepositon assisted by three phase junction. An arrow indicates a movement of ITO during the formation of an array of stripes.

10.1.1.1.   Hydrophilic silicate matrix + CNPs

- **Hydrophilic silicate matrix + CNPs$_{KCl}$ (TMOS$_{gel}$/CNPs$_{KCl}$)**

The active area was modified by deposition of a 20 µl volume of a mixture prepared from 1 µl freshly prepared sol (A) and 100 µl carbon nanoparticle suspension (B). The sol (A) was prepared by mixing 0.5 µl TMOS with 0.125 µl water. Subsequent addition of 27.5 µl 0.04 M HCl initiated the sol-gel process. The mixture was then sonicated for 10 min. The carbon nanoparticle suspension (B) consisted typically of 0.025 g of Emperor 2000 CNPs dispersed in 10 ml aqueous KCl solution (typically 50 mM KCl). Next, sol (A) and carbon nanoparticle suspension (B) were mixed in a sol/suspension ratio of 1:100. The mixture was then sonicated for a further 10 min before being deposited by pipette onto the ITO electrode. After evaporation of water and methanol and 24 h gelation, the film deposit consists of approximately 0.3 mg silicate and 0.25 mg CNPs (45 wt% CNPs).

- **Hydrophilic silicate matrix + CNPs with embedded laccase (TMOS$_{gel}$/CNPs/Lc)**

CNPs suspension was prepared by adding 3 mg of CNPs to 1 ml of water followed by 1 hour sonication. For preparation of the film 500 µl of TMOS was mixed with 27.5 µl of 0.04 M aqueous HCl and 125 µl of CNPs solution. Next 250 µl of the sol

90

was diluted with 225 μl of CNPs solution and 25 μl of 0.1 M phosphate buffer (pH 5.8). Then a 25 μl aliquot of the diluted sol was mixed with 125 μl of Lc or BOx (145 μg of Lc or BOx dissolved in 2 ml of CNPs solution), 75 μl CNPs solution and 25 μl of phosphate buffer. Finally, 25 μl of the sample obtained in last step was diluted in the same way. Every step of solution or sol preparation was followed by sonication. The ITO electrode was modified by drop coating with 20 μl of the solution obtained in the final step using microsyringe. For sol-gel processing and drying these samples were left for at least 20 h at room temperature (22 ± 2 °C) and a relative humidity of 40-50 %. The amount of enzyme and CNPs in the film is estimated to 2.7×10^{-10} mol and 8.5 μg respectively.

This electrode is later called $TMOS_{gel}$/CNPs/Lc and $TMOS_{gel}$/CNPs/BOx. For control experiments the electrodes modified with $TMOS_{gel}$ film ($TMOS_{gel}$) and the same film with embedded laccase ($TMOS_{gel}$/Lc) [345] or carbon nanoparticles ($TMOS_{gel}$/CNPs) was prepared.

10.1.1.2. Hydrophobic silicate matrix + CNPs ($MTMOS_{gel}$/CNPs and $OTEOS_{gel}$/CNPs)

- **$MTMOS_{gel}$/CNPs**

CNPs suspension was prepared by adding 25 mg of CNPs to 10 ml of 50 mM KCl followed by 1 hour sonication. For preparation of the film 500 μl of MTMOS was mixed with 750 μl of methanol and 27.5 μl of 11 M HCl. This mixture was sonicated for 10 minutes and subsequently mixed with CNPs solution, in volume ratio 1:100 and sonicated for 3 minutes. The ITO electrode was modified by 20 μl of the solution obtained in the final step using microsyringe.

- **$OTEOS_{gel}$/CNPs**

CNPs suspension was prepared by adding 15 mg of CNPs to 10 ml of various 0.1 M electrolytes (Na_2SO_3, $NaClO_4$, NaF, NaCl), separately, followed by 1 hour sonication. For preparation of the film 100 μl of MTMOS was mixed with 20 μl of water, 5 μl of ethanol and 7.5 μl of 0.04 M HCl. This mixture was sonicated for 10

91

minutes and subsequently mixed with CNPs solution, in volume ratio 1:100 and sonicated for 3 minutes.

The ITO electrode was modified by 20 μl of the solution obtained in the final step using microsyringe. For sol-gel processing and drying, these samples were left for at least 20 h at ambient atmosphere at room temperature (22 ± 2 °C) and a relative humidity of 40-50 %.

For BOx and Lc modification electrodes were immersed in 1 mg ml^{-1} solution of BOx or Lc in 0.1 M McIlvaine buffer pH 5.0 at $+ 4$ ºC overnight and rinsed with water. These electrodes were later called MTMOS$_{gel}$/CNPs/BOx, MTMOS$_{gel}$/CNPs/Lc, and OTEOS$_{gel}$/CNPs/BOx. For blank experiments the electrode modified with MTMOS$_{gel}$ with embedded carbon nanoparticles film (MTMOS$_{gel}$/CNPs) was prepared.
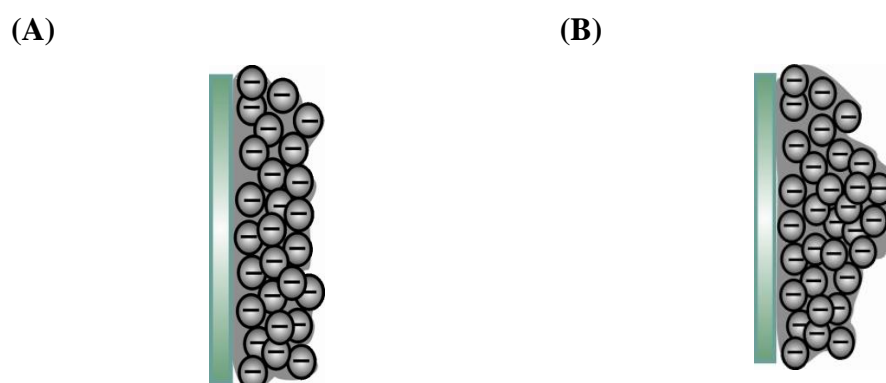
(A)   **(B)**

Fig. 9.2 A scheme of the film prepared from phenylsulfonated carbon nanoparticles embedded in (A) hydrophilic and (B) hydrophobic matrix.

10.1.1.3. Electrodeposition of CNPs-silicate nanocomposites

Electrodeposition of CNPs-silicate nanocomposite was prepared in the form of stripe. CNPs suspensions were prepared by adding 1.5 mg of CNPs to 1 ml of 0.01 M aqueous Na$_2$SO$_3$ followed by 1 h of sonication. Following earlier published procedures for electrodeposition of silicate stripes [346] an ITO electrode (0.8×4 cm^2) was immersed into a cell filled with two immiscible solutions (Fig. 10.1): 3 ml of OTEOS-nitrobenzene mixture (1:29 v/v) and 2 ml of CNPs aqueous suspension. The reference and counter electrodes (RE, CE) were immersed only into the aqueous phase and

a potential of 1.55 V was applied for 7560 s. CNPs-silicate stripe was preapared by an electrochemically assisted sol-gel process at the three phase junction. The sodium sulphite was used to produce the catalyst (hydrated protons) for the sol-gel process during its electrooxidiation. That was confirmed with cyclic voltammogram obtained with the ITO electrode immersed into the immiscible solutions (Fig. 10.3). The electrooxidation of sulphite ions is described by Eq. 10.1. To retain the electroneutrality of the whole system, the generated protons are transferred, from the aqueous to the organic phase in the vicinity of the three phase junction, where are used as catalyst for the sol-gel process.
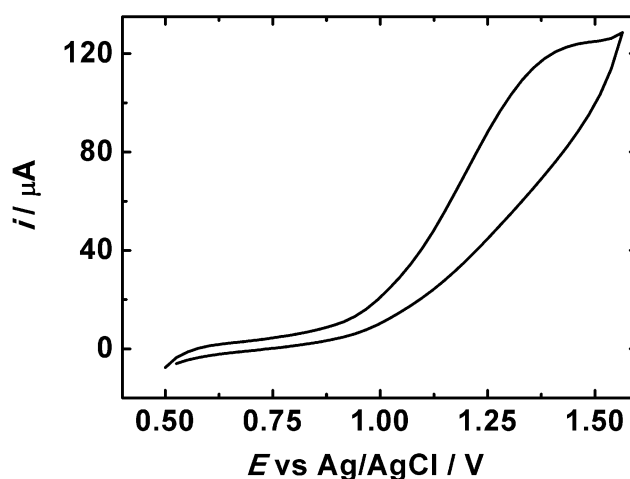
$$SO_3^{2-} + H_2O \rightarrow SO_4^{2-} + 2H^+ + 2e\text{-} \tag{10.1}$$

Fig. 10.3 Cyclic voltammogram (1st scan) of the ITO electrode immersed in 0.01 M Na$_2$SO$_3$ aqueous solution with CNP and OTEOS in nitrobenzene 1:29 v/v ratio (see Scheme 10.1B). Scan rate 100 mV s^{-1}.

To obtain an array of stripes, after each single deposition (1.55 V, 7560 s) the ITO electrode was immersed 2 mm further into the organic phase with a speed 0.7 mm s^{-1} using a dip-coater. If the electrode was instead withdrawn between each step of electrodeposition the nitrobenzene blocked the surface and no deposition took place. Finally, the electrode was withdrawn from the solution and left for 12 h to dry at room temperature. Then, it was washed with water and ethanol.

The surface of the modified electrodes (Fig. 10.4) was defined by masking with scotch tape (geometric area: 0.01 ± 0.002 cm^2 for the stripe and 0.16 cm^2 for the array of

stripes). In the case of the stripe the masking was done under a microscope. First, to allow the tape to stick the traces of carbon material not covered by silicate, adsorbed on the part of the ITO electrode immersed in the aqueous phase, was removed using a scalpel. The tape was attached using sharp tweezers under the microscope and the width of the open gap was measured using the scale of the microscope. The silicate stripe has a width of just under 100 μm and the open gap was about 125 μm wide. The estimated error is about 20%, i.e. a width of between 100 to 150 μm. This gives an area of 0.01 ± 0.002 cm^2 and a current density from 0.67 to 1 mA cm^{-2}.

Enzyme adsorption was performed by immersion of electrodeposited CNPs silicate stripe or the array of stripes into 1 mg ml^{-1} BOx in 0.1 M phosphate buffer (pH 4.8) solution for 2 h at ca. 4 °C.

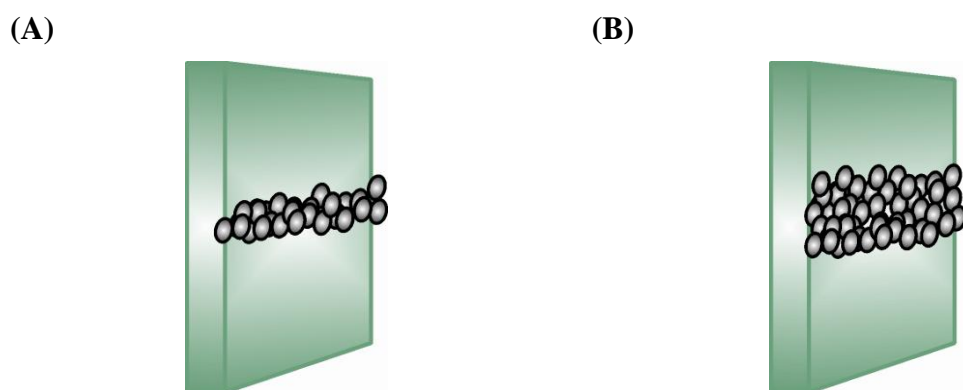**(A)**   **(B)**

Fig. 10.4 A scheme of the electrodeposited CNPs silicate stripe (A) and array of stripes (B).

10.1.2. Multi-step procedures

Through multi-step procedures multilayer film electrodes were prepared according to procedure presented in Fig. 10.5. ITO electrodes were immersed alternately into: a sol containing ionic liquid with imidazolium cationic functional group and negatively charged CNPs suspensions (Fig. 10.5 (1)) or oppositely charged CNPs suspensions (Fig. 10.5 (1)). This procedure was repeated after deposition of desirable number of layers on the electrode surface.

94

(1)

(2)

sol composed of ionic liquid sol-gel precursor and tetramethoxysilane

$\ominus$ = aqueous suspension of carbon nanoparticles modified with negatively charged phenyl sulphonic groups

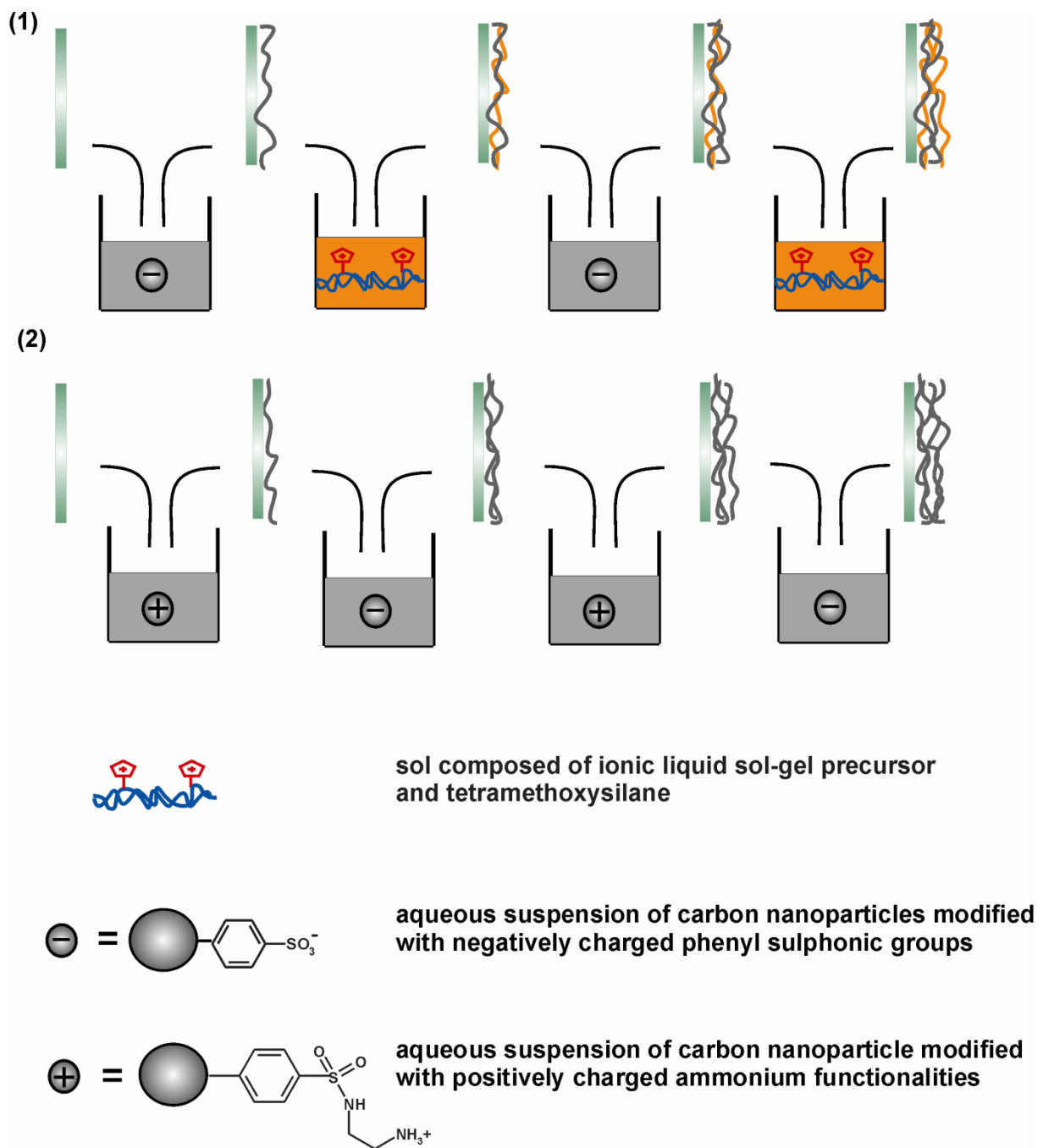$\oplus$ = aqueous suspension of carbon nanoparticle modified with positively charged ammonium functionalities

Fig. 10.5 A scheme of preparation of CNP-imidazolium functionalized silicate multilayers (1) and oppositely charged carbon nanoparticles multilayers (2).

95

10.1.2.1. Sol-gel processed ionic liquid – hydrophilic carbon nanoparticles multilayer film electrode (CNP-imidazolium functionalized silicate layers)

Two solutions, precursor sol (A) and carbon nanoparticles solution (B) were necessary for electrode preparation. The solution (A) was obtained by mixing 0.321 g of 1-methyl-3-(3-trimethoxysilylpropyl)imidazolium bis(trifluoromethyl sulfonyl)imide (1) (see Fig. 15.2), 196 μl of TMOS and 370 μl of formic acid as a catalyst. This mixture was sonicated for 10 min and diluted with methanol at 1:10 volume ratio. The solution (B) was prepared by dissolution of 3 mg of CNPs' in 1 ml of water followed by one hour sonication. First ITO electrode was immersed into solution (B) for 1 min. Next, after rinsing with water electrode it was dipped for 30 s into the diluted sol (A) (Fig. 10.5. (1)). This procedure was repeated after deposition of desirable number of layers on the electrode surface as it is depicted in Fig. 10.6A. The maximum number of layers defined as the number of alternative immersion and withdrawal of the substrate to and from CNPs suspension and sol is equal 10. Further repeating of the procedure results in fragile film.

Electrodes coated by (n) different number of immersion and withdrawal steps to negatively charged CNPs suspension and positively charged imidazolium groups of precursor (1) are called: n CNP-imidazolium functionalized silicate layers. In this studies electrodes coated with one, three, five and ten immersion and withdrawal steps were prepared; one, three, five and ten CNP-imidazolium functionalized silicate layers.

Enzyme adsorption was performed by immersion of n CNP-imidazolium functionalized silicate layers film electrode into following enzymes' solution, separately: 1 mg cm^{-3} bilirubin oxidase or laccase solution in 0.1 M phosphate buffer (pH 4.8) solution for 2 hours.

10.1.2.2. Film electrode prepared from oppositely charged carbon nanoparticles (CNP (+/-))

Suspensions of both types of particles were obtained by mixing 3 mg of particles with 1 ml of water followed by sonication of the mixture for 1 hour. ITO slides were cleaned as described earlier [23] and immersed alternately into the positively and negatively charged CNPs suspension in water for 1 minute (Fig. 10.5. (2)). Every step was followed by drying and immersion in pure water for 2 s to remove weakly bonded

96

particles. The immobilization sequence always ended with negatively charged CNP deposition. The larger number of alternative immersion and withdrawal steps results in darkening of the electrode. When the number of deposition steps was larger than 10 then the film was seen to peel off from the solid surface. This procedure was repeated after deposition of desirable number of layers on the electrode surface as it is depicted in Fig. 10.6B.

Electrodes coated by (*n*) different number of immersion and withdrawal steps to positively and negatively charged CNPs suspension are called: *n*-CNP(+/-). In this studies electrodes coated with one, three, five and ten immersion and withdrawal steps were prepared; one, three, five and ten-CNP(+/-).

Enzyme adsorption was performed by immersion of the *n*-CNP(+/-) film electrode into following enzymes' solution, separately: 1 mg cm^{-3} bilirubin oxidase or laccase solution in 0.1 M phosphate buffer (pH 4.8) solution for 2 hours, 5 mg cm^{-3} glucose oxidase solution in 0.1 M phosphate buffer (pH 7) solution for 24 hours, and 3 mg cm^{-3} myoglobin solution in 0.1 M citrate buffer (pH 4) solution for 24 hours, in ca. 5°C. These electrodes were later called *n*-CNPs(+/-)/BOx, Lc, and GOx or Mb. For blank experiments the electrode coated only with positively charged CNPs and adsorbed BOx (three-CNP(+)/BOx) was prepared.
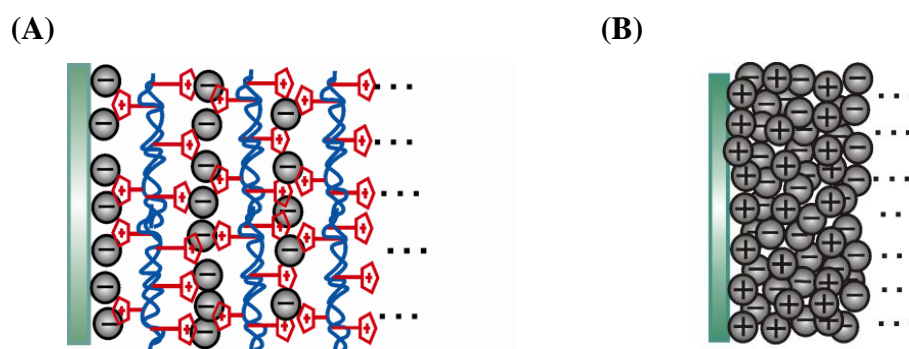
(A) **(B)**

Figure 10.6 A scheme of the surface of (A) CNP-imidazolium functionalized silicate layers and (B) oppositely charged carbon nanoparticles multilayer film electrode prepared by layer by layer method.

10.2. Zinc anode

For testing the electrodes as cathodes in zinc-oxygen hybrid cell a zinc wire (anode) immersed in buffer solution (surface area = 0.023 cm^2). To facilitate the built up of

97

a stable $Zn_3(PO_4)_2 \times 4H_2O$ film during the cell operation, the latter electrode was coated with a Nafion film [290].

11.   Experimental setup

Experiments were carried out at ambient temperature, and pressure under oxygen, air or argon atmosphere.

11.1.   Electrochemical setup

CV and CA experiments were done in a conventional three electrode cell. ITO modified as described in Chapter 10 was used as working electrode, a platinum wire ($d = 0.5$ mm) and $Ag|AgCl|KCl_{sat.}$ were used as counter and reference electrode, respectively.

11.2.   Scanning electrochemical microscopy setup

SECM measurments were performed in a four electrode cell consisting of Pt ultramicroelectrode (UME), $TMOS_{gel}$/CNP/Lc modified ITO electrode as first and second working electrodes, respectively. A platinum wire ($d = 0.5$ mm) and $Ag|AgCl|KCl_{sat.}$ were used as counter and reference electrodes, respectively. The UME tip was obtained by sealing a Pt wire (25 μm diameter) into borosilicate glass capillaries. Its apex was shaped according to literature procedure [347]. The ratio RG between the radius of the insulating glass and the radius r_T of the active tip area was 9.4.

Results and discussion

12. Hydrophilic carbon nanoparticles – hydrophilic sol-gel film electrodes (TMOS$_{gel}$/CNPs$_{KCl}$)

12.1. Introduction

A hydrophilic carbon nanoparticle–sol-gel electrode with good electrical conductivity within the sol-gel matrix was prepared. Sulfonated carbon nanoparticles, with high hydrophilicity and diameter of ca. 8 nm, were co-deposited onto ITO employing a sol-gel technique.

In the following chapter the resulting carbon nanoparticle-sol-gel composite electrodes were characterized as a function of composition and salt (KCl) additive. They were also examined by SEM and cyclic voltammetry.

12.2. The microscopic and electrochemical characterization

To optimize the electrode properties and the CNP aggregation, the starting sol composition was adjusted by changing the CNPs amount and the salt (KCl) concentration. An initial electrochemical characterization of TMOS$_{gel}$/CNPs$_{KCl}$ film modified ITO was conducted in aqueous 0.1 M NaClO$_4$. The presence of the CNPs is immediately revealed by the substantial capacitive charging current (Fig. 12.1). Unsurprisingly, the capacitive current for a 45 wt% carbon nanoparticle deposit (Fig. 12.1 curve 1) is considerably larger compared to that obtained with a 4.5 wt% deposit (Fig. 12.1 curve 2) or that obtained at bare ITO electrodes (not shown). The substantial increase in capacitive background current demonstrates good electrical conductivity throughout the film deposit. A plot of the capacitive current vs the carbon nanoparticle content in film deposits shows a good correlation, although at carbon nanoparticle contents of more than 50 to 60 wt%, film electrodes became mechanically unstable during immersion and removal from solution.
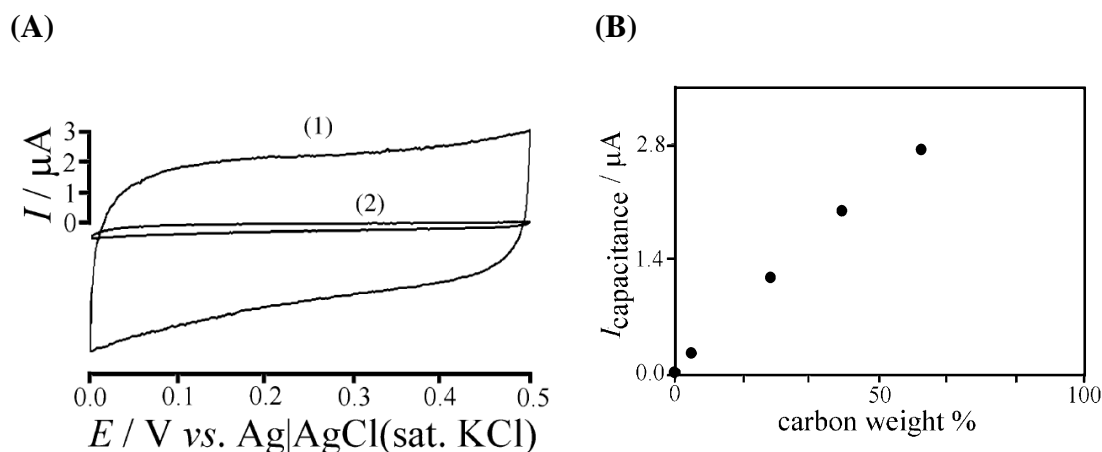
(A)

(B)

Fig. 12.1 (A) Cyclic voltammograms of TMOS$_{gel}$/CNPs$_{KCl}$ film modified ITO electrodes with (1) 45 wt% and (2) 4.5 wt% carbon nanoparticles (prepared using 50 mM KCl aq.) immersed in 0.1 M NaClO$_4$ aqueous solution. (B) Plot of the capacitive current response vs the carbon weight percent in the TMOS$_{gel}$/CNP$_{KCl}$ film electrode. Scan rate 10 mV s^{-1}.

For the 45 wt% carbon nanoparticle electrode (with 0.25 mg CNPs) a specific capacitance of 0.8 F g^{-1} can be calculated. This value seems to be low when compared to other carbon materials like carbon nanofibers [348], but this is believed to be due to a shielding effect in carbon aggregates. For the immobilized carbon in the TMOS$_{gel}$/CNPs$_{KCl}$ film, the observed capacitance corresponds approximately to an active surface area (assuming 10 μF cm^{-2} [349]) of about 10 m^2 g^{-1}. This compares to a calculated surface area of typically 100 m^2 g^{-1} (calculated assuming 8 nm diameter particles) suggesting that approximately 10% of the total carbon surface is active. A substantial part of the apparently inactive surface may be contained within carbon aggregates. SEM images for the carbon nanoparticle material (a) and for the TMOS$_{gel}$/CNPs$_{KCl}$ film electrodes (b, c) are shown in Fig. 12.2. Aggregates of CNPs several microns in diameter are heterogeneously distributed in the composite film. It is likely that they provide percolation paths for electrical conductivity through the film.
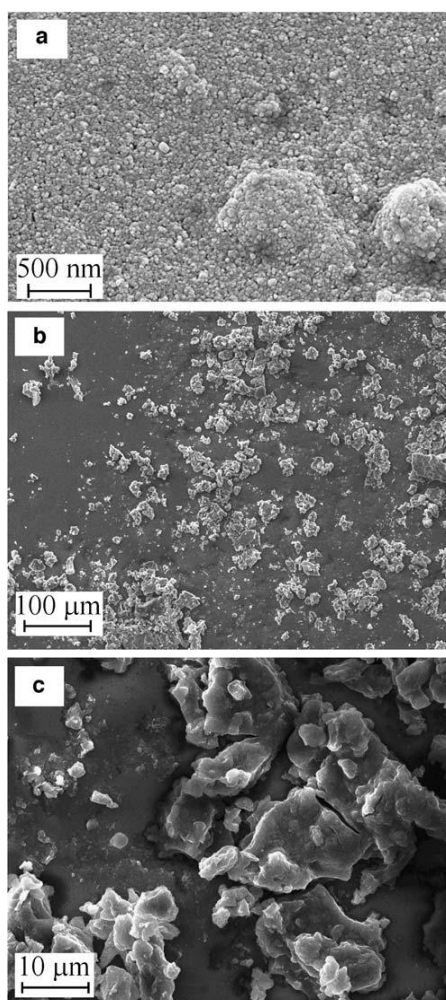
100

Fig. 12.2 SEM images of TMOS$_{gel}$/CNPs$_{KCl}$ film deposits on ITO electrodes: (a) Only carbon nanoparticles deposited from an aqueous dispersion; (b) low magnification image of the TMOS$_{gel}$/CNPs$_{KCl}$ film; (c) high magnification of the TMOS$_{gel}$/CNPs$_{KCl}$ film. The films in (b, c) were obtained from 45 wt% of CNPs (prepared using 50 mM KCl) in sol-gel matrix.

12.2.1. Electrochemical redox reactions

Next, a reversible one electron solution phase redox system was studied. The electro-oxidation of simple redox probe 1,1'-ferrocenedimethanol (Fc(CH$_2$OH)$_2$) was investigated in aqueous 0.1 M NaClO$_4$ (Eq. 12.1).

$$Fc(CH_2OH)_2 \quad \leftrightarrow \quad Fc(CH_2OH)_2^+ + e^- \tag{12.1}$$
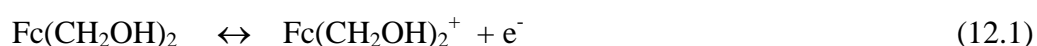
Fig. 12.3A compares voltammograms obtained in a 1 M Fc(CH$_2$OH)$_2$ solution with (1) a 45 wt% CNP electrode, (2) a bare ITO electrode, and (3) a 0 wt% CNPs electrode

101

(only sol-gel film). For the silicate-coated electrode (3) the reduced mobility of 1,1′-ferrocenedimethanol within the gel film is clearly observed. The anodic peak current observed at the 45 wt% CNP–sol-gel electrode (1) is approximately twice comparing to that obtained at a bare ITO electrode (2). In addition to facile electron transfer at the $TMOS_{gel}/CNPs_{KCl}$ film, trapping of solution within the porous carbon structure occurs. As one can observe from voltammogram for electrode (1) a more symmetric voltammetric peak system is developed similar to that obtained for the surface controlled process indicating on entrapment of $Fc(CH_2OH)_2$ within the carbon's pores. The plot of the anodic peak current vs the carbon nanoparticle weight percent content reveals the increase of the peak current probably due to a trapped volume of liquid (Fig. 12.3B). The decrease of the anodic peak current at higher carbon loadings is believed to be due to the mechanical deterioration of the more brittle films with higher carbon content. The behaviour of the porous CNPs–sol-gel electrodes in the presence of an electrochemically reversible solution redox system is dominated in approximately equal amounts by diffusion toward the outer electrode surface and trapped solution within the pores.
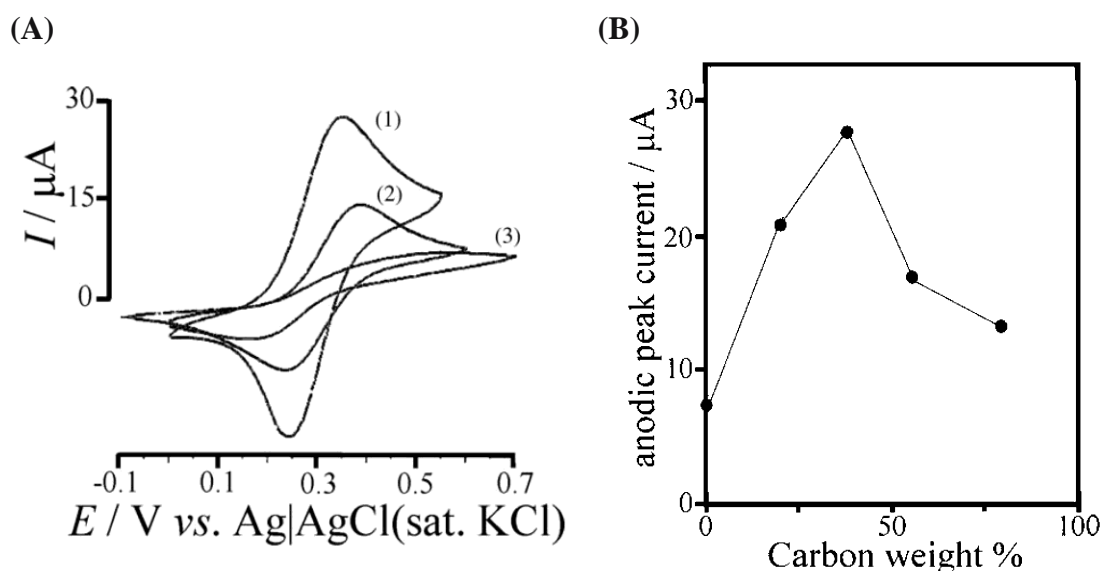
(A)   **(B)**

Fig. 12.3 (A) Cyclic voltammograms of (1) $TMOS_{gel}/CNPs_{KCl}$ (45 wt% CNPs, 50 mM KCl) film modified ITO electrode, (2) a bare ITO electrode, and (3) 0 wt% $TMOS_{gel}/CNPs_{KCl}$ film ITO electrode obtained in 1 mM $Fc(CH_2OH)_2$ solution in 0.1 M $NaClO_4$ aqueous solution. (B) Plot of the anodic peak current vs the CNPs content in the $TMOS_{gel}/CNPs_{KCl}$ film ITO electrode. Scan rate 10 mV s^{-1}.

102

To optimize the electrode formation process, KCl was added to the mixture of sol-gel and carbon nanoparticle suspension. During evaporation of water and methanol and gelation, KCl enrichment causes changes in the carbon nanoparticle aggregation and the resulting in modified composite film structures. Although mechanistic details for this effect are not known, the systematic increase in the anodic current peak for the 1,1′- ferrocenedimethnol oxidation from the diffusion controlled level (at 0 mM KCl) to a considerably increased current (at 50 mM KCl) is clearly observed (Fig. 12.4). The KCl is believed to interact with the carbon aggregates to produce a more accessible and conducting carbon structure. The salt concentration of 50 mM KCl was most beneficial and therefore employed for most of the following experiments.
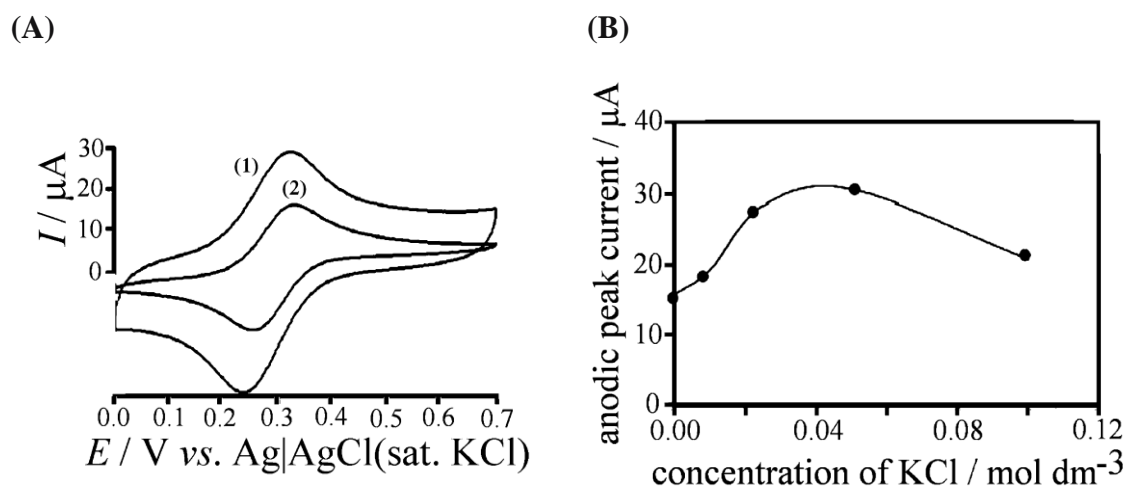
(A)

(B)

Fig. 12.4 (A) Cyclic voltammograms of TMOS$_{gel}$/CNPs$_{KCl}$ film modified ITO electrode with 45 wt% CNPs immersed in Fc(CH$_2$OH)$_2$ solution in 0.1 M NaClO$_4$ aqueous solution. The salt (KCl) content of the deposition solution was varied during the film formation and cyclic voltammograms are shown for (1) no KCl added and (2) 50 mM KCl added. (B) Plot of the anodic peak current vs the KCl concentration in the deposition solution. Scan rate 10 mV s^{-1}.

12.2.2. Electrochemical reactions sensitive on the surface heterogeneity

Two electrode reactions sensitive to electrode heterogeneity surface and its area were tested with obtained electrodes. The examination of slow electrode reaction – electroreduction of hydrogen peroxide in acidic solution provides valuable information on the surface effect because reaction is expected to occur within the whole volume of the film [350, 351].

The examination of the presence of CNPs on the electrochemically highly irreversible reduction of hydrogen peroxide revealed an approximately 20-fold increase of the faradic current for the H_2O_2 reduction (Fig. 12.5A). The current is further increased with higher carbon loading (Fig. 12.5B). In this study, the enhanced reduction is observed probably predominantly caused by the extremely electrochemically active high surface area and of the CNPs and specific geometry of diffusional space. This is confirmed by similar signal-to-noise ratio (calculated as ratio of the current at 0.1 V to that at 0.55 V) equal approximately 10.

(A)   **(B)**
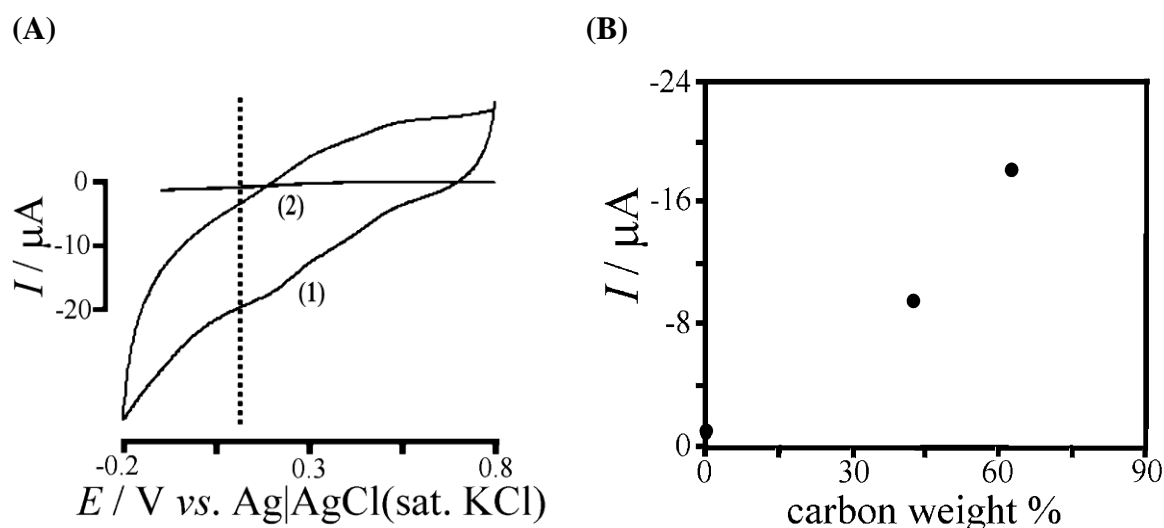
Fig. 12.5 (A) Cyclic voltammograms of (1) a 45 wt% $TMOS_{gel}/CNPs_{KCl}$ film ITO electrode and (2) a bare ITO electrode immersed in 50 mM H_2O_2 solution in 0.1 M H_2SO_4 aqueous solution. (B) Plot of the reduction current vs the CNPs content in the $TMOS_{gel}/CNPs_{KCl}$ film ITO electrode. Scan rate 10 mV s^{-1}.

The voltammetry of redox liquid deposited on the electrode represents another experiment suitable for confirming the surface development of the modified electrode. The efficiency of the electrochemical reaction is proportional to the length of three phase junction electronic conductor|redox liquid|electrolyte solution − the zone where reaction starts (Fig.12.6A,B) [85, 350]. This parameter is substantially increased with nanostructured electrodes [352-355]. Here, a model system − *t*-butylferrocene is used (Fig. 12.6C).
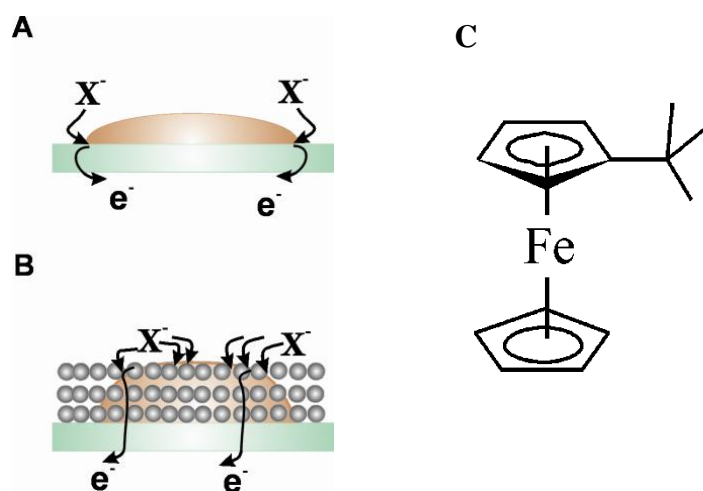
104

Fig. 12.6 (A) The suggested structure of a bare ITO electrode (i) and an ITO electrode covered by CNPs (ii) with redox liquid deposit. The electrochemical reaction predominantly occurs at the ITO electrode-organic liquid-aqueous solution three phase junction and involves electron transfer coupled to anion or cation (not shown for simplicity) transfer. (B) The structural formula of t-butylferrocene. The idea borrowed from ref. [353].

The water insoluble liquid was deposited into porous electrode. In this voltammetric experiment, a peak-shaped response is expected to be associated with the oxidation of *t*BuFc to *t*-butylferricinium cations (*t*BuFc$^+$) (Eq. 12.2) [354].

$$t\text{BuFc(org)} \quad \leftrightarrow \quad t\text{BuFc}^+\text{(org)} \quad + \text{ e}^- \tag{12.2}$$

At a bare ITO electrode, this process is highly ineffective (Fig. 12.7, curve 4) due to the formation of extended droplets which block the electrode surface. However, in the porous structure of the TMOS/CNPs$_{KCl}$ electrode the *t*BuFc liquid is dispersed, and the oxidation can proceed at an extended triple-phase boundary [352-355]. Figure 12.7 shows data for three consecutive potential cycles recorded for a 40 nmol *t*BuFc deposit. The charge under the oxidation peak, approximately 600 μC, is consistent with about 6 nmol electrons being transferred (or 15% of *t*BuFc deposit is converted).
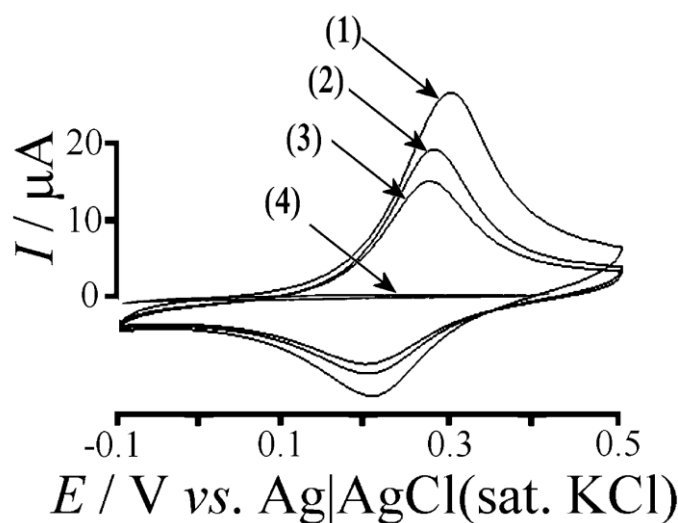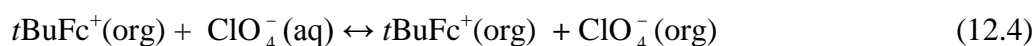
Fig. 12.7 Cyclic voltammograms obtained for the oxidation of tBuFc (40 nmol) immobilized at a 45 wt% TMOS$_{gel}$/CNPs$_{KCl}$ film ITO electrode (50 mM KCl) immersed in 0.1 M NaClO$_4$ aqueous solution: in (1–3) are potential cycles 1 to 3 are shown; (4) cyclic voltammogram obtained under the same conditions at a bare ITO electrode. Scan rate 10 mV s^{-1}.

This behavior of the electrode is related to the development of largely extended three-phase junctions CNP| *tert*-butylferrocene|aqueous electrolyte interface [352, 353, 355]. The efficiency of the reaction (12.2) is similar to obtained with *t*BuFc deposit present on ITO nanoparticles embedded in hydrophobic silicate film [353] but is slightly smaller than on Au covered hydrophobic silicate film (porotrode) [352].

The TMOS$_{gel}$/CNPs$_{KCl}$ film electrode film appears to be wetted by the hydrophobic redox liquid tBuFc, and it retains its electrochemical activity even after several potential cycles. A slow decrease of the voltammetric response can be explained with the slow loss of some produced *t*-butylferricinium cations into the solution phase (Eq. 12.3) [354].

$$t\text{BuFc}^+(\text{org}) \quad \rightarrow \quad t\text{BuFc}^+(\text{aq}) \tag{12.3}$$
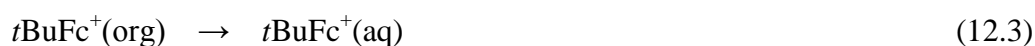
This reaction occurs to maintain charge neutrality of organic deposit. The second competing reaction, the transfer of a counter anion from the aqueous into the organic phase (Eq. 12.4), is likely to occur simultaneously.

$$t\text{BuFc}^+(\text{org}) + \text{ClO}_4^-(\text{aq}) \leftrightarrow t\text{BuFc}^+(\text{org}) + \text{ClO}_4^-(\text{org}) \tag{12.4}$$

106

12.3. Conclusions

A porous electrode modified with hydrophilic CNPs was prepared from a suspension using a sol-gel methodology and drop deposition. The CNPs form micrometer-sized aggregates significantly extending the electrochemically active surface. Namely the double layer capacitance is substantially increased and the effect of the electrode on reversible solution phase redox systems is consistent with other high surface area electrodes. The most significant effect is seen for slow electrode reactions (such as the hydrogen peroxide electroreduction): the magnitude of the current dramatically increases with carbon nanoparticle content. Similarly, a dramatic effect is observed for three-phase junction electrode processes (which suppress capacitive background currents) such as the oxidation of the redox liquid deposit of *tert*-butylferrocene.

13. Hydrophilic carbon nanoparticle-laccase thin film electrode for mediatorless oxygen reduction (TMOS$_{gel}$/CNPs/Lc)

13.1. Introduction

A film composed of hydrophilic carbon nanoparticles (CNPs) with phenyl sulfonic acid functionalities was tested as substrate for mediatorless bioelectrocatalytic oxygen reduction. Laccase and CNPs were immobilized on the electrode surface in a one step procedure − sol drop deposition [356]. Sol-gel processed silicate was chosen as a matrix, because it provides a suitable environment for protein immobilization [357, 358].

The catalytic activity of the enzyme encapsulated in the composite film was studied by cyclic voltammetry, and scanning electrochemical microscopy [359-361]. SECM was used to monitor distribution and activity of the immobilized laccase.

13.2. The microscopic and electrochemical characterization

The surface of the TMOS$_{gel}$/CNPs/Lc electrode was investigated by SEM and AFM (Fig. 13.1A,B). From the SEM image it can be seen that the CNPs form globular structures of the size of tens of nanometers and a well developed surface is formed (Fig. 13.1A). It is difficult to judge whether they are covered by sol-gel processed silicate. Also the AFM image (Fig. 13.1B) shows similar structure of the film. It seems that the

107

modification of CNPs by the protein prevents the nanoparticles aggregation, as it was observed for CNPs entrapped only in silicate matrix (Chapter 12).
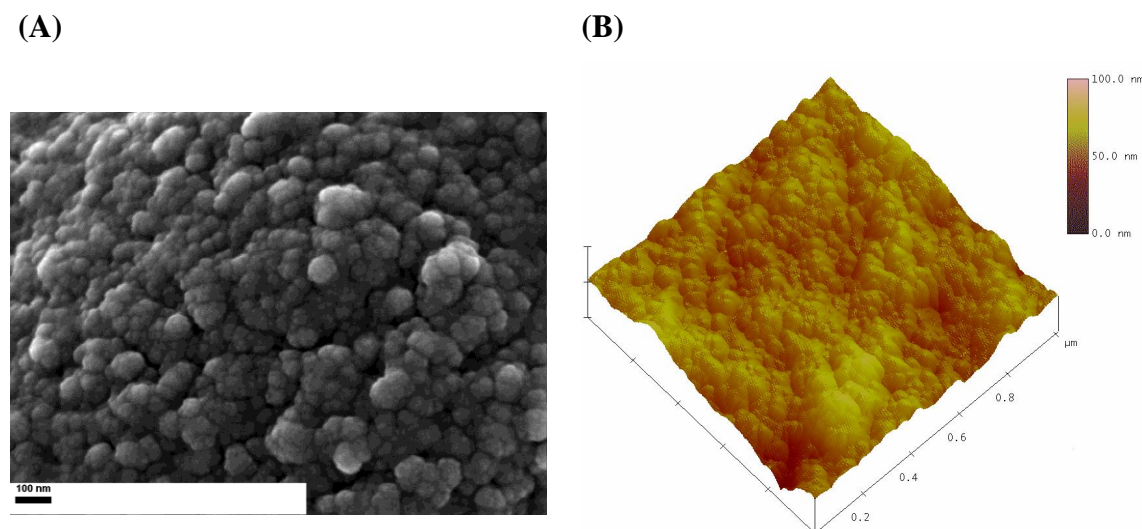
(A)   **(B)**

Fig. 13.1 (A) SEM and (B) AFM images of the TMOS$_{gel}$/CNPs/Lc film ITO electrode. Scale bar 100 nm.

In order to evaluate the electrochemical properties of the prepared electrodes, CV and EIS were applied. As a model the simple redox system $Fe(CN)_6^{3-/4-}$, was selected. The comparison of cyclic voltammograms (Fig. 13.2) and electrochemical impedance spectra (Fig. 13.3) obtained with unmodified, TMOS$_{gel,}$ TMOS$_{gel}$/CNPs and TMOS$_{gel}$/CNPs/Lc ITO electrodes show some effect of the immobilization of the enzyme on CNPs modified electrodes. These include the decrease of the voltammetric peak current, an increase of the difference between the anodic and cathodic peak potentials (Fig. 13.2), and an increase of charge transfer resistance and electrode resistance (Fig. 13.3). This may result from protein adsorption on the CNPs surface. It reduces the number of percolation paths within the film and decrease the probability of electron transfer at the nanoparticle | electrolyte interface, thereby decreasing the heterogeneous electron transfer rate constant [291, 362].

CV also provides the information about the kinetics of the heterogeneous electron process. Recorded curves present quasi − reversible one electron redox reaction (Fig. 13.2). The difference between peaks separation (ΔE_p) for clean electrode is 0.155 V, and it is increasing to 0.189 V and 0.202 V for TMOS$_{gel}$, TMOS$_{gel}$/CNPs/Lc ITO electrode,

108

respectively. The big difference of the potential peak widths for those electrodes reflects the slow electron transport reaction due to the repulsion of $TMOS_{gel}$ and $Fe(CN)_6^{3-/4-}$ ions, and the inert behavior of the enzyme. The smallest ΔE_p, 0.141 V and the highest value of the peak current was obtained for the $TMOS_{gel}$/CNPs electrode. It arises from the good conductivity of the appended CNPs to the silicate matrix, thus the electron transfer is more efficient.
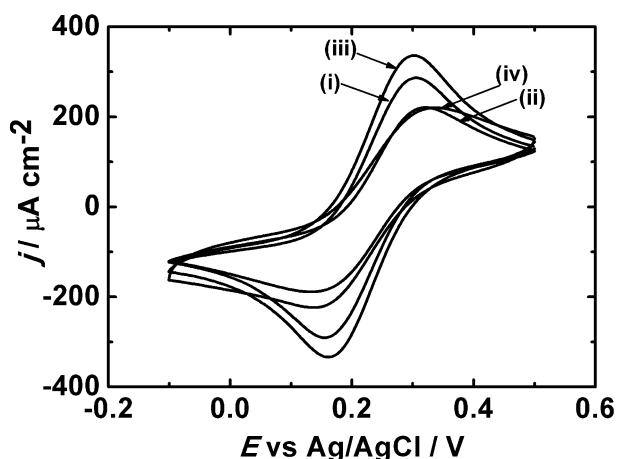

Fig. 13.2 Cyclic voltammograms (2nd scan) of (i) the bare ITO electrode (ii) and coated with $TMOS_{gel}$ (iii) $TMOS_{gel}$/CNPs (iv) $TMOS_{gel}$/CNPs/Lc film ITO electrode immersed in 2.5 mM each of $K_3Fe(CN)_6$ and $K_4Fe(CN)_6$ solution in 0.1 M KCl aqueous solution. Scan rate 10 mV s^{-1}.

EIS was utilized for characterizing the electrical properties of: bare, $TMOS_{gel}$, $TMOS_{gel}$/CNPs and $TMOS_{gel}$/CNPs/Lc ITO electrodes (Fig. 13.3). The measurements were carried out with ferrocyanide ions solution as a redox probe ($Fe(CN)_6^{3-/4-}$ in ration 1:1) that enable the Faradaic impedance to study. The Randles equivalent circuit (Fig. 13.3) consists of the ohmic resistance of the electrolyte solution (R_s), the double layer capacitance (C_{dl}), the Warburg impedance related to the diffusion of the redox probe in the solution (W), and the heterogeneous electron transfer resistance (R_{ct}) and represents a good fit (chi square = $1 - 2 \times 10^{-3}$) to the impedance data (Fig. 13.3). The value of R_{ct} is equal $0.620 \pm 4 \times 10^{-3}$ kΩ, $1.026 \pm 3 \times 10^{-3}$ kΩ, $0.272 \pm 2 \times 10^{-3}$ kΩ and $1.571 \pm 1.4 \times 10^{-2}$ kΩ for bare, $TMOS_{gel}$, $TMOS_{gel}$/CNPs and $TMOS_{gel}$/CNPs/Lc ITO electrode respectively. Clearly the presence of sol-gel processed silicate block the electrode surface and slows down electrode kinetics because of electrostatic repulsion between

film and electroactive anions [363]. The immobilisation of CNPs within the film decreases R_{ct}, because of the increase of the electroactive surface, and the amelioration of electrical conductivity. This occurs despite electrostatic repulsion between sulfonic groups of CNPs and negatively charged redox active anions. Clearly, immobilization of laccase increases R_{ct} ca. 6 times, because its adsorption obstructs the electron transfer [364]. The value of R_s of TMOS$_{gel}$/CNPs/Lc ITO electrode is considerably larger than the others. Since the resistance of the electrode is one of the components of this parameter, immobilized laccase clearly increases the resistance of the CNPs-silicate film. The outcomes from EIS experiments are in good agreement with the results from CV measurements.
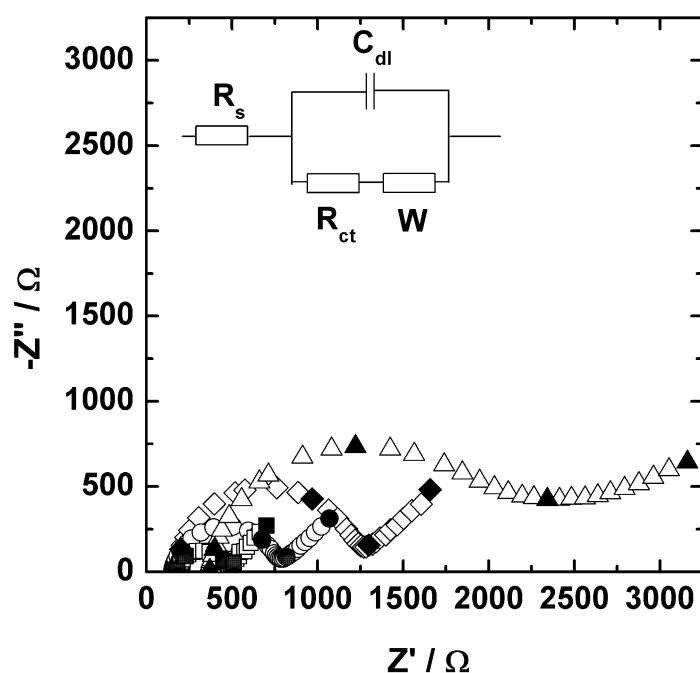

Fig. 13.3 Impedance spectrum presented as Nyquist plot – imaginary part of impedance (-Z'') vs. real one (Z') obtained 2.5 mM each of K₃Fe(CN)₆ and K₄Fe(CN)₆ in 0.1 M KCl aq at a bare ITO electrode (circles) and electrode coated with TMOS$_{gel}$ (diamonds) TMOS$_{gel}$/CNPs (squares) and TMOS$_{gel}$/CNPs/Lc (triangles) film. The frequency difference between data marked with filled symbols is equal one order of magnitude. The frequency range is 0.1 Hz– 10⁵ Hz and the magnitude of perturbation signal is 10 mV (peak-to-peak). The measurements were done at potential equal open circuit voltage. Inset: The Randles equivalent circuit used in fitting.

110

13.3. Bioelectrocatalytic activity

The voltammograms obtained with $TMOS_{gel}$/CNPs/Lc film electrode immersed in McIlvaine buffer (pH 4.8) with different concentrations of oxygen are presented in insert at Fig. 13.4A. For solutions containing oxygen a well defined sigmoidal signal with a current proportional to the O_2 concentration is observed. This signal is absent when laccase is not immobilized in the CNP-silicate film or when laccase is immobilized in a silicate film without CNPs. This clearly indicates enzymatic electrocatalysis without mediator and shows that the presence of CNPs provides favourable conditions for DET between laccase and the electrode. The alternative procedure that involves the addition of the enzyme solution directly to the sol, results in an electrode exhibiting only a minor catalytic current density of the range of 5 $\mu A\ cm^{-2}$ in the same conditions.
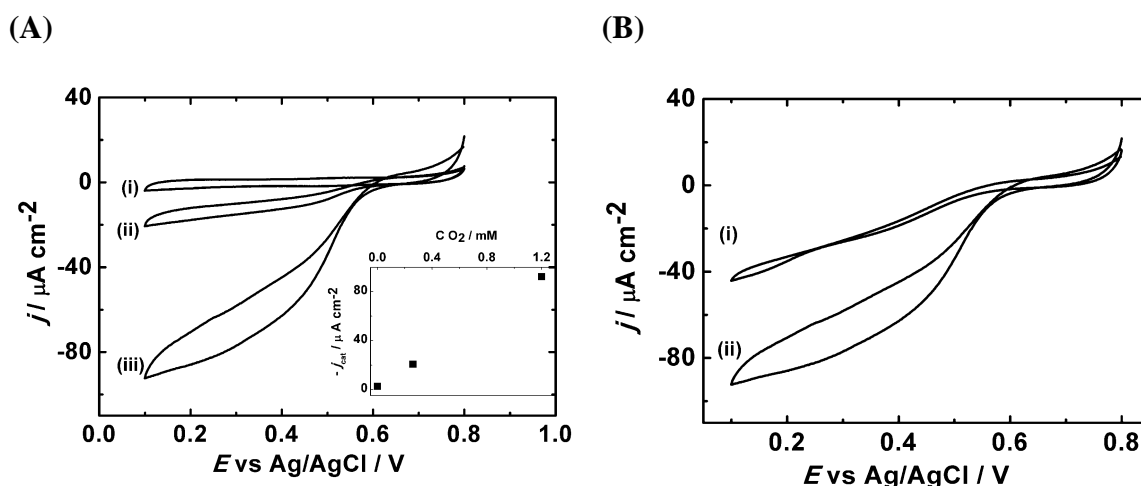
(A)   **(B)**

Fig. 13.4 (A) Cyclic voltammograms (2nd scan) of $TMOS_{gel}$/CNPs/Lc film ITO electrodes immersed in 0.1 M McIlvaine buffer (pH 4.8) saturated with (i) argon (ii) air (iii) and oxygen. Scan rate 1 mV s^{-1}. Inset: Maximum catalytic current density vs. estimated oxygen concentration. (B) Cyclic voltammograms (2nd scan) of $TMOS_{gel}$/CNPs/BOx (i) and $TMOS_{gel}$/CNPs/Lc (ii) films ITO electrode immersed in O_2-saturated 0.1M McIlvaine buffer (pH 5). Scan rate 1 mV s^{-1}.

The mediatorless bioelectrocatalytic reaction of oxygen reduction commences at 0.575 V. Due to lack of faradaic signal in anaerobic conditions we were not able to estimate the redox potential of the immobilised laccase. However, the onset potential of

111

the catalytic wave is close to the reported redox potential of the T1 centre of this enzyme on various carbon materials [147, 255, 365]. Interestingly, analogous BOx-modified electrode exhibited poor catalytic activity (Fig. 13.4B (i)). This indicates that hydrophilic silicate provides more favourable conditions for electron exchange between the Lc and CNPs which might be due to different orientations of the enzymes in hydrophilic sol–gel processed matrices.

Utilization of ABTS^{2-} as mediator for laccase is well known [141]. Therefore, for improving the efficiency of the electrocatalytic process of laccase adsorbed on CNPs and entrapped in silicate matrix that redox probe was used. The experiment was performed with TMOS$_{gel}$/CNPs/Lc and TMOS$_{gel}$/Lc electrodes with ABTS^{2-} dissolved in the McIlvaine buffer (Fig. 13.5).
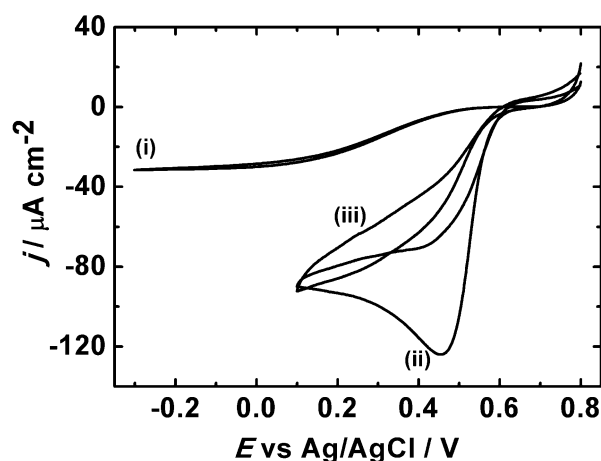
Fig. 13.5 Cyclic voltammograms (2nd scan) of (i) TMOS$_{gel}$/Lc, (iii) TMOS$_{gel}$/CNPs/Lc film ITO electrodes immersed in 0.1 mM ABTS^{2-} solution in O$_2$-saturated 0.1 M McIlvaine buffer (pH 4.8) and (ii) TMOS$_{gel}$/CNPs/Lc film ITO electrode immersed in in O$_2$-saturated 0.1 M McIlvaine buffer (pH 4.8). Scan rate 1 mV s^{-1}.

Obtained results for the TMOS$_{gel}$/CNPs/Lc electrode measured with and without mediator, show that the presence of ABTS^{2-} influences the shape of catalytic wave changing it from sigmoidal to peak-shaped one (Fig. 13.5 (iii)). Such behaviour might result from the depletion of ABTS$^{-\bullet}$ in the vicinity of the electrode's surface. This deficit of the oxidized form is the outcome of its utilization in the electrochemical reaction and its decompostion due to its natural instability. Had the experiment been performed with

112

scan rate lower than 1 mV s^{-1} the ABTS$^{-\bullet}$ would have had enough time to regenerate and the peak would probably disappear. Comparing current densities at 0.2 V, one can see that ABTS^{2-} presence in fact does not improve the bioelectrocatalytic process significantly. Similar result was also observed for the ITO electrode modified only with silicate layer with entrapped laccase (Fig. 13.5 (i)). Obtained current density is ca. 40 µA cm^{-2} smaller than for the sample for which direct electron transport is observed. It is clear that for the latter system the addition of CNPs on which surface laccase is adsorbed to silicate matrix results in: mediatorless bioelectrocatalysis and overpotential dercease for mediated catalysis by about 0.2 V. This probably results from mismatch of the redox potential of T1 site of laccase and mediator.

Voltammetric experiments performed at different scan rates provide qualitative information about the kinetics of the mediatorless electrocatalytic reaction at TMOS$_{gel}$/CNPs/Lc film electrode (Fig. 13.6). The shape of the CVs is scan rate-dependent indicating that the reaction strongly depends on the time scale. Similar behaviour was seen for modified bioelectrocatalysis by laccase entrapped in silicate film [345]. The sigmoidal shape of voltammogram is observed only at scan rates ≤ 4 mV s^{-1}. Also the cathodic and anodic charge ratios (Q_c/Q_a) are significantly larger than unity in the same scan rate range (see inset in Fig. 13.6). The obtained data show that the kinetics of mediatorless bioelectrocatalysis with immobilized laccase is independent of the electrode support and slow [345].
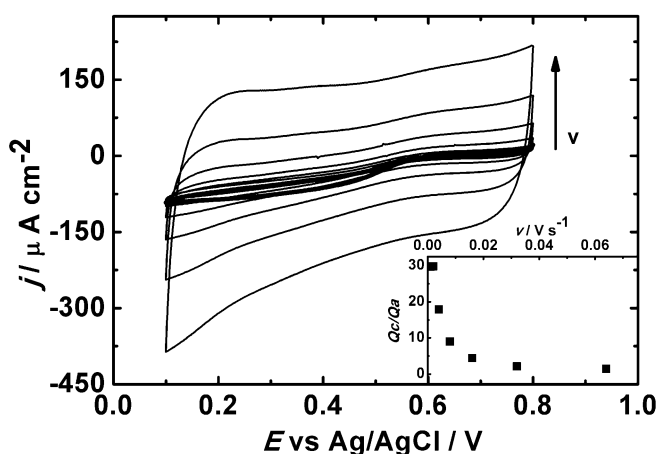

Fig. 13.6 Cyclic voltammograms (2nd scan) of TMOS$_{gel}$/CNPs/Lc film ITO electrode in O$_2$-saturated 0.1 M McIlvaine buffer (pH 4.8) at various scan rates: 64, 32, 16, 8, 4, 2, 1 mV s^{-1}. Inset: Plot of the ratio of cathodic to anodic charge (Q_c/Q_a) vs. scan rate (v). Arrow indicates increasing scan rate.

113

The effect of pH on bioelectrocatalysis with TMOS$_{gel}$/CNPs/Lc was studied in McIlvaine buffers of different pH (Fig. 13.7). The observed maximum of the bioelectrocatalytic activity in the pH range 3.8 − 4.8 is slightly shifted from the value corresponding to the maximum of protein activity (pH 5.3) [366]. This may be caused by local pH shift, because of larger concentration of hydrated protons (as compared to bulk of electrolyte) attracted to oxygen atoms bridging Si atoms as well to unreacted OH⁻ groups [101, 367]. The bioelectrocatalytic current density at neutral pH is about 30 times smaller than its maximal value. This is due to decreased laccase activity, because of a hydroxide anion binding to the T2/T3 coppers ions blocking oxygen access [368].
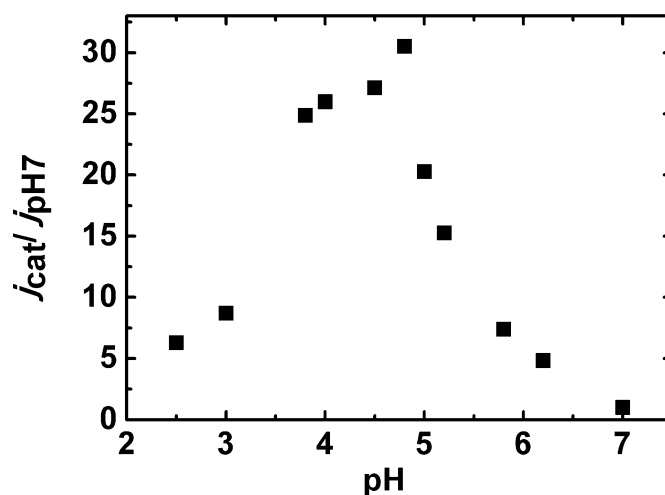

Fig. 13.7 pH dependence of the catalytic current density (j$_{cat}$), divided by current density at pH 7, at potential 0.2 V obtained with TMOS$_{gel}$/CNPs/Lc film ITO electrode immersed in O$_2$-saturated 0.1 M McIlvaine buffer.

13.4. Mapping of the electrode activity with scanning electrochemical microscopy

The activity of the laccase immobilized in CNPs-silicate film was studied by SECM in redox competition mode (RC-SECM) [334, 336]. The idea of this experiment is based on competition for dissolved oxygen between the UME of the SECM and the closely spaced laccase-modified electrode [337]. In order to avoid O_2 depletion in the space between the UME and the substrate, a two-step potential program is applied to the UME at every grid point of the image. In the first step, the UME potential E_T is set to 1.35 V for 3 s causing oxygen generation by water oxidation. Next, E_T is shifted to -0.40 V for diffusion-controlled oxygen reduction reaction (ORR) at the UME for another 3 s (Fig. 13.8).
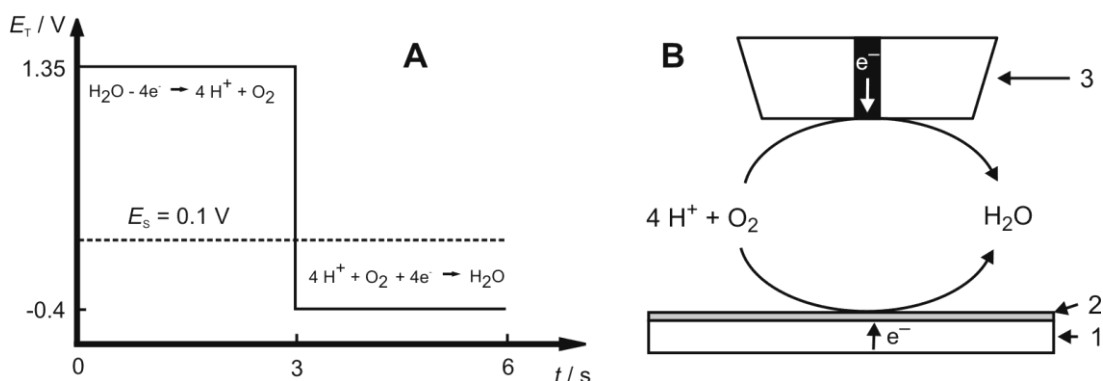

Fig. 13.8 (A) The potential (E_T) program for UME for the RC mode SECM imaging of laccase activity. (B) Schematic of the reactions occurring in the second potential step $3 < t/s < 6$; (1) ITO electrode, (2) $TMOS_{gel}$/CNPs/Lc film ITO electrode and (3) UME tip.

While the UME is located over the active enzyme, its ORR current is smaller because of oxygen consumption by the laccase at the substrate. A two-dimensional image is constructed by plotting the average UME current $i_T(x,y,t)$ between $t = 3.3$ s and $t = 4.0$ s within the potential step at $E_T = -0.4$ V at every point over the $TMOS_{gel}$/CNPs/Lc film. In this image a low absolute i_T represents a locally high laccase activity.

Such images are also influenced by topographic features as they can affect the O_2 diffusion in the interelectrode space. Therefore, two experiments were performed in order to estimate the influence of topographic features of the sample. In the first experiment, the sample electrode was polarized at the potential $E_S = 0.1$ V

115

corresponding to oxygen reduction (Fig. 13.9A). In the second (control) experiment, the sample potential was floating (Fig. 13.9B) [369]. In order to find the active spots, the recorded i_T has to be lower in the RC-SECM experiment (Fig. 13.9A) compared to the control experiment (Fig. 13.9B). The difference between i_T in the two experiments was calculated and is presented as a differential image in Fig. 13.9C. The red areas correspond to higher local laccase activity, whereas the blue areas indicate a lower activity. From this image one can conclude that the active spots are more evenly distributed in the CNPs-silicate matrix than in the case of silicate film without nanoparticles where protein aggregations were observed [369]. This conclusion is also supported by SEM and AFM observation indicating even distribution of the enzyme (see above). It is quite possible that laccase aggregation may be responsible for the lack of the mediatorless bioelectrocatalytic oxygen reduction in the $TMOS_{gel}$/Lc film [370].
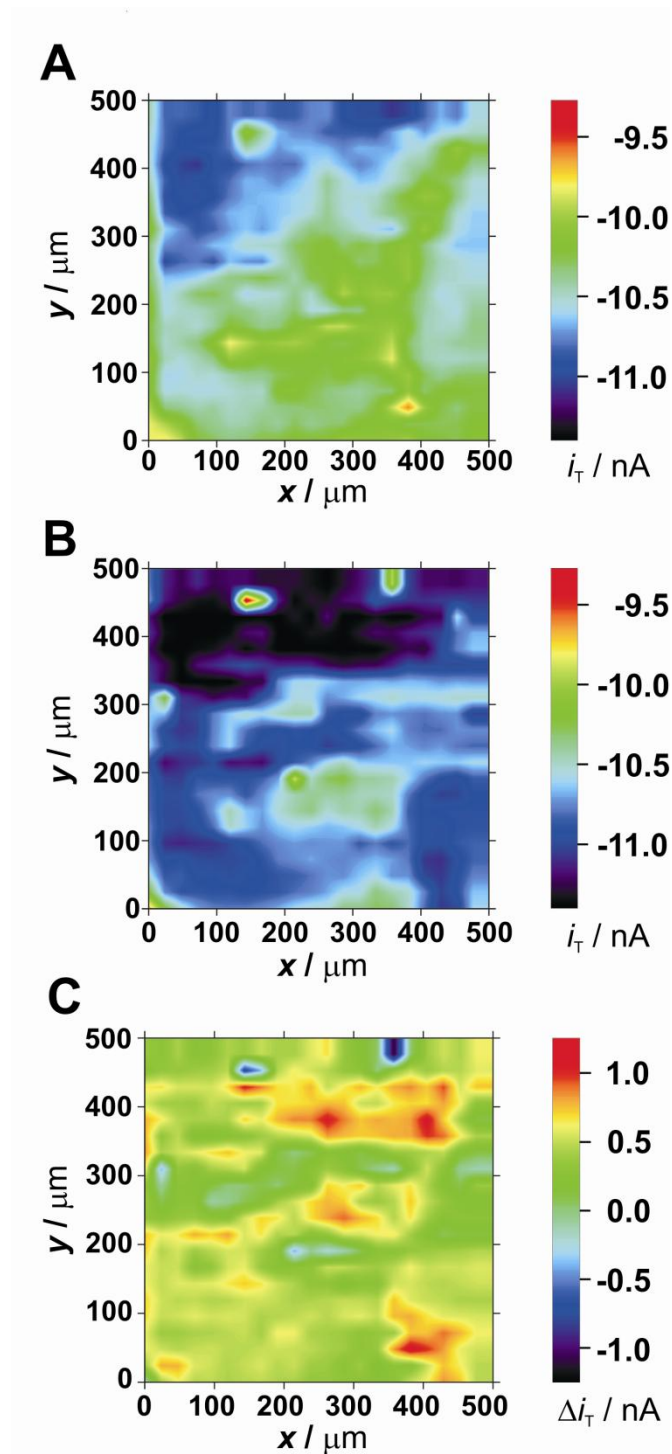
Fig. 13.9 SECM (RC mode) visualization of laccase distribution in TMOS$_{gel}$/CNPs/Lc film ITO electrode in air-saturated 0.1 M McIlvaine buffer (pH 4.8). r_T = 13.15 μm, d =20 μm, v_T = 10 μm s^{-1}. E_T = 1.35 V (3 s) and -0.4 V (3 s); grid spacing is 25 μm. Images are constructed by plotting the average UME current $i_T(x,y,t)$ between t = 3.3 s and t = 4.0 s after stepping to E_T = -0.4 V. The image (A) is recorded with E_S = 0.1 V; and (B) with the sample at open circuit potential. The image (C) was obtained by subtracting the current obtained in control experiment (B) from the current obtained in experiment (A).

117

13.5. Stability of the TMOS$_{gel}$/CNPs/Lc electrode and its application in Zn-O$_2$ hybrid cell

Bearing in mind the potential use of laccase-modified electrodes in energy sources the stability of TMOS$_{gel}$/CNPs/Lc film electrode was tested by chronoamperometry (Fig. 13.10). One hour after application of the potential 0.2 V, the oxygen reduction current decreases by ca. 60%. However, over the next 30 hours it exhibits only a minor decrease ca. 30 μA cm^{-2}.
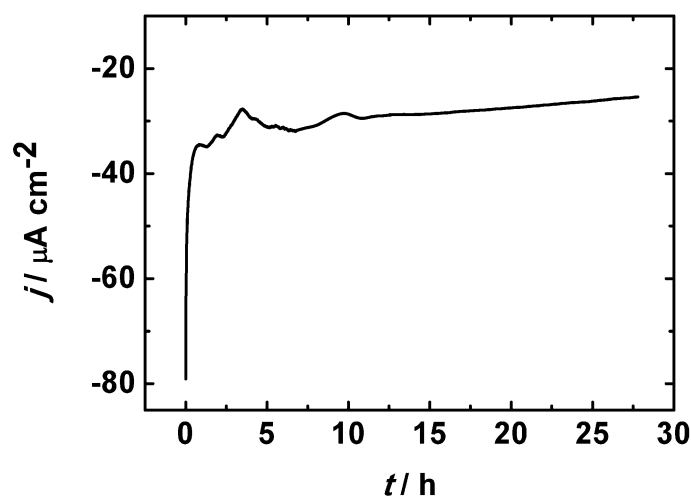

Fig. 13.10 Current density (j) vs. time (t) dependence obtained after application of potential step +0.2 V to TMOS$_{gel}$/CNPs/Lc film ITO electrode immersed in O$_2$-saturated 0.1 M McIlvaine buffer (pH 4.8).

Next, the TMOS$_{gel}$/CNPs/Lc film electrode was tested as biocathode in a zinc-oxygen cell. The cell consists of a TMOS$_{gel}$/CNPs/Lc cathode and a Nafion-coated Zn anode immersed in oxygen saturated 0.1 M McIlvaine buffer (pH 4.8). The voltage was measured for 100 s when the potential was stabilized. It has an open-circuit voltage equal to 1.48 V, below the theoretical value of 1.99 V (Fig. 13.11). The maximum power density is equal to 17.6 μW cm^{-2} at 0.7 V. The considerable decrease of the cell voltage with increasing load is most likely caused by the slow kinetic of the enzymatic reaction on the cathode.
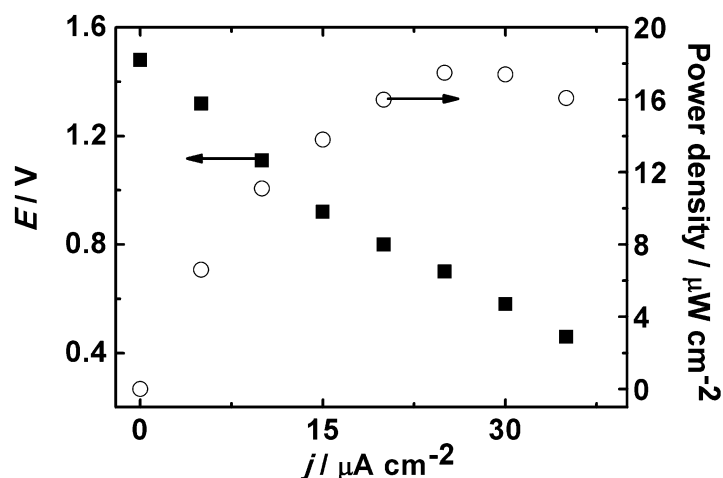
118

Fig. 13.11 Polarisation curve (○) of the Zn-O$_2$ hybrid cell with TMOS$_{gel}$/CNPs/Lc film ITO electrode as biocathode, and the dependence of the power output (■) on the current density in O$_2$-saturated 0.1 M McIlvaine buffer (pH 4.8).

13.6. Conclusions

Electrodes modified with laccase and hydrophilic carbon nanoparticles in nonfunctionalized silicate matrix allows for mediatorless bioelectrocatalytic oxygen reduction. It is probable that the proper enzyme orientation towards nanoparticles allows for efficient electron exchange between CNPs and active site of the enzyme. This can only be achieved if laccase is first mixed with CNPs suspension possibly allowing for adsorption of the enzyme on the CNPs surface. Presumably the electrostatic interactions of positively charged amino acids of Lc such as histidines and cysteins with negatively charged phenyl sulphonate groups on CNPs, facilities the adsorption processes. Additionally, entrapment of that material within silicate matrix enables for stable enzymatic-silicate film formation.

The microscopic examination of the electrode surface shows that laccase' aggregations that were observed in sol-gel processed silicate film deposited on glass are not observed in the presence of CNPs. Clearly, incorporation of both these nanosized components (CNPs and protein molecules) results in their even distribution within the sol-gel processed film. This may also help in achieving direct electrical communication between the electrode and protein's active center.

119

Although, the obtained biocathode was applied successfully in Zn-oxygen hybrid cell its further potential *in vivo* application is limited by laccase's poor activity under physiological conditions.

14. Hydrophobic sol-gel film electrodes

14.1. Introduction

Bilirubin oxidase is superior catalyst for oxygen reduction biocatalysis as compared to laccase [154] in terms of activity under simulated physiological conditions, i.e. at neutral pH and in the presence of Cl^- anions [371], but also its overpotential decrease is comparable with highly potential laccase.

The film electrodes composed of CNPs embedded in hydrophobic silicate matrixes ($MTMOS_{gel}$/CNPs and $OTEOS_{gel}$/CNPs) were characterized. After bilirubin oxidase adsorption they were tested for mediatorless bioelectrocatalysis of oxygen reduction by cyclic voltammetry and chronoamperometry. These electrodes surface were also examined by scanning electron microscopy. One of the electrodes ($MTMOS_{gel}$/CNPs) was also successfully applied as biocathode in Zn-oxygen hybrid cell.

Finally their behaviour will be compared with electrodes based on hydrophilic matrix, in terms of bioelectrocatalytic reaction of oxygen reduction.

14.2. The microscopic characterization

The surface of the film electrode composed of CNPs embedded in sol-gel processed hydrophobic silicate matrix was investigated by SEM (Fig. 14.1). The image shows that CNPs form aggregates of the size from few to few hundreds nanometers, which are more aggregated as compared to hydrophilic matrix (Fig. 13.1.A). The hydrophobic CNPs film's structure is porous but rather compact, and tightly covered with silica (Fig. 14.1). However, the results will further demonstrate that such a structure is sufficiently porous to enable efficient oxygen transport.
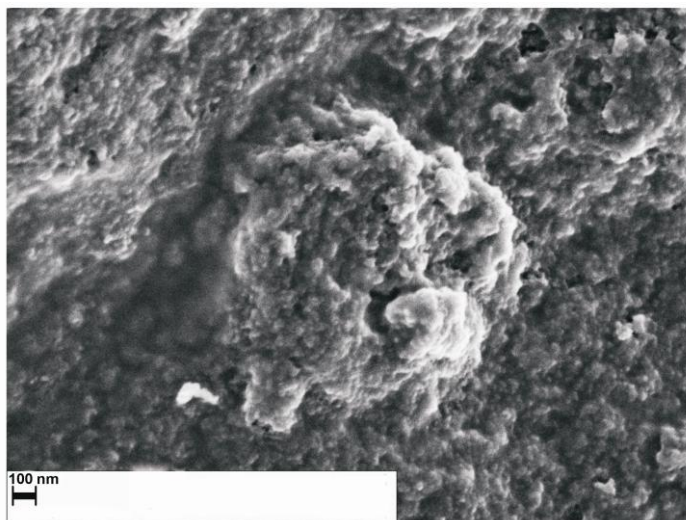
Fig. 14.1 SEM image of the MTMOS$_{gel}$/CNP film ITO electrode.

14.3. Bioelectrocatalytic activity

14.3.1. Mediatorless bioelectrocatalysis on MTMOS$_{gel}$/CNP/BOx electrode

As it is depicted in the inset of the Fig. 14.2 the catalytic current density strongly depends on the concentration of the CNPs within silicate film. The maximal bioelectrocatalytic current was recorded for the electrode modified with CNPs of the concentration equal 2.5 mg ml^{-1}, and for further experiments this electrode was chosen. As one can see from the Fig. 13.2 a well defined sigmoidal curve with a current proportional to the O$_2$ concentration is obtained. This signal is absent when BOx is not adsorbed onto the modified electrode (not shown). The onset potential of catalytic current of the modified electrode for aerobic conditions commences at ca. 0.60 V. That value is close to the formal potential of the T1 centre of BOx [155]. Even for this film some bioelectrocatalytic activity is observed in Ar-saturated solution (Fig. 14.2 (i)). This is probably due to the electroreduction of oxygen trapped within the CNPs-silicate matrix being in contact with the deaerated electrolyte. Clearly, CNPs provide favourable conditions for electron exchange between the electrode and the enzyme's active centre.
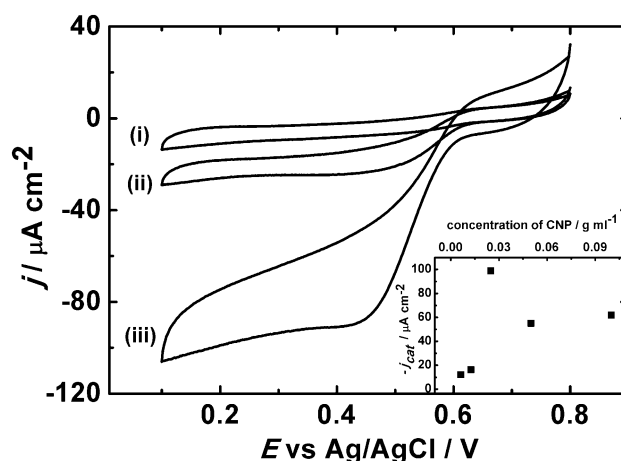
121

Fig. 14.2 Cyclic voltammograms (2nd scan) of MTMOS/CNPs/BOx film ITO electrode with 2.5 mg ml^{-1} CNPs concentrention in deposition sol immersed in (i) Ar and (ii) air and (iii) O_2-saturated 0.1M McIlvaine buffer (pH 5). Scan rate 1 mV s^{-1}. Inset: Current density at 0.2 V vs. CNPs concentration in deposition sol.

The catalytic current density is larger than for carbon nanoparticulate film embedded in a hydrophilic silicate with immobilized bilirubin oxidase. However, if Lc is adsorbed on MTMOS$_{gel}$/CNPs modified electrode the bioelectrocatalytic current density is an order of magnitude smaller than with adsorbed BOx (Fig. 14.3). This indicates that hydrophobic silicate provides more favourable conditions for electron exchange between the BOx and CNPs which might be due to different orientations of the enzyme in hydrophilic and hydrophobic sol–gel processed matrices.
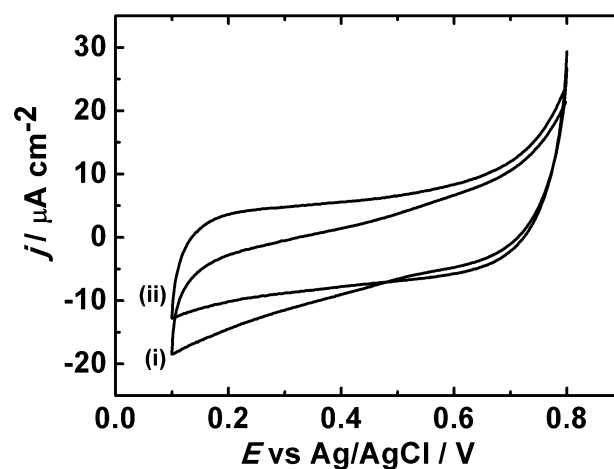

Fig. 14.3 Cyclic voltammograms (2nd scan) of (i) MTMOS$_{gel}$/CNPs and (ii) MTMOS$_{gel}$/CNPs/Lc film ITO electrode immersed in O_2-saturated 0.1 M McIlvaine buffer (pH 5). Scan rate 1 mV s^{-1}.

122

Voltammetric experiments performed at different scan rates provide qualitative information about the kinetics of the mediatorless electrocatalytic reaction at MTMOS$_{gel}$/CNPs/BOx film electrode. As it depicted in Fig. 14.4 the shape of CV is scan rate-dependent indicating that the reaction strongly depends on the time scale. Similar behaviour was recorded for hydrophilic silicate matrix with immobilized laccase and CNPs (Fig. 13.5). Also the sigmoidal shape of voltammogram is observed only at scan rates $\leq$ 4 mV s^{-1}, and the cathodic and anodic charge ratios (Q_c/Q_a) are significantly larger than unity in the same scan rate range (see inset in Fig. 14.4). The results show that the kinetics of mediatorless bioelectrocatalysis with immobilized BOx is slow [345].
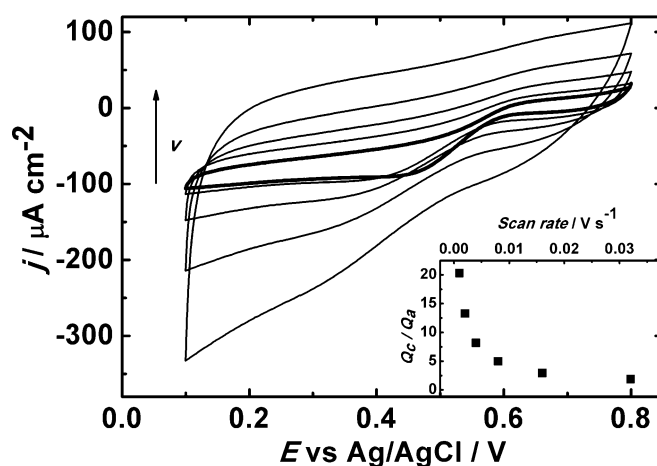

Fig. 14.4 Cyclic voltammograms (2nd scan) of MTMOS$_{gel}$/CNPs/Lc film ITO electrode in O$_2$-saturated 0.1 M McIlvaine buffer (pH 5) at various scan rates: 64, 32, 16, 8, 4, 2, 1 mV s^{-1}. Inset: Plot of the ratio of cathodic to anodic charge (Q_c/Q_a) vs. scan rate (v). Arrow indicates increasing scan rate.

Keeping in mind that such electrode should be applicable *in vivo*, experiments in the buffer of pH 7 and artificial serum were performed. As one can see from obtained CVs, the curves' shape is typical for bioelectrocatalytical process (Fig. 14.5 (i, ii)). Such behaviour is not observed when bilirubin oxidase is not adsorbed onto the surface of modified electrode (Fig. 14.5 (iii)). The onset potential of the catalytic wave is shifted to more negative potential compare to the one recorded for at pH 5, and it commences at 0.50 V, thus increasing the overpotential of oxygen reduction. The catalytic current density recorded in pH 7 is comparable with the one observed for pH 5 (Fig. 14.2), albeit in artificial serum is about 50 % smaller. Nevertheless, the ability of the modified

123

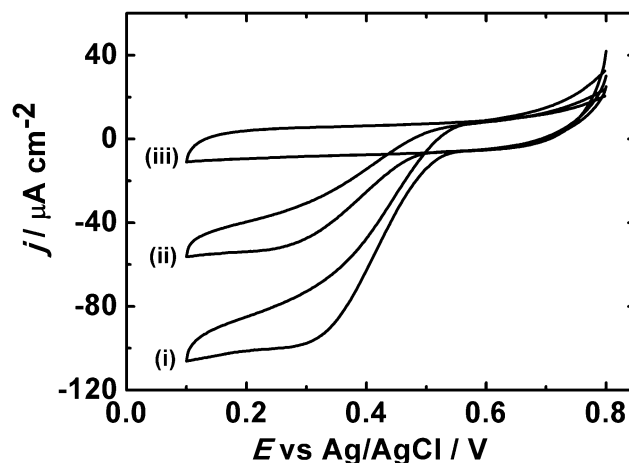electrode to operate effectively in physiological conditions makes it applicable as a cathode in the biofuel cell.

Fig. 14.5 Cyclic voltammograms (2nd scan) of MTMOS$_{gel}$/CNPs/BOx film ITO electrode immersed in O$_2$-saturated (i) 0.1M McIlvaine buffer (pH 7), (ii) artificial serum and, (iii) cyclic voltammogram of MTMOS$_{gel}$/CNPs film ITO electrode immersed in O$_2$-saturated 0.1M McIlvaine buffer (pH 7). Scan rate 1 mV s^{-1}.

14.3.2. Mediatorless bioelectrocatalysis on OTEOS$_{gel}$/CNPs/BOx electrode

The impact of the used salt for the preparation of carbon nanoparticles suspensions, and further for hydrophobic silicate matrix generation (OTEOS$_{gel}$/CNPs), was studied. As one can see from the Fig. 14.6 the BOx after the adsorption on various matrices exhibits mediatorless electrocatalysis towards oxygen reduction. The onset potential of catalytic current of the modified electrodes for aerobic conditions commences at ca. 0.60 V. That value is close to the formal potential of the T1 centre of BOx [155]. The onset potential also depands on the anion of the salt used for film preparation (Fig. 14.6). Such an outcome might results from stronger interaction of protein's T1 center with chloride or fluoride anions and decrease of bioelectrocatalytic activity is seen. The result from that experiment is not clear because one would expect that it exhibited behaviour according to Hofmeister series [372] however in that case it is not observed. It seems that the interactions between ions and protein molecules in this case are influenced by some undetermined factor contradictive to Hofmeister series-like behaviour. Further studies will be required.
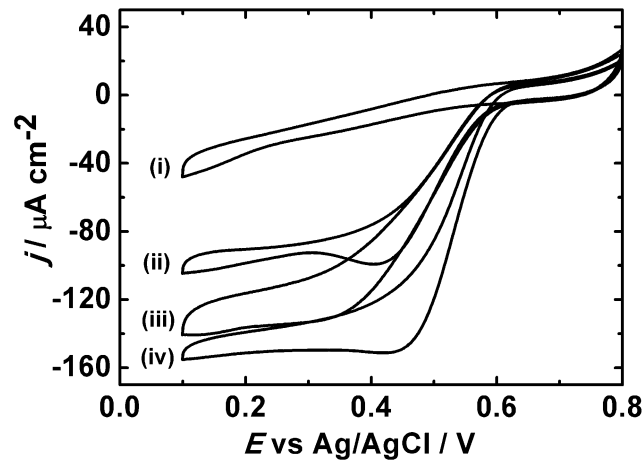
124

Fig. 14.6 Cyclic voltammograms (2nd scan) of OTEOS$_{gel}$/CNPs/BOx film ITO electrode immersed in O$_2$-saturated 0.1 M McIlvaine buffer (pH 5) with various electrolytes used for the preparation of CNPs suspension (i) NaCl (ii) NaF (iii) NaClO$_4$, and (iv) Na$_2$SO$_3$. Scan rate 1 mV s^{-1}.

14.4. Stability of the MTMOS$_{gel}$/CNPs/BOx electrode and its application in Zn-O$_2$ hybrid cell

The stability of MTMOS$_{gel}$/CNPs/BOx film electrode was tested by chronoamperometry (Fig 14.7). One hour after application of the potential 0.2 V, the oxygen reduction current had decreased by ca. 60%. However, over the next 25 hours it exhibits only a minor decrease from 50 to 40 μA cm^{-2}.
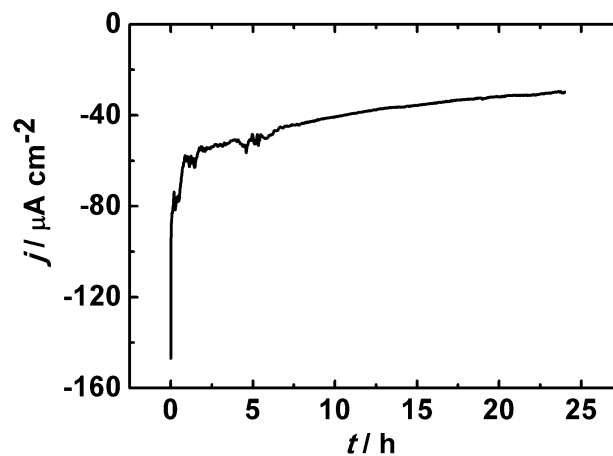

Fig. 14.7 Current density (j) vs. time (t) dependence obtained after application of potential step + 0.2 V to MTMOS$_{gel}$/CNPs/Lc film ITO electrode immersed in O$_2$-saturated 0.1 M McIlvaine buffer (pH 5).

125

The cell consists of MTMOS$_{gel}$/CNPs/BOx cathode and a Nafion-coated Zn anode immersed in: oxygen saturated 0.1 M McIlvaine buffer (pH 5) and artificial serum (Fig. 14.8). The voltage was measured for 100 s when the potential was stabilized. An open-circuit voltage equals to 1.67 V and 1.34 V, at pH 5 and artificial serum, respectively (Fig. 14.8A,B), both below the theoretical value of 1.99 V. The maximum power density is equal to 100 μW cm^{-2} at 1.0 V, and 67 μW cm^{-2} at 0.54 V for pH 5 and artificial serum respectively. The considerable decrease of the cell voltage with increasing load is most likely caused by the slow kinetics of the enzymatic reaction on the cathode. Also one can notice that bioelectrocatalytic oxygen reduction in physiological conditions occurs at much lower potentials, so activation voltage drop is much higher for Zn-O$_2$ hybrid cell than for cell recorded in buffer of pH 5. This is due to lower overpotential of bioelectrocatalytic reaction of oxygen reduction. Additionally, the presence of chloride ions might slightly decrease the BOx's activity. The maximum power density of Zn-O$_2$ hybrid cell constructed from MTMOS$_{gel}$/CNPs/BOx exceeds the one recorded with TMOS$_{gel}$/CNPs/Lc, almost by an order of magnitude. Such result might be explained by that that Lc during measurments might lose its biological activity.

(A)   **(B)**
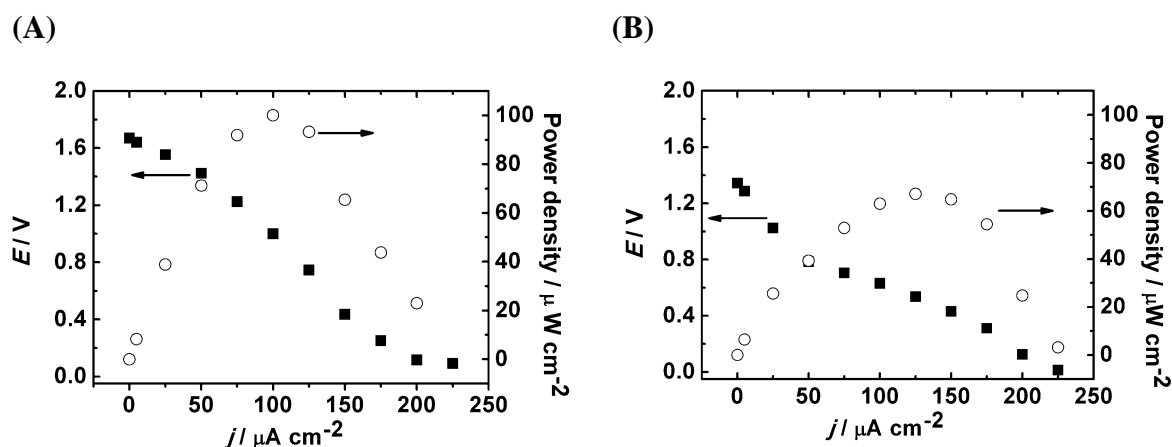
Fig. 14.8 Polarisation curves (●) of the Zn-O$_2$ hybrid cell with MTMOS$_{gel}$/CNPs/BOx film ITO electrode as biocathode, and the dependence of the power output (■) on the current density in O$_2$-saturated (A) 0.1 M McIlvaine buffer (pH 5) and (B) artificial serum.

14.5. Conclusions

The hydrophilic carbon nanoparticles were effectively entrapped within hydrophobic silicate matrixes in the sol-gel process. This electrode material after adsorption on its surface bilirubin oxidase provides favorable conditions for direct electron transfer between the electrode and protein, hence ameliorating the bioelectrocatalytic reaction of oxygen reaction. The obtained electrode was applied successfully as biocathode in a Zn-oxygen hybrid cell operating in 0.1 M McIlvaine buffer (pH 5) and under physiological conditions. The value of maximum power density exceeds almost by an order the values obtained with hydrophilic carbon nanoparticles-laccase thin film biocathode.

15. CNPs-imidazolium functionalized silicate film electrode prepared by layer-by-layer method

15.1. Introduction

The ionic liquid and carbon nanomaterials modified electrodes have become an intensively explored research area [373]. One can find in the literature mostly electrodes modified by non-covalently bonded IL e.g. carbon paste electrodes. However, less attention was paid to the electrodes modified with IL appended film [373].

Here, the hybrid sol-gel processed silicate thin film electrode with cationic appended imidazolium groups is presented. Such electrode was obtained by the sol-gel technology together with LbL method. This approach enables not only to take advantage of electrostatic attraction between charged components (positively charged imidazolium groups and negatively charged CNPs), but also strengthen mechanically the film, because electrostatic self assembly is followed by formation of the inorganic polymer network [236].

The morphology and structure of the surface of CNPs-imidazolium functionalized silicate layers film electrode was investigated by SEM and optical profilometry. The electrochemical properties were evaluated with cyclic voltammetry. These electrodes were examined as a support for laccase and bilirubin oxidase. They exhibit bioelectrocatalytic activity towards oxygen reduction in the presence and absence of accumulated mediator onto their surface.

15.2. The microscopic and electrochemical characterization

The black coloration of the ITO electrode after alternative immersions into CNPs suspension and silicate is increased [83]. This indicates that the film deposition is successful. Change of coloration is observed when sol is composed of non charged precursor TMOS only. CNPs are uniformly distributed within the film as it can be judged by SEM picture (Fig. 15.1). Therefore, the electrostatic interactions between positively charged imidazolium groups of precursor – 1-methyl-3-(3-trimethoxysilylpropyl)imidazolium bis(trifluoromethyl sulfonyl)imide (1) (Fig. 15.2) and negatively charged sulphonic groups of carbon nanoparticles are responsible for film formation (Chapter 10 Fig. 10.5).

Fig. 15.1 SEM image of the ITO electrode coated with five CNPs-imidazolium functionalized silicate layers.
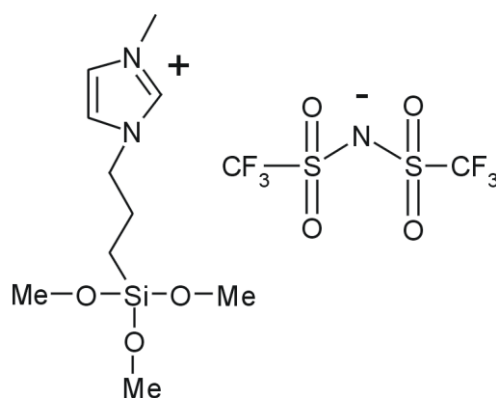

Fig. 15.2 The structural formula of sol-gel precursor 1-methyl-3-(3 trimethoxysilylpropyl)imidazolium bis(trifluoromethyl sulfonyl)imide (1).

128

Additionally, its structure is strengthened due to covalent bonds in silicate structure [101, 374]. We also observed that the mechanical stability of the film obtained with charged precursor (1) is better than obtained by sol drop deposition of CNPs in TMOS based sol – TMOS/CNPs$_{KCl}$ (Chapter 12). The film thickness was estimated from optical profilometry experiment and increases from 250, 690 and 1060 nm for electrode modified with 3, 5 and 10 layers. The removal of the film by scratching is difficult and the fracturing of the film is rather not observed.

The increase of the amount of immobilized CNPs with subsequent immersion and withdrawal steps is confirmed by cyclic voltammetry in aqueous electrolyte (Fig. 15.3). The capacitive current is approximately proportional to the number of layers. CNPs immobilized in silicate matrix and interacting with appended imidazolium groups are in good electric contact forming efficient percolation paths towards ITO surface. This result shows also that the film is not composed of separated layers. The capacitive current obtained with 10 layers electrode is five times larger than obtained with the electrode fabricated by sol drop deposition method TMOS/CNPs$_{KCl}$ (Fig. 12.1). Its capacity is equal 0.5 mF cm^{-2} – 50 times larger than capacity of unmodified ITO indicating proportional increase of electrochemically active area. Taking into account capacity of the CNPs per real surface area (10 μF cm^{-2} [349]) and area of CNPs (approximately 100 m^2 g^{-1}) the amount of the deposited CNPs was calculated to be 50 μg cm^{-2}. This value may be underestimated because not whole surface of CNPs is electrochemically active. The effect of the deposition of CNPs – silicate appended ionic liquid layers on the resistance of the electrochemical cell is not significant. This parameter increases from 210 to 240, 230 and 490 Ω for electrode modified with respectively 3, 5 and 10 layers indicating decrease of the number of percolation paths in thicker films.

Fig. 15.3 Cyclic voltammograms (2nd scan) of (i) a bare ITO electrode and coated with (ii) three (iii) five or (iv) ten CNPs-imidazolium functionalized silicate layers immersed in 0.1 M NaClO$_4$ aqueous solution. Scan rate 10 mV s^{-1}. Inset: Plot of the effect of the CNPs' loading on the capacitive current respone at + 0.5 V.

15.2.1. Electrochemical reactions sensitive on the surface heterogeneity at electrode coated with CNPs-imidazolium functionalized silicate layers

Two electrode reactions sensitive to electrode heterogeneity surface and its area were tested. As it was shown earlier the examination of slow heterogeneous electron transfer reaction as example of irreversible electroreduction of hydrogen peroxide in acidic solution provides valuable information on the surface effect [350, 351]. The voltammetric experiment reveals significant increase of the faradaic current for electrodes with immobilized CNPs (Fig. 15.4). As one can see from the Fig. 15.4, the value of cathodic current density is approximately proportional to the number of deposited layers, reaching ca. 20 fold increase for film composed of the largest amount of CNPs. The potential of current onset is not affected by the presence of CNPs indicating that observed enhancement results only from increase of the electroactive surface but not catalysis.
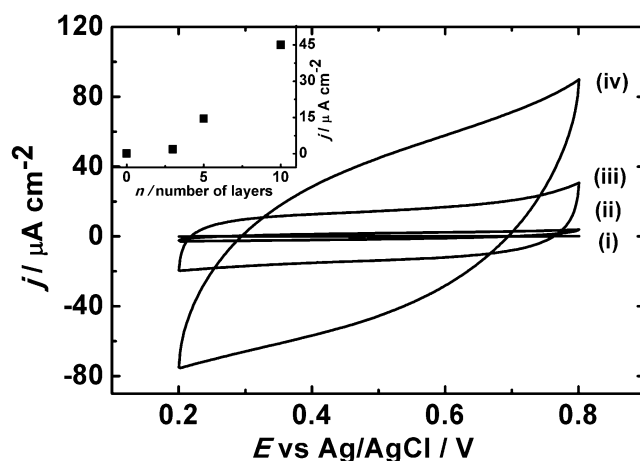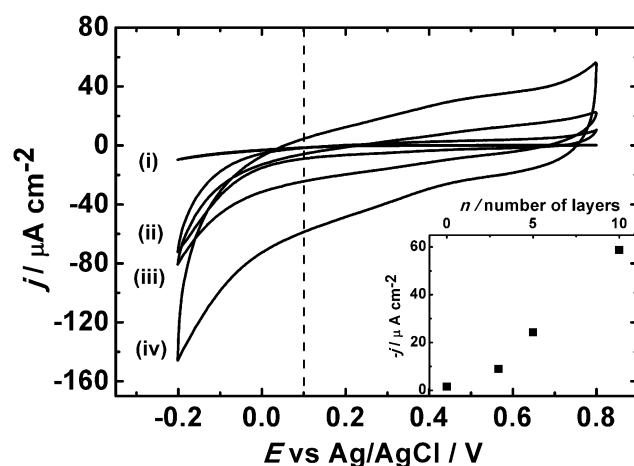
Fig. 15.4 Cyclic voltammograms (2nd scan) of (i) a bare ITO electrode and coated with (ii) three (iii) five or (iv) ten CNPs-imidazolium functionalized silicate layers immersed in 50 mM H_2O_2 solution in 0.1 M H_2SO_4 aqueous solution. Scan rate 10 mV s^{-1}. Inset: Plot of the effect of the CNPs' loading on the reduction current at + 0.1 V.

Next, experiments with the redox liquid were conducted for confirming the surface development of the modified electrode. The obtained peak shaped voltammogram (Fig. 15.5) is associated with redox reaction (Eq. 12.2) [352, 355].
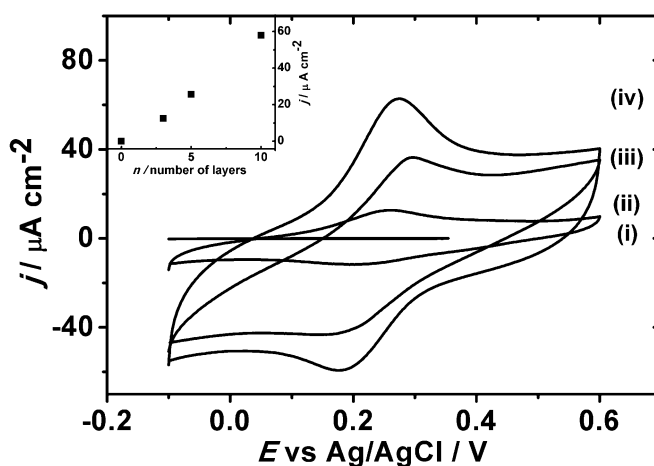

Fig. 15.5 Cyclic voltammograms (2nd scan) obtained for the oxidation-reduction of 50 nmole tBuFc immobilised at (i) a bare ITO electrode and coated with (ii) three (iii) five or (iv) ten CNPs-imidazolium functionalized silicate layers immersed in 0.1 M $NaClO_4$ aqueous solution. Scan rate 10 mV s^{-1}. Inset: Plot of the CNPs' loading on the oxidation current at + 0.25 V.

The voltammetric midpeak potential is shifted by 0.1 V towards positive potentials in comparison to that obtained with tBuFc deposit on bare ITO electrode (0.2 V – midpoint potential). That result indicates that hydrophobic neutral form of the redox probe is more stabilized by hydrophilic material. Most importantly the presence of CNPs increases effectiveness of the electrode process when compared to unmodified ITO and this parameter is proportional to the number of CNPs layers deposited on the electrode surface. Clearly, the porous film structure promotes dispersion of tBuFc liquid and the electrooxidation can proceed at an extended triple phase boundary [352-355]. The efficiency of electrode process determined as the ratio of anodic charge (Q_a) to electric charge corresponding to complete electrooxidation of 50 nmoles of tBuFc (Q_{calc}) increases going from the thinner to the thicker CNPs-imidazolium functionalized silicate layers. Namely, Q_a/Q_{calc} is equal from 0.3% at unmodified ITO to 1.3, 5.2 and 8.0 % for electrode modified with three, five and ten layers of CNPs, respectively. Surprisingly, the film appears to be wetted by the hydrophobic redox liquid tBuFc, and the increased number of CNPs produces significantly increased length of three phase junction electronic conductor|redox liquid|electrolyte solution [352, 355]. During continuous cycling the shape of voltammogram is retained. However, a slow decrease of the peak currents is observed. This may result from ejection of produced tBuFc$^+$ into the solution phase (Eq. 12.3) [354].

15.2.2. Simple electrochemical redox reaction at electrode coated with CNPs-imidazolium functionalized silicate layers

Next, a reversible one electron redox system was examined. The peak shaped voltammogram (Fig. 15.6) obtained in neutral redox probe – $Fc(CH_2OH)_2$ solution indicate simple redox reaction (Eq. 12.1). However the magnitude of the signal is larger than for unmodified ITO electrode. Moreover the peak currents increase in time. After approximately two fold increase of the current is reached the electrode is saturated with trapped redox probe. The current obtained on saturated electrodes increase for three and five layers but decrease for ten layers electrode (Fig. 15.6). Clearly trapping is connected with the increase of the active surface of porous carbon structure and the presence of silicate network. The efficiency of the electrode process seems to be determined by diffusion of reactant towards the outer electrode surface and solution

132

trapped within the pores [351, 353], similar behaviour was also observed for $TMOS_{gel}/CNPs_{KCl}$ modified electrodes.

Fig. 15.6 Cyclic voltammograms (2nd scan) of (i) a bare ITO electrode and coated with (ii) three (iii) five or (iv) ten CNPs-imidazolium functionalized silicate layers immersed in 1 mM Fc(CH₂OH)₂ solution in 0.1 M NaClO₄ aqueous solution. Scan rate 10 mV s⁻¹.

Although, the enhanced voltammetric signal (Fig. 15.7A) due to electrochemical redox reaction:

$$Fe(CN)_6^{4-} \quad \leftrightarrow \quad Fe(CN)_6^{3-} + e^- \tag{15.1}$$

is observed in $K_3Fe(CN)_6$ aqueous solution, which is attributable to redox anions accumulation in the film. This effect is much more pronounced than in the case of uncharged reactant. The increase of the amount of accumulated $Fe(CN)_6^{3-}$ anions is visible when one compares unmodified and 3 and 5 layers modified electrode (Fig. 17.5A). Clearly the increasing number of positively charged imidazolium groups is responsible for this effect. This is also confirmed by positive shift of the midpeak potential obtained with modified electrode which indicates stabilisation of less charged form of redox anion [374].
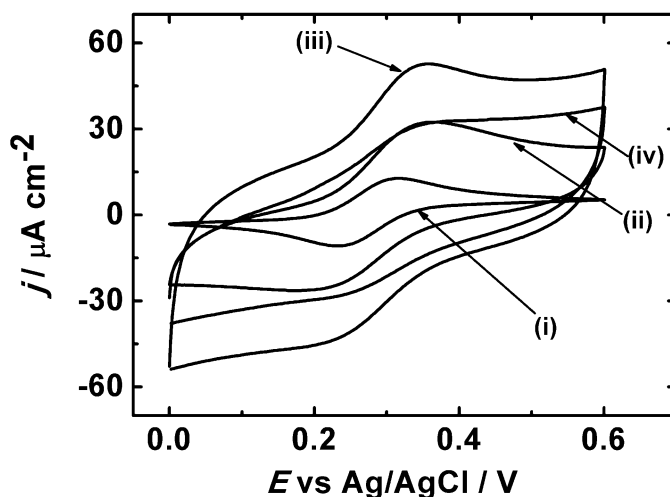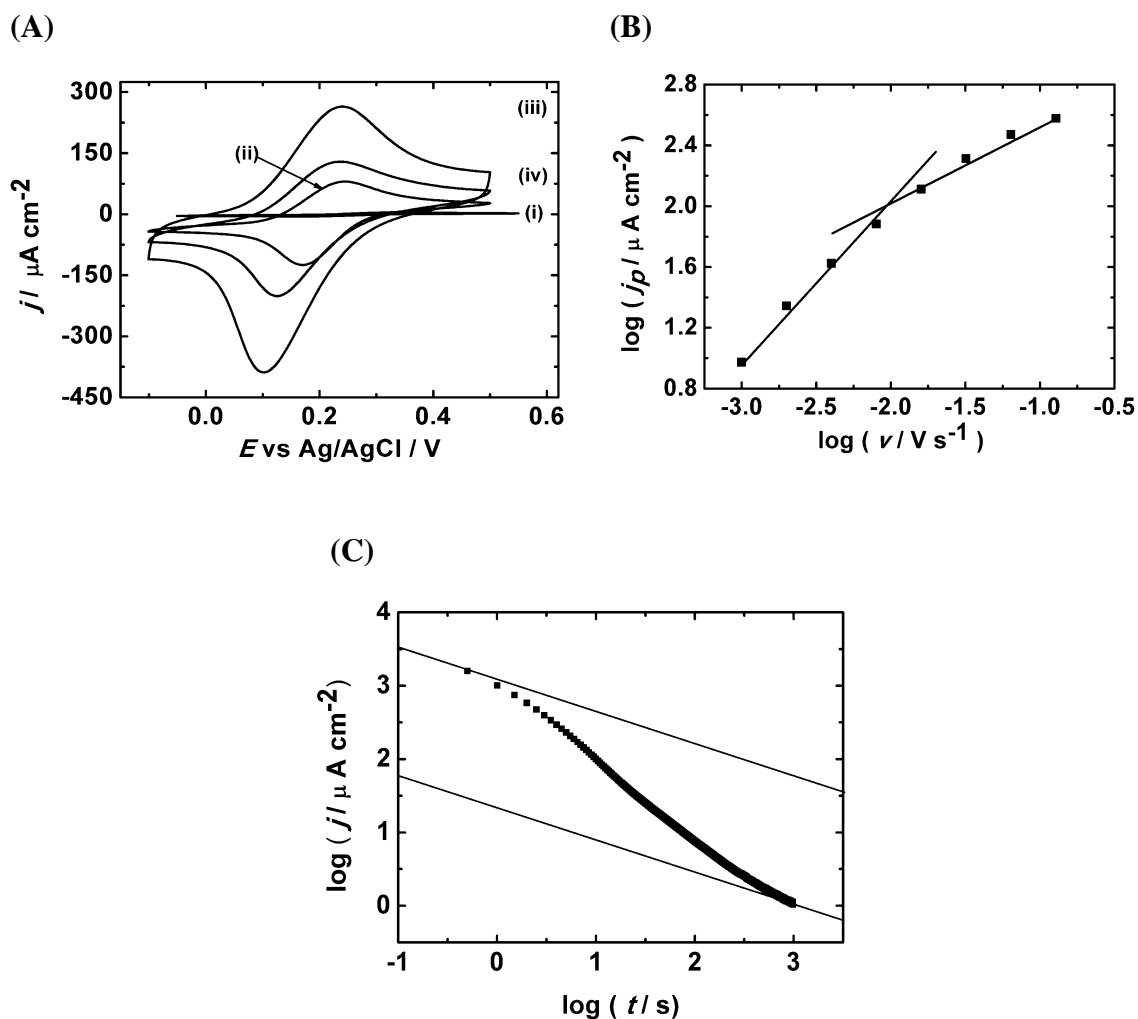
133

(A)

(B)

(C)

Fig. 15.7 (A) Cyclic voltammograms (20th scan) of (i) a bare ITO electrode and coated with (ii) three (iii) five or (iv) ten CNPs-imidazolium functionalized silicate layers immersed in 0.1 mM K_3Fe(CN)_6 solution in 0.1 M NaClO_4 aqueous solution. (B) The logarithmic dependence of anodic peak current density (j_p) on scan rate (v) obtained for the ITO electrode coated with ten CNPs-imidazolium functionalized silicate layers. (C) The logarithmic dependence of the absolute value of cathodic current density (i) on time (t) obtained in chronoamperometric experiments in the same solution with potential step from 0.5 to –0.1 V obtained for ITO electrode coated with ten CNPs-imidazolium functionalized silicate layers. The slope of the solid lines is equal –0.5. Scan rate 10 mV s^{-1}.

Maximal faradaic charge obtained with electrode modified with 5 layers is smaller to that observed in the absence of CNPs modified with phenyl sulphonic groups. Evidently only fraction of cationic groups interacts with CNPs' sulphonic groups of the matrix, and the others can participate in accumulation process. For the electrode modified with

10 layers less effective accumulation is recorded. Such behaviour might result from collapse of silicate matrix close to the electrode surface, thus blocking access of redox active ions. The accumulation process of the redox anions is reversible. More than 50 % of anions are washed out in pure electrolyte after 20 voltammetric scans with scan rate 10 mV s^{-1}. The scan rate dependence of peak currents (Fig. 15.7B) indicates transitions from restricted to unrestricted diffusion. This can be explained by the heterogeneous structure of the film. In long time scale experiment the diffusion space is restricted by neighbouring CNPs. The accumulation of redox active ions is also confirmed by chronoamperometric experiment. The slope of the current vs. time logarithmic plot increases from about 0.5 expected for no restricted diffusion and further decreases back to the approximately the same value (Fig. 15.7C). This shape of the curve is associated with at least 100 times larger concentration of the redox active anions within the film than in bulk solution.

The mechanism of accumulation of ABTS^{2-} (Fig. 15.8) – organic dianion with two sulphonic functional groups and extended π electron system is different.
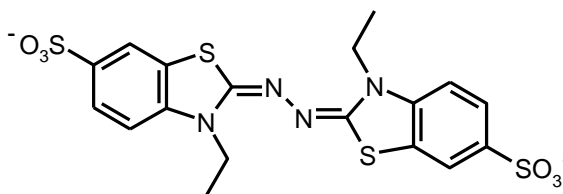

Fig. 15.8 2, 2'-azinobis (3-ethylbenzothiazoline-6-sulfonate) ABTS^{2-} [221].

The efficiency of this process is similar to that of Fe(CN)$_6^{3-}$ anions, but it is irreversible – no ABTS^{2-} anions are washed out when the electrode is immersed into aqueous solution (Fig. 15.9).
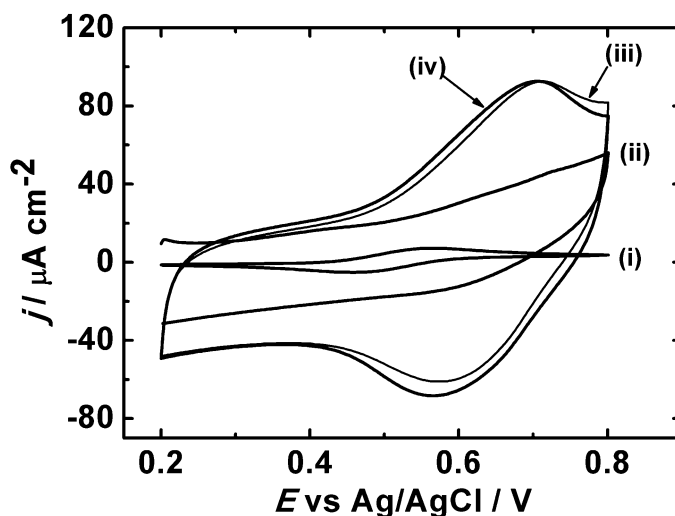
135

Fig. 15.9 Cyclic voltammograms of (i) a bare ITO electrode or coated with (ii) ten CNPs-imidazolium functionalized silicate layers immediately after immersion and (iii) after 20th scans immersed in 0.1 mM ABTS^{2-}solution in 0.1 M phospate buffer (pH 4.8). Curve (iv) was obtained with the same electrode transferred to pure phosphate buffer after 20 scans. Scan rate 10 mV s^{-1}.

This irreversibility is not observed in the absence of CNPs in the film obtained from the same sol by sol drop deposition. Therefore, not only electrostatic interactions with imidazolium group are responsible for this effect but also the extended π electron aromatic system of ABTS^{2-}and carbon nanoparticles which are modified with sulphonic groups. The peak current density is proportional to the number of immersion and withdrawal cycles (Fig. 15.10). Clearly, when a larger amount of material is deposited at the electrode surface, greater amount of mediator ions is accumulated. Also the increase of capacitive current related to the electroactive surface is observed.
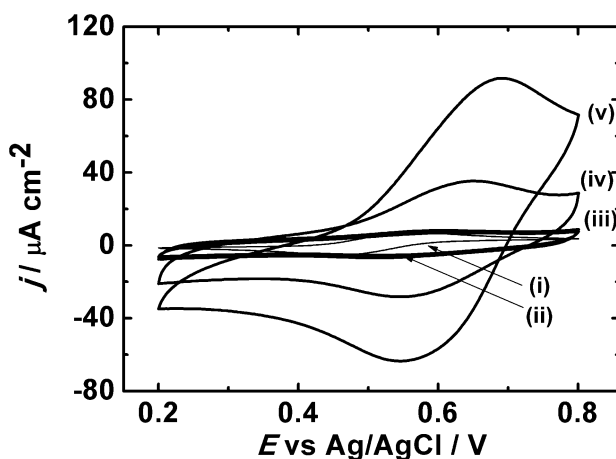
Fig. 15.10 Cyclic voltammograms of (i) a bare ITO electrode and coated with (ii) three (iii) five or (iv) ten CNPs-imidazolium functionalized silicate layers with adsorbed ABTS^{2-} immersed in 0.1 M phosphate buffer (pH 4.8). Scan rate 10 mV s^{-1}.

The midpeak potential corresponding to one electron oxidation-reduction process:

$$ABTS^{2-} \leftrightarrow ABTS^{\bullet-} + e^- \qquad\qquad (15.2)$$

is shifted by 0.15 V towards positive potential in comparison with the bare electrode ITO in the presence of mediator in the solution. This indicates stabilization of less negatively charged component of ABTS$^{2-/\bullet-}$ redox couple by imidazolium groups appended to silicate matrix. The stabilization of the reduced form of the mediator indicates attraction between its sulfonic functional groups and imidazolium functional groups of silicate. Moreover, the peak current dependence on scan rate can be approximated by a polynomial with exponent between 0.5 and 1.0 indicating some attached ABTS^{2-} mobility. The difference between peak potentials (ΔE) is increasing with the larger *n*. It reaches a maximum of 0.1 V for n = 10. Such a big difference may occur due to some mobility of the encapsulated mediator – which is held by the positive charge of the functional groups of the silicate polymer – as exemplified by the observed peak-currents scan-rate dependence.
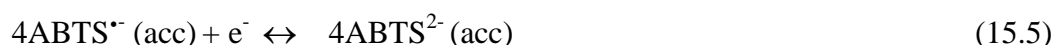
15.3. Bioelectrocatalytic activity

The adsorbed redox active ABTS^{2-} dianions were used as immobilised mediators in bioelectrocatalytic reaction of oxygen reduction catalyzed by multicopper enzymes – laccase or bilirubin oxidase. The accumulated mediator is oxidized by one of the

137

multicopper oxidases [375]:

$$MCOx(4Cu^{2+}) + 4ABTS^{2-} (acc) \leftrightarrow 4ABTS^{\bullet-} (acc) + MCOx(4Cu^{+}) \qquad (15.3)$$

$$MCOx(4Cu^{+}) + O_2 + 4H^{+} \rightarrow 2H_2O + MCOx(4Cu^{2+}) \qquad (15.4)$$

and these steps are followed by electrochemical regeneration of the mediator:

$$4ABTS^{\bullet-} (acc) + e^{-} \leftrightarrow 4ABTS^{2-} (acc) \qquad (15.5)$$

Indeed, the prepared electrode with immobilized mediator is effective for bioelectrocatalytic process. However, the bioelectrocatalytic reaction catalyzes by laccase occurs only if the enzyme is dissolved in the solution, and the electrode is modified with 10 layers (Fig. 15.11). Then, the electrode architecture enables close contact between adsorbed $ABTS^{2-}$ and large laccase molecule from solution. If the Lc is adsorbed onto modified electrode no bioelectrocatalysis is observed (not shown).
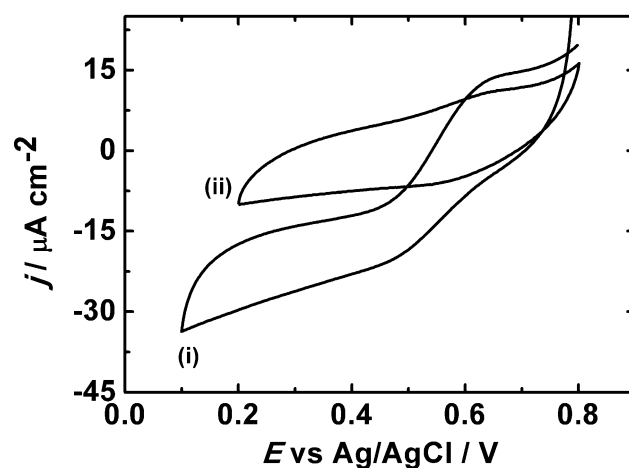
Fig. 15.11 Cyclic voltammograms (2nd scan) of ITO electrode coated with ten CNPs-imidazolium functionalized silicate layers and with adsorbed $ABTS^{2-}$ immersed in O_2-saturated 0.1 M phospate buffer (pH 4.8) in the (i) presence and (ii) absence of laccase in solution. Scan rate 1 mV s^{-1}.

In the case of the same electrodes with adsorbed BOx the onset potential of oxygen reduction is comparable with Lc ones (Fig. 15.12). The maximum current density is obtained for electrode prepared by five immersion and withdrawal steps

138

(Fig. 15.12 (iii)). The obtained result may be explain with that the smaller void of electrode restrict accumulation of the enzyme in the film electrode.
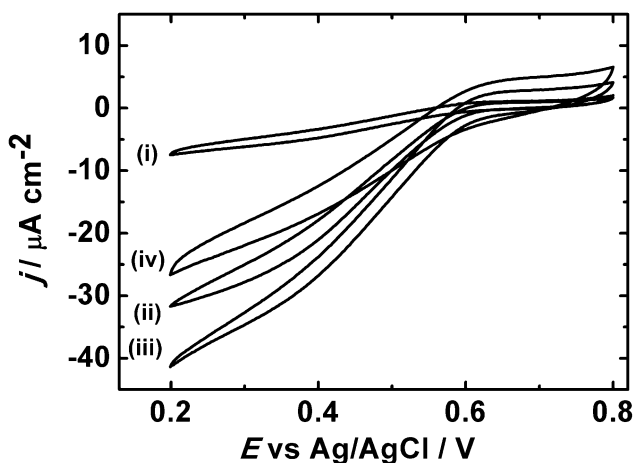

Fig. 15.12 Cyclic voltammograms (2nd scan) of ITO electrode coated with (i) one (ii) three (iii) five or (iv) ten CNPs-imidazolium functionalized silicate layers with adsorbed ABTS^{2-} and BOx immersed in O$_2$-saturated 0.1 M phosphate buffer (pH 4.8). Scan rate 1 mV s^{-1}.

In the absence of accumulated mediator, the modified electrodes with adsorbed BOx exhibits even smaller catalytic activity towards oxygen reduction (Fig. 15.13). The catalytic current is about half of that observed with accumulated ABTS^{2-}. This can be interpreted as the opening of a new reaction path due to immobilization of mediator.
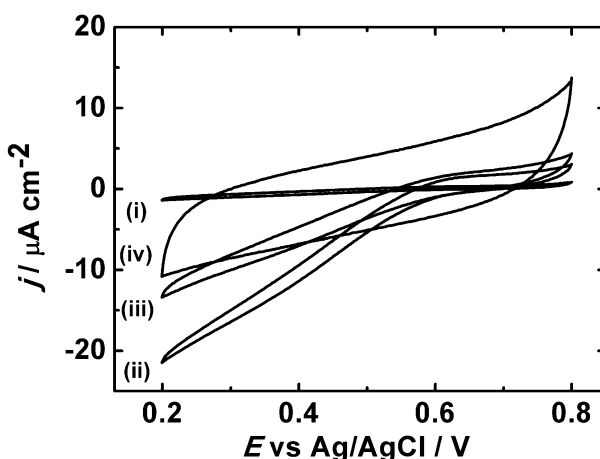

Fig .15.13 Cyclic voltammograms (2nd scan) of ITO electrode coated with (i) one (ii) three (iii) five or (iv) ten CNPs-imidazolium functionalized silicate layers with adsorbed BOx immersed in O$_2$-saturated 0.1 M phosphate buffer (pH 4.8). Scan rate 1 mV s^{-1}.

139

15.4. Conclusions

The combination of sol containing ionic liquid precursor with imidazolium cationic functional group and carbon nanoparticles modified with sulphonic anionic groups enables to prepare electrode with controlled amount of conductive nanoparticles. The electrostatic interactions and sol-gel matrix formation result in mechanically stable films with uniform distribution of carbon nanoparticles. The electrode exhibits increased efficiency of surface dependent electrode process. Moreover, the excess of imidazolium binding sites enable accumulation of redox active ions whereas the same binding sites and surface of carbon nanoparticles provides suitable surface for irreversible adsorption of organic anion with extended pi electron system. The modified electrodes exhibits mediated (with adsorbed BOx and dissolved Lc), and mediatorless (with adsorbed BOx) bioelectrocatalytic activity towards oxygen reduction reaction. However, low current density eliminates them as a potential cathode for biofuel cell.

The application of another linker (silicate submicroparticles with appended imidazalium functional groups), which is based on the same ionic liquid precursor (1) as was used in this chapter, for the prepartion of carbon nanoparticle-film electrode by LbL method with adsorbed BOx enables to obtain efficient bioelectrocatalysis [376]. As depicted at the Fig. 15.4, the catalytic signal is increasing with the amount of material, and the highest current density (greater than 300 $\mu A\ cm^{-2}$) was observed for the electrode with the largest amount of material whrease for electrode with CNPs-imidazolium functionalized silicate layers the maximal activity is seen for three immersion and withdrawl steps. It appears that for this electrode low bioelectrocatalytic activity results not from the presence of the imidazolium groups but from the blocking of CNPs by deposited sol decreasing its electrical conductivity.
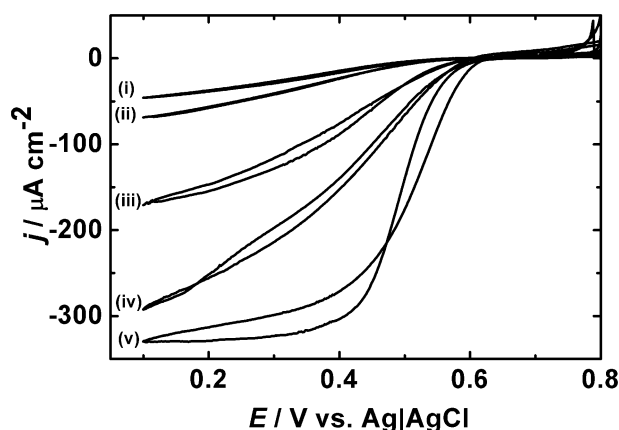
Fig. 15.14 Cyclic voltammograms of ITO electrode coated with (i) one (ii) two (iii) eight (iv) sixteen (v) and thirty-two CNPs – imidazolium functionalized silicate submicroparticles layers with adsorbed BOx immersed in O_2-saturated 0.1 M phosphate buffer (pH 4.8). Scan rate 1 mV s^{-1}[376].

16. Film electrode prepared from oppositely charged carbon nanoparticles

16.1. Introduction

In order to improve the electrochemical properties of the modified electrode, and to prepare better platform for enzymes' immobilization, in this section the bottom up approach was utilized for the preparation of the entirely carbon film electrode. In contrast to pulsed discharged plasma CVD [377] or various pyrolysis based techniques [378] that approach is easy, fast and quit cheap. In this procedure no polymeric matrix is involved [82] (Chapter 12). It allows for the preparation of nanoparticulate carbon film with electrochemical properties different from bulk carbon materials. Such material is attractive for sensing and biosensing applications [379] or for efficient bioelectrocatalysis [375].

Herein, the ITO electrode was made of the carbon nanoparticles of opposite charge using a layer-by-layer method. Hydrophilic CNPs with phenyl sulfonic acid and ammonium [98] functionalities were employed as negatively and positively charged element of the film, respectively.

The electrodes were studied by SEM, AFM and tested by voltammetry in the presence of different reagents including the enzymes such as bilirubin oxidase, glucose oxidase and myoglobin.

16.2.   The microscopic and electrochemical characterization

The SEM image of the ITO electrode obtained by single pair of immersion and withdrawal steps (one-CNPs(+/-)) shows complete coverage by nanoparticulate material (Fig.16.1A), because characteristic tens of nanometer size features of ITO electrode surface are not noticeable. After further immersion and withdrawal steps (Fig. 16.1B) some aggregation of carbon material is visible. Clearly, electrostatic attraction of carbon nanoparticle aggregates allows for carbon film formation.

(A)   **(B)**
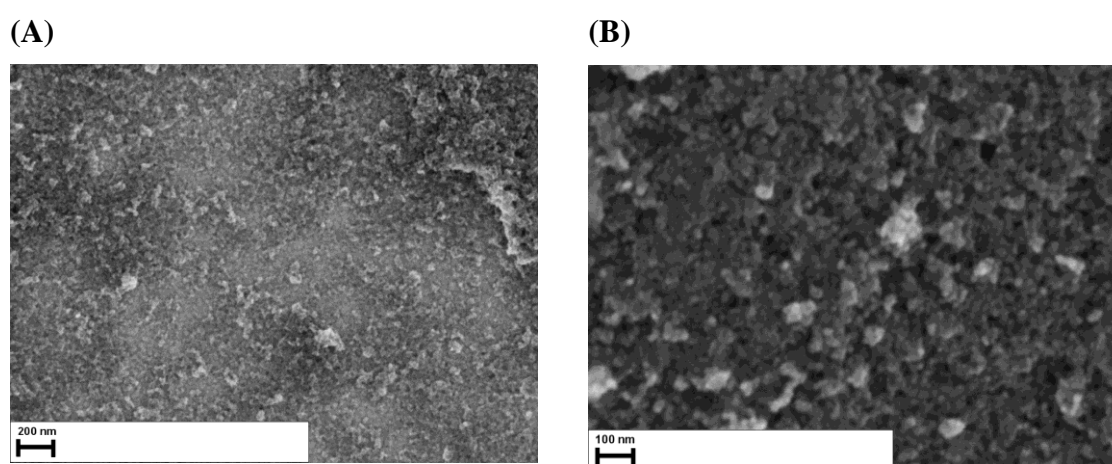
Fig. 16.1 SEM image of the (A) one-CNPs(+/-) and (B) three-CNPs(+/-) film ITO electrode.

The AFM image provided more qualitative information about the size and distribution of carbon nanoparticles aggregates. As one can see from such an image, which was obtained for the electrode coated by ten immersion and withdrawal steps (ten-CNPs(+/-)) that the film is quite smooth with some single aggregates of few hundred nanometer size (Fig. 16.2).
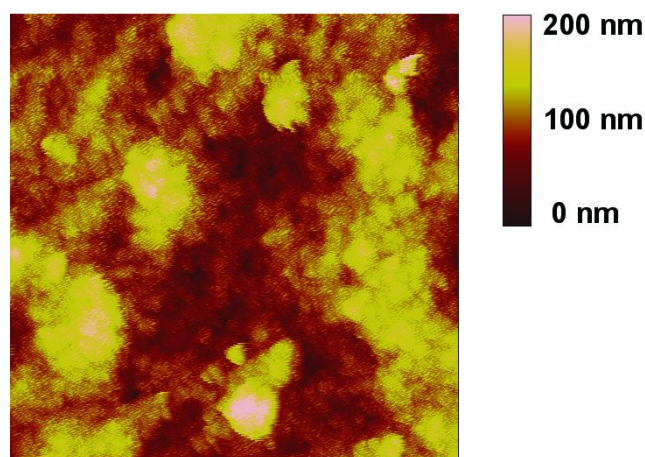
142

Fig. 16.2 AFM image of the ten-CNPs(+/-) film ITO electrode.

The average thickness of ITO electrode coated by one, three, five and ten immersion and withdrawal steps is 35 ± 15 nm, 100 ± 20 nm, 160 ± 30 nm and 320 ± 50 nm (Fig. 16.3A), respectively, as revealed by the measurements of the AFM profiles (see for the three-CNPs(+/-) film ITO electrode Fig. 16.3B).

(A)

(B)
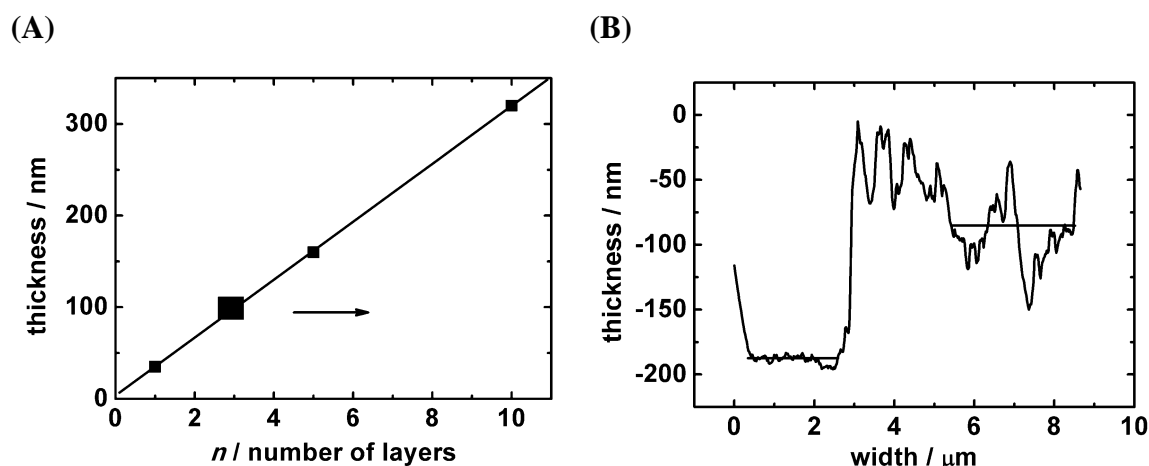
Fig. 16.3 (A) Depandance of thickness of CNPs(+/-) films on the number of layers (n). (B) High profile along a line used for estimation of thickness of three-CNPs(+/-) film.

There is some effect of deposition of oppositely charged carbon nanoparticles on the resistance of the electrochemical cell. This parameter decreases from 311 to 294, 266 and 256 Ω for electrode modified by 1, 3, 5, and 10 immersion and withdrawal steps, respectively. Clearly, the deposited carbon nanoparticles are interconnected

forming efficient electron percolation pathways, thus their electrical conductivity increase.

In order to evaluate the electrochemical properties of the prepared electrodes, firstly, the electroactive window of the three-CNPs(+/-) film electrode was examined in 0.1 M $NaClO_4$ deareated aqueous solution and in 0.1 M deaereted phosphate buffer (not shown). It ranges from -1.0 to 1.1 V and -1.0 to 0.9 V, and is slightly narrowed as compared to other carbon electrodes material [380]. No significant change in the background current is seen after excursion up to 0.3 V (or down to -0.3) beyond potential window.

The voltammetric experiments performed in hydrogen peroxide aqueous acidic solution reveal two important properties of the electrode (Fig. 16.4). Firstly, the capacitive current (observed in the positive potential range) is proportional to the number of alternative immersion and withdrawal steps, and the differential capacity of the film reaches 0.1 Fcm^{-2}. Secondly, the current density corresponding to slow electrode reaction – H_2O_2 electroreduction is also proportional to the number of alternative immersion and withdrawal steps. The result shows that the substrate of the electrode reaction is small enough to diffuse through the voids of the nanoparticulate film to reach whole available electrochemically active surface. Both effects indicate an increase of the electrochemically active surface related to the amount of the film material and good contact with the ITO substrate.

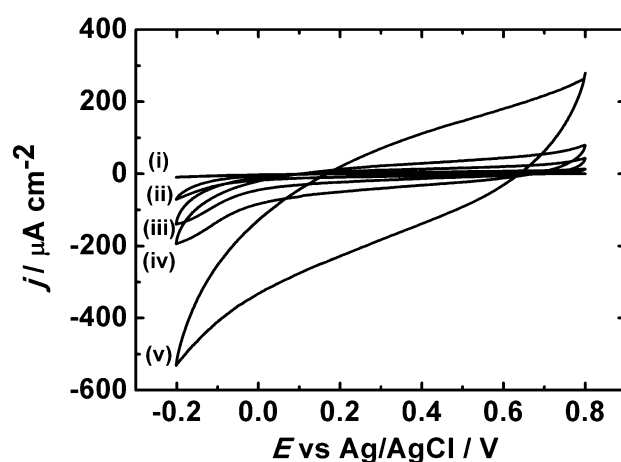Fig. 16.4 Cyclic voltammograms (2nd scan) of (i) a bare ITO electrode and coated with (ii) one (iii) three (iv) five and (v) ten-CNPs(+/-) immersed in 0.05 M H_2O_2 solution in 0.1 M H_2SO_4 aqueous solution. Scan rate 10 mV s^{-1}.

144

As described in the Chapter 12 and 15 the voltammetry of redox liquid deposited on the electrode is suitable experiment that demonstrates the effect of electroactive surface development and heterogeneity of the film structure. Here also tBuFc was used as a model system. The voltammetric midpeak potential is shifted by 0.2 V towards positive potentials in comparison to that obtained with tBuFc deposit on ITO electrode (Fig. 16.5). This quite surprisingly result, indicates stabilisation of hydrophobic neutral form of the redox probe by hydrophilic material. Most importantly the presence of CNPs increases efficiency of the electrode process, when compared to unmodified ITO, and this parameter is proportional to the number of CNPs layers deposited on the electrode surface. Perhaps the porous film structure promotes dispersion of tBuFc liquid and the electrooxidation can proceed at an extended triple phase boundary [352, 354, 355]. The increase of the charge under the oxidation peak is consistent with increase of electrochemical conversion of 50 nmoles of tBuFc deposit from 0.3% at unmodified ITO to 3, 17, 28 and 32 % for electrode modified with one, three, five and ten layers of CNPs. These values are higher in comparison to the ones obtained for electrodes covered by the CNPs-imidazolium functionalized silicate layers and $TMOS_{gel}/CNPs_{KCl}$ film. That can be caused by (i) good electrical conductivity (ii) organic liquid not entirely coating the hydrophilic surface and thereby increasing the three phase boundary region. The hydrophilic film appears to be wetted by the hydrophobic redox liquid tBuFc, and the increased number of CNPs, produce significantly increased length of three phase junction electronic conductor|redox liquid|electrolyte solution [352-355]. Likewise to CNPs-imidazolium functionalized silicate layers modified electrode during continuous cycling the shape of voltammogram is retained, and a slow decrease of the peak currents is observed. This behaviour may result from ejection of produced tBuFc$^+$ into the solution phase (Chapter 12 Eq. 12.3) [352-355].
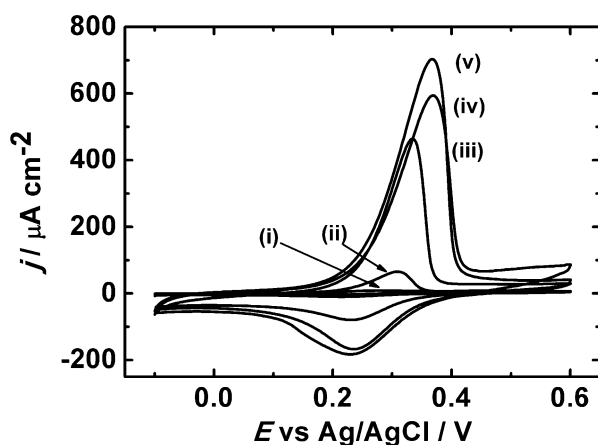
Fig. 16.5 Cyclic voltammograms (2nd scan) obtained for the oxidation-reduction of 50 nmole tBuFc immobilised at (i) a bare ITO electrode and coated with (ii) one (iii) three (iv) five and (v) ten-CNPs(+/-) immersed in 0.1 M NaClO$_4$ aqueous solution. Scan rate 10 mV s^{-1}.

The increasing voltammetric signal obtained in the redox probe – ABTS^{2-} solution reveals not only a reversible oxidation-reduction process but also accumulation of this redox probe. After transfer of this electrode to pure electrolyte solution, the surface voltammetry of ABTS$^{2-/\bullet-}$ redox couple is observed (Fig. 16.6). Its redox potential compared with solution voltammetry on ITO electrode is unchanged. Therefore, redox probe accumulation occurs due to interaction of its extended π electrons system and that of carbon particle. The increase of the peak current with the amount of deposited nanoparticulate material provides further evidence of extension of the electrochemically active surface.
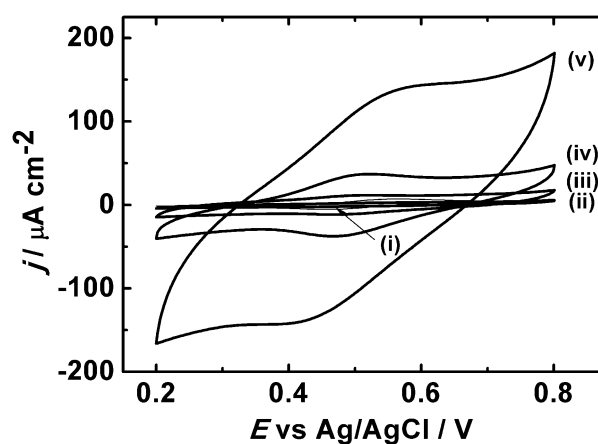

Fig. 16.6 Cyclic voltammograms of (i) a bare ITO electrode and coated with (ii) one (iii) three (iv) five and (v) ten-CNPs(+/-) and with adsorbed ABTS^{2-} immersed in 0.1 M phosphate buffer (pH 4.8). Scan rate 10 mV s^{-1}.

146

Additionally, the voltammetric experiments performed in the presence of simple redox reactants such as $Fe(CN)_6^{3-}$ and $Ru(NH_3)_6^{3+}$ does not indicate any accumulation effect (Fig. 16.7). This indicates strong electrostatic interactions between both components of the film contributing to its stability. Also, as one can see, from the cyclic voltammograms obtained for the electrode modified by three immersion and withdrawal steps and bare ITO electrode that the presence of carbon nanoparticulate material increases the capacitive current demonstrating a well developed electroactive surface area. However the increase of the faradaic current is not observed because the electrochemical reaction occurs only at the outer layer of carbon nanoparticles.

(A)   **(B)**
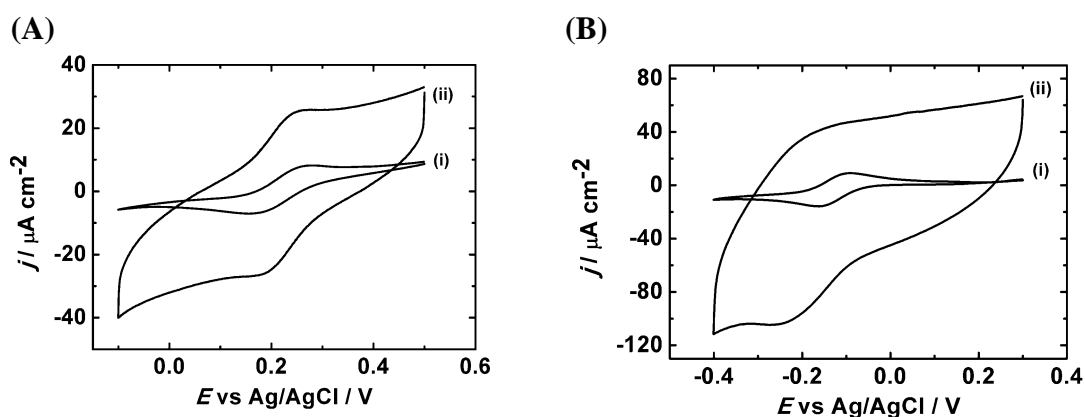
Fig. 16.7 Cyclic voltammograms (2nd scan) of (i) a bare ITO electrode and coated with three-CNPs(+/-) immersed in (A) 0.1 mM $K_3Fe(CN)_6$ solution and (B) 0.1 mM $Ru(NH_3)_6Cl_3$ solution in 0.1 M $NaClO_4$ aqueous solution. Scan rate 10 mV s^{-1}.

16.3. Bioelectrocatalytic activity

The sigmoidal shape of voltammogram obtained with CNPs(+/-) modified electrodes by adsorbed BOx in oxygen saturated solution (Fig. 16.8A) indicates the carbon nanoparticulate film promotes mediatorless bioelectrocatalysis of oxygen reduction with good efficiency [86, 255]. However, the largest catalytic current is obtained for an electrode prepared by three cycles of immersion and withdrawal. Contrary to small hydrogen peroxide molecules, the protein is too large to diffuse through any voids on the electrode surface during adsorption process [381]. The onset potential of bioelectrocatalytic ORR commences at ca. 0.6 V, found to be close to the formal potential of the T1 copper of BOx [155]. The catalytic current is absent when the

147

electrode is modified only with carbon nanoparticles (Fig. 16.8B (v)). Though, the negligible one is recoded when the electrode is modified only with positively charged carbon nanoparticles and adsorbed enzyme (three-CNPs(+)/BOx) (Fig. 16.8B (vi)). This result reveals that for efficient bioelectrocatalysis, the film formation from the oppositely charged CNPs with adsorbed BOx is required.

(A)   **(B)**
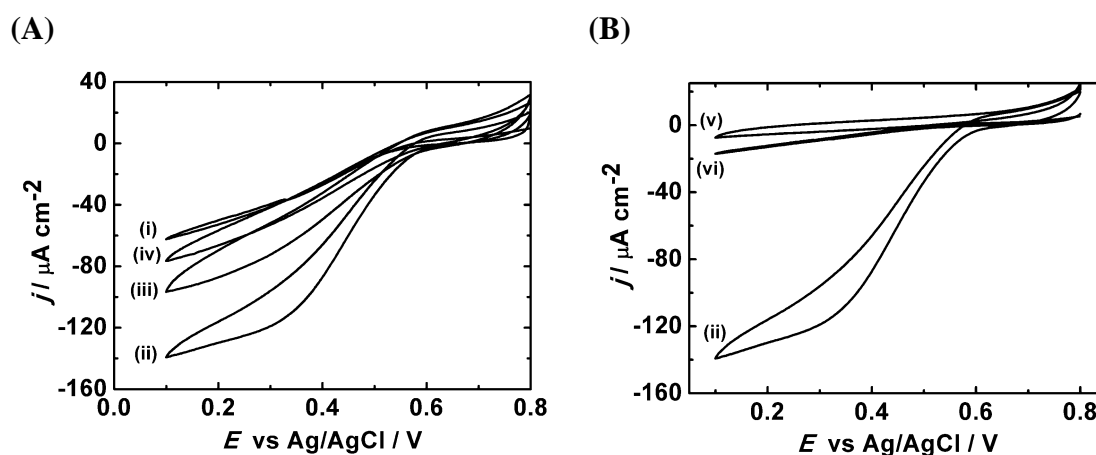
Fig. 16.8 (A) Cyclic voltammograms (2nd scan) of ITO electrode coated with (i) one (ii) three (iii) five and (iv) ten-CNPs(+/-)/BOx immersed in O_2-saturated 0.1 M phosphate buffer (pH 4.8). (B) Cyclic voltammograms of (ii) three-CNPs(+/-)/BOx (vi) three-CNPs(+)/BOx and (v) three-CNPs(+/-) film ITO electrode immersed in O_2-saturated 0.1 M phosphate buffer (pH 4.8). Scan rate 1 mV s^{-1}.

However, if the Lc is adsorbed on carbon nanoparticulate film electrode the bioelectrocatalytic current density is 2 orders of magnitude smaller than with adsorbed BOx (Fig. 16.9). Such outcome may be explained with Lc's molecules being less resistance on adsorption on functionalized materials than BOx's molecules. Such phenomena might occur if there are too strong interactions between the protein and the substrate. That in turn leads to loss of enzyme's biological activity.

148

Fig. 16.9 Cyclic voltammograms (2nd scan) of three-CNPs(+/-) film ITO electrode with adsorbed Lc in (i) O_2 and (ii) Ar-saturated 0.1 M phosphate buffer (pH 4.8). Scan rate 1 mV s^{-1}.
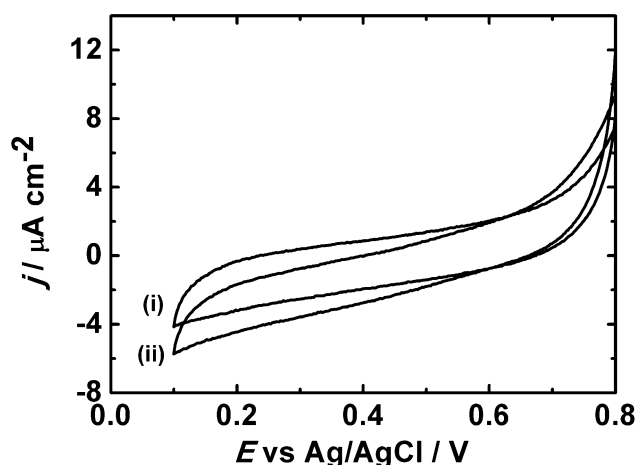
16.4. Zn-O$_2$ hybrid cell

The cell was assembled of ITO coated by positively and negatively charged CNPs (three-CNPs(+/-)) as a cathode and a Nafion-coated Zn anode immersed in oxygen saturated 0.1 M McIlvaine buffer (pH 4.8) or in artifical serum (Fig. 16.10). The voltage was measured for 100 s when the potential was stabilized. The hybrid cell has an open-circuit voltage equal to 1.60 V and 1.29 V, respectively, below the theoretical value of 1.99 V. The maximum power density for buffer of pH 4.8 and aritical serum are equal to 114 μW cm^{-2} at 0.65 V and 47.0 μW cm^{-2} at 0.47 V, respectively (Fig. 16.10A,B). The considerable decrease of the cell voltage with increasing load is similar to the previously studied carbon nanoparticles based ITO electrodes (see Chapter 13 and 14), and probably brought about like before by the slow kinetic of the enzymatic reaction on the cathode. The performance of these Zn-O$_2$ hybrid cells, in buffer with pH 4.8 as well as in artificial serum, are comparable to those obtained with MTMOS$_{gel}$/CNPs/BOx biocathode (Chapter 14). Nevertheless, cells with MTMOS$_{gel}$/CNPs/BOx as biocathodes exhibit slightly enhanced performances. The most reasonable explanation, of that outcome, might be the hydrophobic properties of MTMOS$_{gel}$/CNPs/BOx that assure proper environment for enzymes' immobilization.

149
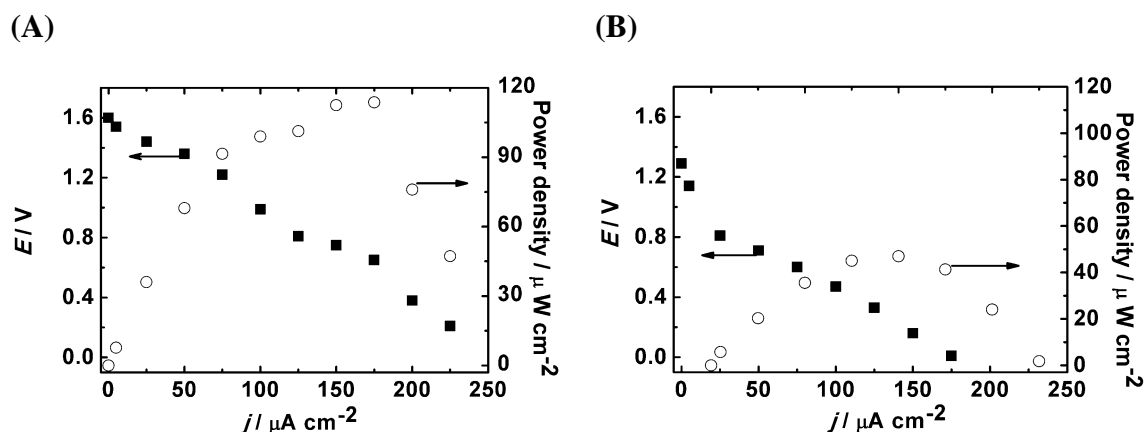
Fig. 16.10 Polarisation curves (●) of the zinc-oxygen hybrid cell, with three-CNPs(+/-)/BOx film ITO electrode as biocathode and the dependence of the power output (■) on the current density in O_2-saturated (A) 0.1 M phosphate buffer (pH 4.8) and (B) artificial serum.

16.5. Electrochemistry of the adsorbed myoglobin

16.5.1. Direct myoglobin voltammetry on the modified electrode

The voltammetry performed on film electrode prepared from opposietly charged nanoparticles with adsorbed myoglobin reveals direct and reversible electron transfer (Fig. 16.11).
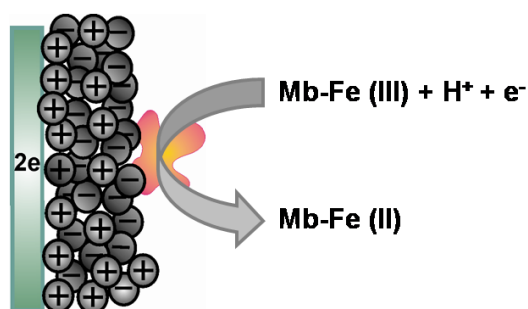
Fig. 16.11 The illustration of direct communication between the CNPs(+/-) film ITO electrode and Mb.

Clearly one can observe, a pair of well-defined redox peaks of the heme Fe(III)/Fe(II) redox couple (Fig. 16.12 (iii)).

150
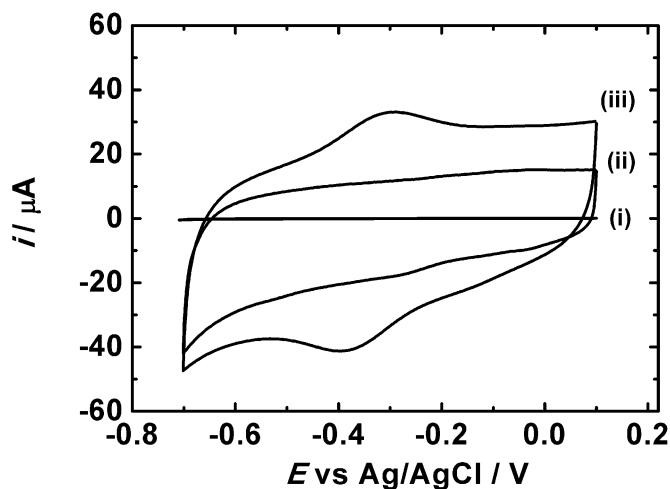
Fig. 16.12 Cyclic voltammograms (2nd scan) of (i) a bare ITO electrode and coated with (ii) three-CNPs(+/-) (iii) three-CNPs(+/-)/Mb immersed in Ar-saturated 0.1 M phosphate buffer (pH 7). Scan rate 100 mV s^{-1}.

The peak current is proportional to the number of immersion and withdrawal steps (Fig. 16.13). However, the increase is less visible for larger amounts of nanoparticulate material, because the protein's molecules, due to their size, are being adsorbed only at the outer layers of carbon nanoparticlute film.

The formal redox potential $E^{o'}$ of the three-CNPs(+/-)/Mb film electrode was evaluated as the midpoint of cathodic and anodic peak potentials is equal to -0.34 V which is close to the reported in literature [325].

Fig. 16.13 Cyclic voltammograms (2nd scan) of ITO electrode coated with (i) one (ii) three (iii) five and (iv) ten-CNPs(+/-)/BOx immersed in Ar-saturated 0.1 M phosphate buffer (pH 7). Scan rate 100 mV s^{-1}.

151

The scan rate dependence of cathodic and anodic peaks current shows that peak current vary linearly with the potential scan rate, confirming a surface-controlled 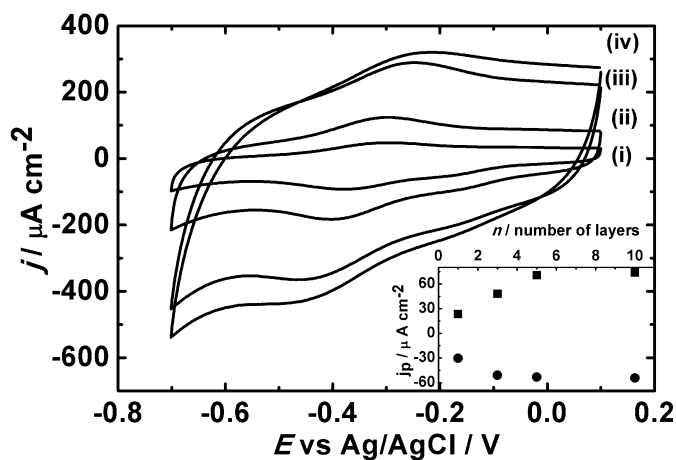process of adsorbed Mb at the modified electrode (Fig. 16.14). The heterogeneous electron transfer rate constant (k_s) and electron transfer coefficient (α) of the Mb on the modified electrode was estimated using Laviron's peak separation method [382]. The relationship follows that equations (Eq. 16.1-16.3) [382].

$$E_{pc} = E^{0'} + \frac{RT}{\alpha nF} \ln \frac{RTk}{\alpha nF} \ln v \tag{16.1}$$

$$E_{pa} = E^{0'} + \frac{RT}{(1-\alpha)nF} \ln \frac{RTk}{(1-\alpha)nF} + \frac{RT}{(1-\alpha)nF} \ln v \tag{16.2}$$

$$\log k_S = \alpha \log(1-\alpha) + (1-\alpha)\log\alpha - \log\frac{RT}{nFv} - \frac{\alpha(1-\alpha)nF\Delta E_p}{2.3RT} \tag{16.3}$$

These values were determined from the plot of peak potential (E_{pa} and E_{pc}) vs. logarithm of the scan rates (Fig. 16.14B). The α was estimated at 0.53 from the slopes of two straight lines at higher scan rate and then k_s was calculated as 0.86 s^{-1} (Fig. 16.14B). The obtained value of k_s indicates that the redox process of adsorbed Mb on the carbon nanoparticulate film electrode is quasi-reversible.

(A) **(B)**

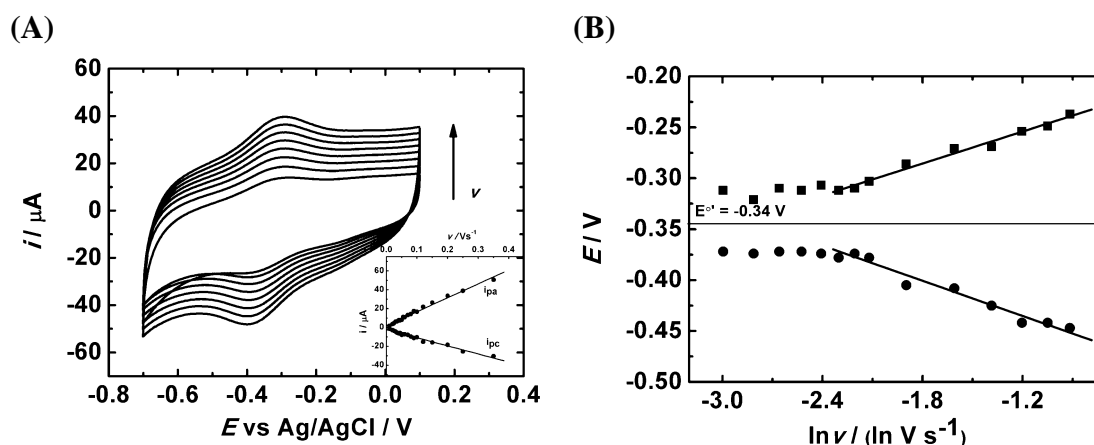Fig. 16.14 (A) Cyclic voltammograms (2nd scan) of three-CNPs(+/-)/Mb film ITO electrode immersed in Ar-saturated 0.1 M phosphate buffer (pH 7) at different scan rates: 50, 60, 70, 80, 90, 100, 110, 120 mV s^{-1}. Inset: The plot of cathodic and anodic peak current vs. scan rate. (B) Plots of anodic peak potential (■) and cathodic peak potential (♦) against the logarithm of scan rate.

152

The total surface average concentration (Γ_T) of the electroactive, adsorbed Mb on carbon nanoparticulate film electrode was estimated by the cathodic charge integration using the following equation:

$$\Gamma_T = Q/nFA \tag{16.4}$$

where Q is the charge (C), n is the number of transfer electrons, F is the Faraday constant, and A is the surface area of carbon nanoparticulate film electrode. The Γ_T was calculated as 9.34×10^{-9} mol cm^{-2}.

The direct electron transfer of Mb is a reaction in which protons are involved (Fig. 16.11) [162], therefore the effect of pH value of the supporting electrolyte was studied. The Fig. 16.15 depicts the pH effect on protein voltammetry. The formal potential is shifted towards more negative value with increasing pH value with a slope of -29.4 mV pH^{-1}. This result is unexpected since it is almost equal to a half of the theoretical value of -59 mV pH^{-1} at 25 ºC [291] for reversible one-electron and one proton coupled electrochemical reaction between the electrode surface and heme of the Mb. The explanation for this discrepancy is not yet clear and requires further studies. Similar results were also obtained by other groups [383, 384].
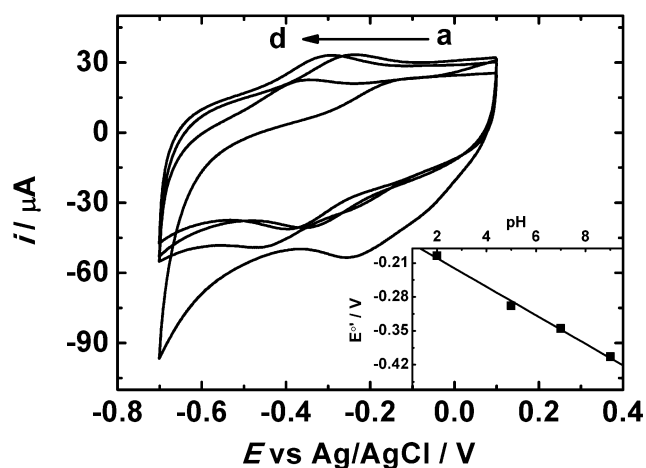

Fig. 16.15 Cyclic voltammograms (2nd scan) of three-CNPs(+/-)/Mb film ITO electrode immersed in Ar-saturated 0.1 M phosphate with different pH values of (a-d) 2, 5, 7 and 9. Scan rates 100 mV s^{-1}. Inset: The plot of formal potentials vs pH.

16.5.2. Electrocatalytic activity of the modified electrode with adsorbed myoglobin

One can observe that the catalytic current of the H_2O_2 reduction is proportional to its concentration in the solution (Fig. 16.17). That mechanism can be presented by the Fig. 16.16:
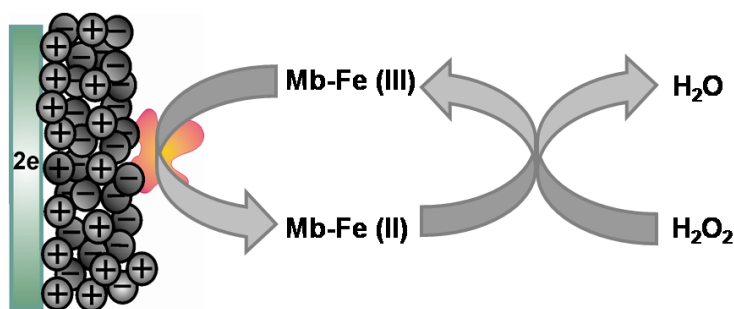
Fig. 16.16 A schematic diagram of the bioelectrocatalytic reaction of hydrogen peroxide reduction via Mb adsorbed at the CNPs(+/-) film ITO electrode.

This electrode shows a linear range towards the H_2O_2 reduction from 0.2 mM to 1mM with the detection limit (signal to noise) equal to be 12 μm. It reaches the plateau at 1.2 mM, thus revealing the characteristics of the Michaelis-Menten kinetic mechanism. The apparent Michealis-Menten constant (K_M^{app}) that provides the information about the interaction of the enzyme with its substrate can be calculated from the electrochemical version of the Lineweaver-Burk equation [385]:

$$\frac{1}{I_{SS}} = \frac{1}{I_{max}} + \frac{K_M^{app}}{I_{max}C}$$

(16.6)

where, I_{SS} is the steady-state current after the addition of substrate, I_{max} is the maximum current measured under saturated substrate conditions, and C is the bulk concentration of the substrate. The K_M^{app} was calculated from the slope (K_M^{app}/I_{max}) and the intercept ($1/I_{max}$) for the plot of the reciprocals of the I_{SS} vs. H_2O_2 concentration (C). It is equal 0.6 mM indicating that the adsorbed enzyme has low biological affinity to its substrate. If one would like apply such electrode as H_2O_2 biosensor active element this material has to be optimized.

154

Fig. 16.17 Cyclic voltammograms (2nd scan) of three-CNPs(+/-)/Mb film ITO electrode immersed in Ar-saturated 0.1 M phosphate buffer (pH 7.0) containing (a) 0 (b) 0.31 (c) 0.51 (d) 0.63 and (f) 1.18 mM of H_2O_2. Scan rate100 mV s^{-1}. The inset: The plot of the catalytic currents at -0.45 V vs H_2O_2 concentration.

16.6. Electrochemistry of the adsorbed glucose oxidase

16.6.1. Direct glucose oxidase voltammetry on the modifed electrode

The carbon nanoparticulate film electrodes apart from promoting myoglobin direct electron transfer, turns out to be also an excellent support for facilitating direct communication of glucose oxidase with electrode surface (Fig. 16.18). On voltammogram obtained with adsorbed GOx one can observe a pair of well defined reversible peaks of the FAD/FADH$_2$ redox couple only if the GOx is adsorbed on the carbon nanoparticulate film electrode (Fig. 16.19).
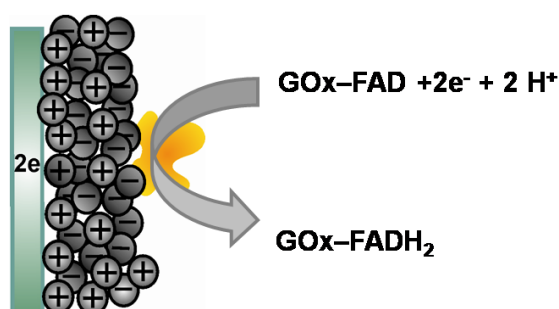
Fig. 16.18 The illustration of direct communication between the CNPs(+/-) film ITO electrode and GOx.

It indicates that direct electron transfer occurs between the enzyme's active centre and electrode surface. The formal potential ($E°'$) of GOx was estimated as -0.43 V (vs. Ag/AgCl) which is close to the reported in literature (see for example [316]), with 59 mV peak-to-peak separation at 50 mV s^{-1} (Fig. 16.19 (ii)).
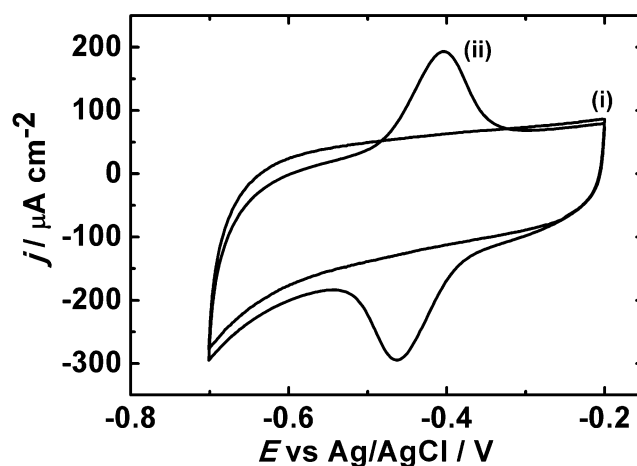
Fig. 16.19 Cyclic voltammograms (2nd scan) of (i) a bare ITO electrode and coated with (ii) three-CNPs/GOx immersed in Ar-saturated 0.1 M phosphate buffer (pH 7). Scan rates 100 mV s^{-1}.

The peak current is proportional to the number of immersion and withdrawal steps (results not shown). However, similarly to Mb modified electrode, and most likely for the same reason, the increase is less visible for larger amounts of nanoparticulate material (see Chapter 16.5.1).

To ensure that the redox process of GOx is surface controlled on the modified electrode, the scan rate dependence was performed (Fig. 16.20). It revealed that the redox peak current vary linearly. The heterogeneous electron transfer rate constant and electron transfer coefficient of the GOx on the modified electrode was also estimated using Laviron's peak separation method [382], (see Chapter 16.5.1) and are equal to: 0.34 s^{-1} and 0.46, for k_s and α, respectively. The obtained result indicates that the redox process of adsorbed GOx on the carbon nanoparticulate film electrode is also quasi-reversible.

The surface average concentration of the electroactive GOx adsorbed on carbon nanoparticulate film electrode was calculated according the equation (16.4) and equals to 9.83×10^{-9} mol cm^{-2}.
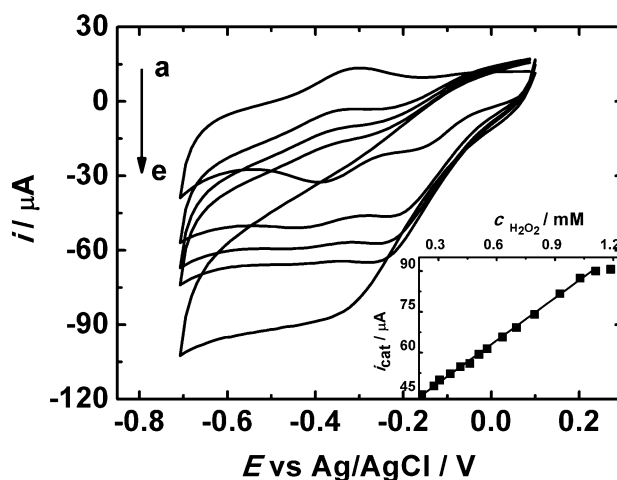
156

Fig. 16.20 (A) Cyclic voltammograms (2nd scan) of three-CNPs(+/-)/GOx film ITO electrode immersed in Ar-saturated 0.1 M phosphate buffer (pH 7) at different scan rates: 1, 5, 10, 20, 40, 50, 60, 80, 100 mV s^{-1}. Inset: The plot of cathodic and anodic peak current vs scan rate.

The direct electron transfer of GOx is a two-electron coupled with two-proton reaction which is described via such reaction (Eq. 6.8). Therefore to study the pH effect the experiments in various pH were performed. As is the depicted in Fig. 16.21 the peak current is shifted towards more negative values when the pH increases in the range of 5-9. It varies linearly with the slope close to the theoretical value (59 mV pH^{-1} [291]) equals to 64 mV pH^{-1}.

Recently, the distinction if the FAD is in or outside the protein's shell is a controversial subject in the literature [316]. At that moment, from the experiments that have been carried out, it is hard to find whether the observed DET is from the bounded FAD to GOx or the cofactor is free, outside the protein's shell, resulting in MET. Such analysis requires further experiments that have to be performed.

Fig. 16.21 Cyclic voltammograms (2nd scan) of three-CNPs(+/-)/GOx film ITO electrode immersed in Ar-saturated 0.1 M phosphate with different pH values of (a-d) 5, 6, 7, and 9. Scan rates 50 mV s^{-1}. Inset: The plot of the formal potential vs pH.

16.6.2. Electrocatalytic activity of the modified electrode with adsorbed glucose oxidase

Oxygen as a natural co-substrate for GOx is taking a part in enzymatic reaction of glucose oxidation (Fig. 16.22). Therefore, the electrocatalytic ability of the carbon nanoparticulate film electrodes for oxidation of glucose was investigated.
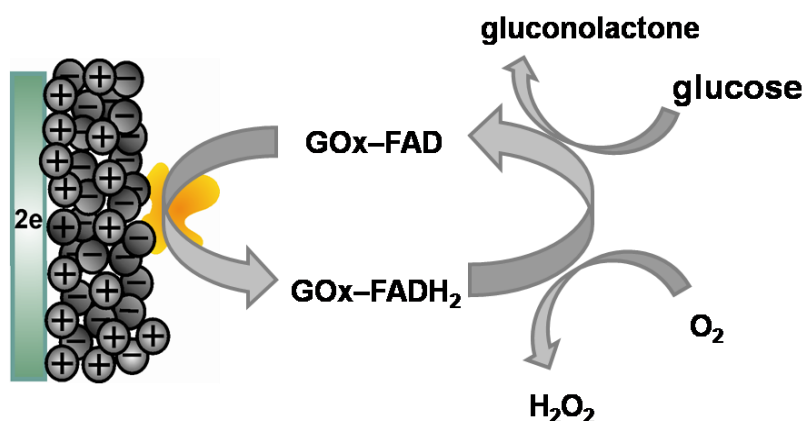
Fig. 16.22 Schematic illustration of the bioelectrocatalytic reaction of glucose oxidation in the presence of oxygen (natural cofactor) at the CNPs(+/-) film ITO electrode.

158

Cyclic voltammograms of the modified electrode with adsorbed GOx in PBS (pH 7) saturated with oxygen, in the absence and presence different concentration of glucose, were recorded (Fig. 16.23). In O_2 saturated solution the reduction peak current, originating from reduction of O_2 and H_2O_2, appears while the oxidation peak current significantly decreases (Fig. 16.23 (ii)) as compare to deareated conditions (Fig. 16.23 (i)). After the injection of the glucose to the oxygen saturated solution the reduction peak currents are decreasing (Fig. 16.23 (iii, iv)). Such behaviour is due to the decrease of oxygen concentration owing to its consumption in the enzyme-catalyzed reaction between GOx and glucose. The glucose does not undergo the oxidation in the absence of enzyme in this potential range. As one can see from the insert at Fig. 16.23 the reduction current depends linearly on the glucose concentration in the solution. It exhibits a wide and linear range (0 – 20 mM). However, if one would like to use this electrode as first generation glucose biosensor there is still room for optimization.
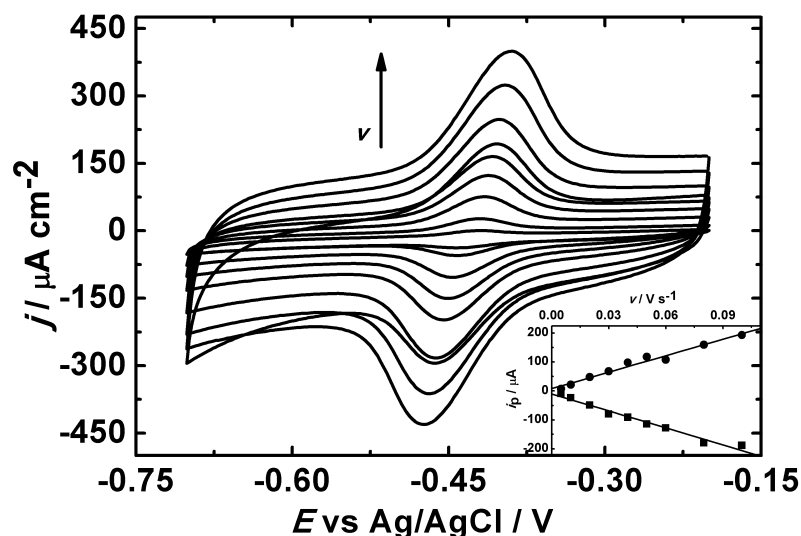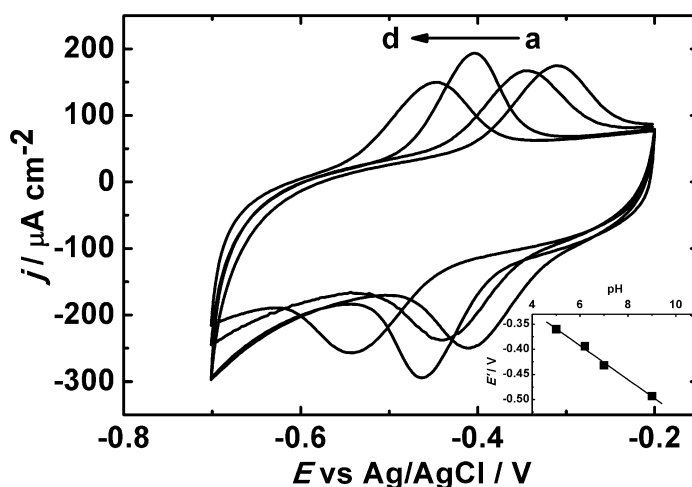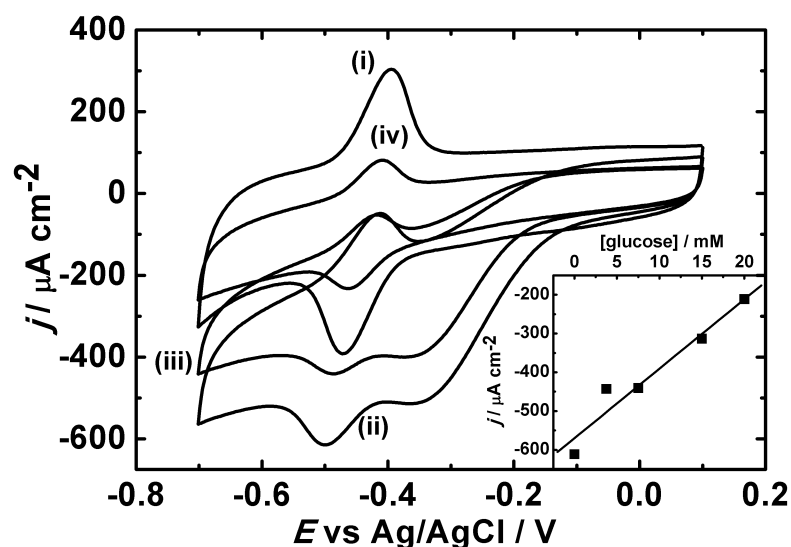

Fig. 16.23 Cyclic voltammograms (2nd scan) of three-CNP(+/-)/GOx film ITO electrode immersed in 0.1 M phosphate buffer (pH 7) under (i) anaerobic conditions in absence of glucose, (ii) aerobic conditions in absence of glucose, and (iii) under aerobic conditions with 3.75 mM glucose and (iv) 20 mM glucose. Scan rates 50 mV s^{-1}. Inset: The plot of catalytic current at -0.49 V vs glucose concentrations.

If the natural cofactor is replaced by the artificial mediator e.g. ferrocenemonocarboxylic acid (FMCA), bioelectrocatalytic oxidation of glucose occurs

159

(Fig. 16.24). The electrocatalytic oxidation of glucose at three-CNPs(+/-)/GOx film electrode occurs only if the mediator is in the solution (Fig. 16.25).
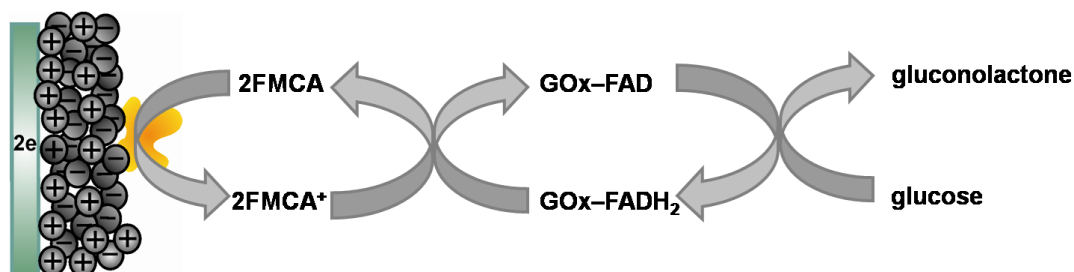
Fig. 16.24 A schematic diagram of the bioelectrocatalytic reaction of glucose oxidation via GOx in the presence of mediator (FMCA and its oxidized form FMCA$^+$) at the CNPs(+/-) film ITO electrode.
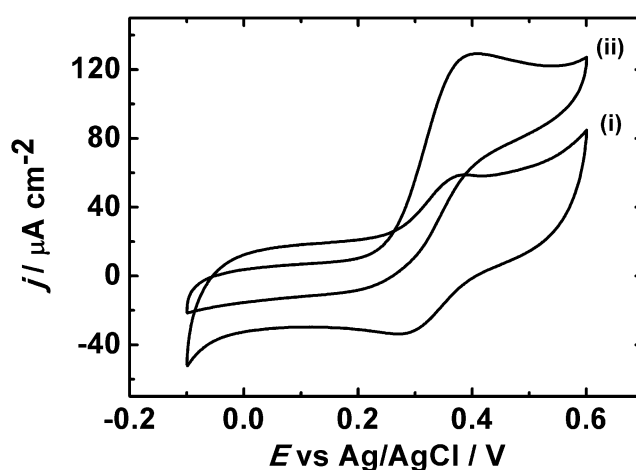
Fig. 16.25 Cyclic voltammograms (2nd scan) of three-CNPs(+/-)/GOx film ITO electrode obtained in 0.5 mM FMCA solution in O$_2$-saturated phosphate buffer (pH 7) (i) in the absence, and (ii) in the presence of 5 mM of glucose. Scan rate 10 mV s^{-1}.

16.7. Conclusions

A stable carbon nanoparticulate film electrode was obtained employing carbon nanoparticles with opposite charges by layer-by-layer approach. The amount of deposited carbon material can be controlled by the number of immersion and withdrawal steps. Even single alternative immersion and withdrawal step produces film covering the entire electrode surface. The increase in electrochemically active surface

by consecutive immersion and withdrawal steps was demonstrated for selected electrode reactions.

The proposed procedure represents an example of a novel way of nanoparticulate film formation by alternative deposition of the conductive nanoparticles of opposite charges [381] also almost unexplored for film electrodes [86, 374]. The carbon nanoparticulate film electrode can be employed as platform for number of redox proteins' immobilizations. One can observe the bioelectrocatalytic activity towards the oxygen reduction reaction after BOx adsorption as well as direct electron transfer and electrocatalytic acitivity after Mb and GOx adsorption. These electrodes after further improvement may be employed for the construction of various biodevices such as biofuel cells and biosensors.

17. Electrodeposited carbon-silicate nanocomposites assisted by a three-phase junction

17.1. Introduction

Electrodepositon of silicate materials have attracted recently some interest [386]. In its simplest form an electrode surface creates a catalyst of H^+ or OH^- ions by the application of a sufficiently positive or negative potential [130]. The dramatic change of pH causes the pre-hydrolysed sol to gel at the electrode surface forming a silicate matrix. Such films exhibit thickness ranging from several nanometres [386] to microns [387] depending on the applied potential, sol concentration, electrode material and deposition time.

In this chapter this approach will be applied to carbon–silicate nanocomposite preparation. The procedure involves single-step electrodeposition assisted by an electrode|organic-phase|aqueous-electrolyte three-phase junction. A water insoluble silicate precursor is dissolved in the organic phase whereas catalysts are electrochemically generated in the aqueous phase [346]. A stable aqueous suspension of CNPs was used allowing CNPs to be embedded into the silicate. This method leads to the formation of a narrow carbon–silicate stripe. To increase the active surface area several parallel stripes were deposited.The morphology and structure of the nanocomposites were thoroughly investigated by AFM, SEM, optical and infrared

161

mapping. The electrodes were examined as a support for bilirubin oxidase – an enzyme showing bioelectrocatalytic activity towards oxygen reduction.

17.2. The microscopic characterization

Electrodes were prepared according the procedure described in Chapter 10. That result in deposition of carbon-silicate stripe and an array of stripes. It is noteworthy that blank experiments show no deposition of silicate material without applied current, and only few islands of adsorbed CNPs on the ITO electrode, could be found. Owing to that the CNPs solution is too opaque for any spectroscopic measurement and the meniscus around the cell vessel distorts the view of the junction from the side by optical microscopy.

The optical microscope and SEM images of Fig. 17.1A,B allow the surface morphology of the ITO electrode modified with CNPs-silicate composites to be investigated. Fig. 17.1A (i) shows a black, ca. 100 μm wide stripe in the vicinity of the three-phase junction. The time of electrodeposition significantly influences neither its structure nor its width. However, its shape is strongly dependent on the CNPs concentration in the aqueous phase. A blurry and wider stripe was obtained for CNPs concentration of greater than 1.5 mg cm^{-3}. Unfortunatly the attempt to deposit an array of stripe leads to the formation of a film between the individual stripes (Fig. 17.1A (ii)) with the CNPs rather evenly distributed over a large area. SEM images reveal significant differences in the surface morphology of the single stripe and the film. The single stripe (Fig. 17.1B (i)) forms a porous structure like a carbon-sponge, whereas the array of stipes is more compact and contains fissures (Fig. 17.1B (ii)). More qualitative information about the size and distribution of the CNPs aggregates are provided by AFM images (Fig. 17.1C). The film is quite smooth (Fig. 17.1C (ii)) with small aggregates on the surface, whereas the single stripe is thicker with larger CNPs aggregates and deep holes throughout the structure (Fig. 17.1C (i)). The average thickness of the single stripe and the film are 1625 ± 140 nm and 715 ± 85 nm, respectively, as revealed by the measurement of the AFM profiles.
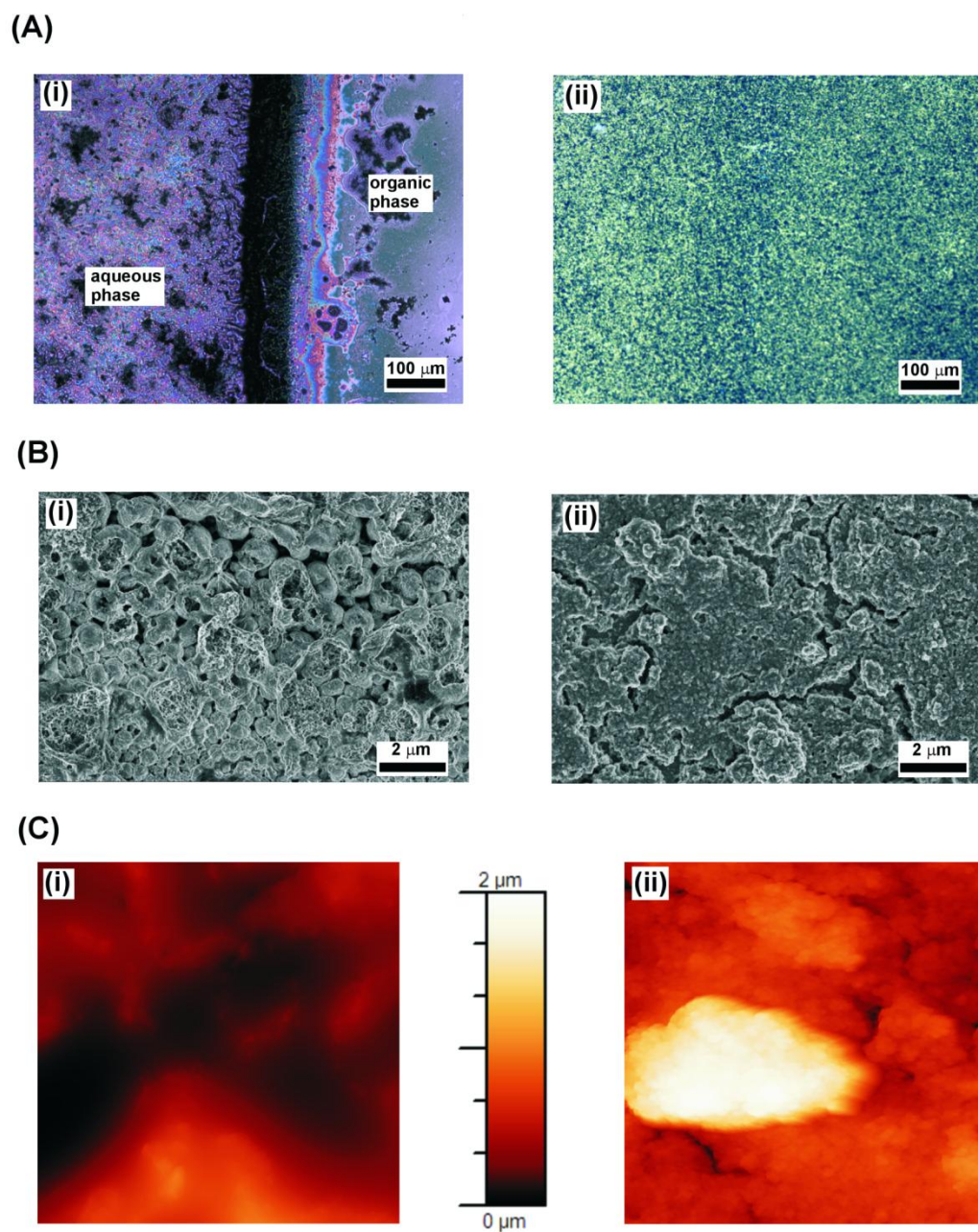
162

Fig. 17.1 (A) Optical (B) SEM and (C) AFM (scale bar 1 µm) images of the electrodeposited CNPs silicate (i) stripe and (ii) array of stripes on ITO electrodes.

163

17.3. FTIR characterization

FTIR spectroscopy was used to confirm gel-network formation [388, 389]. The spectrum of the sol-gel processed silicate on the ITO surface (Fig. 17.2A (a)) was compared with the precursor spectrum (Fig. 17.2A (b)). The latter is composed of strong bands due to Si–O–CH$_3$ groups superimposed on the contribution from groups in the hydrocarbon chains. The most prominent change introduced by the sol-gel process (Fig. 17.2A (a)) is a very strong band from the Si–O–Si network (1125 cm^{-1}) replacing the Si–O–C modes at 1170 cm^{-1} [388, 389]. The bands at 2985/2893 cm^{-1}, 1464/1393 cm^{-1} correspond to methylene asymmetric/symmetric stretching and bending in the hydrocarbon chains. The band at 965 cm^{-1} is a characteristic for methylene groups bonded to silicon atoms and corresponds to the CH$_2$ twisting mode. Upon gelation the band at 965 cm^{-1} does not change significantly, as shown in Fig. 17.2A (a). Fig. 17.2A (c) shows the spectrum from CNPs. The intrinsic infrared bands of CNPs are weak because their oscillations do not change the dipole moment. However, they show an intensive background depending on the aggregation and possible impurities [390, 391]. The intense band at 1082 cm^{-1} is attributed to the sulfonate surface groups. To investigate the CNPs-silicate distribution on the stripe-array electrode an infrared map was studied. Fig. 17.2B compares a regular optical micrograph of the film with its infrared images − showing the correlation between the actually measured spectrum and the octyl functionalized silicate (Fig. 17.2A (a)) and CNP (Fig. 17.2A (c)) spectra as the reference. Fig. 17.2B shows that the gel spots appear in the same places as CNPs spectra, suggesting that CNPs are easily incorporated in the gelated material. Both correlation maps show horizontal stripes. The position of the stripes coincides with the position of the three-phase junction during the sequential immersion steps. Consequently, we can conclude that the sol-gel process takes place mainly at the three phase junction. However, between the stripes there is an additional deposit of a film-like CNPs-silicate material. Moreover, the places rich in gelated material form rather large shapes suggesting that the CNPs are not aggregated during the process occurring at the three-phase junction.

164
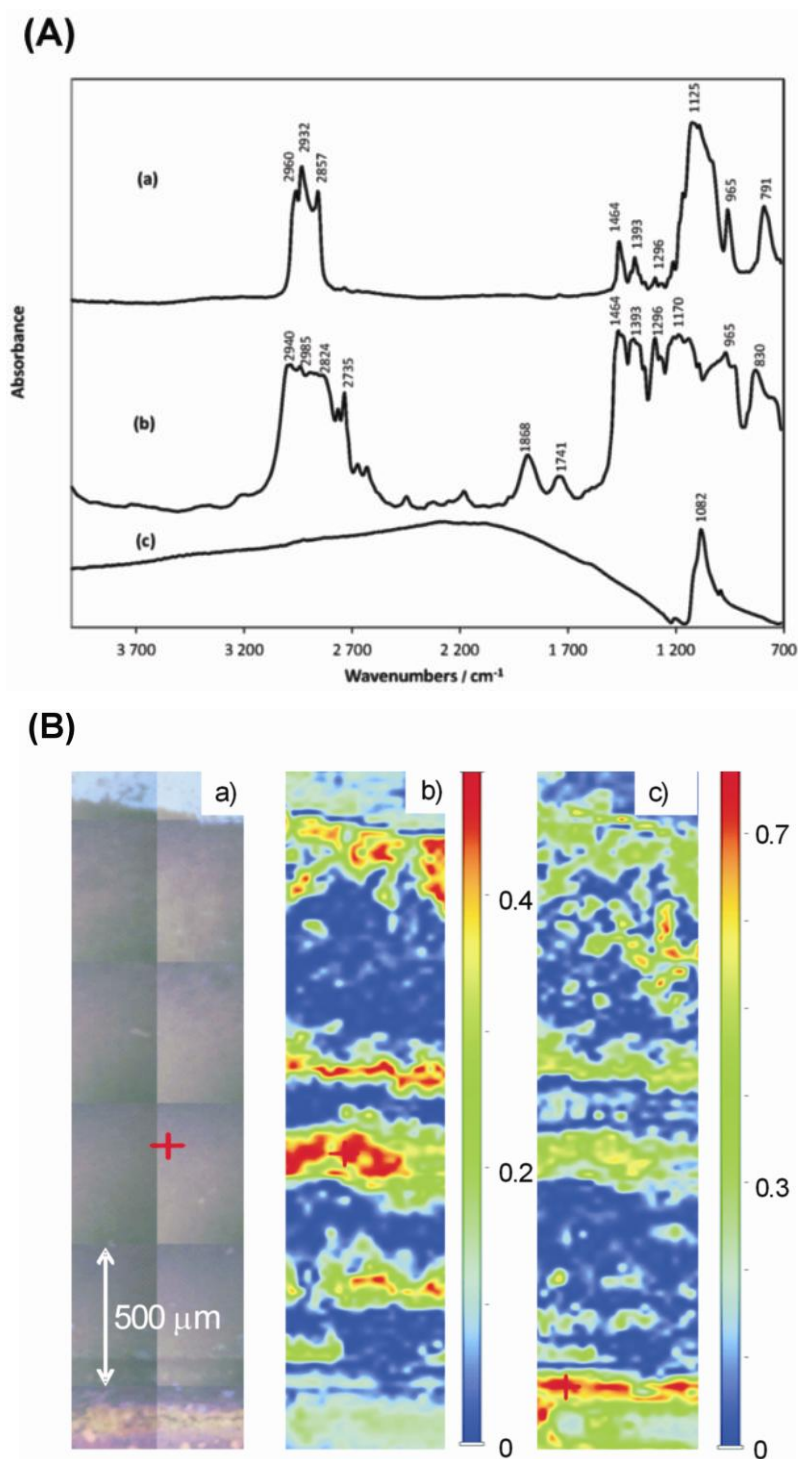
Fig. 17.2 (A) Infrared spectra of (a) gelated OTEOS, (b) OTEOS precursor and (c) CNPs. (B) Optical micrograph of the electrodeposited CNPs silicate array of stipe (a) and infrared correlation maps of gelated OTEOS (b) and CNPs (c). The vertical bars depict the correlation values.

165

17.4.   The electrochemical characterization

In order to evaluate the electrochemical properties of the prepared electrodes cyclic voltammetric measurements were performed using three different redox probes of different size and charge: $Fe(CN)_6^{3-/4-}$, $Fc(CH_2OH)_2^{0/+}$, and $Ru(NH_3)_6^{3+/2+}$ (Fig. 17.3). The stripe modified electrode exhibits higher current than the film formed between the stripes for all of the redox probes. This shows that the active surface area of the stripe is bigger than the film of the same material probably due to the porous structure of the stripe. Moreover, the stripe is probably loaded with a larger amount of CNPs per area than the film. This affects both the capacitive and the Faradaic currents since the phenylsulfonic CNPs functional groups are responsible for $Fc(CH_2OH)_2^{0/+}$, $Ru(NH_3)_6^{3+/2+}$ cation attraction to the carbon–silicate nanocomposites and repulsion of a negatively charged $Fe(CN)_6^{3-/4-}$. For all of the cases peak-shaped voltammograms were recorded indicating that entrapped CNPs are electrically connected with the ITO electrode and accessible for the redox probes. On the stripe electrodes the CVs of the redox probes are not typically peak-shaped, but have a somewhat sigmoidal character. This could indicate a contribution from non-linear diffusion.

Fig. 17.3 Cyclic voltammograms of electrodeposited CNPs silicate (i) stripe (ii) array of stripes (iii) and bare ITO electrode immersed in 0.5 mM $Fe(CN)_6^{3-}$ and 0.5 mM $Fe(CN)_6^{4-}$, 1 mM $Ru(NH_3)_6^{3+}$ or 1 mM $Fc(CH_2OH)_2$ solutions in 0.1 M $NaClO_4$ aqueous solution. Scan rate 5 mV s^{-1}.

166

17.5. Bioelectrocatalytic activity

The ITO electrodes modified with carbon–silicate nanocomposites were used as support for enzyme immobilization and their biocatalytic activity was tested (Fig. 17.4). Well-defined electrocatalytic waves were obtained for both stripe and film electrodes in oxygen saturated buffer, which vanished after deaeration. The oxygen reduction commences at ca. 0.60 V for both electrodes, close to the formal potential of the T1 center of BOx [155]. The obtained results show that adsorbed BOx exhibits mediatorless catalysis towards the four-electron reduction of O_2 to water [181, 255, 279]. Also, a blank experiment was performed for the bare ITO electrode with adsorbed BOx which exhibits mediatorless catalysis but its efficiency is negligible (ca. 0.02 mA cm^{-2}). The highest catalytic current density was recorded for the stripe electrode ca. 0.8 ± 0.13 mA cm^{-2} at 0.2 V (Fig. 17.4A curve O_2), which is about three times higher than for the film and eight-times greater than for other carbon nanoparticulate silicate films. The reasonable explanation of this behaviour might be in the carbon-sponge structure of stripe that provides suitable active area for efficient oxygen transport to the enzyme and higher enzyme loading. It is also possible that the stripe has some contribution from non-linear diffusion (edge effect) [278] what increases the diffusion limited current density. In the case of the film, the geometric area of it includes not only the array of stripes, but also the compact film between them that probably has a lower enzyme loading due to the compactness of the surface. Such a structure might result in smaller current density.
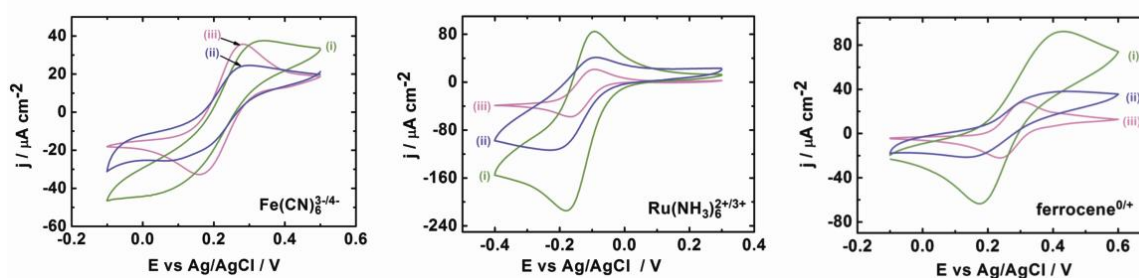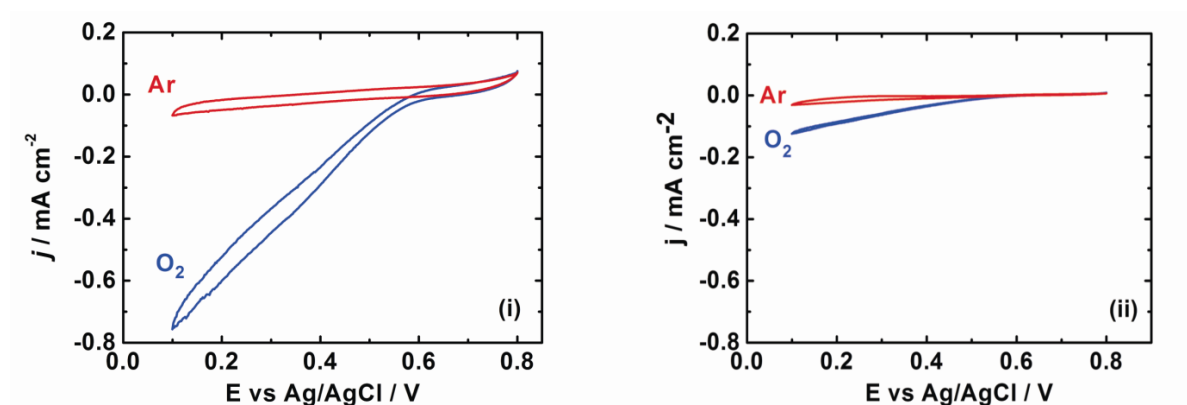
Fig. 17.4 Cyclic voltammograms of electrodeposited CNPs silicate (i) stripe and (ii) array of stripes modified with BOx on ITO electrode immersed in oxygen (O₂) and argon (Ar) saturated 0.1 M McIlvaine buffer (pH 4.8). Scan rate 1 mV s⁻¹.

17.6. Conclusions

Single-step electrodeposition of sol-gel carbon–silicate nanocomposites with the help of the electrode|organic-phase|aqueous-electrolyte three-phase junction has been demonstrated. Using this method it is possible to obtain either an isolated stripe or continuous interconnected stripes. This method also opens new possibilities for a construction of sensors with controllable geometry and morphology. Carbon–silicate stripes and films are convenient hosts for BOx immobilization since both exhibit mediatorless bioelectrocatalysis of oxygen reduction. The efficiency of the biocatalytic process is greatest for the carbon-sponge stripe, probably due to high enzyme loading and good oxygen accessibility of the structure.

168

18. Carbon nanoparticles – multicopper oxidases – biocathodes based on mediatorless electron transfer
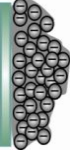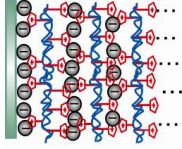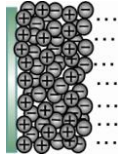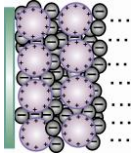
The construction of efficient biocathodes for biofuel cells, with high current density, low overpotential and good stability, is still a challenging task. The application of carbon nanomaterials ensures good electrical contact between the enzyme's active centre and the electrode surface; therefore they are widely applied for biocathode construction (see for example [2, 184]).

In this research carbon nanoparticles were deposited on the electrode surface via various avenues. On the surface of modified electrodes laccase or bilirubin oxidase, were immobilized. These electrodes were further studied in terms of bioelectrocatalytic reaction of oxygen reduction.

As one can see form the Table 1 different preparation procedures lead to the generation of biocathodes with different catalytic efficiencies (as measured by current density). For electrodes based on hydrophilic silicate the presence of laccase ensures more efficient catalysis whereas in the hydrophobic films bilirubin oxidase is more effective.

The current densities resulting from mediatorless bioelectrocatalysis of the obtained film electrodes range from a few up to 150 μA cm^{-2}. Other studi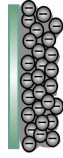es show that electrode architecture based on carbon nanoparticles and silicate submicroparticles is even more favourable [376]. For electrodeposited CNPs silicate stripes, and multi-layers film electrodes with CNPs-silicate submicroparticles functionalized with imidazolium groups current densities above 0.5 and 0.3 mA cm^{-2}, respectively, were recorded. These values are similar to those obtained with: bilirubin oxidase adsorbed on nanostructed sol-gel/pyrene-functionalized CNTs [181], CCE enriched with carbon nanoparticles [205], platinum [273] and gold [274] nanoparticles. Among the studied film electrodes the best efficiency was obtained for multi-layers film electrodes with CNPs-silicate submicroparticles functionalized with imidazolium groups. Unfortunately, none of the presented biocathodes' current density is close to maximal efficiencies (above 1 mA cm^{-2}) reported in the literature [206, 255, 283]. Such problems could potentially be overcome by utilization of 3D macroporous materials for electrodes modification. Such materials increase the electroactive surface, the enzyme loading and improve the access of substrate (oxygen) to the enzyme.

Table 1 The comparison of the efficiency of the bioelectrocatalytic reaction of oxygen reduction on carbon nanoparticles-MCOx modified electrodes (in all cases the onset potential of ORR is ca. 0.6 V).

Electrode	Current density at 0.2 V ($\mu A\ cm^{-2}$) pH 4.8	Scheme
Hydrophilic silicate film $TMOS_{gel}$/CNPs/Lc $TMOS_{gel}$/CNPs/BOx	 -90 -30	
Hydrophobic silicate film $MTMOS_{gel}$/CNPs/BOx $MTMOS_{gel}$/CNPs/Lc $OTEOS_{gel}$/CNPs/BOx	 -98 -14 -151	
CNPs silicate nanocomposites stripe/BOx array of stripes/BOx	 580 -90	
Three–(CNPs-imidazolium functionalized silicate layers film electrode)/BOx	-21	
Film electrode prepared from oppositely charged carbon nanoparticles three-CNPs(+/-)/BOx three-CNPs(+/-)/Lc	 -130 -4	
Thirty-two-(CNPs-silicate submicroparticles functionalized with imidazolium functional groups)/BOx [376]	-320	

170

19. Zn-O$_2$ hybrid cells – summary

Th operating voltage of a Zn-O$_2$ hybrid cell, based on a Zn anode and a biocathode, is larger than that of a typical biofuel cell, which makes it a competitive power source. Recently a number of these devices with biocathodes modified with multicopper oxidases have been reported [203, 294, 295]. However, their main disadvantage is restricted time of operation due to the limited amount of Zn (which is consumed during the electrochemical reaction), and enzyme's poor stability. Therefore these cells are suitable for small energy consumption devices. Recently Feraponotova's group has made progress in this area, constructing such cell powering an electronic timer for 38 days [294].

The Zn-O$_2$ cells assembled in research for this thesis, compared to others found in the literature in terms of power densities still require significant improvement (Table 2). Here their maximum power densities range from 17 to 114 μW cm^{-2} at pH 5. The highest ones were obtained for cells with bilirubin oxidase-based biocathodes modified with oppositely charged carbon nanoparticles or a hydrophobic silicate matrix with entrapped carbon nanoparticles. These values are similar to those obtained for Zn-O$_2$ cells combined with nanostructed sol-gel/pyrene-functionalized CNTs biocathodes [181], and twice as high as the maximum power density obtained for Zn-O$_2$ cells combined with ITO nanoparticle based biocathodes [293] (Table 2). Unfortunately, obtained power densities are almost an order of magnitude smaller than recently reported example (up to 3.5 mW cm^{-2} [260]) (Table 2).

In order to enhance the efficiency of Zn-O$_2$ hybrid cells one should work on improvement of biocathode properties as it is the case of biofuel cells. This is possible via the application of more efficient enzymes or by amelioration of the electrical contact between the enzyme and the electrode's surface through various methods of surface modification e.g. covalent bonding of laccase to carbon nanotubes [260, 295]. Also the utilization of whole microbial organisms instead of enzymes might prolong the life-time of such cells.

171

Table 2 Parameters of Zn-O$_2$ cells with various MCOx-biocathodes based on mediatorless bioelectrocatalysis.

MCOx-biocathode in Zn-O$_2$ cells	OCP/V	P$_{max}$/µW cm^{-2}	O$_2$ saturated buffer	Ref.
Air-breathing CCE/BOx	1.09	41.3 at 0.58V	0.1 M phosphate buffer pH 5	[203]
CCE-CNPs10/BOx	1.52	220 at 0.45V	air-saturated 0.1 M phosphate buffer pH 5	[392]
	1.48	300 at 0.6V	Artificial serum	
ITO/PSA/SWCNT/MTMOS/BOx	1.55	108 at 0.90V	0.1 M McIlvaine buffer pH 4.8	[181]
ITO/ITO$_{NP}$/BOx$_{ads}$	1.6	43 at 0.86V	0.1 M McIlvaine buffer pH 4.8	[293]
ITO/ITO$_{NP}$/BOx$_{encap}$	1.63	54 at 1.10 V		
ITO/VACNT/MTMOS/Lc	1.64	115 at 1.25V	0.1 M McIlvaine buffer pH 4.8	[234]
ITO/VACNT/PSA/MTMOS/Lc	1.70	275 at 1.50V		
Graphite sheet/AEBA/Lc	1.6	1190 at 0.41V	0.05 M succinate buffer pH 4.5	[264]
GCE/SWCNT-AQ-side/SWCNT-AQ-side /Lc + Nafion/modified Nafion *	1.52	3500 at 0.5 V	0.1M McIlvaine buffer pH 5.2/ 0.2M NaNO$_3$	[260]
	*1.52	*2740 at 0.44V		
GCE/SWCNT–(CH2)$_2$–NH$_2$/Lc	1.50	1000 at 0.80V	0.15 M McIlvaine buffer pH 5.3	[295]
Graphitized carbon cloth/Lc	1.76	400 at 0.5V	air-saturated 0.05 M potassium sulphate/0.01 M sodium citrate buffer pH 5.0	[294]
ITO/TMOS$_{gel}$/CNPs/Lc	1.48	17.4 at 0.7V	0.1 M McIlvaine buffer pH 4.8	This work
ITO/MTMOS$_{gel}$/CNPs/BOx	1.67	100 at 1.0V	0.1 M McIlvaine buffer pH 4.8	This work
	1.34	67.0 at 0.54V	Artificial serum	
ITO/three-CNPs(+/-)/BOx	1.60	114 at 0.65V	0.1M McIlvaine buffer pH 4.8	This work
	1.29	47.0 at 0.47 V	Artificial serum	

20.   General conclusions

Ensuring a good electrical contact between the enzyme's active centre and the electrode surface is a challenging task. Many attempts have been undertaken to achieve it, mainly by improving the electrical conductivity and increasing the dimensionality and porosity of the modified electrode. Also this thesis attempts to solve this problem with application of carbon nanoparticles and various methods for their immobilisation at the electrode surface.

Here five types of electrodes modified with carbon nanoparticles and various enzymes were constructed and studied:

- Hydrophilic carbon nanoparticle thin film electrode with entrapped laccase or bilirubin oxidase.

- Hydrophobic sol-gel film electrode with entrapped carbon nanoparticles and adsorbed bilirubin oxidase or laccase.

- Carbon nanoparticles-imidazolium functionalized silicate layers film electrode prepared by a layer-by-layer method with adsorbed laccase or bilirubin oxidase.

- Film electrodes prepared from oppositely charged carbon nanoparticles with adsorbed bilirubin oxidase, laccase, glucose oxidase or myoglobin.

- Electrodeposited at a three-phase junction solid|liquid|liquid carbon-silicate nanocomposites with adsorbed bilirubin oxidase.

These electrodes were studied mainly from a bioelectrocatalytic point of view to be further applied as biocathodes in Zn-O hybrid cells or as hydrogen peroxide or glucose biosensors.

The most important conclusions from this thesis are the following:

- A simple procedure of electrode modification with conductive, oppositely charged carbon nanoparticles, demonstrated for the first time, results in stable carbon nanoparticulate film. This material is a superior platform for immobilization of various redox proteins (bilirubin oxidase, laccase, myoglobin and glucose oxidase).

- It is possible to obtain stable carbon nanoparticles silicate composite by electrochemically driven sol-gel process.

173

- The presence of carbon nanoparticles in film electrode allows for direct electronic communication between enzyme and electrode. The efficiency of this process depends on the method of immobilization.

- The direct signal from the enzyme's active center was recorded for electrodes modified with oppositely charged carbon nanoparticles and adsorbed myoglobine or glucose oxidase. In the case of the latter enzyme the signal is extremely well defined. These electrodes were also successfully applied for hydrogen peroxide and glucose sensing.

- The highest current density of bioelectrocatalytic oxygen reduction was recorded for the electrode modified with electrodeposited carbon-silicate stripe assisted by the three phase junction with adsorbed bilirubin oxidase.

21. Bibliography

[1] T. Miyake, S. Yoshino, T. Yamada, K. Hata, M. Nishizawa, J. Am. Chem. Soc., 133 (2011) 5129.

[2] A. Zebda, C. Gondran, A. Le Goff, M. Holzinger, P. Cinquin, S. Cosnier, Nat. Comm., 2 (2011) 370.

[3] R.F. Lane, A.T. Hubbard, J. Phys. Chem., 77 (1973) 1411.

[4] R.A. Durst, A.J. Baumner, R.W. Murray, R.P. Buck, C.P. Andrieux, Pure Appl. Chem., 69 (1997) 1317.

[5] L.C. Clark, C. Lyons, Ann. N. Y. Acad. Sci., 102 (1962) 29.

[6] S.J. Updike, G.P. Hicks, Nature, 214 (1967) 986.

[7] P. Yeh, T. Kuwana, Chem. Lett., (1977) 1145.

[8] M.J. Eddowes, H.A.O. Hill, J. Chem. Soc. Chem. Commun., 21 (1977) 771.

[9] L.V. Radushkevich, V.M. Lukyanovich, Russ. J. Phys. Chem. A, 26 (1952) 88.

[10] S. Iijima, Nature, 354 (1991) 56.

[11] J.J. Gooding, Electrochim. Acta, 50 (2005) 3049.

[12] S.N. Kim, J.F. Rusling, F. Papadimitrakopoulos, Adv. Mater., 19 (2007) 3214.

[13] W. Yang, K.R. Ratinac, S.P. Ringer, P. Thordarson, J.J. Gooding, F. Braet, Angew. Chem. Int. Ed., 49 (2010) 2114.

[14] J. Wang, Analyst, 130 (2005) 421.

[15] G. Lota, K. Fic, E. Frackowiak, Energy Environ. Sci., 4 (2011) 1592.

[16] P. Coquay, E. Flahaut, E. De Grave, A. Peigney, R.E. Vandenberghe, C. Laurent, J. Phys. Chem. B, 109 (2005) 17825.

[17] T. Guo, P. Nikolaev, A. Thess, D.T. Colbert, R.E. Smalley, Chem. Phys. Lett., 243 (1995) 49.

[18] Y. Liu, S. Xiaolong, Z. Tingkai, Z. Jiewu, M. Hirscher, P. Fritz, Carbon, 42 (2004) 1852.

[19] M. Trojanowicz, Trends in Anal. Chem., 25 (2006) 480.

[20] X.-L. Luo, J.-J. Xu, J.-L. Wang, H.-Y. Chen, Chem. Commun., (2005) 2169.

[21] B.J.C. Thomas, A.R. Boccaccini, M.S.P. Shaffer, J. Am. Ceram. Soc., 88 (2005) 980.

[22] M. Musameh, J. Wang, A. Merkoci, Y. Lin, Electrochem. Commun., 4 (2002) 743.

[23] H.R. Zare, N. Nasirizadeh, Electrochim. Acta, 52 (2007) 4153.

[24] A. Salimi, C.E. Banks, R.G. Compton, Analyst, 129 (2004) 225.

[25] T.-K. Hong, D.W. Lee, H.J. Choi, H.S. Shin, B.-S. Kim, ACS Nano, 4 (2010) 3861.

[26] B. Habibi, M.H. Pournaghi-Azar, Electrochim. Acta, 55 (2011) 5492.

[27] M.S.P. Shaffer, A.H. Windle, Adv. Mater., 11 (1999) 937.

[28] V.G. Gavalas, R. Andrews, D. Bhattacharyya, L.G. Bachas, Nano Lett., 1 (2001) 719.

[29] J. Wang, Electroanalysis, 17 (2005) 7.

[30] A. Hirsch, Angew. Chem. Int. Ed., 41 (2002) 1853.

[31] C.E. Banks, A. Crossley, C. Salter, S.J. Wilkins, R.G. Compton, Angew. Chem. Int. Ed., 45 (2006) 2533.

[32] P.J. Britto, K.S.V. Santhanam, P.M. Ajayan, Bioelectrochem. Bioenerg., 41 (1996) 121.

[33] J. Wang, M. Musameh, Y. Lin, J. Am. Chem. Soc., 125 (2003) 2408.

[34] R.N. Goyal, V.K. Gupta, S. Chatterjee, Biosens. Bioelectron., 24 (2009) 3562.

[35] B.E.K. Swamy, B.J. Venton, Analyst, 132 (2007) 876.

[36] X. Chen, Y. Yang, M. Ding, Anal. Chim. Acta, 557 (2006) 52.

[37] R.T. Kachoosangi, G.G. Wildgoose, R.G. Compton, Electroanalysis, 20 (2008) 2495.

[38] H. Xu, L. Zeng, S. Xing, Y. Xian, G. Shi, L. Jin, Electroanalysis, 20 (2008) 2655.

[39] J. Wang, S.B. Hocevar, B. Ogorevc, Electrochem. Commun., 6 (2004) 176.

[40] M. Huang, H. Jiang, X. Qu, Z. Xu, Y. Wang, S. Dong, Chem. Commun., (2005) 5560.

[41] M. Zhou, Y. Zhai, S. Dong, Anal. Chem., 81 (2009) 5603.

[42] A. Lesniewski, Electrodes modifed with imidazolium functionalized materials, PhD Thesis, Institute of Physical Chemistry, Polish Academy of Sciences, Warsaw, 2010.

[43] A. Salimi, R. Hallaj, M. Ghadermazi, Talanta, 65 (2005) 888.

[44] J. Li, S. Guo, Y. Zhai, E. Wang, Anal. Chim. Acta, 649 (2009) 196.

[45] K.S. Novoselov, A.K. Geim, S.V. Morozov, D. Jiang, Y. Zhang, S.V. Dubonos, I.V. Grigorieva, A.A. Firsov, Science, 306 (2004) 666.

[46] C.N.R. Rao, A.K. Sood, K.S. Subrahmanyam, A. Govindaraj, Angew. Chem. Int. Ed., 48 (2009) 7752.

[47] S. Park, R.S. Ruoff, Nat. Nanotechnol., 4 (2009) 217.

[48] S. Guo, S. Dong, Chem. Soc. Rev., 40 (2011) 2644.

[49] Y. Shao, J. Wang, H. Wu, J. Liu, I.A. Aksay, Y. Lin, Electroanalysis, 22 (2010) 1027.

[50] M. Pumera, Chem. Rec., 9 (2009) 211.

[51] A. Reina, X. Jia, J. Ho, D. Nezich, H. Son, V. Bulovic, M.S. Dresselhaus, J. Kong, Nano Lett., 9 (2008) 30.

[52] A. Dato, V. Radmilovic, Z. Lee, J. Phillips, M. Frenklach, Nano Lett., 8 (2008) 2012.

[53] K.S. Subrahmanyam, L.S. Panchakarla, A. Govindaraj, C.N.R. Rao, J. Phys. Chem. C, 113 (2009) 4257.

[54] C. Zhu, S. Guo, Y. Fang, S. Dong, ACS Nano, 4 (2010) 2429.

[55] J.H. Lee, D.W. Shin, V.G. Makotchenko, A.S. Nazarov, V.E. Fedorov, Y.H. Kim, J.-Y. Choi, J.M. Kim, J.-B. Yoo, Adv. Mater., 21 (2009) 4383.

[56] H.-L. Guo, X.-F. Wang, Q.-Y. Qian, F.-B. Wang, X.-H. Xia, ACS Nano, 3 (2009) 2653.

[57] V.Y. Aristov, G. Urbanik, K. Kummer, D.V. Vyalikh, O.V. Molodtsova, A.B. Preobrajenski, A.A. Zakharov, C. Hess, T. Hanke, B. Buchner, I. Vobornik, J. Fujii, G. Panaccione, Y.A. Ossipyan, M. Knupfer, Nano Lett., 10 (2010) 992.

[58] L. Jiao, X. Wang, G. Diankov, H. Wang, H. Dai, Nat. Nanotechnol., 5 (2010) 321.

[59] K.R. Ratinac, W. Yang, J.J. Gooding, P. Thordarson, F. Braet, Electroanalysis, 23 (2011) 803.

[60] H. Yamaguchi, G. Eda, C. Mattevi, H. Kim, M. Chhowalla, ACS Nano, 4 (2010) 524.

[61] G. Eda, G. Fanchini, M. Chhowalla, Nat. Nanotechnol., 3 (2008) 270.

[62] Z.-S. Wu, S. Pei, W. Ren, D. Tang, L. Gao, B. Liu, F. Li, C. Liu, H.-M. Cheng, Adv. Mater., 21 (2009) 1756.

[63] J. Shen, Y. Hu, C. Li, C. Qin, M. Shi, M. Ye, Langmuir, 25 (2009) 6122.

[64] R.Y.N. Gengler, A. Veligura, A. Enotiadis, E.K. Diamanti, D. Gournis, C. Józsa, B.J. van Wees, P. Rudolf, Small, 6 (2010) 35.

[65] X. Li, G. Zhang, X. Bai, X. Sun, X. Wang, E. Wang, H. Dai, Nat. Nanotechnol., 3 (2008) 538.

[66] Z. Wei, D.E. Barlow, P.E. Sheehan, Nano Lett., 8 (2008) 3141.

[67] Z. Tang, S. Shen, J. Zhuang, X. Wang, Angew. Chem. Int. Ed., 49 (2010) 4603.

[68] J. Liu, S. Fu, B. Yuan, Y. Li, Z. Deng, J. Am. Chem. Soc., 132 (2010) 7279.

[69] C. Zhu, S. Guo, P. Wang, L. Xing, Y. Fang, Y. Zhai, S. Dong, Chem. Commun., 46 (2010) 7148.

[70] C. Shan, H. Yang, J. Song, D. Han, A. Ivaska, L. Niu, Anal. Chem., 81 (2009) 2378.

[71] H.-G. Liao, H. Wu, J. Wang, J. Liu, Y.-X. Jiang, S.-G. Sun, Y. Lin, Electroanalysis, 22 (2010) 2297.

[72] C.X. Guo, Z.S. Lu, Y. Lei, C.M. Li, Electrochem. Commun., 12 (2010) 1237.

[73] A. Cao, Z. Liu, S. Chu, M. Wu, Z. Ye, Z. Cai, Y. Chang, S. Wang, Q. Gong, Y. Liu, Adv. Mater., 22 (2010) 103.

[74] N.G. Shang, P. Papakonstantinou, M. McMullan, M. Chu, A. Stamboulis, A. Potenza, S.S. Dhesi, H. Marchetto, Adv. Funct. Mater., 18 (2008) 3506.

[75] J. Li, S. Guo, Y. Zhai, E. Wang, Electrochem. Commun., 11 (2009) 1085.

[76] M.H. Parvin, Electrochem. Commun., 13 (2011) 366.

[77] Y.-K. Kim, H.-K. Na, Y.W. Lee, H. Jang, S.W. Han, D.-H. Min, Chem. Commun., 46 (2010) 3185.

[78] M.S. Goh, M. Pumera, Electrochem. Commun., 12 (2010) 1375.

[79] C.K. Chua, A. Ambrosi, M. Pumera, Electrochem. Commun., 13 (2011) 517.

[80] J.A. Belmont, R.M. Amici, C.P. Galloway, US patent 5851280, 1998-12-22, Cabot Corporation.

[81] E.M. Dannenberg, L. Paquin, H. Gwinnell, 4, New York, 1992, pp. 1037.

[82] A.M. Zimer, R. Bertholdo, M.T. Grassi, A.J.G. Zarbin, L.H. Mascaro, Electrochem. Commun., 5 (2003) 983.

[83] M. Amiri, S. Shahrokhian, F. Marken, Electroanalysis, 19 (2007) 1032.

[84] L. Rassaei, M.J. Bonne, M. Sillanpaa, F. Marken, New J. Chem., 32 (2008) 1253.

[85] L. Rassaei, M. Sillanpää, F. Marken, Electrochim. Acta, 53 (2008) 5732.

[86] A. Lesniewski, M. Paszewski, M. Opallo, Electrochem. Commun., 12 (2010) 435.

[87] A. Lesniewski, J. Niedziolka-Jonsson, C. Rizzi, L. Gaillon, J. Rogalski, M. Opallo, Electrochem. Commun., 12 (2010) 83.

[88] A. Celebanska, D. Tomaszewska, A. Lesniewski, M. Opallo, Biosens. Bioelectron., 26 (2011) 4417.

[89] S. Macdonald, K. Szot, J. Niedziolka, F. Marken, M. Opallo, J. Solid State Electrochem., 12 (2008) 287.

[90] F. Ghorbani-Bidkorbeh, S. Shahrokhian, A. Mohammadi, R. Dinarvand, Electrochim. Acta, 55 (2010) 2752.

[91] F. Ghorbani-Bidkorbeh, S. Shahrokhian, A. Mohammadi, R. Dinarvand, J. Electroanal. Chem., 638 (2010) 212.

[92] S. Shahrokhian, M. Ghalkhani, Electrochem. Commun., 11 (2009) 1425.

[93] S. Shahrokhian, E. Jokar, M. Ghalkhani, Microchim. Acta, 170 (2010) 141.

[94] L. Vidal, A. Chisvert, A. Canals, E. Psillakis, A. Lapkin, F. Acosta, K.J. Edler, J.A. Holdaway, F. Marken, Anal. Chim. Acta, 616 (2008) 28.

[95] M. Amiri, S. Shahrokhian, E. Psillakis, F. Marken, Anal. Chim. Acta, 593 (2007) 117.

[96] N. Cheng, R.A. Webster, M. Pan, S. Mu, L. Rassaei, S.C. Tsang, F. Marken, Electrochim. Acta, 55 (2010) 6601.

[97] S.M. MacDonald, P.D.I. Fletcher, Z.-G. Cui, M. Opallo, J. Chen, F. Marken, Electrochim. Acta, 53 (2007) 1175.

[98] J.D. Watkins, R. Lawrence, J.E. Taylor, S.D. Bull, G.W. Nelson, J.S. Foord, D. Wolverson, L. Rassaei, N.D.M. Evans, S.A. Gascon, F. Marken, Phys. Chem. Chem. Phys., 12 (2010) 4872.

[99] J.D. Watkins, K. Lawrence, J.E. Taylor, T.D. James, S.D. Bull, F. Marken, Electroanalysis, 23 (2011) 1320.

[100] M. Tsionsky, G. Gun, V. Glezer, O. Lev, Anal. Chem., 66 (1994) 1747.

[101] C.J. Brinker, G.W. Scherer, Sol-gel science : The Physics and Chemistry of Sol-Gel Processing, Academic Press, Boston, 1990.

[102] L. Rabinovich, O. Lev, Electroanalysis, 13 (2001) 265.

[103] L. Zhu, C. Tian, J. Zhai, R. Yang, Sensor Actuat. B, 125 (2007) 254.

[104] A. Salimi, H. MamKhezri, R. Hallaj, Talanta, 70 (2006) 823.

[105] A. Salimi, V. Alizadeh, H. Hadadzadeh, Electroanalysis, 16 (2004) 1984.

[106] A. Salimi, M. Roushani, Electrochem. Commun., 7 (2005) 879.

[107] A. Salimi, S. Pourbeyram, Talanta, 60 (2003) 205.

[108] A. Salimi, R. Hallaj, Electroanalysis, 16 (2004) 1964.

[109] Q. Sheng, H. Yu, J. Zheng, Electrochim. Acta, 52 (2007) 7300.

[110] H. Razmi, H. Heidari, E. Habibi, J. Solid State Electrochem., 12 (2008) 1579.

[111] B. Haghighi, A. Rahmati-Panah, S. Shleev, L. Gorton, Electroanalysis, 19 (2007) 907.

[112] M.R. Majidi, K. Asadpour-Zeynali, S.A. Hosseini, Electroanalysis, 19 (2007) 364.

[113] W. Nogala, E. Rozniecka, I. Zawisza, J. Rogalski, M. Opallo, Electrochem. Commun., 8 (2006) 1850.

[114] W. Nogala, E. Rozniecka, J. Rogalski, M. Opallo, J. Electroanal. Chem., 608 (2007) 31.

[115] J.F. Rusling, B. Wang, S.-e. Yun, Electrochemistry of Redox Enzymes, Bioelectrochemistry, John Wiley & Sons, Ltd, 2008, pp. 39.

[116] L. Cao, Introduction: Immobilized Enzymes: Past, Present and Prospects, Carrier-bound Immobilized Enzymes, Wiley-VCH Verlag GmbH & Co. KGaA, 2006, pp. 1.

[117] J.M. Montornes, M.S. Vreeke, I. Katakis, Glucose Biosensors, Bioelectrochemistry, John Wiley & Sons, Ltd, 2008, pp. 199.

[118] G.T.R. Palmore, Biofuel Cells, Bioelectrochemistry, John Wiley & Sons, Ltd, 2008, pp. 359.

[119] R.A. Bullen, T.C. Arnot, J.B. Lakeman, F.C. Walsh, Biosens. Bioelectron., 21 (2006) 2015.

[120] M.H. Osman, A.A. Shah, F.C. Walsh, Biosens. Bioelectron., 26 (2011) 3087.

[121] A.K. Sarma, P. Vatsyayan, P. Goswami, S.D. Minteer, Biosens. Bioelectron., 24 (2009) 2313.

[122] M.J. Cooney, V. Svoboda, C. Lau, G. Martin, S.D. Minteer, Energy Environ. Sci., 1 (2008) 320.

[123] G. Güven, R. Prodanovic, U. Schwaneberg, Electroanalysis, 22 (2010) 765.

[124] J. Kim, J.W. Grate, P. Wang, Chem. Eng. Sci., 61 (2006) 1017.

[125] L.S. Wong, F. Khan, J. Micklefield, Chem. Rev., 109 (2009) 4025.

178

[126] M. Pellissier, F. Barričre, A.J. Downard, D. Leech, Electrochem. Commun., 10 (2008) 835.

[127] F.H. Dickey, J. Phys. Chem., 59 (1955) 695.

[128] S. Braun, S. Rappoport, R. Zusman, D. Avnir, M. Ottolenghi, Mater. Lett., 10 (1990) 1.

[129] H. Frenkel-Mullerad, D. Avnir, J. Am. Chem. Soc., 127 (2005) 8077.

[130] M.M. Collinson, Accounts Chem. Res., 40 (2007) 777.

[131] S. Yang, W.-Z. Jia, Q.-Y. Qian, Y.-G. Zhou, X.-H. Xia, Anal. Chem., 81 (2009) 3478.

[132] R.K. Iler, J. Colloid Interface Sci., 21 (1966) 569.

[133] G. Decher, J.-D. Hong, Makromol. Chem. Macromol. Symp., 46 (1991) 321.

[134] X. Zhang, H. Chen, H. Zhang, Chem. Commun., (2007) 1395.

[135] G. Decher, Science, 277 (1997) 1232.

[136] J. Zhang, M. Feng, H. Tachikawa, Biosens. Bioelectron., 22 (2007) 3036.

[137] F. Lisdat, R. Dronov, H. Mohwald, F.W. Scheller, D.G. Kurth, Chem. Commun., (2009) 274.

[138] E.I. Solomon, U.M. Sundaram, T.E. Machonkin, Chem. Rev., 96 (1996) 2563.

[139] T. Sakurai, K. Kataoka, Chem. Rec., 7 (2007) 220.

[140] M.R. Tarasevich, A.I. Yaropolov, V.A. Bogdanovskaya, S.D. Varfolomeev, Bioelectrochem. Bioenerg., 6 (1979) 393.

[141] G.T.R. Palmore, H.-H. Kim, J. Electroanal. Chem., 464 (1999) 110.

[142] S. Shleev, J. Tkac, A. Christenson, T. Ruzgas, A.I. Yaropolov, J.W. Whittaker, L. Gorton, Biosens. Bioelectron., 20 (2005) 2517.

[143] M. Sosna, J.-M. Chretien, J.D. Kilburn, P.N. Bartlett, Phys. Chem. Chem. Phys., 12 (2010) 10018.

[144] K. Mizutani, M. Toyoda, K. Sagara, N. Takahashi, A. Sato, Y. Kamitaka, S. Tsujimura, Y. Nakanishi, T. Sugiura, S. Yamaguchi, K. Kano, B. Mikami, Acta Crystallogr., Sect. F: Struct. Biol. Cryst. Commun., 66 (2010) 765.

[145] J.A. Cracknell, T.P. McNamara, E.D. Lowe, C.F. Blanford, Dalton Trans., 40 (2011) 6668.

[146] H.P. Call, I. Mucke, J. Biotechnol., 53 (1997) 163.

[147] S. Shleev, A. Christenson, V. Serezhenkov, D. Burbaev, A. Yaropolov, L. Gorton, T. Ruzgas, Biochem. J., 385 (2005) 745.

[148] B.R.M. Reinhammar, T.I. Vänngåd, Eur. J. Biochem., 18 (1971) 463.

[149] P. Schneider, M.B. Caspersen, K. Mondorf, T. Halkier, L.K. Skov, P.R. Ostergaard, K.M. Brown, S.H. Brown, F. Xu, Enzyme Microb. Technol., 25 (1999) 502.

[150] A. Klonowska, C. Gaudin, A. Fournel, M. Asso, J. Le Petit, M. Giorgi, T. Tron, Eur. J. Biochem., 269 (2002) 6119.

[151] S. Shleev, M. Klis, Y. Wang, J. Rogalski, R. Bilewicz, L. Gorton, Electroanalysis, 19 (2007) 1039.

[152] E. Nazaruk, A. Michota, J. Bukowska, S. Shleev, L. Gorton, R. Bilewicz, J. Biol. Inorg. Chem., 12 (2007) 335.

[153] K. Stolarczyk, E. Nazaruk, J. Rogalski, R. Bilewicz, Electrochim. Acta, 53 (2008) 3983.

[154] N. Mano, H.-H. Kim, Y. Zhang, A. Heller, J. Am. Chem. Soc., 124 (2002) 6480.

[155] P. Ramirez, N. Mano, R. Andreu, T. Ruzgas, A. Heller, L. Gorton, S. Shleev, Biochimi.Biophys. Acta, 1777 (2008) 1364.

179

[156] E.I. Solomon, R. Sarangi, J.S. Woertink, A.J. Augustine, J. Yoon, S. Ghosh, Accounts Chem. Res., 40 (2007) 581.
[157] A. Heller, B. Feldman, Chem. Rev., 108 (2008) 2482.
[158] J. Wang, Chem. Rev., 108 (2008) 814.
[159] N. Mano, F. Mao, A. Heller, ChemBioChem, 5 (2004) 1703.
[160] E. Nazaruk, S. Smolinski, M. Swatko-Ossor, G. Ginalska, J. Fiedurek, J. Rogalski, R. Bilewicz, J. Power Sources, 183 (2008) 533.
[161] J.A. Cracknell, K.A. Vincent, F.A. Armstrong, Chem. Rev., 108 (2008) 2439.
[162] A.M. Bond, Inorg. Chim. Acta, 226 (1994) 293.
[163] J. Niu, Y. Guo, S. Dong, J. Electroanal. Chem., 399 (1995) 41.
[164] X. Zuo, S. He, D. Li, C. Peng, Q. Huang, S. Song, C. Fan, Langmuir, 26 (2009) 1936.
[165] Q.-L. Sheng, J.-B. Zheng, X.-D. Shang-Guan, W.-H. Lin, Y.-Y. Li, R.-X. Liu, Electrochim. Acta, 55 (2010) 3185.
[166] T. Takano, J. Mol. Biol., 110 (1977) 569.
[167] F. Patolsky, Y. Weizmann, I. Willner, Angew. Chem. Int. Ed., 43 (2004) 2113.
[168] J. Liu, A. Chou, W. Rahmat, M.N. Paddon-Row, J.J. Gooding, Electroanalysis, 17 (2005) 38.
[169] A. Le Goff, M. Holzinger, S. Cosnier, Analyst, 136 (2011) 1279.
[170] K. Gong, Y. Yan, M. Zhang, L. Su, S. Xiong, L. Mao, Anal. Sci., 21 (2005) 1383.
[171] S.K. Vashist, D. Zheng, K. Al-Rubeaan, J.H.T. Luong, F.-S. Sheu, Biotechnol. Adv., 29 (2011) 169.
[172] K. Balasubramanian, M. Burghard, Anal. Bioanal. Chem., 385 (2006) 452.
[173] W. Jia, S. Schwamborn, C. Jin, W. Xia, M. Muhler, W. Schuhmann, L. Stoica, Phys. Chem. Chem. Phys., 12 (2010) 10088.
[174] X. Yu, D. Chattopadhyay, I. Galeska, F. Papadimitrakopoulos, J.F. Rusling, Electrochem. Commun., 5 (2003) 408.
[175] J.J. Davis, R.J. Coles, H. Allen, O. Hill, J. Electroanal. Chem., 440 (1997) 279.
[176] L. Zhang, W. Gong, Y. Pan, Y. Zhang, Russ. J. Electrochem., 44 (2008) 1271.
[177] H. Zhou, T.-H. Lu, H.-X. Shi, Z.-H. Dai, X.-H. Huang, J. Electroanal. Chem., 612 (2008) 173.
[178] F. Gao, L. Viry, M. Maugey, P. Poulin, N. Mano, Nat. Comm., 1 (2010) 2.
[179] L. Xiang, Y. Lin, P. Yu, L. Su, L. Mao, Electrochim. Acta, 52 (2007) 4144.
[180] S.C. Wang, F. Yang, M. Silva, A. Zarow, Y. Wang, Z. Iqbal, Electrochem. Commun., 11 (2009) 34.
[181] M. Jönsson-Niedziolka, A. Kaminska, M. Opallo, Electrochim. Acta, 55 (2010) 8744.
[182] É. Lojou, X. Luo, M. Brugna, N. Candoni, S. Dementin, M. Giudici-Orticoni, J. Biol. Inorg. Chem., 13 (2008) 1157.
[183] F. Tasca, M.N. Zafar, W. Harreither, G. Noll, R. Ludwig, L. Gorton, Analyst, 136 (2011) 2033.
[184] M. Opallo, R. Bilewicz, Adv. Phys. Chem., 2011 (2011) 1.
[185] C. Gomez, S. Shipovskov, E.E. Ferapontova, J. Renewable Sustainable Energy, 2 (2010) 013103.
[186] Y. Yan, W. Zheng, L. Su, L. Mao, Adv. Mater., 18 (2006) 2639.
[187] S. Mantha, V.A. Pedrosa, E.V. Olsen, V.A. Davis, A.L. Simonian, Langmuir, 26 (2010) 19114.

[188] G. Strack, H.R. Luckarift, R. Nichols, K. Cozart, E. Katz, G.R. Johnson, Chem. Commun., 47 (2011) 7662.

[189] M. Pumera, A. Ambrosi, A. Bonanni, E.L.K. Chng, H.L. Poh, Trends in Anal. Chem., 29 (2010) 954.

[190] S. Campuzano, J. Wang, Electroanalysis, 23 (2011) 1289.

[191] W. Zheng, H.Y. Zhao, J.X. Zhang, H.M. Zhou, X.X. Xu, Y.F. Zheng, Y.B. Wang, Y. Cheng, B.Z. Jang, Electrochem. Commun., 12 (2010) 869.

[192] C. Liu, S. Alwarappan, Z. Chen, X. Kong, C.-Z. Li, Biosens. Bioelectron., 25 (2010) 1829.

[193] J.-F. Wu, M.-Q. Xu, G.-C. Zhao, Electrochem. Commun., 12 175.

[194] K. Liu, J. Zhang, G. Yang, C. Wang, J.-J. Zhu, Electrochem. Commun., 12 402.

[195] S.P. Kumar, R. Manjunatha, C. Nethravathi, G.S. Suresh, M. Rajamathi, T.V. Venkatesha, Electroanalysis, 23 (2010) 842.

[196] X. Wu, Y. Hu, J. Jin, N. Zhou, P. Wu, H. Zhang, C. Cai, Anal. Chem., 82 (2010) 3588.

[197] W. Song, D.-W. Li, Y.-T. Li, Y. Li, Y.-T. Long, Biosens. Bioelectron., 26 3181.

[198] K. Wang, Q. Liu, L. Dai, J. Yan, C. Ju, B. Qiu, X. Wu, Anal. Chim. Acta, In Press, Corrected Proof (2011).

[199] K.-J. Huang, D.-J. Niu, X. Liu, Z.-W. Wu, Y. Fan, Y.-F. Chang, Y.-Y. Wu, Electrochim. Acta, 56 (2011) 2947.

[200] J. Gun, O. Lev, Anal. Chim. Acta, 336 (1996) 95.

[201] K. Wang, Q. Liu, L. Dai, J. Yan, C. Ju, B. Qiu, X. Wu, Anal. Chim. Acta, 695 (2011) 84.

[202] Y. Liu, X. Qu, H. Guo, H. Chen, B. Liu, S. Dong, Biosens. Bioelectron., 21 (2006) 2195.

[203] W. Nogala, A. Celebanska, G. Wittstock, M. Opallo, Fuel Cells, 10 (2010) 1157.

[204] L. Deng, L. Shang, Y. Wang, T. Wang, H. Chen, S. Dong, Electrochem. Commun., 10 (2008) 1012.

[205] W. Nogala, A. Celebanska, K. Szot, G. Wittstock, M. Opallo, Electrochim. Acta, 55 (2010) 5719.

[206] V. Flexer, N. Brun, O. Courjean, R. Backov, N. Mano, Energy Environ. Sci., 4 (2011) 2097.

[207] Y. Yuan, Y. Jeon, J. Ahmed, W. Park, S. Kim, J. Electrochem. Soc., 156 (2009) B1238.

[208] X. Xu, J. Chen, W. Li, Z. Nie, S. Yao, Electrochem. Commun., 10 (2008) 1459.

[209] J.-J. Yu, F.-Q. Zhao, B.-Z. Zeng, J. Solid State Electrochem., 12 (2008) 1167.

[210] J. Tang, B. Su, D. Tang, G. Chen, Biosens. Bioelectron., 25 (2010) 2657.

[211] S. Sampath, O. Lev, Anal. Chem., 68 (1996) 2015.

[212] H. Chen, S. Dong, Biosens. Bioelectron., 22 (2007) 1811.

[213] J. Niu, J. Yang Lee, Annal. Commun., 36 (1999) 81.

[214] M. El Kaoutit, I. Naranjo-Rodriguez, K.R. Temsamani, J.L. Hidalgo-Hidalgo de Cisneros, Biosens. Bioelectron., 22 (2007) 2958.

[215] G. Alarcon, M. Guix, A. Ambrosi, M.T. Ramirez Silva, M.E. Palomar Pardave, A. Merkoçi, Nanotechnology, 21 (2010) 245502.

[216] S.K. Ozoner, M. Yalvac, E. Erhan, Curr. Appl. Phys., 10 (2010) 323.

[217] J.B. Davis, H.F. Yarbrough, Science, 137 (1962) 615.

[218] A.T. Yahiro, S.M. Lee, D.O. Kimble, Biochimi.Biophys. Acta, 88 (1964) 375.

[219] I. Willner, E. Katz, F. Patolsky, A. F. Buckmann, J. Chem. Soc., Perkin Trans. 2, (1998) 1817.
[220] E. Katz, I. Willner, A.B. Kotlyar, J. Electroanal. Chem., 479 (1999) 64.
[221] S.L. Scott, W.J. Chen, A. Bakac, J.H. Espenson, J. Phys. Chem., 97 (1993) 6710.
[222] T. Chen, S.C. Barton, G. Binyamin, Z. Gao, Y. Zhang, H.-H. Kim, A. Heller, J. Am. Chem. Soc., 123 (2001) 8630.
[223] N. Mano, F. Mao, A. Heller, J. Am. Chem. Soc., 125 (2003) 6588.
[224] F. Mao, N. Mano, A. Heller, J. Am. Chem. Soc., 125 (2003) 4951.
[225] C. Fernández-Sánchez, T. Tzanov, G.M. Gübitz, A. Cavaco-Paulo, Bioelectrochemistry, 58 (2002) 149.
[226] B. Palys, A. Bokun, J. Rogalski, Electrochim. Acta, 52 (2007) 7075.
[227] K.J. Davies, M.E. Delsignore, J. Biol. Chem., 262 (1987) 9908.
[228] J. Rogalski, A.L. Dawidowicz, A. Leonowicz, Acta Biotechnol., 10 (1990) 261.
[229] S.D. Maleknia, J.W.H. Wong, K.M. Downard, Photochem. Photobiol. Sci., 3 (2004) 741.
[230] W.E. Farneth, M.B. D'Amore, J. Electroanal. Chem., 581 (2005) 197.
[231] R. Bilewicz, M. Opallo, Biocathodes for Dioxygen Reduction in Biofuel Cells, Fuel Cell Science, John Wiley & Sons, Inc., 2010, pp. 169.
[232] E. Nazaruk, K. Sadowska, K. Madrak, J.F. Biernat, J. Rogalski, R. Bilewicz, Electroanalysis, 21 (2009) 507.
[233] K. Sadowska, K. Stolarczyk, J.F. Biernat, K.P. Roberts, J. Rogalski, R. Bilewicz, Bioelectrochemistry, 80 (2010) 73.
[234] A. Zloczewska, M. Jönsson-Niedziolka, J. Rogalski, M. Opallo, Electrochim. Acta, 56 (2011) 3947.
[235] K. Karnicka, K. Miecznikowski, B. Kowalewska, M. Skunik, M. Opallo, J. Rogalski, W. Schuhmann, P.J. Kulesza, Anal. Chem., 80 (2008) 7643.
[236] M. Jönsson, K. Szot, J. Niedziolka, J. Rogalski, K. Karnicka, P.J. Kulesza, M. Opallo, J. Nanosci. Nanotechnol., 9 (2009) 2346.
[237] E. Nazaruk, K. Sadowska, J. Biernat, J. Rogalski, G. Ginalska, R. Bilewicz, Anal. Bioanal. Chem., 398 (2010) 1651.
[238] J. Fei, H.-K. Song, G.T.R. Palmore, Chem. Mater., 19 (2007) 1565.
[239] L. Brunel, J. Denele, K. Servat, K.B. Kokoh, C. Jolivalt, C. Innocent, M. Cretin, M. Rolland, S. Tingry, Electrochem. Commun., 9 (2007) 331.
[240] S. Cosnier, D. Shan, S.-N. Ding, Electrochem. Commun., 12 (2010) 266.
[241] S.-N. Ding, M. Holzinger, C. Mousty, S. Cosnier, J. Power Sources, 195 (2010) 4714.
[242] A. Habrioux, G. Merle, K. Servat, K.B. Kokoh, C. Innocent, M. Cretin, S. Tingry, J. Electroanal. Chem., 622 (2008) 97.
[243] A. Habrioux, K. Servat, S. Tingry, K.B. Kokoh, Electrochem. Commun., 11 (2009) 111.
[244] L. Hussein, G. Urban, M. Kruger, Phys. Chem. Chem. Phys., 13 (2011) 5831.
[245] A. Habrioux, T. Napporn, K. Servat, S. Tingry, K.B. Kokoh, Electrochim. Acta, 55 (2011) 7701.
[246] I.V. Berezin, V.A. Bogdanovskaya, S.D. Varfolomeev, M.R. Tarasevich, A.I. Yaropolov, Doklady Akademii Nauk SSSR., 240 (1978) 615.
[247] M.R. Tarasevich, Bioelectrochem. Bioenerg., 6 (1979) 587.
[248] M.R. Tarasevich, V.A. Bogdanovskaya, E.F. Gavrilova, S.B. Orlov, J. Electroanal. Chem., 206 (1986) 217.

182

[249] Y. Miura, S. Tsujimura, S. Kurose, Y. Kamitaka, K. Kataoka, T. Sakurai, K. Kano, Fuel Cells, 9 (2009) 70.

[250] R. Kontani, S. Tsujimura, K. Kano, Bioelectrochemistry, 76 (2009) 10.

[251] M. Pita, S. Shleev, T. Ruzgas, V.M. Fernandez, A.I. Yaropolov, L. Gorton, Electrochem. Commun., 8 (2006) 747.

[252] M. Klis, E. Maicka, A. Michota, J. Bukowska, S. Sek, J. Rogalski, R. Bilewicz, Electrochim. Acta, 52 (2007) 5591.

[253] B.A. Kuznetsov, G.P. Shumakovich, O.V. Koroleva, A.I. Yaropolov, Biosens. Bioelectron., 16 (2001) 73.

[254] J. Gallaway, I. Wheeldon, R. Rincon, P. Atanassov, S. Banta, S.C. Barton, Biosens. Bioelectron., 23 (2008) 1229.

[255] S. Tsujimura, Y. Kamitaka, K. Kano, Fuel Cells, 7 (2007) 463.

[256] M.R. Tarasevich, Y.G. Chirkov, V.A. Bogdanovskaya, A.V. Kapustin, Electrochim. Acta, 51 (2005) 418.

[257] R.P. Ramasamy, H.R. Luckarift, D.M. Ivnitski, P.B. Atanassov, G.R. Johnson, Chem. Commun., 46 (2010) 6045.

[258] X. Li, H. Zhou, P. Yu, L. Su, T. Ohsaka, L. Mao, Electrochem. Commun., 10 (2008) 851.

[259] M. Jönsson-Niedziolka, K. Szot, J. Rogalski, M. Opallo, Electrochem. Commun., 11 (2009) 1042.

[260] K. Stolarczyk, M. Sepelowska, D. Lyp, K. Zelechowska, J.F. Biernat, J. Rogalski, K.D. Farmer, K.N. Roberts, R. Bilewicz, Bioelectrochemistry, in press (2011).

[261] L. Deng, F. Wang, H. Chen, L. Shang, L. Wang, T. Wang, S. Dong, Biosens. Bioelectron., 24 (2008) 329.

[262] M. Dagys, K. Haberska, S. Shleev, T. Arnebrant, J. Kulys, T. Ruzgas, Electrochem. Commun., 12 (2010) 933.

[263] L. Deng, L. Shang, D. Wen, J. Zhai, S. Dong, Biosens. Bioelectron., 26 (2010) 70.

[264] J. Martinez-Ortiz, R. Flores, R. Vazquez-Duhalt, Biosens. Bioelectron., 26 (2011) 2626.

[265] C.F. Blanford, R.S. Heath, F.A. Armstrong, Chem. Commun., (2007) 1710.

[266] C.F. Blanford, C.E. Foster, R.S. Heath, F.A. Armstrong, Faraday Discuss., 140 (2009) 319.

[267] M.S. Thorum, C.A. Anderson, J.J. Hatch, A.S. Campbell, N.M. Marshall, S.C. Zimmerman, Y. Lu, A.A. Gewirth, J. Phys. Chem. Lett., 1 (2010) 2251.

[268] C. Vaz-Dominguez, S. Campuzano, O. Rüdiger, M. Pita, M. Gorbacheva, S. Shleev, V.M. Fernandez, A.L. De Lacey, Biosens. Bioelectron., 24 (2008) 531.

[269] W. Gellett, J. Schumacher, M. Kesmez, D. Le, S.D. Minteer, J. Electrochem. Soc., 157 (2010) B557.

[270] G. Gupta, C. Lau, B. Branch, V. Rajendran, D. Ivnitski, P. Atanassov, Electrochim. Acta, 56 (2011) 10767.

[271] S. Shleev, G. Shumakovich, O. Morozova, A. Yaropolov, Fuel Cells, 10 (2010) 726.

[272] S. Calabrese Barton, Electrochim. Acta, 50 (2005) 2145.

[273] Y.-M. Yan, I. Baravik, R. Tel-Vered, I. Willner, Adv. Mater., 21 (2009) 4275.

[274] K. Murata, K. Kajiya, N. Nakamura, H. Ohno, Energy Environ. Sci., 2 (2009) 1280.

[275] D. Ivnitski, K. Artyushkova, P. Atanassov, Bioelectrochemistry, 74 (2008) 101.

[276] S. Shleev, A. El Kasmi, T. Ruzgas, L. Gorton, Electrochem. Commun., 6 (2004) 934.

[277] S. Tsujimura, T. Nakagawa, K. Kano, T. Ikeda, Electrochemistry 72 (2004) 437.

[278] X. Li, L. Zhang, L. Su, T. Ohsaka, L. Mao, Fuel Cells, 9 (2009) 85.

[279] G. Göbel, F. Lisdat, Electrochem. Commun., 10 (2008) 1691.

[280] K. Schubert, G. Goebel, F. Lisdat, Electrochim. Acta, 54 (2009) 3033.

[281] G. Merle, A. Habrioux, K. Servat, M. Rolland, C. Innocent, K.B. Kokoh, S. Tingry, Electrochim. Acta, 54 (2009) 2998.

[282] J. Lim, N. Cirigliano, J. Wang, B. Dunn, Phys. Chem. Chem. Phys., 9 (2007) 1809.

[283] D. Wen, X. Xu, S. Dong, Energy Environ. Sci., 4 (2011) 1358.

[284] G. Gupta, C. Lau, V. Rajendran, F. Colon, B. Branch, D. Ivnitski, P. Atanassov, Electrochem. Commun., 13 (2011) 247.

[285] A. Heller, Phys. Chem. Chem. Phys., 6 (2004) 209.

[286] Y. Beyl, D.A. Guschin, S. Shleev, W. Schuhmann, Electrochem. Commun., 13 (2011) 474.

[287] P. Rowinski, C. Kang, H. Shin, A. Heller, Anal. Chem., 79 (2007) 1173.

[288] V. Coman, R. Ludwig, W. Harreither, D. Haltrich, L. Gorton, T. Ruzgas, S. Shleev, Fuel Cells, 10 (2010) 9.

[289] A. Heller, Anal. Bioanal. Chem., 385 (2006) 469.

[290] W. Shin, J. Lee, Y. Kim, H. Steinfink, A. Heller, J. Am. Chem. Soc., 127 (2005) 14590.

[291] A.J. Bard, L.R. Faulkner, Electrochemical methods : Fundamentals and Applications, 2nd ed., Wiley, New York, 2001.

[292] M. Smolander, H. Boer, M. Valkiainen, R. Roozeman, M. Bergelin, J.E. Eriksson, X.C. Zhang, A. Koivula, L. Viikari, Enzyme Microb. Technol., 43 (2008) 93.

[293] E. Rozniecka, M. Jonsson-Niedziolka, J.W. Sobczak, M. Opallo, Electrochim. Acta, 56 (2011) 8739.

[294] U.B. Jensen, S. Lorcher, M. Vagin, J. Chevallier, S. Shipovskov, O. Koroleva, F. Besenbacher, E.E. Ferapontova, Electrochim. Acta, in press (2011).

[295] E. Nazaruk, M. Karaskiewicz, K. Zelechowska, J.F. Biernat, J. Rogalski, R. Bilewicz, Electrochem. Commun., 14 (2011) 67.

[296] D.R. Thevenot, K. Toth, R.A. Durst, G.S. Wilson, Biosens. Bioelectron., 16 (2001) 121.

[297] N.J. Ronkainen, H.B. Halsall, W.R. Heineman, Chem. Soc. Rev., 39 (2010) 1747.

[298] E.-H. Yoo, S.-Y. Lee, Sensors, 10 (2010) 4558.

[299] Y. Xiao, F. Patolsky, E. Katz, J.F. Hainfeld, I. Willner, Science, 299 (2003) 1877.

[300] B. Wang, B. Li, Q. Deng, S. Dong, Anal. Chem., 70 (1998) 3170.

[301] I. Willner, B. Basnar, B. Willner, FEBS J., 274 (2007) 302.

[302] P.T. Kissinger, Biosens. Bioelectron., 20 (2005) 2512.

[303] J.E. Frew, H.A.O. Hill, Anal. Chem., 59 (1987) 933A.

[304] S. Vaddiraju, I. Tomazos, D.J. Burgess, F.C. Jain, F. Papadimitrakopoulos, Biosens. Bioelectron., 25 (2010) 1553.

[305] H.V. Malmstadt, H.L. Pardue, Anal. Chem., 33 (1961) 1040.

[306] H.P. Silverman, J.M. Brake, US patent 3506544, 1970-04-14, Magma Coorporation.

[307] A.E.G. Cass, G. Davis, G.D. Francis, H.A.O. Hill, W.J. Aston, I.J. Higgins, E.V. Plotkin, L.D.L. Scott, A.P.F. Turner, Anal. Chem., 56 (1984) 667.

[308] A. Chaubey, B.D. Malhotra, Biosens. Bioelectron., 17 (2002) 441.

[309] N.K. Cenas, J.J. Kulys, Bioelectrochem. Bioenerg., 8 (1981) 103.

[310] M.E. Ghica, C.M.A. Brett, Anal. Chim. Acta, 532 (2005) 145.

[311] P.N. Bartlett, S. Booth, D.J. Caruana, J.D. Kilburn, C. Santamaria, Anal. Chem., 69 (1997) 734.

[312] Y. Degani, A. Heller, J. Phys. Chem., 91 (1987) 1285.

[313] C.G.J. Koopal, B. de Ruiter, R.J.M. Nolte, J. Chem. Soc. Chem. Commun., (1991) 1691.

[314] C. Deng, J. Chen, X. Chen, C. Xiao, L. Nie, S. Yao, Biosens. Bioelectron., 23 (2008) 1272.

[315] W. Liang, Y. Zhuobin, Sensors, 3 (2003) 544.

[316] C. Cai, J. Chen, Anal. Biochem., 332 (2004) 75.

[317] L. Kuznetsova, M. Tarasevich, V. Bogdanovskaya, Russ. J. Electrochem., 36 (2000) 716.

[318] M. Delvaux, A. Walcarius, S. Demoustier-Champagne, Biosens. Bioelectron., 20 (2005) 1587.

[319] Q. Sheng, J. Zheng, Biosens. Bioelectron., 24 (2009) 1621.

[320] Z. Zhang, J. Zhou, A. Tang, Z. Wu, G. Shen, R. Yu, Biosens. Bioelectron., 25 (2010) 1953.

[321] A. Ramanavicius, A. Ramanaviciene, Fuel Cells, 9 (2009) 25.

[322] P. Cinquin, C. Gondran, F. Giroud, S. Mazabrard, A. Pellissier, F. Boucher, J.-P. Alcaraz, K. Gorgy, F. Lenouvel, S. Mathe, P. Porcu, S. Cosnier, PLoS One, 5 (2011) e10476.

[323] L. Shi, X. Liu, W. Niu, H. Li, S. Han, J. Chen, G. Xu, Biosens. Bioelectron., 24 (2009) 1159.

[324] Y. He, J. Zheng, K. Li, Q. Sheng, N. Qiao, Chinese J. Chem., 28 (2010) 2507.

[325] L. Zhao, H. Liu, N. Hu, Anal. Bioanal. Chem., 384 (2006) 414.

[326] S. Wang, F. Xie, G. Liu, Talanta, 77 (2009) 1343.

[327] L.-S. Duan, Q. Xu, F. Xie, S.-F. Wang, Int. J. Electrochem. Sci., 3 (2008) 118

[328] L. Zhao, H. Liu, N. Hu, J. Colloid Interface Sci., 296 (2006) 204.

[329] G.-X. Ma, T.-H. Lu, Y.-Y. Xia, Bioelectrochemistry, 71 (2007) 180.

[330] M.J. Esplandiu, M. Pacios, L. Cyganek, M. del Valle, Nanotechnology, 20 (2009) 355502.

[331] C. You, X. Yan, J. Kong, D. Zhao, B. Liu, Electrochem. Commun., 10 (2008) 1864.

[332] F.A. Armstrong, H.A. Heering, J. Hirst, Chem. Soc. Rev., 26 (1997) 169.

[333] R.S. Nicholson, I. Shain, Anal. Chem., 36 (1964) 706.

[334] G. Wittstock, M. Burchardt, S.E. Pust, Y. Shen, C. Zhao, Angew. Chem. Int. Ed., 46 (2007) 1584.

[335] S.E. Pust, W. Maier, G. Wittstock, Z. Phys. Chem., 222 (2008) 1463.

[336] K. Eckhard, X.X. Chen, F. Turcu, W. Schuhmann, Phys. Chem. Chem. Phys., 8 (2006) 5359.

[337] K. Karnicka, K. Eckhard, D.A. Guschin, L. Stoica, P.J. Kulesza, W. Schuhmann, Electrochem. Commun., 9 (2007) 1998.

[338] SEM, http://www.purdue.edu/rem/rs/sem.html, Accessed on 2012-01-13.

[339] AFM, http://www.wittstock.chemie.uni-oldenburg.de/en/research/methods/afm.html, Accessed on 2012-01-13.

[340] Z. Kęcki, Podstawy spektroskopii molekularnej, PWN, Warszawa, 1972.

[341] K. Freischlad, Laser Focus World, 46 (2010).

[342] J. Rogalski, A. Dawidowicz, E. Jozwik, A. Leonowicz, J. Mol. Catal. B: Enzym., 6 (1999) 29.

[343] C. Nunes Kirchner, S. Szunerits, G. Wittstock, Electroanalysis, 19 (2007) 1258.

[344] G. Wittstock, T. Asmus, T. Wilhelm, Fresenius. J. Anal. Chem., 367 (2000) 346.

[345] I. Zawisza, J. Rogalski, M. Opallo, J. Electroanal. Chem., 588 (2006) 244.

[346] J. Niedziolka, M. Opallo, Electrochem. Commun., 10 (2008) 1445.

[347] C. Kranz, M. Ludwig, H.E. Gaub, W. Schuhmann, Adv. Mater., 7 (1995) 568.

[348] F. Marken, M.L. Gerrard, I.M. Mellor, R.J. Mortimer, C.E. Madden, S. Fletcher, K. Holt, J.S. Foord, R.H. Dahm, F. Page, Electrochem. Commun., 3 (2001) 177.

[349] P. Żółtowski, J. Power Sources, 1 (1976) 285.

[350] F. Marken, R.D. Webster, S.D. Bull, S.G. Davies, J. Electroanal. Chem., 437 (1997) 209.

[351] M. De Leo, A. Kuhn, P. Ugo, Electroanalysis, 19 (2007) 227.

[352] K.J. McKenzie, J. Niedziolka, C.A. Paddon, F. Marken, E. Rozniecka, M. Opallo, Analyst, 129 (2004) 1181.

[353] J. Niedziolka, K. Szot, F. Marken, M. Opallo, Electroanalysis, 19 (2007) 155.

[354] J.D. Wadhawan, R.G. Evans, R.G. Compton, J. Electroanal. Chem., 533 (2002) 71.

[355] J. Niedziolka, M.A. Murphy, F. Marken, M. Opallo, Electrochim. Acta, 51 (2006) 5897.

[356] D. Quan, Y. Kim, W. Shin, B. Kor. Chem. Soc., 25 (2004) 1195.

[357] S. Braun, S. Rappoport, R. Zusman, D. Avnir, M. Ottolenghi, Mater. Lett., 10 (1990) 1.

[358] D. Avnir, S. Braun, O. Lev, M. Ottolenghi, Chem. Mater., 6 (1994) 1605.

[359] H.-Y. Liu, F.-R.F. Fan, C.W. Lin, A.J. Bard, J. Am. Chem. Soc., 108 (1986) 3838.

[360] A.J. Bard, F.-R.F. Fan, J. Kwak, O. Lev, Anal. Chem., 61 (1989) 132.

[361] R.C. Engstrom, M. Weber, D.J. Wunder, R. Burgess, S. Winquist, Anal. Chem., 58 (1986) 844.

[362] Y. Liu, L. Huang, S. Dong, Biosens. Bioelectron., 23 (2007) 35.

[363] S.V. Patwardhan, N. Mukherjee, S.J. Clarson, Silicon Chem., 1 (2002) 47.

[364] Y. Liu, L. Huang, S. Dong, Biosens. Bioelectron., 23 (2007) 35.

[365] S. Shleev, A. Jarosz-Wilkolazka, A. Khalunina, O. Morozova, A. Yaropolov, T. Ruzgas, L. Gorton, Bioelectrochemistry, 67 (2005) 115.

[366] M.M. Bradford Anal. Biochem., 72 (1976) 248.

[367] G. Shul, K.J. McKenzie, J. Niedziolka, E. Rozniecka, B. Palys, F. Marken, C.M. Hayman, B.R. Buckley, P.C.B. Page, M. Opallo, J. Electroanal. Chem., 582 (2005) 202.

[368] C. Fernandez-Sanchez, T. Tzanov, G.M. Gubitz, A. Cavaco-Paulo, Bioelectrochemistry, 58 (2002) 149.

[369] W. Nogala, M. Burchardt, M. Opallo, J. Rogalski, G. Wittstock, Bioelectrochemistry, 72 (2008) 174.

[370] J.L. Fernandez, N. Mano, A. Heller, A.J. Bard, Angew. Chem. Int. Ed., 43 (2004) 6355.

[371] N. Mano, H.H. Kim, Y.C. Zhang, A. Heller, J. Am. Chem. Soc., 124 (2002) 6480.

[372] R.L. Baldwin, Biophys. J., 71 (1996) 2056.

[373] M. Opallo, A. Lesniewski, J. Electroanal. Chem., 656 (2011) 2.

[374] A. Lesniewski, J. Niedziolka, B. Palys, C. Rizzi, L. Gaillon, M. Opallo, Electrochem. Commun., 9 (2007) 2580.

[375] S. Tsujimura, H. Tatsumi, J. Ogawa, S. Shimizu, K. Kano, T. Ikeda, J. Electroanal. Chem., 496 (2001) 69.

[376] K. Szot, R.P. Lynch, A. Lesniewski, E. Majewska, J. Sirieix-Plenet, L. Gaillon, M. Opallo, Electrochim. Acta, 56 (2011) 10306.

[377] M. Noda, H. Yukawa, M. Matsushima, H. Uchida, M. Umeno, Diamond Relat. Mater., 18 (2009) 426.

[378] O. Niwa, T. Horiuchi, H. Tabei, J. Electroanal. Chem., 367 (1994) 265.

[379] X. Luo, A. Morrin, A.J. Killard, M.R. Smyth, Electroanalysis, 18 (2006) 319.

[380] R.L. McCreery, Chem. Rev., 108 (2008) 2646.

[381] D. Lee, M.F. Rubner, R.E. Cohen, Nano Lett., 6 (2006) 2305.

[382] E. Laviron, J. Electroanal. Chem., 101 (1979) 19.

[383] Y. Hu, N. Hu, Y. Zeng, Microchem. J., 65 (2000) 147.

[384] S. Liu, H. Ju, Electroanalysis, 15 (2003) 1488.

[385] R.A. Kamin, G.S. Wilson, Anal. Chem., 52 (1980) 1198.

[386] F. Qu, R. Nasraoui, M. Etienne, Y.B.S. Come, A. Kuhn, J. Lenz, J. Gajdzik, R. Hempelmann, A. Walcarius, Electrochem. Commun., 13 (2011) 138.

[387] P.N. Deepa, M. Kanungo, G. Claycomb, P.M.A. Sherwood, M.M. Collinson, Anal. Chem., 75 (2003) 5399.

[388] H.K. Park, T.H. Ha, K. Kim, Langmuir, 20 (2004) 4851.

[389] J. Niedziolka, B. Palys, R. Nowakowski, M. Opallo, J. Electroanal. Chem., 578 (2005) 239.

[390] T. Belin, F. Epron, Mat. Sci. Eng. B, 119 (2005) 105.

[391] S. Ohmori, T. Saito, M. Tange, B. Shukla, T. Okazaki, M. Yumura, S. Iijima, J. Phys. Chem. C, 114 (2010) 10077.

[392] W. Nogala, Dioxygen reduction on enzyme modified carbon ceramic electrodes, PhD Thesis, Institute of Physical Chemistry, Polish Academy of Sciences, Warsaw, 2010.

22. Published papers

List of papers, which have evolved from doctoral thesis:

1. "Introducing hydrophilic carbon nanoparticles into hydrophilic sol-gel film electrodes."
   S.M. MacDonald, K. Szot, J. Niedziółka, F. Marken, M. Opallo
   J. Solid State Electrochem., 12 (2008) 287-293

2. "Sol-gel processed ionic liquid – hydrophilic carbon nanoparticles multilayer film electrode prepared by layer-by-layer method."
   K. Szot, A. Leśniewski, J. Niedziółka, M. Jonsson, C. Rizzi, L. Gaillon, F. Marken, J. Rogalski, M. Opallo
   J. Electroanal. Chem., 623 (2008) 170-176

3. "Hydrophilic carbon nanoparticle-laccase thin film electrode for mediatorless oxygen reduction. SECM activity mapping and application in zinc-oxygen battery."
   K. Szot, W. Nogala, J. Niedziolka-Jönsson, M. Jönsson-Niedziolka, F. Marken, J. Rogalski, C. Nunes Kirchner, G Wittstock, M. Opallo
   Electrochim. Acta, 54 (2009) 4620-4625

4. "Three dimensional film electrode prepared from oppositely charged carbon nanoparticles as efficient enzyme host."
   K. Szot, J. D. Watkins, S. D. Bull, F. Marken, M. Opallo
   Electrochem. Commun., 12 (2010) 737-739

5. "Bioelectrocatalytic mediatorless oxygen reduction at carbon ceramic electrodes modified with bilirubin oxidase."
   W. Nogala, A. Celebanska, K. Szot, G. Wittstock, M. Opallo
   Electrochim. Acta, 55 (2010) 5719-5724

6. "One-step electrodeposition of carbon-silicate sponge assisted by a three-phase junction for efficient bioelectrocatalysis."
   K. Szot, M. Jönsson-Niedziolka, B. Palys, J. Niedziolka-Jönsson
   Electrochem. Commun., 13 (2011) 556-569

7. "The effect of linker of electrodes prepared from sol–gel ionic liquid precursor and carbon nanoparticles on oxygen electroreduction bioelectrocatalysis."
   K. Szot, R.P. Lynch, A. Lesniewski, E. Majewska, J. Sirieix-Plenet, L. Gaillon, M. Opallo
   Electrochim. Acta, 56 (2011) 10306-10312

188

Others papers with my co-authorship:

1. "A porous ITO nanoparticle modified electrode for the immobilization of redox liquids."
   J. Niedziółka, K. Szot, F. Marken, M. Opallo
   Electroanalysis, 19 (2007) 155-161

2. "Bio-electrocatalytic dioxygen reduction at hybrid silicate - polyallylamine film with encapsulated laccase."
   K. Szot, J. Niedziółka, J. Rogalski, F. Marken, M. Opallo
   J. Electroanal. Chem., 612 (2008) 1-8

3. "Adsorption of 2,2'-azino-bis(3-ethylbenzothiazoline-6-sulfonate) on multiwalled carbon nanotubes – silicate film: application to bioelectrocatalytic oxygen reduction."
   M. Jonsson, K. Szot, J. Niedziółka, J. Rogalski, K. Karnicka, P. Kulesza, M. Opallo
   J. Nanosci. Nanotechnol., 9 (2009) 2346-2352

4. "Pyrene Sulfonate Functionalised Single-Walled Carbon Nanotubes for Mediatorless Oxygen Bioelectrocatalysis."
   M. Jönsson-Niedziolka, K. Szot, J Rogalski, M. Opallo
   Electrochem. Commun., 11 (2009) 1042-1044

5. "In Situ Micro-Raman Studies of Syringaldazine-entrapped Composite Electrodes Modified with Laccase."
   G. Z. Zukowska, W. Nogala, Y. Svartsov, M. Marcinek, J. Rogalski, K. Szot, M. Opallo
   ECS Trans. 25 (2009) 29-44

6. "Scanning electrochemical microscopy activity mapping of electrodes modified with laccase encapsulated in sol-gel processed matrix."
   W. Nogala, K. Szot, M. Burchardt, M. Jönsson-Niedziolka, J. Rogalski, G Wittstock, M. Opallo
   Bioelectrochemistry, 79 (2010) 101-107

7. "Feedback mode SECM study of laccase and bilirubin oxidase immobilised in a sol–gel processed silicate film."
   W. Nogala, K. Szot, M. Burchardt, F. Roelfs, J. Rogalski, M. Opallo, G. Wittstock Analyst, 135 (2010) 2051-2058

189